

AFFDL-TR-71-62

VOLUME VI

Volume VI. Wind Tunnel Test of a Powered
Tilt-Rotor Dynamic Model on a
Simulated Free Flight Suspension System

John E. Tomassoni
Robert B. Taylor
Leon N. Delarm
Edward B. Schagrin
The Boeing Company, Vertol Division
Philadelphia, Pennsylvania

TECHNICAL REPORT AFFDL-TR-71-62, VOLUME VI

October 1971

APPROVED FOR PUBLIC RELEASE
DISTRIBUTION UNLIMITED

Air Force Flight Dynamics Laboratory
Aeronautical Systems Division
Air Force Systems Command
Wright-Patterson Air Force Base, Ohio

Contracts

FOREWORD

This report was prepared by the Boeing Company, Vertol Division, Philadelphia, Pennsylvania, for the Air Force Flight Dynamics Laboratory, Wright-Patterson Air Force Base, Ohio, under Phase II of Contract F33615-69-C-1577. The contract objective is to develop design criteria and aerodynamic prediction techniques for the folding tilt rotor concept through a program of model testing and analysis.


The contract was administered by the Air Force Flight Dynamics Laboratory with Mr. Daniel E. Fraga (FV) as Project Engineer.

This report covers the period from January to July 1971.

The reports published under this contract for Design Studies and Model Tests of the Stowed Tilt Rotor Concept are:

Volume I	Parametric Design Studies
Volume II	Component Design Studies
Volume III	Performance Data for Parametric Study
Volume IV	Wind Tunnel Test of the Conversion Process of a Folding Tilt Rotor Aircraft Using a Semi-Span Unpowered Model
Volume V	Wind Tunnel Test of a Powered Tilt Rotor Performance Model
Volume VI	Wind Tunnel Test of a Powered Tilt Rotor Dynamic Model on a Simulated Free Flight Suspension System
Volume VII	Wind Tunnel Test of the Dynamics and Aerodynamics of Rotor Spinup, Stopping and Folding on a Semi-Span Folding Tilt Rotor Model
Volume VIII	Summary of Structural Design Criteria and Aerodynamic Prediction Techniques
Volume IX	Value Engineering Report

This report has been reviewed and is approved.


Ernest J. Cross, Jr.
Lt. Colonel, USAF
Chief, Prototype Division

ABSTRACT

This report presents the results of a wind tunnel test on a powered dynamic model of the Boeing M-160 tilt rotor aircraft with 5.5 foot diameter rotors. The model was tested in the Boeing V/STOL 20 X 20 foot wind tunnel during January-February 1971 and was supported to simulate free flight conditions with mount frequencies much lower than the dynamic aircraft frequencies. Blade loads, wing loads, flying qualities and skittishness in ground effect data were obtained.

SUMMARY

The test was conducted to obtain data in several different technical categories and the summary of the results is given below.

Rotating blade frequencies for the first three modes have been measured and correlate very well with predictions. (Figure 5.2, Section 5).

Blade load data were obtained in hover, transition, and cruise attitudes. The hover results show that the sensitivity of the blade loads to cyclic pitch are not affected by ground effect, but ground effect does increase the minimum blade load at zero cyclic. Increased collective pitch increased the blade load sensitivity to cyclic pitch. (Figures 6-1 to 6-58, Sections 6.1 through 6.4).

Blade alternating loads were essentially unaffected by differential collective between the two rotors but waveforms changed considerably (Section 6.1, Figure 6-12).

Low amplitude stall flutter inception occurred at $\theta_{.75} = 11^\circ$, but torsional blade loads were low up to the highest blade angle tested of 14° (Section 6.1, Figures 6-19 and 6-20).

Results show that in transition the minimum blade alternating chord bending load increases with increasing dynamic pressure. Flap bending loads were not significantly affected by dynamic pressure. Increased collective pitch decreased the minimum alternating chord bending load. Fuselage pitch and yaw caused large changes in alternating chord bending load with little effect on flap bending. (Section 6.2, Figures 6-22 through 6-44).

Alternating blade loads in cruise attitude were significantly lower than those encountered in hover and transition. However, the alternating chord bending sensitivity to cyclic was greater than in hover. (Section 6.3, Figures 6-45 through 6-58).

At a dynamic pressure of 6.65 psf corresponding to full-scale cruise of 140 knots, 5 degrees of yaw produced alternating chord bending loads equivalent to that due to 0.85 degrees of cyclic in hover. Alternating flap bending loads were insensitive to yaw. (Section 6.3.1 and 6.3.2).

Contrails

Whirl flutter, static divergence, ground and air resonance were not encountered over the range of conditions tested. However, near zero damping occurred in the blade chordwise bending motion at tilt angles tested (0°, 40°, 60°, 90°) at low dynamic pressures and near zero thrust conditions. Further analysis of these data are being conducted. (Section 7.3.2, Figures 7-18 through 7-23).

The model was very stable in its rigid body modes. The rotors increased rigid body stability in hover and cruise attitude (Section 8, Figures 8-1 through 8-7).

Skittishness in ground effect was found to exist, but motion is non-divergent, low amplitude ($\pm 2^\circ$) and very low frequency. Results indicate that skittishness on the full scale aircraft can be adequately stabilized by stability augmentation system required for normal flight conditions (Section 9.0, Figures 9-1 and 9-2).

TABLE OF CONTENTS

	PAGE
1.0 INTRODUCTION	1
2.0 OBJECTIVES.	2
3.0 TEST DESCRIPTION.	5
3.1 MODEL DESCRIPTION.	5
3.2 DYNAMIC SCALE RELATIONSHIPS	7
3.3 MODEL INSTRUMENTATION	8
3.4 AIR JET SHAKER.	8
3.5 MODEL WIND TUNNEL INSTALLATION	8
4.0 MODEL UNPOWERED FREQUENCY AND DAMPING DATA	20
4.1 RIGID BODY	20
4.2 BLADE FREQUENCIES.	20
5.0 ROTATING BLADE FREQUENCY MEASUREMENTS.	27
6.0 BLADE LOADS	43
6.1 HOVER BLADE LOADS.	43
6.1.1 EFFECT OF CYCLIC PITCH.	44
6.1.2 ROTOR-ROTOR INTERFERENCE	45
6.1.3 EFFECT OF COLLECTIVE PITCH	45
6.1.4 ROTOR START-UP AND SHUT-DOWN.	46
6.1.5 LOW FORWARD SPEED	46
6.1.6 STALL FLUTTER.	46

Contrails

TABLE OF CONTENTS (CONTINUED)

	PAGE
6.2 TRANSITION BLADE LOADS	69
6.2.1 EFFECT OF CYCLIC PITCH.	69
6.2.2 EFFECT OF MODEL YAW.	70
6.2.3 EFFECT OF MODEL PITCH	70
6.2.4 STALL FLUTTER.	70
6.3 CRUISE CONFIGURATION BLADE LOADS.	94
6.3.1 EFFECT OF CYCLIC PITCH.	94
6.3.2 EFFECT OF MODEL YAW.	94
6.3.3 EFFECT OF MODEL PITCH	95
6.3.4 EFFECT OF COLLECTIVE PITCH	95
6.4 BLADE RESPONSE TO MODEL DISTURBANCE.	110
7.0 VEHICLE DYNAMICS.	113
7.1 PREDICTED FREQUENCY AND DAMPING SPECTRUM	113
7.2 VEHICLE FREQUENCIES	113
7.2.1 ROTORS NON-ROTATING.	113
7.2.2 ROTATING ROTORS	115
7.3 ELASTIC MODE STABILITY	116
7.3.1 INPUT DISTURBANCES	117
7.3.2 BLADE CHORD BENDING MODE OSCILLATION	117

TABLE OF CONTENTS (CONTINUED)

	PAGE
8.0 FLYING QUALITIES.	142
8.1 INSTALLED RIGID BODY DYNAMICS.	142
8.2 PITCH AND ROLL SPRINGS	142
8.3 HOVER CHARACTERISTICS	143
8.3.1 RIGID BODY DAMPING	143
8.3.2 COLLECTIVE PITCH EFFECTIVENESS - ROLL CONTROLLABILITY	143
8.3.3 CYCLIC PITCH EFFECTIVENESS - PITCH CONTROLLABILITY.	143
8.4 TRANSITION AND CRUISE CHARACTERISTICS	144
9.0 SKITTISHNESS	153
9.1 GROUND EFFECT	153
9.2 EFFECT OF ADDED ROLL STIFFNESS	153
10.0 CONCLUSIONS	157
10.1 BLADE LOADS.	157
10.2 VEHICLE DYNAMICS	157
10.3 FLYING QUALITIES	157
10.4 SKITTISHNESS	158

TABLE OF CONTENTS (CONTINUED)

	PAGE
11.0 RECOMMENDATIONS	159
12.0 REFERENCES	160
13.0 APPENDICES	161
A. MODEL MASS PROPERTIES	161
B. ROTOR BLADE AND WING PROPERTIES	163
C. RUN LOG	172

LIST OF FIGURES (CONT.)

<u>NUMBER</u>	<u>TITLE</u>	<u>PAGE</u>
3-1	1/10 SCALE POWERED DYNAMIC TILT ROTOR MODEL - M-160	12
3-2	CALCULATED BLADE FREQUENCY SPECTRUM, $\theta_{.75}=3^\circ$	13
3-3	MODEL INSTALLATION AND BLADE AZIMUTH LOCATION AT TIME OF 1/REV INDICATOR	14
3-4	FULL-SCALE VELOCITY - MODEL DYNAMIC PRESSURE RELATIONSHIP	15
3-5	ILLUSTRATION OF BLADE FLAPWISE AND CHORDWISE MOTION WITH RESPECT TO DISC PLANE BASED ON BLADE BENDING MOMENT STRAIN GAGES AT 0.10R	16
3-6	AIR JET SHAKER INSTALLATION	17
3-7	CALIBRATION OF AIR POWERED SHAKERS.	18
3-8	TEST CONDITION RANGE.	19
4-1	VARIATION OF BLADE FREQUENCY WITH RUNS,	25
4-2	BLADE MODAL DAMPING FROM TWEAK TESTS, $\Omega = 0$	26
5-1	SCHEMATIC OF BAFFLE TEST SETUP.	29

LIST OF FIGURES

<u>FIGURE</u>	<u>TITLE</u>	<u>PAGE</u>
5-2	PREDICTED AND MEASURED ROTOR BLADE NATURAL FREQUENCIES FOR $\theta_{.75} = 3$ DEG.	30
5-3	ALTERNATING CHORD BENDING RESPONSE TO BAFFLES .	31
5-4	ALTERNATING FLAP BENDING RESPONSE TO BAFFLES .	32
5-5	1ST HARMONIC CHORD BENDING RESPONSE TO BAFFLES.	33
5-6	1ST HARMONIC FLAP BENDING RESPONSE TO BAFFLES .	34
5-7	2ND HARMONIC CHORD BENDING RESPONSE TO BAFFLES.	35
5-8	2ND HARMONIC FLAP BENDING RESPONSE TO BAFFLES .	36
5-9	3RD HARMONIC CHORD BENDING RESPONSE TO BAFFLES.	37
5-10	3RD HARMONIC FLAP BENDING RESPONSE TO BAFFLES .	38
5-11	4TH HARMONIC CHORD BENDING RESPONSE TO BAFFLES.	39
5-12	4TH HARMONIC FLAP BENDING RESPONSE TO BAFFLES .	40
5-13	5TH HARMONIC CHORD BENDING RESPONSE TO BAFFLES.	41
5-14	5TH HARMONIC FLAP BENDING RESPONSE TO BAFFLES .	42
6-1	WAVE-FORM OF ALTERNATING BLADE LOADS FOR A SERIES OF CYCLIC PITCH ANGLES - RIGHT BLADE AT .10R, $\theta_{.75} = 9.0^\circ$, $\omega = 750$ RPM, HOVER, RUN 31 .	48
6-2	EFFECT OF CYCLIC PITCH ON RIGHT ROTOR ALTERNATING CHORD BENDING MOMENT IN HOVER IGE FOR $i_N = 90$ DEG. $\theta_{.75} = 4.7$ DEG., AND 825 RPM, RUN 61(16). . . .	49
6-3	EFFECT OF CYCLIC PITCH ON RIGHT ROTOR ALTERNATING FLAP BENDING MOMENT IN HOVER IGE FOR $i_N = 90$ DEG., $\theta_{.75} = 4.7$ DEG., AND 825 RPM, RUN 61(16).	50

LIST OF FIGURES (CONT.)

<u>FIGURE</u>	<u>TITLE</u>	<u>PAGE</u>
6-4	EFFECT OF CYCLIC PITCH ON RIGHT ROTOR ALTERNATING CHORD BENDING MOMENT IN HOVER MODE FOR $i_N = 90$ DEG., $\theta_{.75} = 4$ DEG., AND 750 RPM, RUN 23(7)	51
6-5	EFFECT OF CYCLIC PITCH ON RIGHT ROTOR ALTERNATING FLAP BENDING MOMENT IN HOVER MODE FOR $i_N = 90$ DEG., $\theta_{.75} = 4$ DEG., AND 750 RPM, RUN 23(7)	52
6-6	EFFECT OF CYCLIC PITCH ON RIGHT ROTOR ALTERNATING CHORD BENDING MOMENT IN HOVER MODE FOR $i_N = 90$ DEG., $\theta_{.75} = 10.6$ DEG., AND 825 RPM, RUN 61(3)	53
6-7	EFFECT OF CYCLIC PITCH ON RIGHT ROTOR ALTERNATING FLAP BENDING MOMENT IN HOVER MODE FOR $i_N = 90$ DEG., $\theta_{.75} = 10.6$ DEG., AND 825 RPM, RUN 61(3)	54
6-8	EFFECT OF CYCLIC PITCH ON RIGHT ROTOR ALTERNATING CHORD BENDING MOMENT IN HOVER MODE FOR $i_N = 90$ DEG., $\theta_{.75} = 10.1$ DEG., AND 825 RPM, RUN 65(12)	55
6-9	EFFECT OF CYCLIC PITCH ON RIGHT ROTOR ALTERNATING FLAP BENDING MOMENT IN HOVER MODE FOR $i_N = 90$ DEG., $\theta_{.75} = 10.1$ DEG., AND 825 RPM, RUN 65(12)	56
6-10	EFFECT OF CYCLIC PITCH ON RIGHT ROTOR ALTERNATING CHORD BENDING MOMENT IN HOVER MODE FOR $i_N = 90$ DEG., $\theta_{.75} = 11$ DEG., AND 825 RPM, RUN 62(17)	57

LIST OF FIGURES (CONT.)

<u>FIGURE</u>	<u>TITLE</u>	<u>PAGE</u>
6-11	EFFECT OF CYCLIC PITCH ON RIGHT ROTOR ALTERNATING FLAP BENDING MOMENT IN HOVER IGE FOR $i_N = 90$ DEG., $\theta_{.75} = 11$ DEG., AND 825 RPM, RUN 62(17)	58
6-12	RIGHT BLADE RESPONSE TO DIFFERENTIAL COLLECTIVE, HOVER, RUN 26(8-11)	59
6-13	EFFECT OF COLLECTIVE PITCH ON RIGHT ROTOR STEADY FLAP BENDING MOMENT IN HOVER OGE FOR $i_N =$ 90 DEG., $\theta_2 = -.75$ DEG., AND 750 RPM, RUN 32(4)	60
6-14	EFFECT OF ROTOR START-UP AND SHUT-DOWN ON RIGHT HAND ALTERNATING CHORD BENDING MOMENT IN HOVER OGE FOR $i_N = 90$ DEG., $\theta_{.75} = 3.2$ DEG., AND $\theta_2 = 0$ DEG., RUN 24	61
6-15	EFFECT OF ROTOR START-UP AND SHUT-DOWN ON RIGHT HAND ALTERNATING FLAP BENDING MOMENT IN HOVER OGE FOR $i_N = 90$ DEG., $\theta_{.75} = 3.2$ DEG., AND $\theta_2 = 0$ DEG., RUN 24	62
6-16	ROTOR SPEED DURING START-UP AND SHUT-DOWN IN HOVER OGE FOR $i_N = 90$ DEG., $\theta_{.75} = 3.2$ DEG., AND $\theta_2 = 0$ DEG., RUN 24	63
6-17	EFFECT OF CYCLIC PITCH ON RIGHT ROTOR ALTER- NATING CHORD BENDING MOMENT IN HOVER OGE FOR $i_N = 90$ DEG., $\theta_{.75} = 4$ DEG., 750 RPM, AND $q = 0.06$ PSF, RUN 33(2-6)	64
6-18	EFFECT OF CYCLIC PITCH ON RIGHT ROTOR ALTER- NATING FLAP BENDING MOMENT IN HOVER OGE FOR $i_N = 90$ DEG., $\theta_{.75} = 4$ DEG., 750 RPM, AND $q = 0.06$ PSF, RUN 33(2-6)	65
6-19	EFFECT OF COLLECTIVE PITCH ON BLADE TORSIONAL RESPONSE IN HOVER FOR $i_N = 90$ DEG., $\theta_2 = 0$ DEG.	66

LIST OF FIGURES (CONT.)

<u>FIGURE</u>	<u>TITLE</u>	<u>PAGE</u>
6-20	EFFECT OF COLLECTIVE PITCH ON BLADE TORSION AMPLITUDE - HOVER, $\Omega = 830$ RPM, RUNS 60 and 61	67
6-21	ROTOR THRUST - DETERMINED FROM WING STEADY FLAP BENDING MOMENT - RIGHT SIDE-HOVER	68
6-22	EFFECT OF DYNAMIC PRESSURE ON RIGHT ROTOR ALTERNATING CHORD BENDING MOMENT IN TRANSITION FOR $i_N = 60$ DEG., $\theta_{.75} = 9.8$ DEG., AND 790 RPM, RUN 39(6,8,9,12)	71
6-23	EFFECT OF DYNAMIC PRESSURE ON RIGHT ROTOR ALTERNATING FLAP BENDING MOMENT IN TRANSITION FOR $i_N = 60$ DEG., $\theta_{.75} = 9.8$ DEG., AND 790 RPM, RUN 39(6,8,9,12)	72
6-24	EFFECT OF DYNAMIC PRESSURE ON RIGHT ROTOR ALTERNATING CHORD BENDING MOMENT IN TRANSITION FOR $i_N = 60$ DEG., $\theta_{.75} = 14.2$ DEG., AND 790 RPM, RUN 41(8,12)	73
6-25	EFFECT OF DYNAMIC PRESSURE ON RIGHT ROTOR ALTERNATING FLAP BENDING MOMENT IN TRANSITION FOR $i_N = 60$ DEG., $\theta_{.75} = 14.2$ DEG., AND 790 RPM, RUN 41(8,12)	74
6-26	EFFECT OF DYNAMIC PRESSURE ON RIGHT ROTOR ALTERNATING CHORD BENDING MOMENT IN TRANSITION FOR $i_N = 60$ DEG., $\theta_{.75} = 16$ DEG., AND 790 RPM (RUN 41(17,24)).	75
6-27	EFFECT OF DYNAMIC PRESSURE ON RIGHT ROTOR ALTERNATING FLAP BENDING MOMENT IN TRANSITION FOR $i_N = 60$ DEG., $\theta_{.75} = 16$ DEG., AND 790 RPM, RUN 41(17,24)	76

LIST OF FIGURES (CONT.)

<u>FIGURE</u>	<u>TITLE</u>	<u>PAGE</u>
6-28	EFFECT OF DYNAMIC PRESSURE ON BLADE MINIMUM ALTERNATING CHORD BENDING LOAD IN TRANSITION FOR $i_N = 60$ DEG.	77
6-29	EFFECT OF CYCLIC PITCH ON RIGHT HAND BLADE ALTERNATING LOADS IN TRANSITION - $i_N = 40$ DEG., $\theta_{.75} = 16.2$ DEG., $q = 2.0$ PSF, AND $\Omega = 790$ RPM, RUN 43(3).	78
6-30	EFFECT OF CYCLIC PITCH ON RIGHT HAND BLADE ALTERNATING LOADS IN TRANSITION $i_N = 40$ DEG., $\theta_{.75} = 20.0$ DEG., $q = 4.0$ PSF, AND $\Omega = 790$ RPM, RUN 43(8).	79
6-31	EFFECT OF CYCLIC PITCH ON RIGHT HAND BLADE ALTERNATING LOADS IN TRANSITION - $i_N = 40$ DEG., $\theta_{.75} = 23$ DEG., $q = 5.25$ PSF, AND $\Omega = 790$ RPM, RUN 43(14)	80
6-32	EFFECT OF MODEL YAW ANGLE ON RIGHT ROTOR ALTERNATING CHORD BENDING MOMENT IN TRANSI- TION FOR $i_N = 60$ DEG., $\theta_{.75} = 16$ DEG., $q = 4.1$ PSF, $\theta_2 = 5.8$ DEG., AND 790 RPM, RUN 41(27).	81
6-33	EFFECT OF MODEL YAW ANGLE ON RIGHT ROTOR ALTERNATING FLAP BENDING MOMENT IN TRANSITION FOR $i_N = 60$ DEG., $\theta_{.75} = 16$ DEG., $q = 4.1$ PSF, $\theta_2 = 5.8$ DEG., AND 790 RPM, RUN 41(27).	82
6-34	EFFECT OF MODEL YAW ANGLE ON RIGHT ROTOR ALTERNATING CHORD BENDING MOMENT IN TRANSITION FOR $i_N = 40$ DEG., $\theta_{.75} = 20$ DEG., $q = 4$ PSF, $\theta_2 = 3.8$ DEG., AND 790 RPM, RUN 43(10).	83

LIST OF FIGURES (CONT.)

<u>FIGURE</u>	<u>TITLE</u>	<u>PAGE</u>
6-35	EFFECT OF MODEL YAW ANGLE ON RIGHT ROTOR ALTERNATING FLAP BENDING MOMENT IN TRANSITION FOR $i_N = 40$ DEG., $\theta_{.75} = 20$ DEG., $q = 4$ PSF, $\theta_2 = 3.8$ DEG., AND 790 RPM, RUN 43(10)	84
6-36	EFFECT OF MODEL YAW ANGLE ON RIGHT ROTOR ALTERNATING CHORD BENDING MOMENT IN TRANSITION FOR $i_N = 40$ DEG., $\theta_{.75} = 23$ DEG., $q = 5.25$ PSF, $\theta_2 = 4.3$ DEG., AND 790 RPM, RUN 43(16)	85
6-37	EFFECT OF MODEL YAW ANGLE ON RIGHT ROTOR ALTERNATING FLAP BENDING MOMENT IN TRANSITION FOR $i_N = 40$ DEG., $\theta_{.75} = 23$ DEG., $q = 5.25$ PSF, $\theta_2 = 4.3$ DEG., AND 790 RPM, RUN 43(16)	86
6-38	EFFECT OF MODEL PITCH ANGLE ON RIGHT ROTOR ALTERNATING CHORD BENDING MOMENT IN TRANSITION FOR $i_N = 60$ DEG., $\theta_{.75} = 16$ DEG., $q = 4.1$ PSF, $\theta_2 = 5.8$ DEG., AND 790 RPM, RUN 41(26)	87
6-39	EFFECT OF MODEL PITCH ANGLE ON RIGHT ROTOR ALTERNATING FLAP BENDING MOMENT IN TRANSITION FOR $i_N = 60$ DEG., $\theta_{.75} = 16$ DEG., $q = 4.1$ PSF, $\theta_2 = 5.8$ DEG., AND 790 RPM, RUN 41(26)	88
6-40	EFFECT OF MODEL PITCH ANGLE ON RIGHT ROTOR ALTERNATING CHORD BENDING MOMENT IN TRANSITION FOR $i_N = 40$ DEG., $\theta_{.75} = 20$ DEG., $q = 4$ PSF, $\theta_2 = 3.8$ DEG., AND 790 RPM, RUN 43(9)	89
6-41	EFFECT OF MODEL PITCH ANGLE ON RIGHT ROTOR ALTERNATING FLAP BENDING MOMENT IN TRANSITION FOR $i_N = 40$ DEG., $\theta_{.75} = 20$ DEG., $q = 4$ PSF, $\theta_2 = 3.8$ DEG., AND 790 RPM, RUN 43(9)	90

LIST OF FIGURES (CONT.)

<u>FIGURE</u>	<u>TITLE</u>	<u>PAGE</u>
6-42	EFFECT OF DYNAMIC PRESSURE ON BLADE RESPONSE AT TORSIONAL FREQUENCY, (f = 65 CPS), IN TRANSITION, $i_N = 60$ DEG. . . .	91
6-43	BLADE TORSION RESPONSE IN TRANSITION - RIGHT BLADE - .15R.	92
6-44	EFFECT OF FUSELAGE DISPLACEMENT ON BLADE ALTERNATING TORSION RESPONSE AT ITS TORSION NATURAL FREQUENCY-RIGHT BLADE - .15R, $i_N = 40$ DEG.	93
6-45	EFFECT OF CYCLIC PITCH ON RIGHT ROTOR ALTERNATING CHORD BENDING MOMENT IN CRUISE FOR $i_N = 0$ DEG., $\theta_{.75} = 24.5$ DEG., $q = 5$ PSF, AND 790 RPM, RUN 37(33-37)	96
6-46	EFFECT OF CYCLIC PITCH ON RIGHT ROTOR ALTERNATING FLAP BENDING MOMENT IN CRUISE FOR $i_N = 0$ DEG., $\theta_{.75} = 24.5$ DEG., $q = 5$ PSF, AND 790 RPM, RUN 37(33-37)	97
6-47	EFFECT OF MODEL YAW ANGLE ON RIGHT ROTOR ALTERNATING CHORD BENDING MOMENT IN CRUISE FOR $i_N = 0$ DEG., $\theta_{.75} = 26.7$ DEG., $q = 6$ PSF, $\theta_2 = -0.7$ DEG., AND 790 RPM, RUN 38(4)	98
6-48	EFFECT OF MODEL YAW ANGLE ON RIGHT ROTOR ALTERNATING FLAP BENDING MOMENT IN CRUISE FOR $i_N = 0$ DEG., $\theta_{.75} = 26.7$ DEG., $q = 6$ PSF, $\theta_2 = -0.7$ DEG., AND 790 RPM, RUN 38(4)	99
6-49	EFFECT OF MODEL YAW ANGLE ON RIGHT ROTOR ALTERNATING CHORD BENDING MOMENT IN CRUISE FOR $i_N = 0$ DEG., $\theta_{.75} = 30.7$ DEG., $q = 7$ PSF, $\theta_2 = -0.7$ DEG., AND 790 RPM, RUN 38(10)	100

LIST OF FIGURES (CONT.)

<u>FIGURE</u>	<u>TITLE</u>	<u>PAGE</u>
6-50	EFFECT OF MODEL YAW ANGLE ON RIGHT ROTOR ALTERNATING FLAP BENDING MOMENT IN CRUISE FOR $i_N = 0$ DEG., $\theta_{.75} = 30.7$ DEG., $q = 7$ PSF, $\theta_2 = -0.7$ DEG., AND 790 RPM, RUN 38(10)	101
6-51	EFFECT OF MODEL PITCH ANGLE ON RIGHT ROTOR ALTERNATING CHORD BENDING MOMENT IN CRUISE FOR $i_N = 0$ DEG., $\theta_{.75} = 26.7$ DEG., $q = 6$ PSF, $\theta_2 = -0.7$ DEG., AND 790 RPM, RUN 38(3)	102
6-52	EFFECT OF MODEL PITCH ANGLE ON RIGHT ROTOR ALTERNATING FLAP BENDING MOMENT IN CRUISE FOR $i_N = 0$ DEG., $\theta_{.75} = 26.7$ DEG., $q = 6$ PSF, $\theta_2 = -0.7$ DEG., AND 790 RPM, RUN 38(3)	103
6-53	VARIATION OF MODEL YAW WITH MODEL PITCH ANGLE IN CRUISE FOR $i_N = 0$ DEG., $\theta_{.75} = 26.7$ DEG., $q = 6$ PSF, $\theta_2 = -0.7$ DEG., AND 790 RPM, RUN 38(3)	104
6-54	EFFECT OF MODEL PITCH ANGLE ON RIGHT ROTOR ALTERNATING CHORD BENDING MOMENT IN CRUISE FOR $i_N = 0$ DEG., $\theta_{.75} = 30.7$ DEG., $q = 7$ PSF, $\theta_2 = -0.7$ DEG., AND 790 RPM, RUN 38(9)	105
6-55	EFFECT OF MODEL PITCH ANGLE ON RIGHT ROTOR ALTERNATING FLAP BENDING MOMENT IN CRUISE FOR $i_N = 0$ DEG., $\theta_{.75} = 30.7$ DEG., $q = 7$ PSF, $\theta_2 = -0.7$ DEG., AND 790 RPM, RUN 38(9)	106
6-56	VARIATION OF MODEL YAW WITH MODEL PITCH ANGLE IN CRUISE FOR $i_N = 0$ DEG., $\theta_{.75} = 30.7$ DEG., $q = 7$ PSF, $\theta_2 = -0.7$ DEG., AND 790 RPM, RUN 38(9)	107

LIST OF FIGURES (CONT.)

<u>FIGURE</u>	<u>TITLE</u>	<u>PAGE</u>
6-57	EFFECT OF COLLECTIVE PITCH ANGLE ON RIGHT ROTOR STEADY FLAP BENDING MOMENT IN CRUISE FOR $i_N = 0$ DEG., $q = 6$ PSF, $\theta_2 = -0.5$ DEG., AND 790 RPM, RUN 37(41).	108
6-58	EFFECT OF COLLECTIVE PITCH ANGLE ON RIGHT ROTOR STEADY FLAP BENDING MOMENT IN CRUISE FOR $i_N = 0$ DEG., $\theta_2 = -0.4$ DEG., AND 790 RPM, RUN 37	109
6-59	BLADE RESPONSE TO PITCH DISTURBANCE IN HOVER, $\theta_{.75} = 6$ DEG., $\theta_2 = -.5$ DEG., $\Omega = 830$ RPM, RUN 65.	111
6-60	BLADE RESPONSE TO PITCH DISTURBANCE IN CRUISE ATTITUDE, $\theta_{.75} = 28$ DEG., $\Omega = 790$ RPM, $q = 7.0$ PSF, $i_N = 0$ DEG., RUN 50.	112
7-1	FREQUENCY SPECTRUM FOR SYMMETRICAL HOVER MODES	119
7-2	DAMPING SPECTRUM FOR SYMMETRICAL HOVER MODES, $\theta_{.75} = 11$ DEG.	120
7-3	DAMPING SPECTRUM FOR SYMMETRICAL HOVER MODES, $\theta_{.75} = 0$ DEG.	121
7-4	FREQUENCY SPECTRUM FOR ANTI-SYMMETRICAL HOVER MODES	122
7-5	DAMPING SPECTRUM FOR ANTI-SYMMETRICAL HOVER MODES	123
7-6	WING FLAP BENDING RESPONSE TO SYMMETRICAL EXCITATION -- NON-ROTATING BLADES, $i_N =$ 90 DEG.	124
7-7	WING CHORD BENDING RESPONSE TO SYMMETRICAL EXCITATION -- NON-ROTATING BLADES, $i_N = 90$ DEG.	125

Contrails

LIST OF FIGURES (CONT.)

<u>FIGURE</u>	<u>TITLE</u>	<u>PAGE</u>
7-8	WING TORSION RESPONSE TO SYMMETRIC EXCITATION -- NON-ROTATING BLADES, $i_N = 90$ DEG.	126
7-9	WING FLAP BENDING RESPONSE TO ANTI- SYMMETRIC EXCITATION -- NON-ROTATING BLADES, $i_N = 90$ DEG.	127
7-10	WING CHORD BENDING RESPONSE TO ANTI- SYMMETRIC EXCITATION--NON-ROTATING BLADES, $i_N = 90$ DEG.	128
7-11	WING TORSION RESPONSE TO ANTI-SYMMETRIC EXCITATION--NON-ROTATING BLADES, $i_N = 90$ DEG.	129
7-12	WING FLAP BENDING RESPONSE TO SYMMETRIC EXCITATION- $\Omega = 790$ RPM, $q = 0$, $\theta_{.75} = 6$ DEG., $i_N = 0$ DEG.	130
7-13	WING CHORD BENDING RESPONSE TO SYMMETRIC EXCITATION - $\Omega = 790$ RPM, $q = 0$, $\theta_{.75} = 6$ DEG., $i_N = 0$ DEG.	131
7-14	WING TORSION RESPONSE TO SYMMETRIC EXCITATION- $\Omega = 790$ RPM, $q = 0$, $\theta_{.75} = 6$ DEG., $i_N = 0$ DEG.	132
7-15	WING FLAP BENDING RESPONSE TO SYMMETRIC EXCITATION - $\Omega = 825$ RPM, $q = 0$, $\theta_{.75} = 10$ DEG., $i_N = 90$ DEG.	133
7-16	WING CHORD BENDING RESPONSE TO SYMMETRIC EXCITATION - $\Omega = 825$ RPM, $q = 0$, $\theta_{.75} = 10$ DEG., $i_N = 90$ DEG, RUN 52	134
7-17	WING TORSION RESPONSE TO SYMMETRIC EXCITATION -- $\Omega = 825$ RPM, $q = 0$, $\theta_{.75} = 10$ DEG., $i_N = 90$ DEG., RUN 52.	135

Contracts

LIST OF FIGURES (CONT.)

<u>FIGURE</u>	<u>TITLE</u>	<u>PAGE</u>
7-18	LOW FREQUENCY OSCILLATION OCCURRENCES- RELATIONSHIP TO ZERO THRUST	136
7-19	BEAT FREQUENCY RESPONSE OSCILLOGRAM - RIGHT BLADE AND WING, $i_N = 60$ DEG., RUN 40 (12)	137
7-20	CORRELATION OF OBSERVED LOW FREQUENCY MODE DAMPING WITH PREDICTION - $q = 0$	138
7-21	REGIONS OF LOW FREQUENCY OSCILLATION OCCURRENCES	139
7-22	SUMMARY OF CONDITIONS AT WHICH LOW FREQUENCY OSCILLATION OCCURRED.	140
7-23	CORRELATION OF BLADE FREQUENCY OBTAINED FROM BEAT OSCILLATION DURING EMERGENCY SHUTDOWN, $i_N = 60$ DEG, RUN 40 (12).	141
8-1	PITCH AND ROLL DAMPING DECREMENTS - HOVER CONDITION	146
8-2	RIGID BODY DAMPING IN HOVER	147
8-3	EFFECT OF COLLECTIVE PITCH ON WING STEADY FLAP BENDING MOMENT	148
8-4	EFFECT OF CYCLIC PITCH ON WING STEADY TORQUE LOAD ILLUSTRATING CONTROL EFFEC- TIVENESS	149
8-5	CYCLIC PITCH CONTROL POWER	150
8-6	EFFECT OF DYNAMIC PRESSURE ON RIGID BODY PITCH FREQUENCY AND DAMPING	151
8-7	EFFECT OF DYNAMIC PRESSURE ON THE RIGID BODY PITCH FREQUENCY AND DAMPING WITH ROTORS OFF.	152
9-1	MODEL ROLL STABILITY - IN GROUND EFFECT	155
9-2	ROLL STABILITY IN AND OUT OF GROUND EFFECT - WITHOUT SPRINGS.	156

LIST OF FIGURES (CONT.)

<u>NUMBER</u>	<u>TITLE</u>	<u>PAGE</u>
B-1	1/10 SCALE M-160 ROTOR BLADE FLAPWISE STIFFNESS	165
B-2	1/10 SCALE M-160 ROTOR BLADE CHORDWISE STIFFNESS	166
B-3	1/10 SCALE M-160 ROTOR BLADE TORSIONAL STIFFNESS	167
B-4	1/10 SCALE M-160 WING FLAPWISE STIFFNESS . .	168
B-5	1/10 SCALE M-160 WING CHORDWISE STIFFNESS .	169
B-6	1/10 SCALE M-160 WING TORSIONAL STIFFNESS .	170
B-7	ROTOR BLADE THICKNESS AND AIRFOIL DISTRIBUTION.	171

LIST OF TABLES

	<u>PAGE</u>
3-1 MODEL DIMENSIONS.	9
3-2 MEASUREMENT LIST.	10
4-1 TWEAK TEST RESULTS.	22
4-2 PRE-TEST RIGID BODY FREQUENCY AND DAMPING - POWER ON AND WIND OFF	24
7-1 WING FREQUENCIES AND DAMPING FROM TWEAK TEST. .	113
7-2 SHAKE TEST INDEX - ROTORS NON-ROTATING.	114
7-3 SHAKE TEST INDEX - ROTATING ROTORS.	115
7-4 WING FREQUENCY SUMMARY.	116
8-1 RIGID BODY DAMPING DATA SUMMARY	145
B-1 BLADE PROPERTIES	164

Contracts

LIST OF SYMBOLS AND SIGN CONVENTION

c	- Blade chord	- ft or inch
c _{.75}	- Blade chord at .75R	- ft
$C_{M\delta_2}$	- Pitching moment coefficient due to cyclic pitch	-
C_T	- Thrust coefficient = $\frac{T}{\pi \rho V_T^2 R^2}$	-
D	- Rotor Diameter	- ft or inch
f	- Frequency	- cps
h	- Height of rotor disc plane above ground level	- ft
IGE	- In ground effect	-
i_N	- Nacelle tilt angle	deg
M	- Pitching moment	- lb in.
N	- Number of blades	-
n	- Rotor speed	- RPS
OGE	- Out of ground effect	-
q	- Freestream dynamic pressure	- lb/ft ²
q_m	- Freestream dynamic pressure, model scale	- lb/ft ²
q^*	- $q (\cos^2 i_N)$	- lb/ft ²
R	- Blade radius	- ft or inch
r	- Radial distance from rotor center to blade station	- ft or inch

LIST OF SYMBOLS AND SIGN CONVENTION

T	- Thrust	- lb
V	- Velocity	- ft/sec or knots
V_m	- Freestream velocity, model scale	- ft/sec
V_T	- Rotor tip velocity	- ft/sec
α	- Fuselage pitch angle(positive-nose up)	- deg
γ	- Fuselage roll angle(positive-right wing down)	- deg
δ	- Horizontal stabilizer from angle (positive - leading edge up)	- deg
$\beta_{.75}$	- Blade collective pitch angle (positive - blade leading edge up)	- deg
β_2	- Blade cyclic pitch angle(positive-blade leading edge rotated down on the advancing blade) (See Figure 3-3)	- deg
ξ	- Viscous damping coefficient = c/c_c	-
ρ	- Air density	- slugs/ft ²
σ	- $\frac{Nc}{\pi R}$	-
φ	- Rotor blade azimuth(See Figure 3-3)	- deg
ω	- Frequency	- cpm or rad/sec
ω_n	- Blade nth natural coupled frequency	(n = 1,2,---)CPS or CPM
ω_{t_1}	- Blade torsion frequency	- rad/sec
ψ	- Fuselage yaw angle(positive-nose right)	- deg
Ω	- Rotor speed	- RPM

LIST OF SYMBOLS AND SIGN CONVENTION

LOAD SIGN CONVENTION*

- Blade and wing flapwise bending moment - positive, compression on upper surface
- Blade and wing chordwise bending moment - positive, compression on trailing edge
- Blade and wing torsion - positive, leading edge rotated nose up

*With respect to strain gages

1.0 INTRODUCTION

VTOL aircraft with forward tilting rotors mounted on nacelles at the wing tips experience large aerodynamic changes as the rotors are tilted from the hover attitude through the transition regime to cruise flight. Freedom of the aircraft to move and to elastically deform under these changing aerodynamic conditions can have an effect on the rotor blade loads, flying qualities, and aeroelastic stability of the aircraft.

These aspects must be examined in sufficient detail so that design criteria may be developed which account for aeroelastic effects. In addition, existing analytical methods must be verified so that full scale aircraft designs can proceed with technical confidence.

One step toward the achievement of the above objectives is to perform wind tunnel tests on a full span dynamically scaled model on a mount that permits some freedom of motion. Boeing-Vertol Wind Tunnel Test No. 047 of the VR054D model mounted on a pole support conducted in January 1970, demonstrated the feasibility of this type model testing, the results of which are reported in Reference 1.

This document contains the results of wind tunnel tests conducted during January and February 1971 by Boeing-Vertol on the same model, with certain refinements, in support of the Phase II contract for the Design Studies and Model Tests of the Stowed Tilt Rotor Concept.

2.0 OBJECTIVES

The test program was performed to obtain data under conditions ranging from hover through tilt transition and low speed cruise. The general objectives were to:

- a) Provide blade and wing loads data, both steady and dynamic, throughout the transition flight envelope.
- b) Explore the flutter and divergence boundaries of the rotor and wing including the whirl mode.
- c) Obtain data which can be used to calculate the effects of gust penetration and maneuvers.
- d) Provide aerodynamic data which include aeroelastic effects.

The specific program objectives are listed below:

Blade Dynamics

- 1) Determine the non-rotating and rotating blade frequencies and damping values. Check against technical predictions.
 - Data have been obtained from baffle tests and are reported in Section 5.0 with analysis correlation.

Simulated Free Flight Suspension System

- 2) Determine the effect of the support system (vertical guide, umbilical, and restraining cables) on the model behavior.
 - Prior to the power and wind on runs with the model installed in the wind tunnel test section, tests were performed to determine the effect of the umbilical and snubber cables on the rigid body modes. Corresponding data are presented in Section 4.0. These effects are small.

Contrails

Hover

- 3) Determine blade loads as a function collective pitch, cyclic pitch and ground proximity.
 - Data are presented in Section 6.1.
- 4) Determine blade loads, collective pitch and C_T/σ at stall flutter.
 - Data are presented in Section 6.1.
- 5) Determine the tendency for the model to have air resonance.
 - No air resonance was encountered, as predicted. See Section 7.
- 6) Measure the response of the model to rigid body disturbances.
 - A limited amount of data indicated that, in hover, the rotor substantially increases the rigid body stability (damping) over the unpowered condition. See Section 8.0.
- 7) Determine the effect of IGE on rotor control derivatives.
 - Results presented in Section 8.3 indicate ground effect to be negligible.

Transition

- 8) Determine rotor stall limits as a function of airspeed.
 - No stall limits were encountered during this test.
- 9) Determine blade loads in the transition region.
 - Details are presented in Section 6.2.

Contrails

- 10) Determine if aeroelastic instabilities occur in the transition region.
 - No whirl flutter or air resonance was found during this test.
 - Low frequency oscillations associated with the blade chordwise bending mode occurred at various conditions near zero thrust. Details are discussed in Section 7.3.2.
- 11) Determine model response to rigid body disturbances.
 - A limited amount of data indicates stability in the rigid body modes. See Section 8.4.

Cruise

- 12) Measure blade loads in cruise and their change with q collective pitch, cyclic pitch, aircraft pitch and yaw.
 - Details are presented in Section 6.3.
- 13) Determine if aeroelastic instabilities occur in the cruise attitude.
 - See answer given to Question (10).

Maneuver and Gust Penetration

- 14) Measure blade loads responses to rapid aircraft attitude changes.
 - Details are presented in Section 6.4.

3.0 TEST DESCRIPTION

Run numbers are designated as run XX (Y). XX indicates run number and the number noted in the brackets designates the area of the oscillograph tape analyzed.

3.1 MODEL DESCRIPTION

The model shown in Figure 3-1 is a powered, 1/10 scale full span dynamic model aerodynamically representative of the M-160,55' rotor diameter tilt rotor aircraft. Its construction consists of scaled stiffness beams in all members with segmented balsa structure providing the required aerodynamic contours. Additional properties are contained in References 1, 2 and 3 and dimensions are listed in Table 3-1.

The collective and monocyclic pitch of the rotor blades and the incidence angle of the horizontal tail are remotely adjustable. The nacelle tilt angle is manually adjustable. An internal rider assembly permits the model to be mounted on a single vertical cable in the wind tunnel. The model is supported by a soft spring (bungee) to carry its total weight when shut down. This mounting system provides vertical, pitch, roll and yaw freedoms. Additional significant features are:

a. Nacelles

- o Manually tiltable from 25° below horizontal reference plane to 15° aft of vertical plane by using fixed pre-set links.
- o Tilt axis is located at 40% wing chord.

b. Rotor

- o 5.5 foot diameter.
- o Distance between rotor centers is 6.78 feet.
- o Power is provided by an air turbine motor located in the fuselage which transmits power through a chain drive to a shaft interconnecting the rotors.
- o Hover RPM (Froude scaling) - 825 RPM, $V_T = 237.5$ fps
Full scale values are - 261 RPM, $V_T = 750$ FPS.

Contrails

c. Blades

- o Soft in-plane, segmented
- o Dynamically-scaled with monocoat covering across segments (See Appendix B for aerodynamic and aeroelastic properties).
- o Calculated blade natural frequencies per Figure 3-2.
- o Mass center, pitch axis and shear center are located at 25% chord.
- o Collective pitch - remotely controllable between -5° to 40°
- o Monocyclic pitch - remotely controllable between $+15^{\circ}$ to -15° with input azimuth angle at 108° (See Figure 3-3).

d. Model Mass and Stiffness Properties

- o See Appendix A and B

e. Miscellaneous

- o The fuselage is flexible but not directly scaled.
- o The tail surfaces were stiffened from the original design with a layer of 1/32" balsa. Also, 45 gms was added to each tip of the horizontal tail (Run 29) to eliminate the tail shake.
- o The horizontal tail surface is remotely adjustable for pitch trim.
- o The model was equipped with pitch and roll axis springs to simulate a simple feedback control system.

3.2 DYNAMIC SCALE RELATIONSHIPS

The model was designed to maintain a Froude No. ratio (model to full scale) = 1.0 so that resulting loads contain the proper gravitational influences. Figure 3-4 shows the relationship between the model dynamic pressure and full scale velocity. The following table lists the scale factors for model to full scale:

<u>Parameter</u>	<u>Scale Factor</u>
Length	$L = 1/10$
Mass	L^3
Time	$L^{1/2}$
Frequency	$L^{-1/2}$
Froude No.	1.0
Force	L^3
Moment	L^4
Pressure	L
Stiffness (EI & GJ)	L^5
Density (Sea Level)	1.0

3.3 MODEL INSTRUMENTATION

A complete list of the measurements made with their respective locations is presented in Table 3-2. Yaw position was measured with a wind vane mounted in a nose boom (Figure 3-1). Pitch and roll displacements were measured utilizing position potentiometers attached between the model and the vertical cable. Two oscillographs were used to measure right blade and wing loads. All measurements were recorded on the computer system. One blade on each rotor was instrumented. See Figure 3-3. The full scale velocity to model dynamic pressure relationships and the nacelle tilt angle reached during the tests are presented in Figure 3.4.

Since the blade strain gages were bonded to the blade spar, resulting blade flapwise and chordwise motions construed from bending moments will always be with respect to the blade and not with respect to the rotor disc plane. For instance, at cruise collective angles ($0.75 \approx 30^\circ$), the chordwise bending moment would result primarily from out-of-disc plane deformation, and flapwise bending moment would result primarily from in-disc plane motion. This is illustrated in Figure 3-5.

3.4 AIR JET SHAKER

Solenoid controlled air jet shakers were mounted on each nacelle 4 inches from the tilt axis (See Figure 3-6) with the air hoses running from the umbilical to the shaker through the wing. These were developed specifically for this model test to provide a source of excitation which would not be affected by model rigid body motion or offer restraints to rigid body freedom. Calibrations based on frequency and air pressure were conducted before the test. The results are presented in Figure 3-7.

3.5 MODEL WIND TUNNEL INSTALLATION

The model was installed as shown in Figure 3-1 in the center of the test section. The vertical guide was a 1/4 inch diameter multiple strand cable anchored at the test section ceiling and weighted with 400 lbs. underneath the test section floor to provide the required fore-aft and lateral mounted frequency (1.0 cps). Snubber cables were installed to serve the dual purpose of restraining the model for safety purposes, and to displace the model during test as required. The umbilical was installed as shown in Figure 3-1 to minimize its effect on the total system mass stiffness and damping. For the skittishness test a platform extending across the test section floor at an elevation of 4 feet was installed. The model was lowered to the desired "ground" proximity for these tests. Figure 3-8 contains the design flight conditions and the general range of those at which the model was tested.

TABLE 3-1
MODEL DIMENSIONS

<u>Rotor</u>	
Number of blades	3
Radius	2.750 ft
Solidity	.0857
Effective Disc Area	23.750 ft ²
Blade Area	2.034 ft ²
Airfoil	See Fig. B-7

<u>Wing</u>	
Airfoil	NACA 63 ₄ 421 (Modified)
Span (Nacelle C _L to Nacelle C _L)	6.78 ft
Chord (Constant)	.858 ft
Thickness Ratio, constant root to tip	.21
Area	5.85 ft ²
Aspect Ratio	7.93
Nacelle Pitch Axis	40% Chord
Wing Angle of Attack with Respect to Fuselage Waterline	2.5 Deg

<u>Horizontal Tail</u>	
Airfoil	NACA 0015
Root Chord	.708 ft
Tip Chord	.416 ft
Span	3.00 ft
Area	1.68 ft ²
Aspect Ratio	5.34

<u>Vertical Tail</u>	
Airfoil	NACA 0015
Root Chord	1.45 ft
Tip Chord	.94 ft
Span	1.04 ft
Aspect Ratio	0.87

TABLE 3-2
MEASUREMENT LIST - LOADS

MEASUREMENT AND LOCATION	RECORDER		COMPUTER
	CEC #1	CEC #2	
<u>ROTOR BLADE LOADS</u>			
FLAPWISE AND CHORDWISE BEND MOMENT	R		L,R L,R
TORSION	R		L,R
<u>WING LOADS</u>			
FLAPWISE AND CHORDWISE BEND MOMENT		R	L,R
DIFFERENTIAL TORSION		R	L,R

NOTE: ALL DATA CHANNELS HAD FREQUENCY RESPONSE GREATER THAN 100 HERTZ FOR LOADS
ALL DATA ON ON-LINE PRINT-OUT GREATER THAN 50 HERTZ FOR ACCELERATION
L = LEFT, R = RIGHT

MEASUREMENT LIST - ACCELERATION

MEASUREMENT AND LOCATION	RECORDER		COMPUTER
	CEC #1	CEC #2	
NACELLES - NORMAL AND AXIAL			L,R
WING - VERTICAL - WING TIP			L,R
FUSELAGE NOSE AND CG - VERTICAL AND LATERAL			X
FUSELAGE CG - LONGITUDINAL			X

TABLE 3-2 (CONTD.)
MEASUREMENT LIST - MISCELLANEOUS

MEASUREMENT	RECORDER			FREQ. RESPONSE
	CEC #1	CEC #2	COMPUTER	
COLLECTIVE AND CYCLIC 4	LEFT ROTOR		L, R	0
	RIGHT ROTOR	L, R	L, R	0
FUSELAGE POSITION	PITCH, YAW	PITCH, ROLL, YAW	PITCH, ROLL, YAW	5
HORIZONTAL STABILIZER ANGLE			X	0
ROTOR SPEED	X	X	X	
1/REV LOCATOR	X	X	X	20
VERTICAL SUPPORT LOAD	X	X	X	5
SHAKER FREQUENCY	X	X	X	20
DYNAMIC PRESSURE	X		X	0

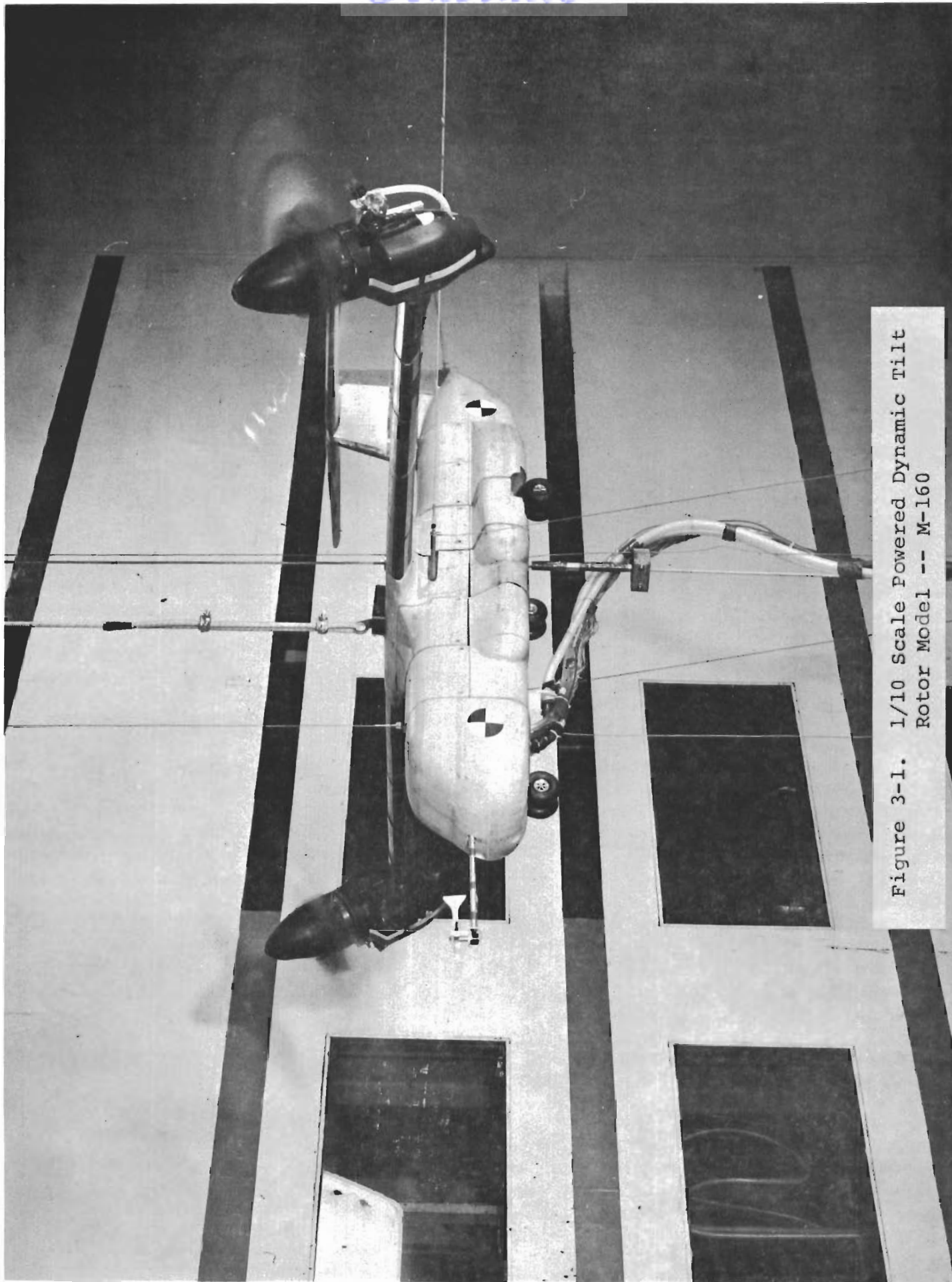


Figure 3-1. 1/10 Scale Powered Dynamic Tilt Rotor Model -- M-160

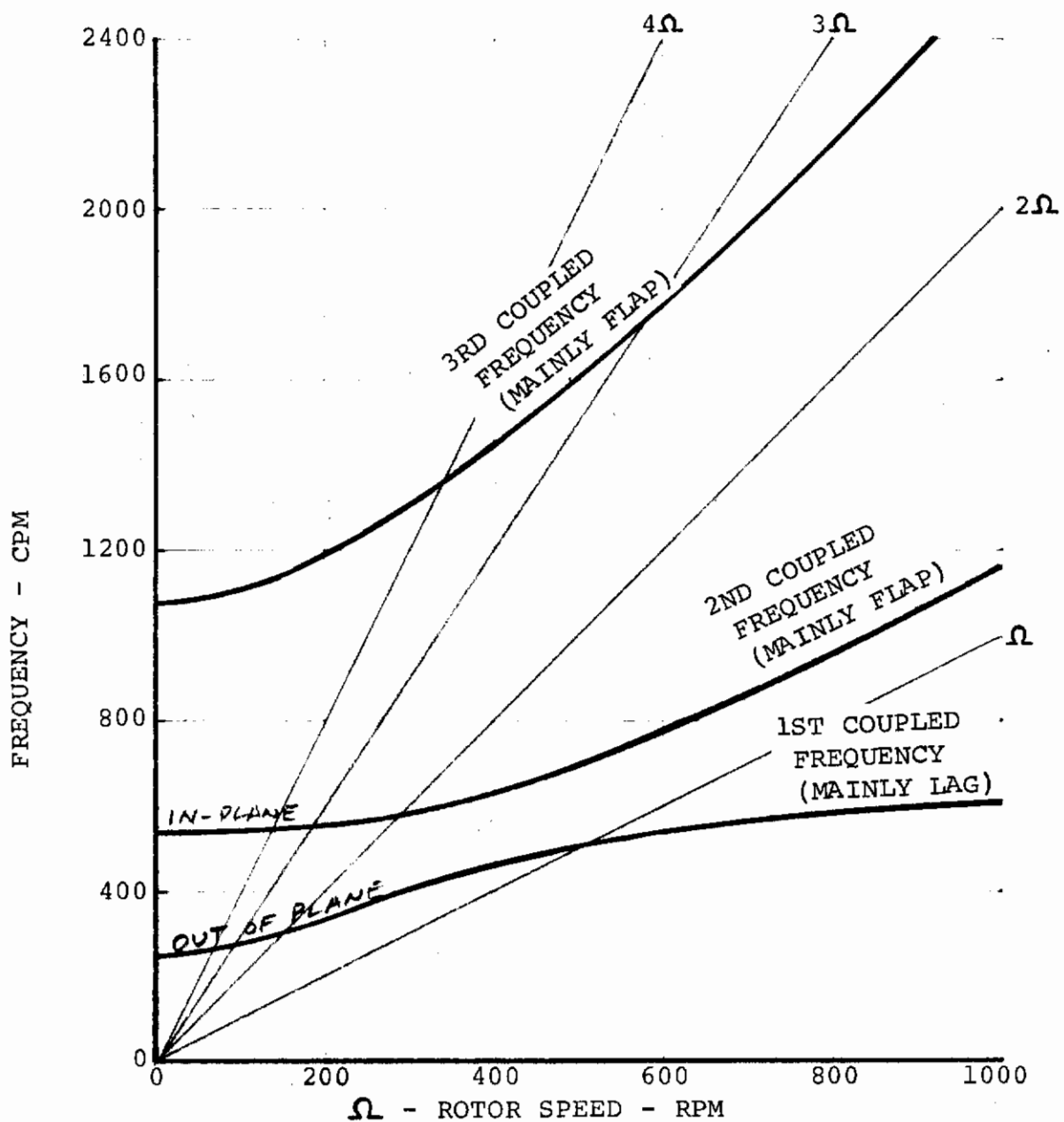


FIGURE 3-2. CALCULATED BLADE FREQUENCY SPECTRUM
 $\theta_{.75} = 3^\circ$

Contrails

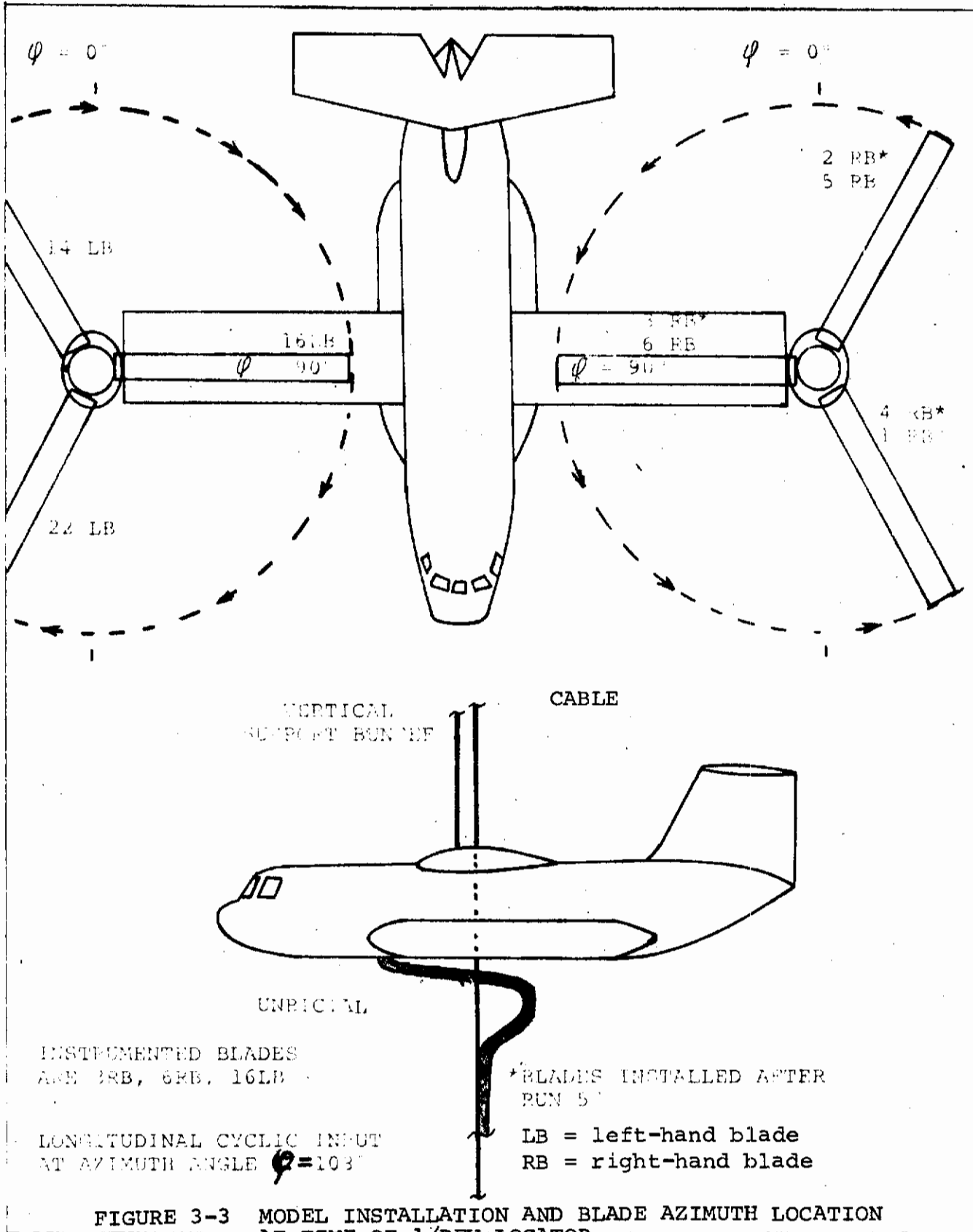


FIGURE 3-3 MODEL INSTALLATION AND BLADE AZIMUTH LOCATION AT TIME OF 1/REV LOCATOR

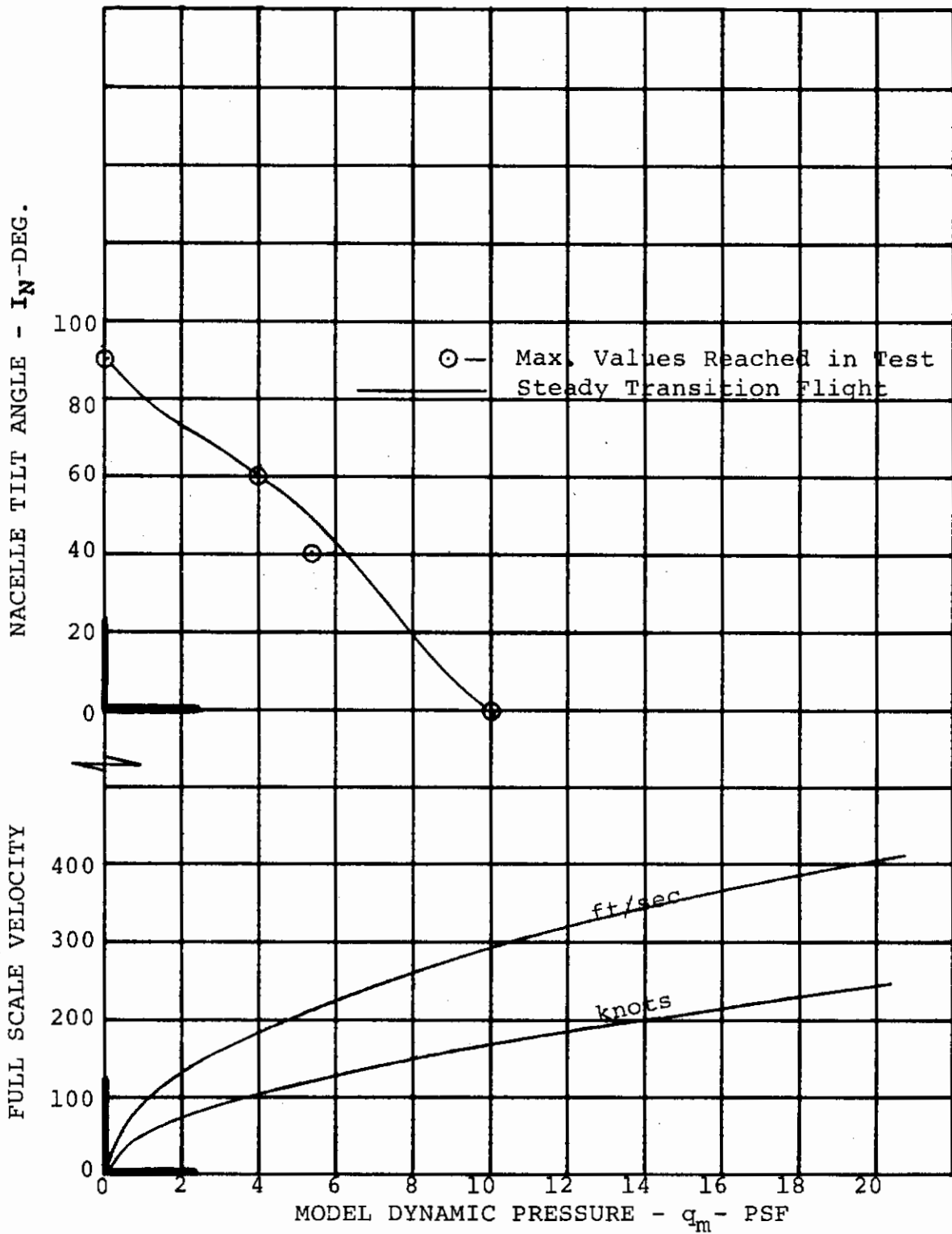


FIGURE 3-4. - FULL SCALE VELOCITY - MODEL DYNAMIC PRESSURE RELATIONSHIP

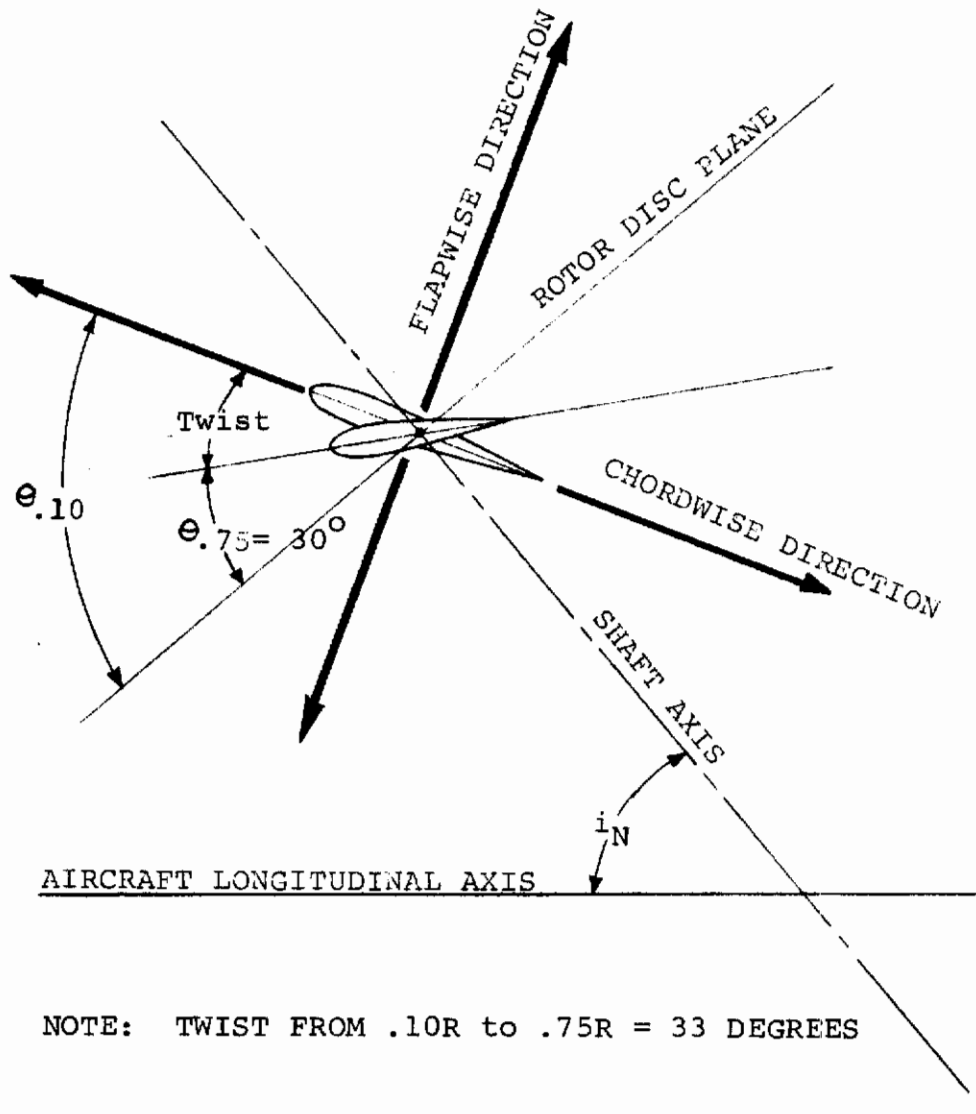


FIGURE 3-5. ILLUSTRATION OF BLADE FLAPWISE AND CHORDWISE MOTION WITH RESPECT TO DISC PLANE BASED ON BLADE BENDING MOMENT STRAIN GAGES AT 0.10R

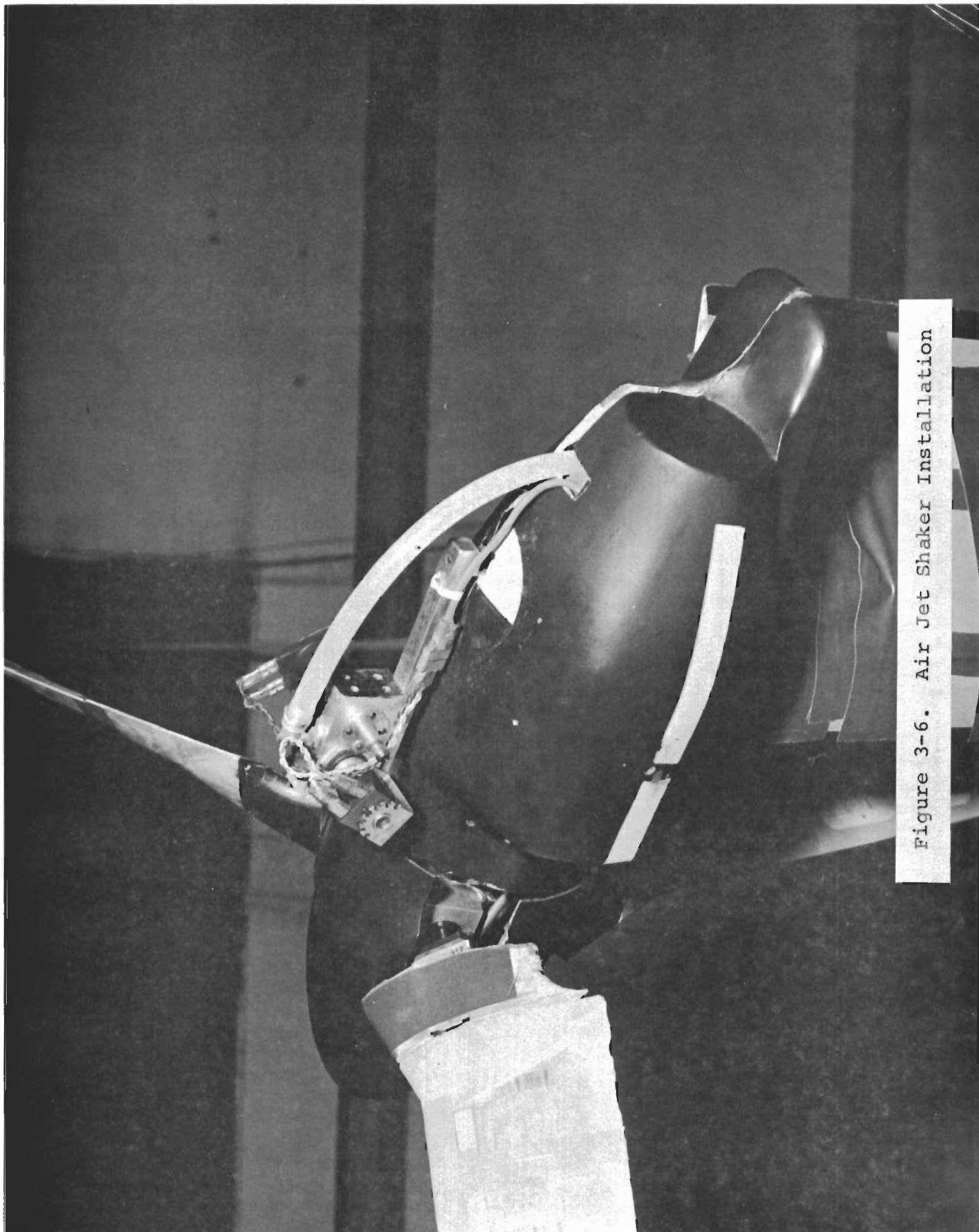


Figure 3-6. Air Jet Shaker Installation

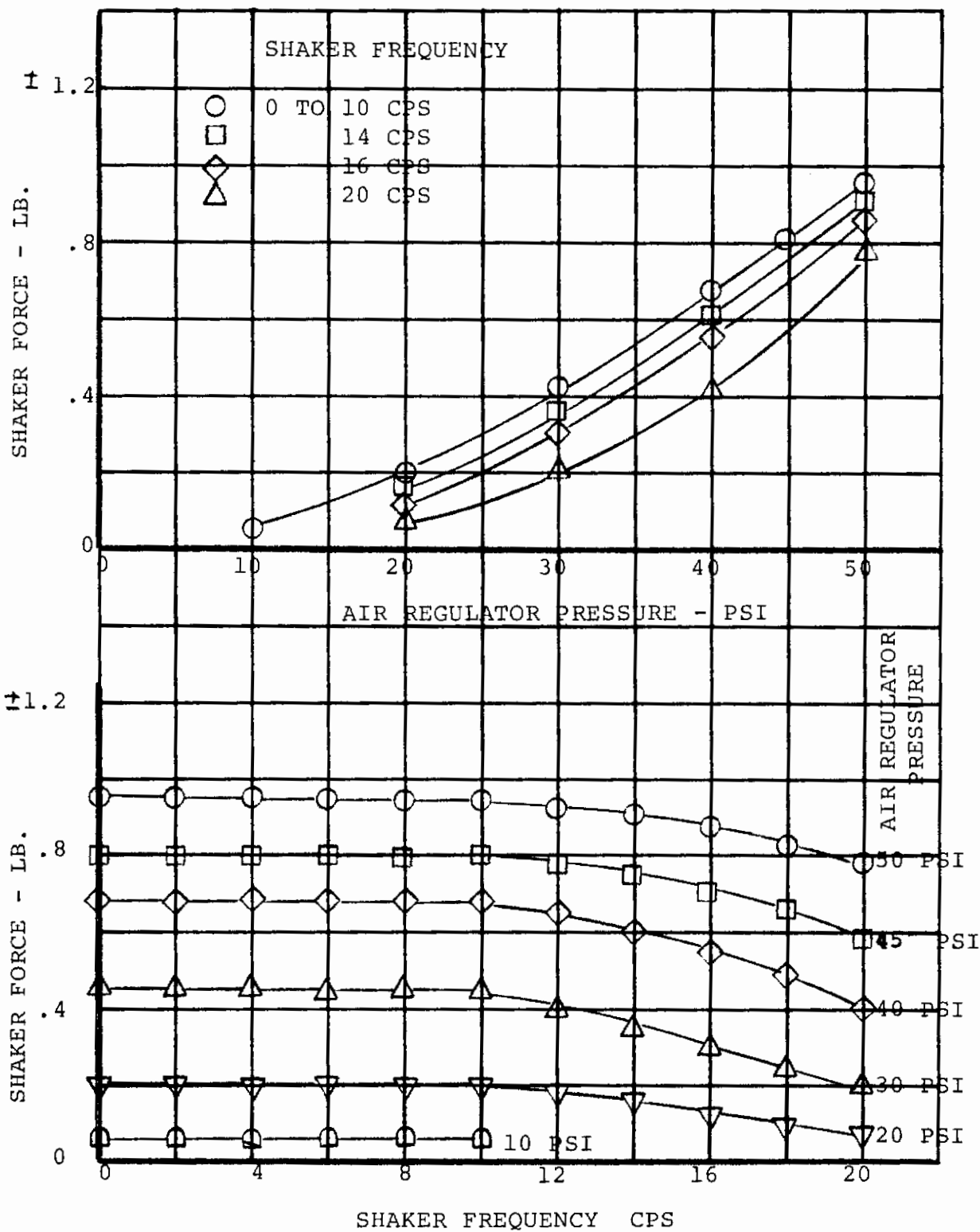


FIGURE 3-7. CALIBRATION OF AIR POWERED SHAKERS

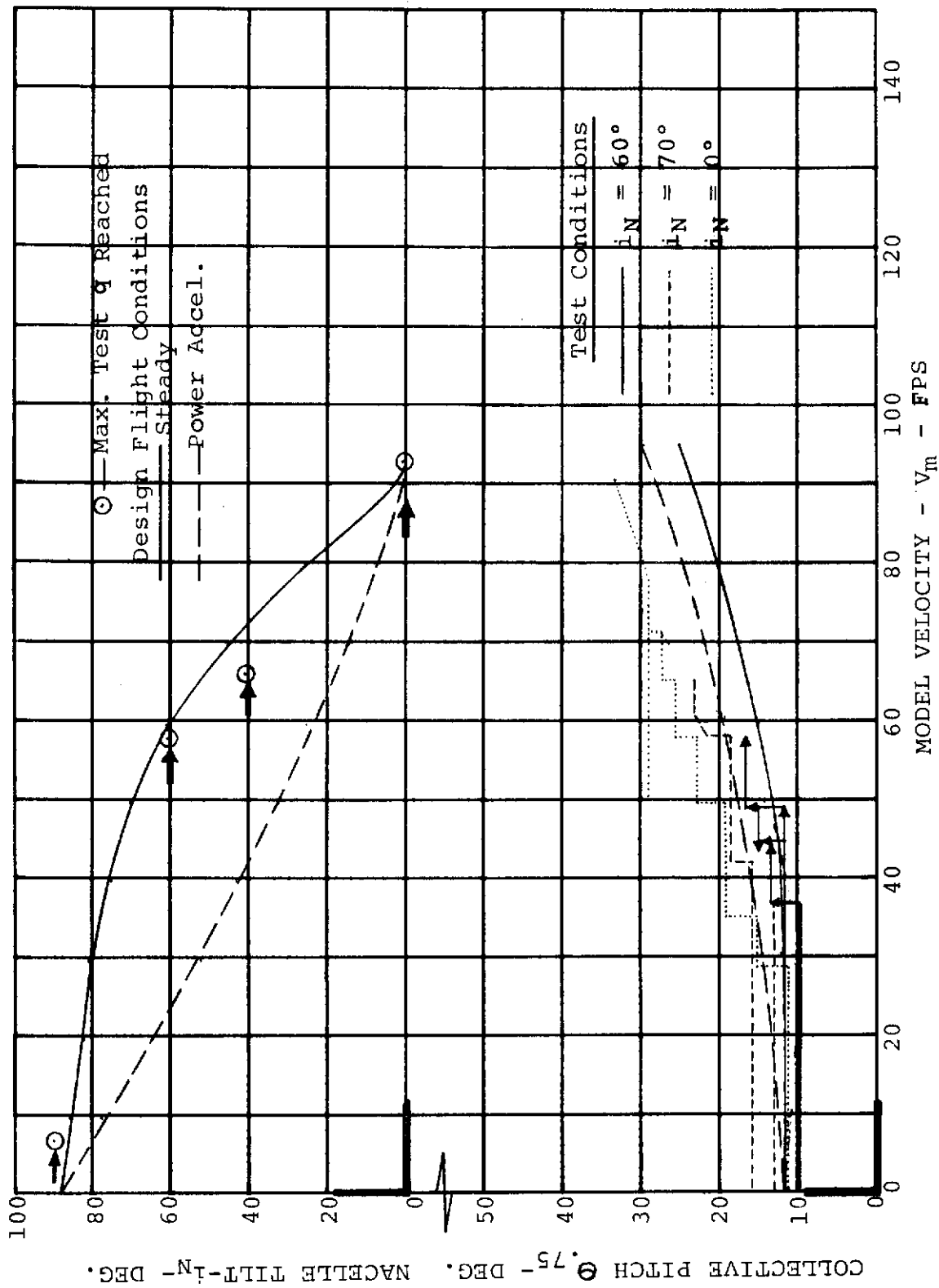


FIGURE 3-8. - TEST CONDITION RANGE

4.0 MODEL UNPOWERED FREQUENCY AND DAMPING DATA

The model was tweak tested by manually bending or pushing the model to an initial deflection to approximately each mode shape, and suddenly releasing the model to measure frequency and decay. This was performed periodically throughout the program and the corresponding results are listed in Table 4-1. The data corresponding to the run numbers in Table 4-1 with pre as a prefix are data taken immediately before the run and with a post prefix are taken immediately after a run. Inconsistency among the frequency and damping values may be due in part to the manner in which the model was excited. Some modes were difficult to excite without causing others to respond also. All tweak data were reduced from the CEC records. The damping values are equivalent viscous damping coefficients. In general, the model was highly damped in all modes (rigid body as well as elastic) relative to typical values for full-scale structures. Although the higher damping is not expected to affect blade loads resulting from forced conditions, it could cause unconservatism where system stability is involved.

4.1 RIGID BODY

A summary of the rigid body frequency and damping data including the mount effects are provided in Table 4.2. Prior to the powered tests, Runs 6 through 10 were conducted which found the umbilical (which consisted of two air hoses and a wire bundle) to have no effect on the model rigid body frequencies and damping as mounted, therefore the data is essentially free of mount effects. Also, the addition of the snubber cables, when loose, were found to have no effect. The snubber cables when tightened increased the rigid body frequencies. The magnitude of restraint depended upon the operator (different ones during different test periods) as well as the manner in which the snubbing load was applied. Vertical support was provided with a bungee cable anchored to the test section ceiling from the model center of gravity. No problems were encountered with this arrangement during the test up to the maximum test dynamic pressure of 10.0 psf.

4.2 BLADE FREQUENCIES

During the course of testing it was noted that the monocoat material on the blades was cracking. Corresponding reduction in blade tweak frequencies also resulted as shown in Figure 4-1. This suggests that the monocoat contributed significantly to the blade stiffness.

Contrails

SN-13 blade was tweak-tested on 3/10/71 (after the completion of wind tunnel tests) to determine the effects of monocoat on blade frequency. This blade was cantilevered at its shoulder (without pitch shaft) and the following results were obtained:

	<u>Fully Monocoated</u>	<u>Outer Five Segments Cut</u>	<u>All Segments Cut</u>
Flap Bending	3.6 cps	3.6 cps	3.5 cps
Chord Bending	13.2 cps	12.3 cps	10.6 cps

As indicated above, the monocoat had little effect on flap bending frequency but a large effect on the chord bending frequency. This was caused by the fact that the monocoat was loose between segments, and since the difference from the blade flap bending elastic axis to the monocoat was small there was no change in the flap bending frequencies. A large change in the chordwise bending frequency resulted because of its greater distance from the neutral axis. Blade damping coefficient variation with time shows considerable scatter but no basic variation with time, Figure 4-2.

Contrails
TABLE 4-1

TWEAK TEST RESULTS

RUN	RIGID BODY			BLADE				WING		
	PITCH	ROLL	YAW	FB	CB	2FB	T	FB	CB	T
PRE 1 (2)				4.15	8.7	19.6				
BAFFLE TEST				.019	.014	.026				
PRE 3				4.1	9.0	18.4				
BAFFLE TEST				.017	.004	-				
PRE 11				4.15	9.2	19.2		5.15	11.0	18.0
				.017	-	-		.027	-	-
11				4.2	9.2				10.9	17.6
									.017	.012
PRE 14	1.5	.54						5.1		18.
	.06	.016						.03		-
POST 14				4.1	9.1	19.6				
				.014	-	-				
POST 28	1.5	.54		4.0	9.0	18.7		5.1	10.9	
	.027	.028		.016	-	.01		.031		
PRE 30				4.0	8.8	18.5				
				.022	.012	-				
POST 30	1.5									
	.09									
PRE 35				3.9	8.8	18.5	73.	5.2	10.5	15.3
				.03	.01	.018	.027	-	-	-
PRE 39				4.0	8.8	18.5	75.	5.1	10.3	
				.031	.017			.032	.017	
PRE 44	1.5	.55		3.9	8.4	17.9	69.	5.1	10.5	17.
	.07	.02		.022	.027	.022	.027	.041	.015	-
PRE 56	1.4	.53		3.9	8.4	17.6	69.	5.1	10.5	
	.065	.024		.021	.01	.032	.03	.026	-	
PRE 57	1.5	.60						5.4	10.7	16.8
	.05	.02						.022	.012	.010
				<u>BLADES OFF</u>						
POST 60	1.5			3.9	8.3	18.3	70.	5.1	10.3	18.4
	.046			.03	.013	.017	-	.04	-	-

NOTE: (1) 1st No. in Box is Frequency - CPS; 2nd is Damping Coef. %/c_c
 (2) Pre means immediately prior to run. Post means immediately after run.

TABLE 4-1 (continued)

TWEAK TEST RESULTS

RUN	RIGID BODY			BLADE				WING		
	PITCH	ROLL	YAW	FB	CB	2FB	T	FB	CB	T
POST 62	.87	.30								
	.14	.10								
POST 67		.40		3.9	8.3	17.6		5.1	10.4	17.0
		-		.017	.015	.02		.055	-	-
POST 60 LEFT BLADE					8.5	19.3				
POST 62 MODEL SNUBBED	3.0	1.2								
POST 67 LEFT BLADE					8.0					

TABLE 4-2

PRE-TEST RIGID BODY FREQUENCY AND DAMPING -- POWER AND WIND OFF

MODE	WITHOUT UMBILICAL WITHOUT SNUBBERS			WITH UMBILICAL No Snub. Snub LooseSnub Tight										
	$i_N = 90^\circ$			$i_N = 0^\circ$										
	f	ξ	Run	f	ξ	Run								
PITCH	1.5	.027	Run 6	1.5	.026	Run 7	1.5	.023	Run 8	1.5	.032	Run 9	3.5	-
ROLL	.56	.012		.56	.014		.58	.014		.59	.014		1.5	-
YAW	.50	.015		.48	.014		.47	.013		.47	.014		.50	-
VERTICAL	.57	.10		.57	.10		.57	.10						
LATERAL	1.02	.004		1.02	.004		1.02	.005		1.02	.004		1.04	-
LONGITUDINAL	SAME AS LATERAL													

f = frequency - CPS

ξ = damping coefficient - %

Contrails

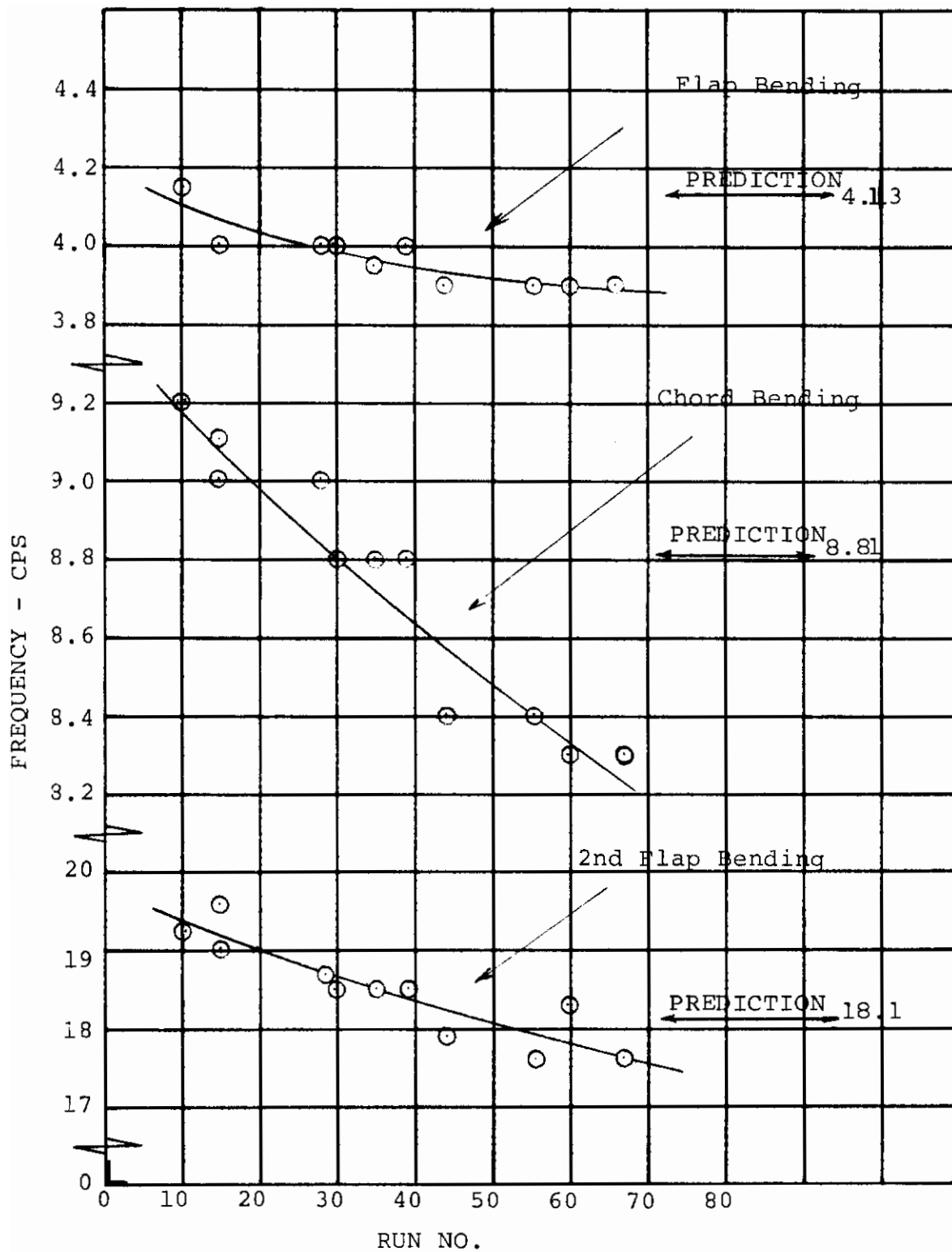


FIGURE 4-1. - VARIATION OF BLADE FREQUENCY WITH RUNS. ROTOR RPM = 0.

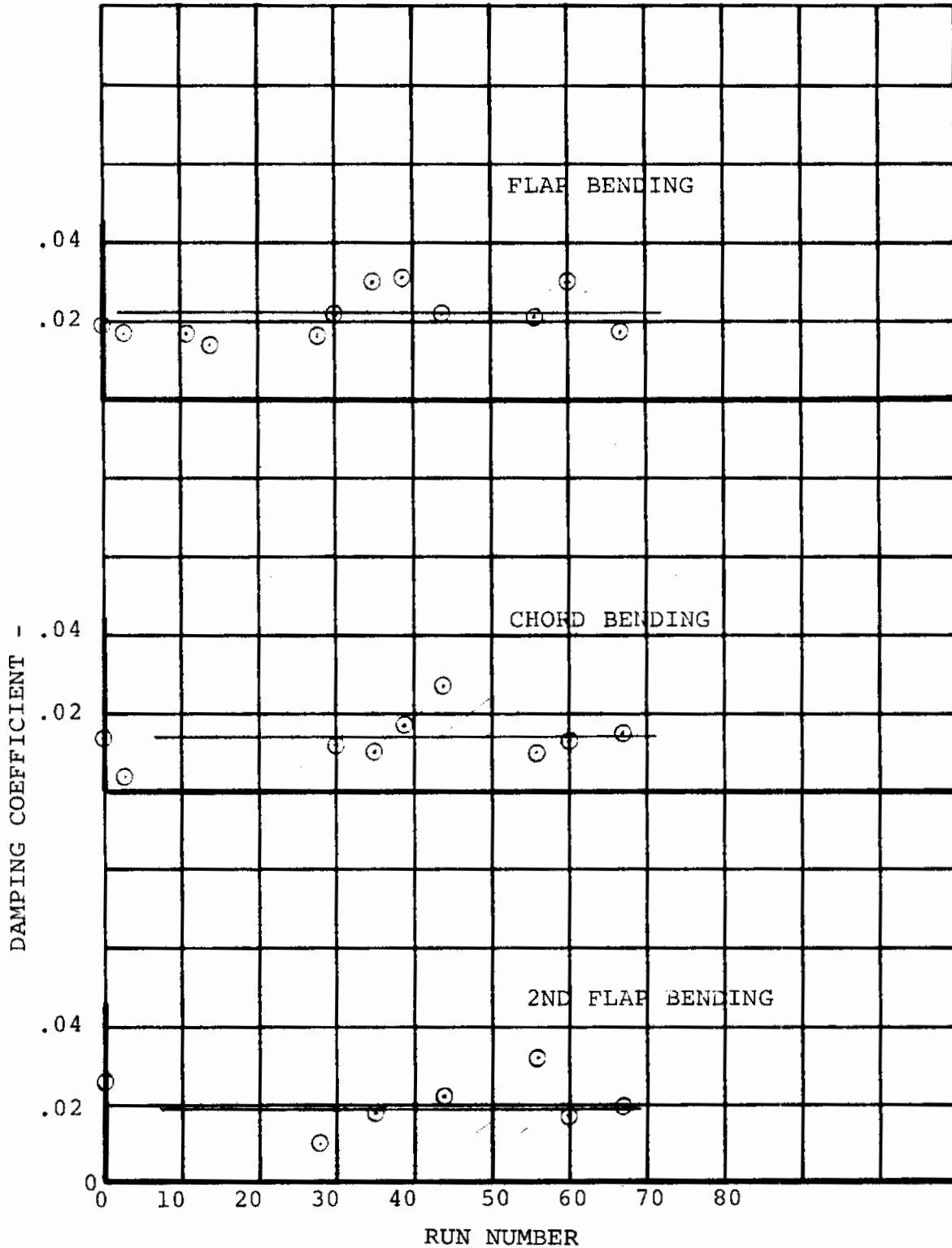


FIGURE 4-2. BLADE MODAL DAMPING FROM TWEAK TESTS
 $\zeta = 0$

5.0 ROTATING BLADE FREQUENCY MEASUREMENTS

One of the test objectives was to determine the rotating blade frequencies in hover and correlate the results with a coupled blade frequency analysis. Test results show good agreement with analysis for the first three blade modes over the RPM range tested.

Substantiation of the rotating blade frequencies was accomplished through the use of a baffle configuration used on a previously tested rotor for blade frequency measurement. The baffle arrangement is shown in Figure 5-1. Baffle combinations of 1, 2, 3 and 4 were used.

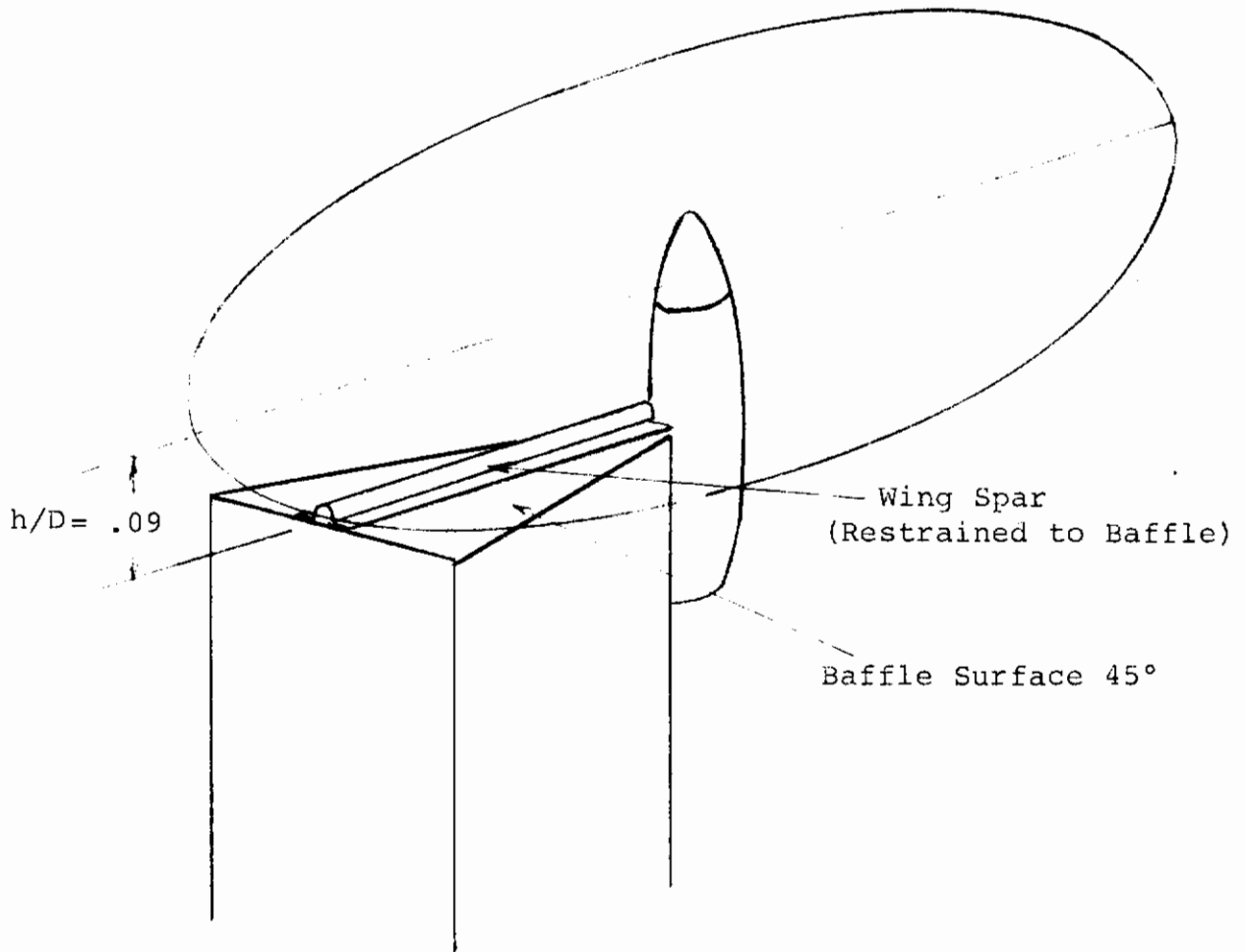
A comparison of the baffle test results with prediction is shown in Figure 5-2 and shows good agreement with prediction for the first three modes. The test data used to determine the 1, 2, 3, 4 and 5 per rev blade frequencies is shown in Figures 5-3 through 5-14. The alternating chord and flap bending data in Figures 5-3 and 5-4 show a high response at 550 RPM. Alternating chord bending response in Figures 5-5 and 5-6 show the same amplification near 550 RPM. The blade loads were near fatigue allowables at 550 RPM and only oscillograph records were taken in this RPM range since harmonic analysis of the data required additional running time per data point. The second harmonic test data in Figures 5-7 and 5-8 show a sharp response to the two baffle configurations at 130 and 280 RPM. Analysis results indicate the first two modes to be highly coupled in this RPM range but the 2 per rev crossing at 130 RPM was predicted to be predominantly a flapping mode and the 2 per rev crossing at 280 RPM predominantly a chordwise mode. The high chord bending response at 280 RPM and high flap bending at 130 RPM substantiate the predicted 2 per rev blade frequencies and also the predicted modal predominance.

The third harmonic blade bending response to the baffles is shown in Figures 5-9 and 5-10. The chord bending data show a large response at 100 and 170 RPM to the 3 per rev baffle configuration and the flap bending data shows a response to 3 baffles at 90 RPM. The largest third harmonic flap bending response occurred between 500 and 600 RPM being twice as large as the second harmonic flap bending response between 500 and 600 RPM as shown in Figure 5-8 and six times as large

Contrails

as the fourth harmonic flap bending response as shown in Figure 5-10 for the same RPM range. This indicates that the third harmonic flap bending response is due to a 3 per rev frequency crossing on a higher flapping mode and not due to the one per rev chordwise frequency crossing at 550 RPM. Although the third harmonic flap bending data is sparse between 500 and 600 RPM, the RPM corresponding to the highest flapping response (570 RPM) was determined to be the 3 per rev crossing for the second flap mode.

The fourth harmonic blade bending response is shown in Figures 5-11 and 5-12. The chord bending response shows a large amplification at 135 RPM and 360 RPM for the 4 per rev baffle configuration and the flap bending response shows little amplification at 135 RPM and a large amplification at 360 RPM. The large response at 135 RPM is due to a 4 per rev crossing on the second mode (predominantly chordwise) and the flap bending response at 360 RPM is due to a 4 per rev crossing on the third mode (primarily second flap). Although a 5 per rev baffle configuration was not tested, the test results show a significant fifth harmonic response. The fifth harmonic blade bending response is shown in Figures 5-13 and 5-14 and show a chord bending amplification at 110 RPM and 265 RPM and a flap bending amplification at 265 RPM. The response to 110 RPM is due to a 5 per rev frequency crossing on the second mode and the response at 265 RPM is due to a 5 per rev frequency crossing on the third mode.



Note: Model was partially assembled.

Tests were conducted with
1, 2, 3 and 4 baffles.

Figure 5-1. Schematic of Baffle Test Set-Up

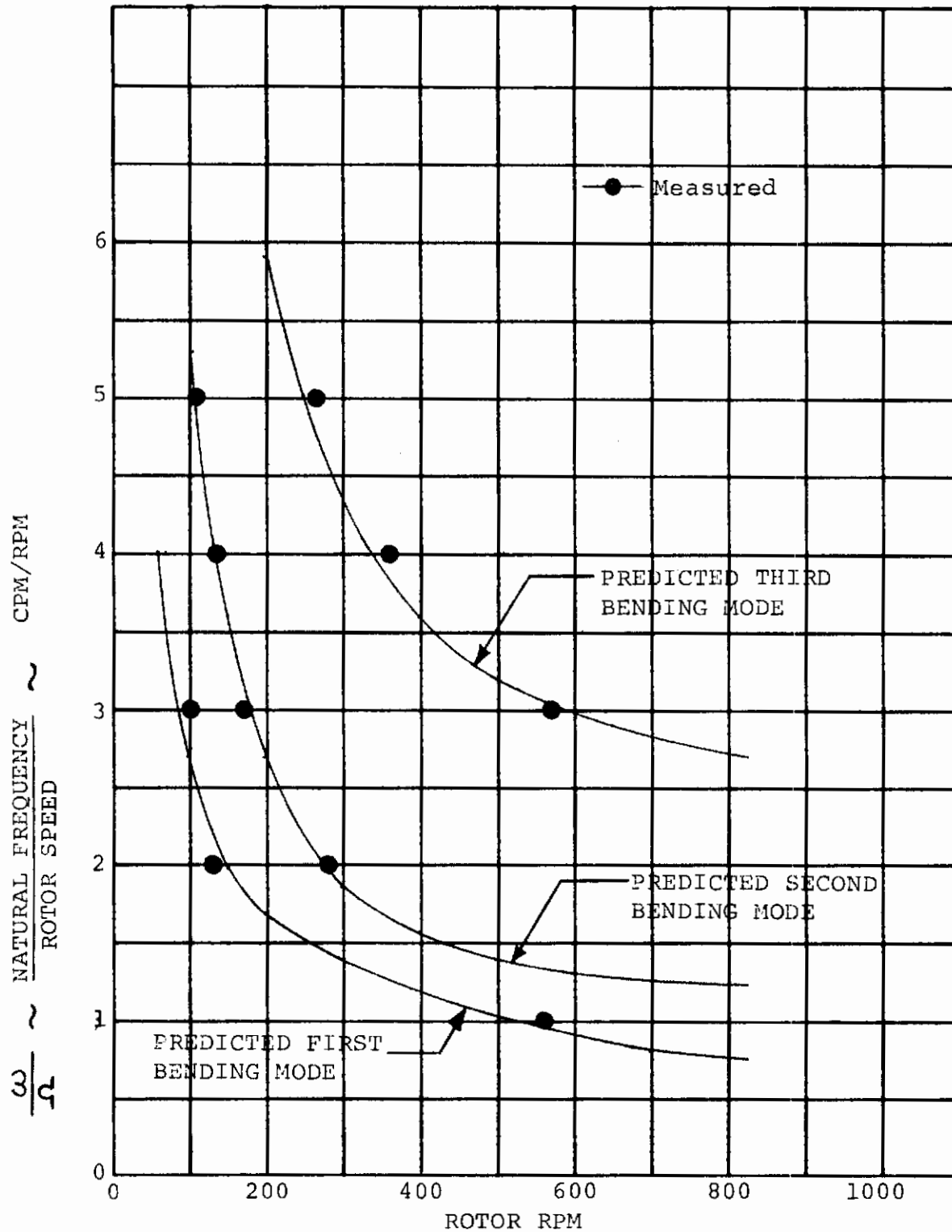


FIGURE 5-2. PREDICTED AND MEASURED ROTOR BLADE NATURAL FREQUENCIES FOR $\theta_{.75} = 3$ DEG.

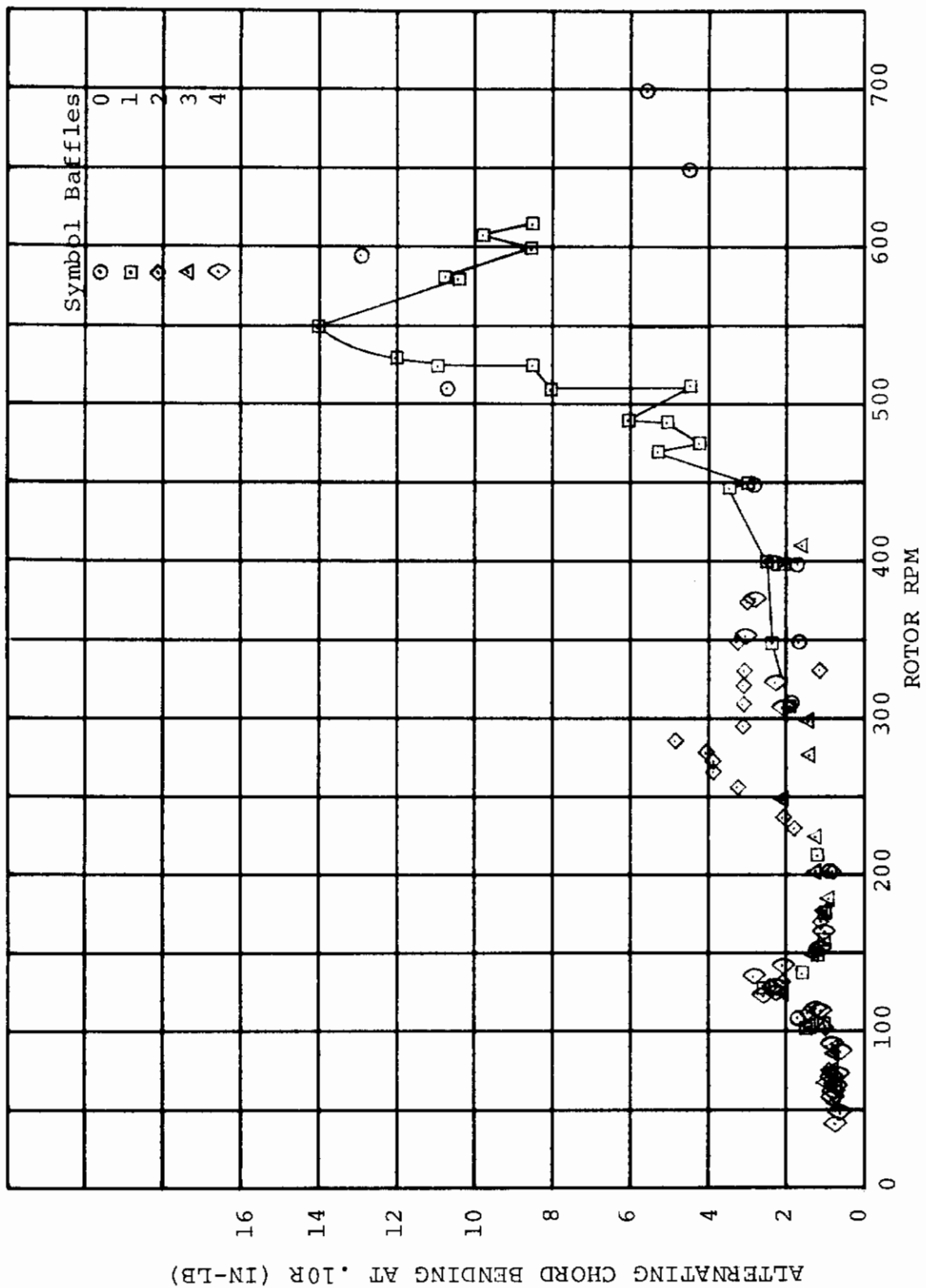


FIGURE 5-3. ALTERNATING CHORD BENDING RESPONSE TO BAFFLES

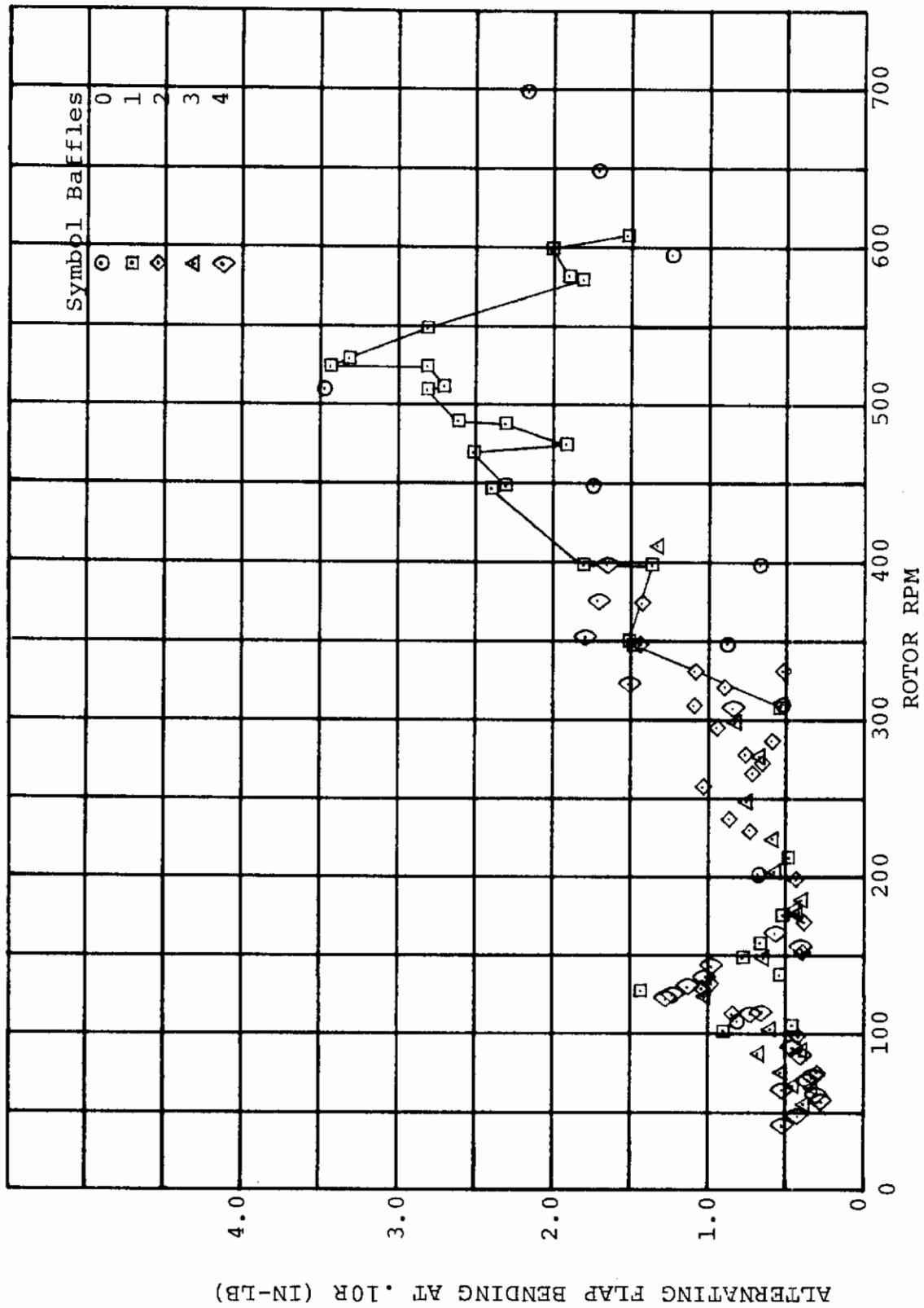


FIGURE 5-4. ALTERNATING FLAP BENDING RESPONSE TO BAFFLES

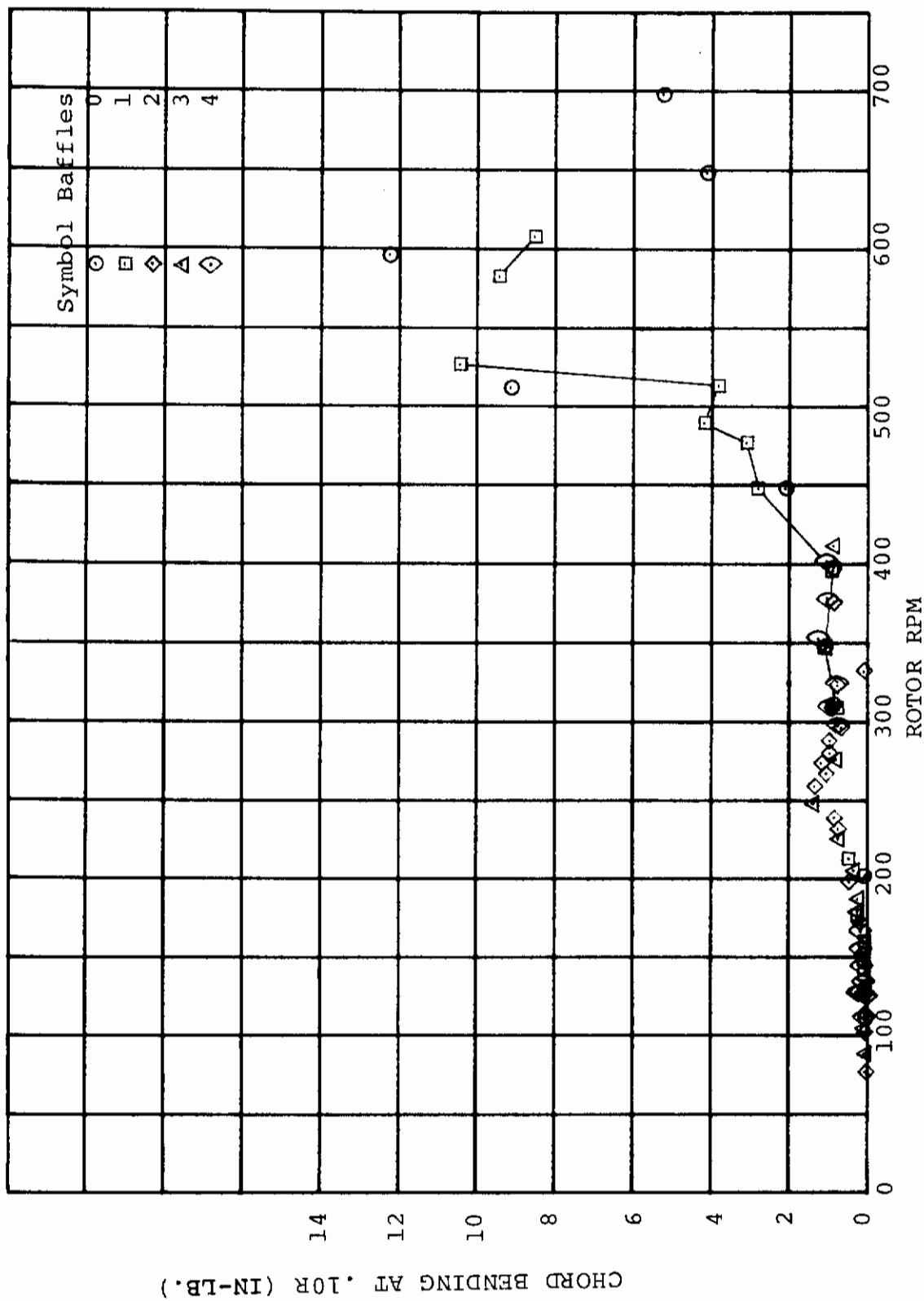


FIGURE 5-5. 1ST HARMONIC CHORD BENDING RESPONSE TO BAFFLES

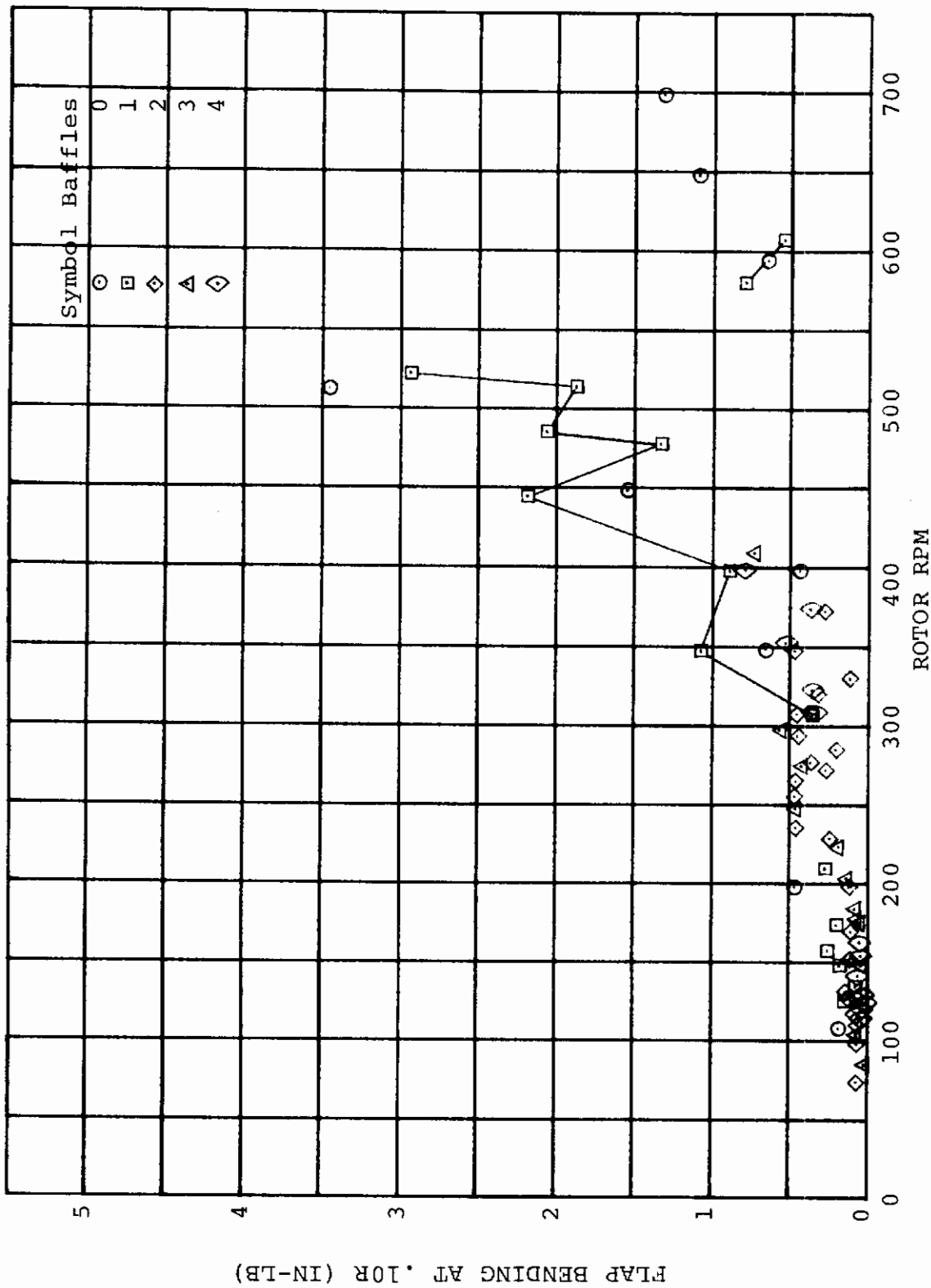


FIGURE 5-6. 1ST HARMONIC FLAP BENDING RESPONSE TO BAFFLES

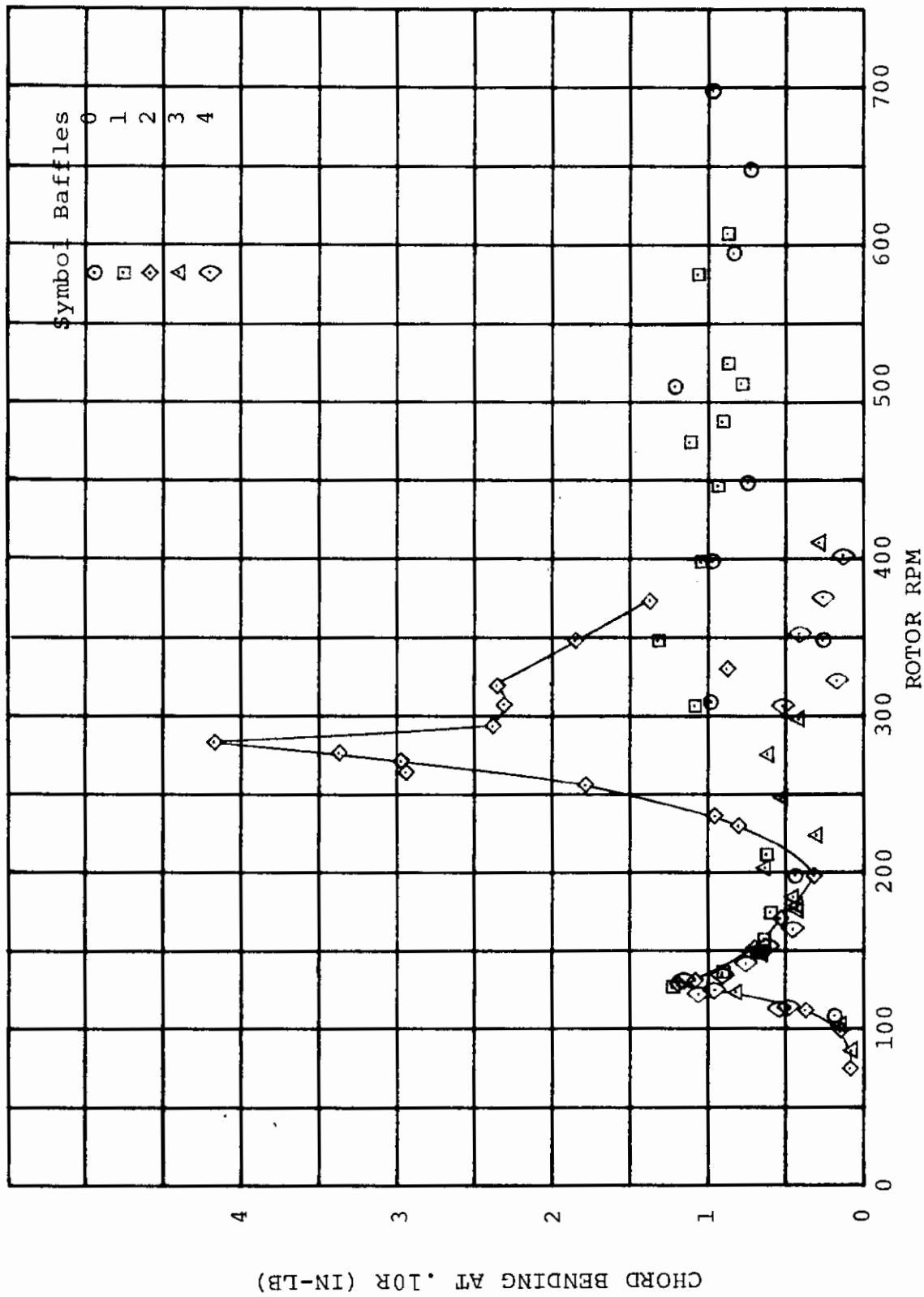


FIGURE 5-7. 2ND HARMONIC CHORD BENDING RESPONSE TO BAFFLES

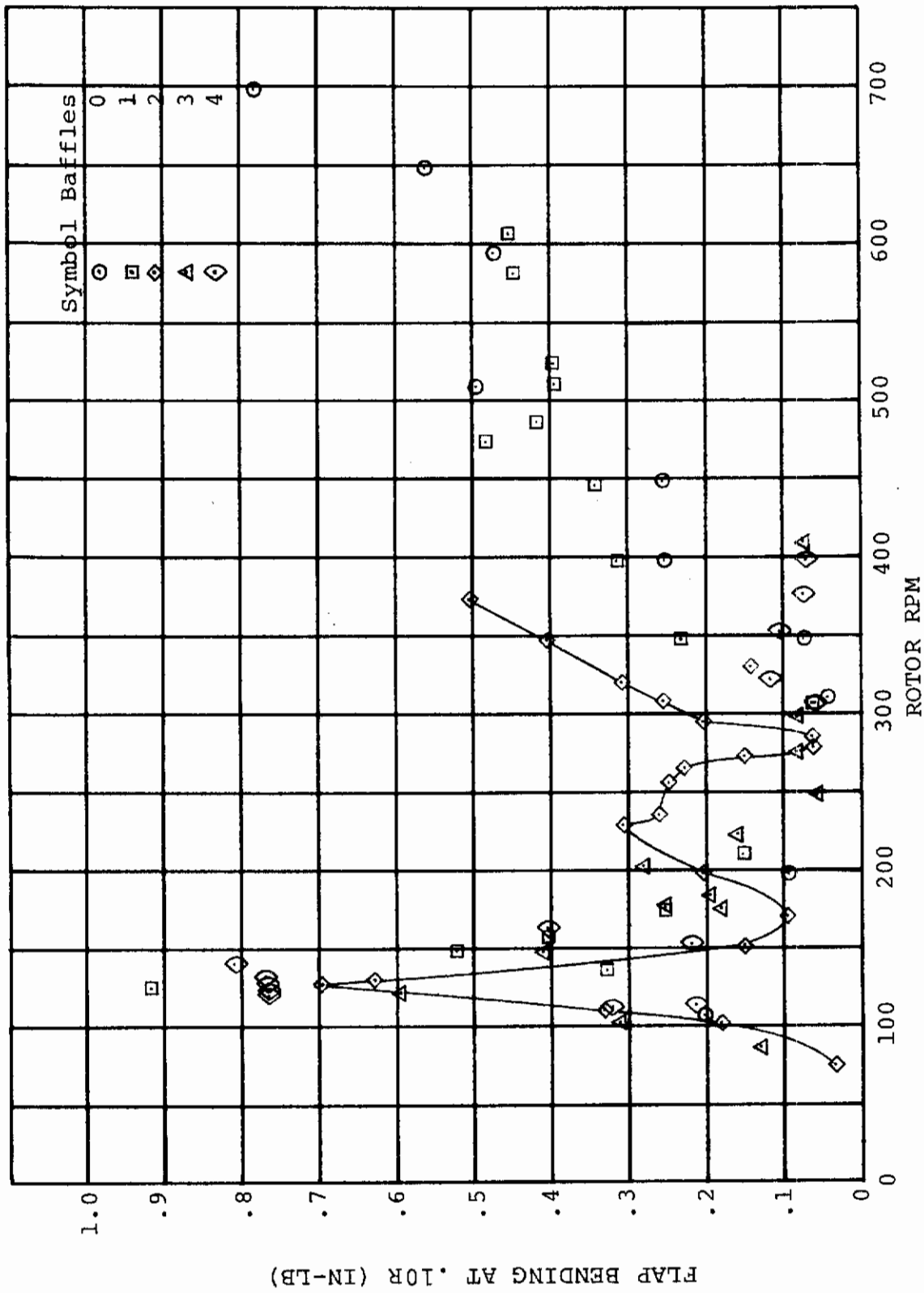


FIGURE 5-8. 2ND HARMONIC FLAP BENDING RESPONSE TO BAFFLES

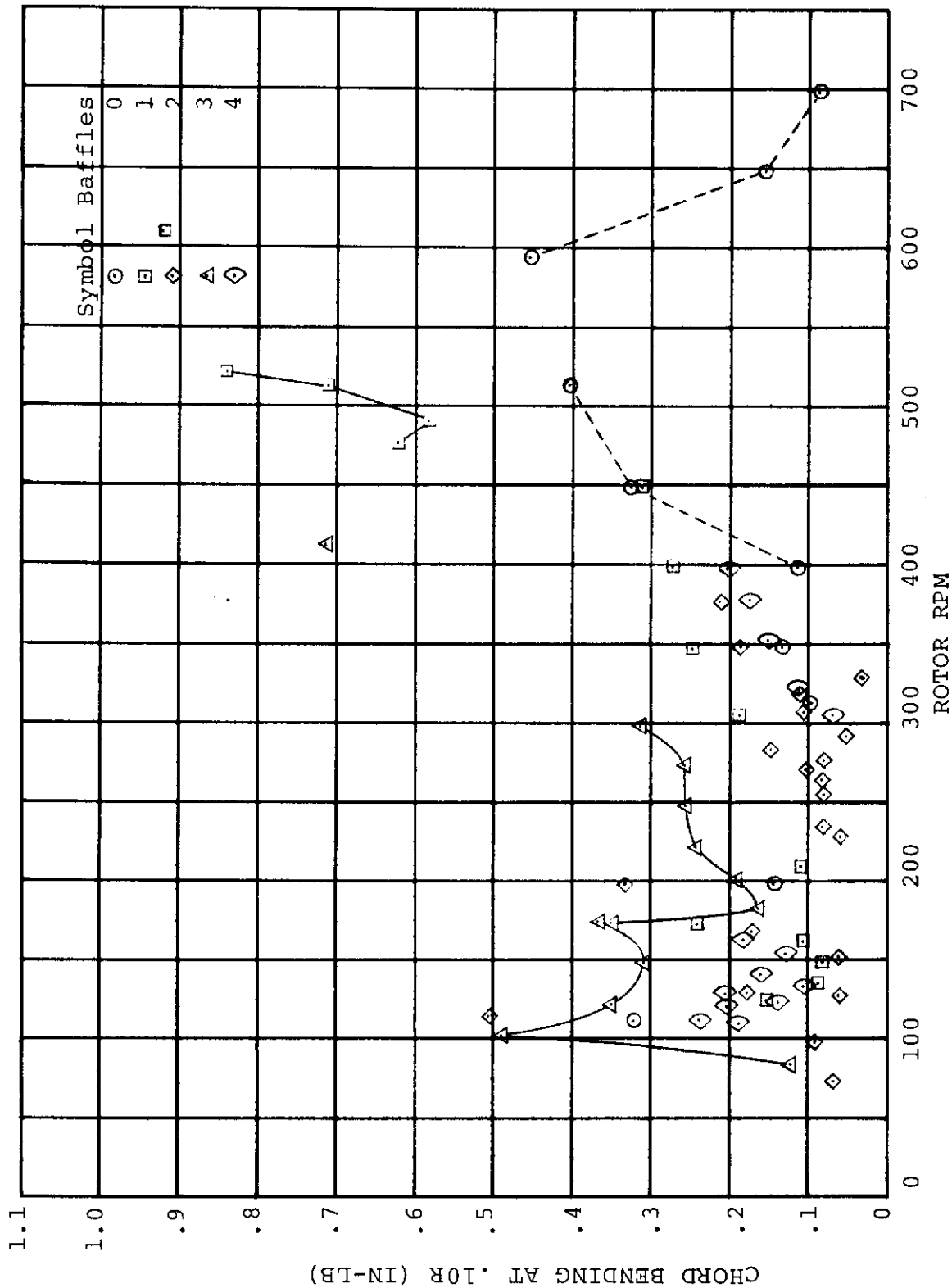


FIGURE 5-9. 3RD HARMONIC CHORD BENDING RESPONSE TO BAFFLES

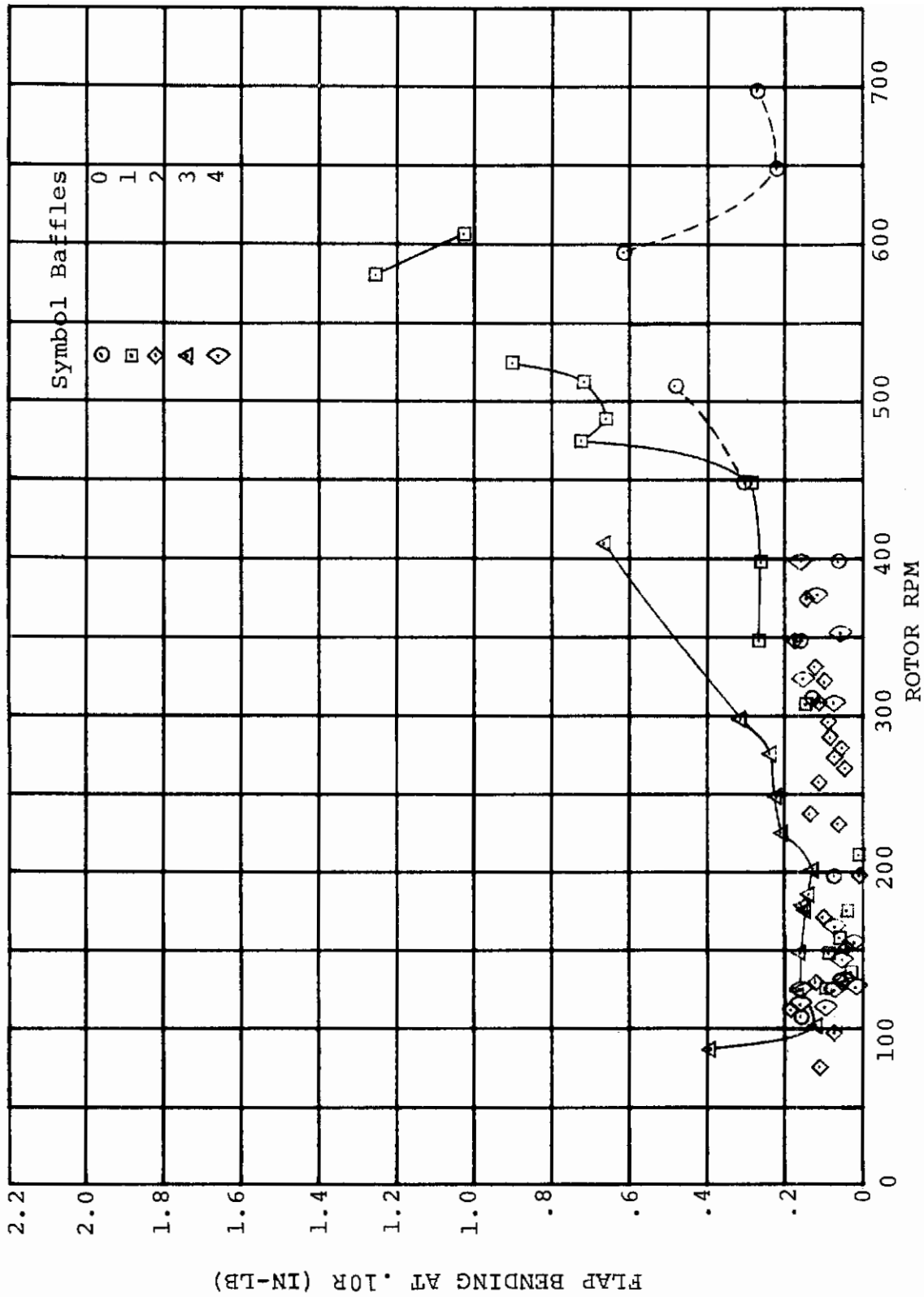


FIGURE 5-10. 3RD HARMONIC FLAP BENDING RESPONSE TO BAFFLES

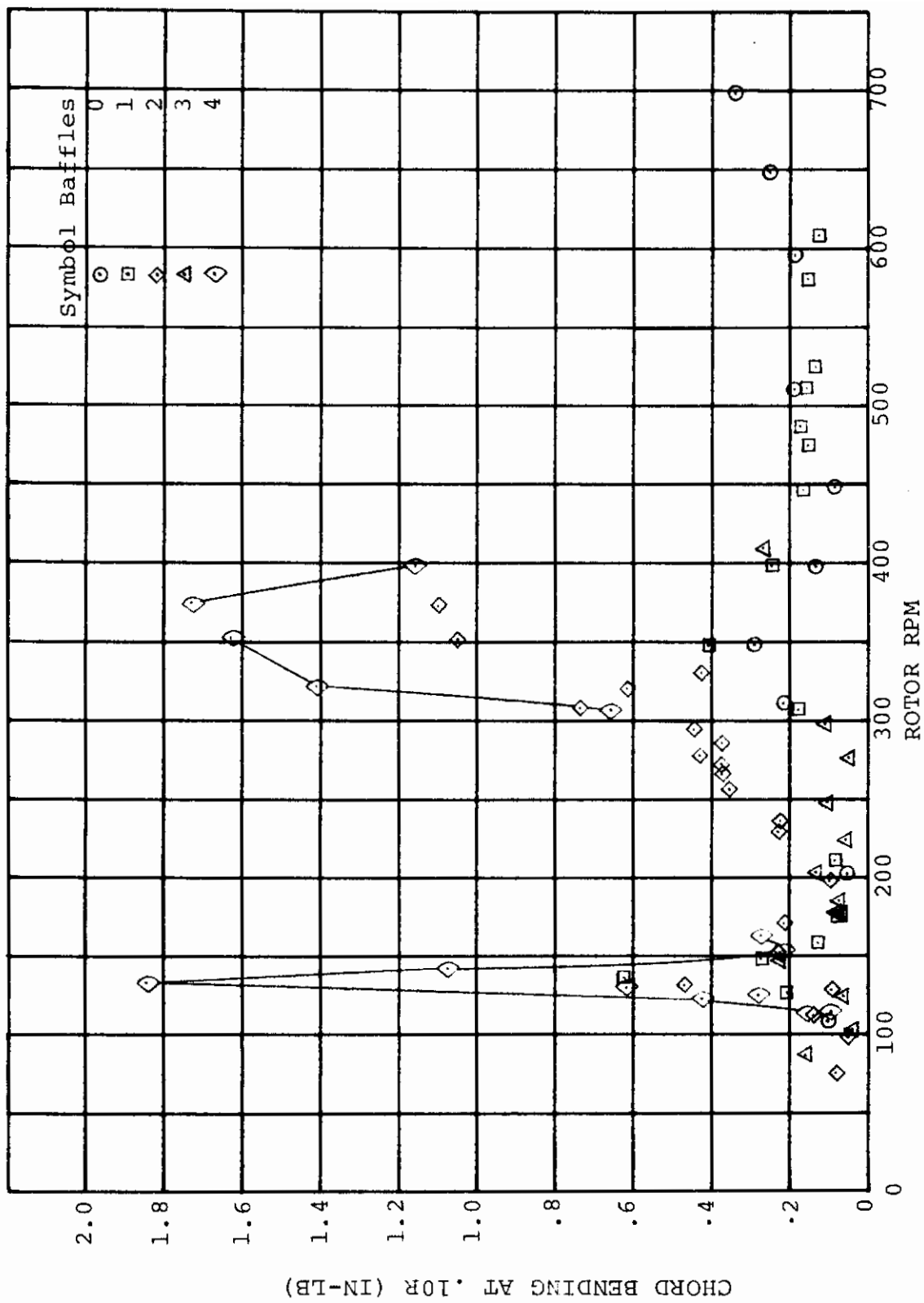


FIGURE 5-11. 4TH HARMONIC CHORD BENDING RESPONSE TO BAFFLES

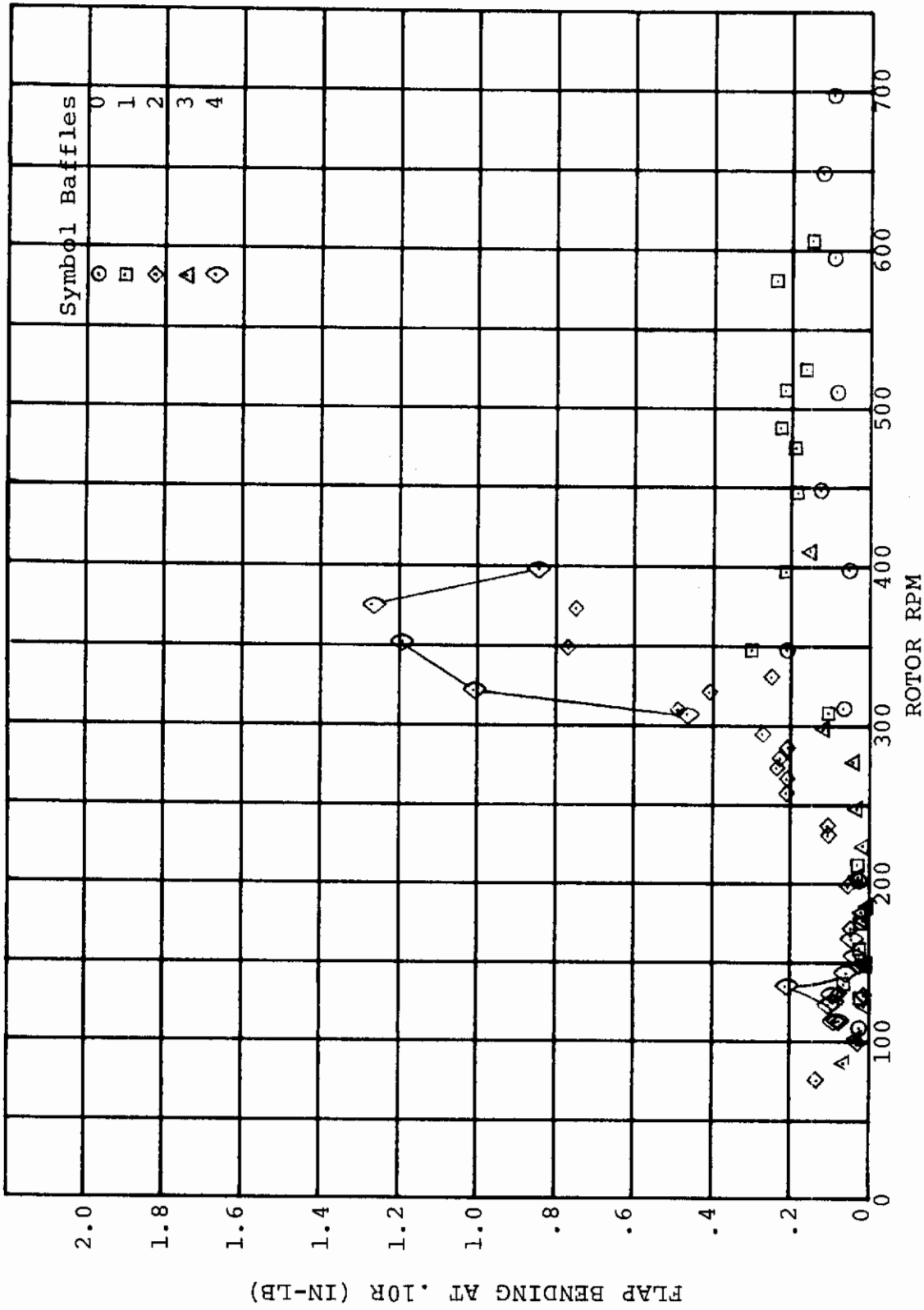


FIGURE 5-12. 4TH HARMONIC FLAP BENDING RESPONSE TO BAFFLES

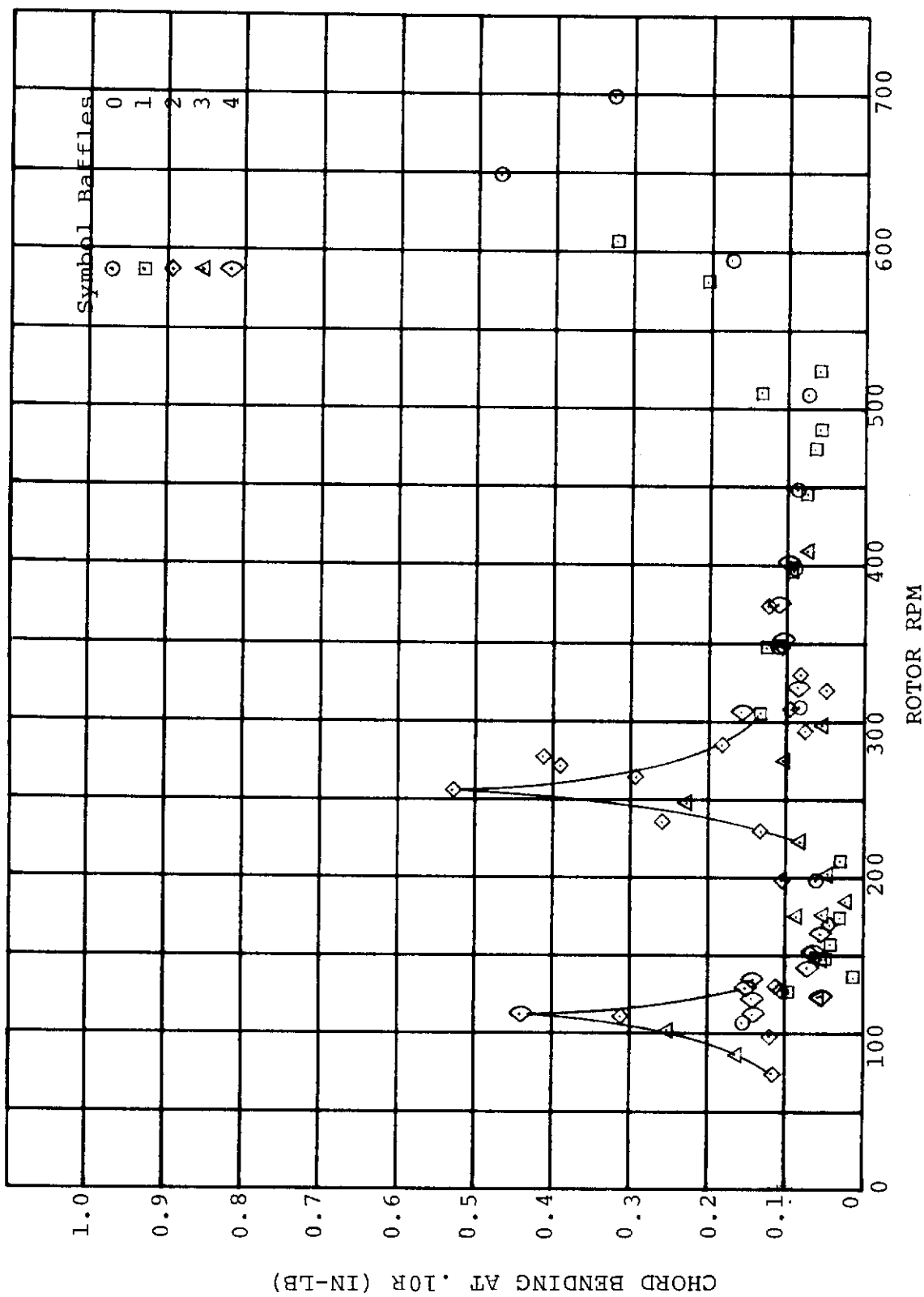


FIGURE 5-13. 5TH HARMONIC CHORD BENDING RESPONSE TO BAFFLES

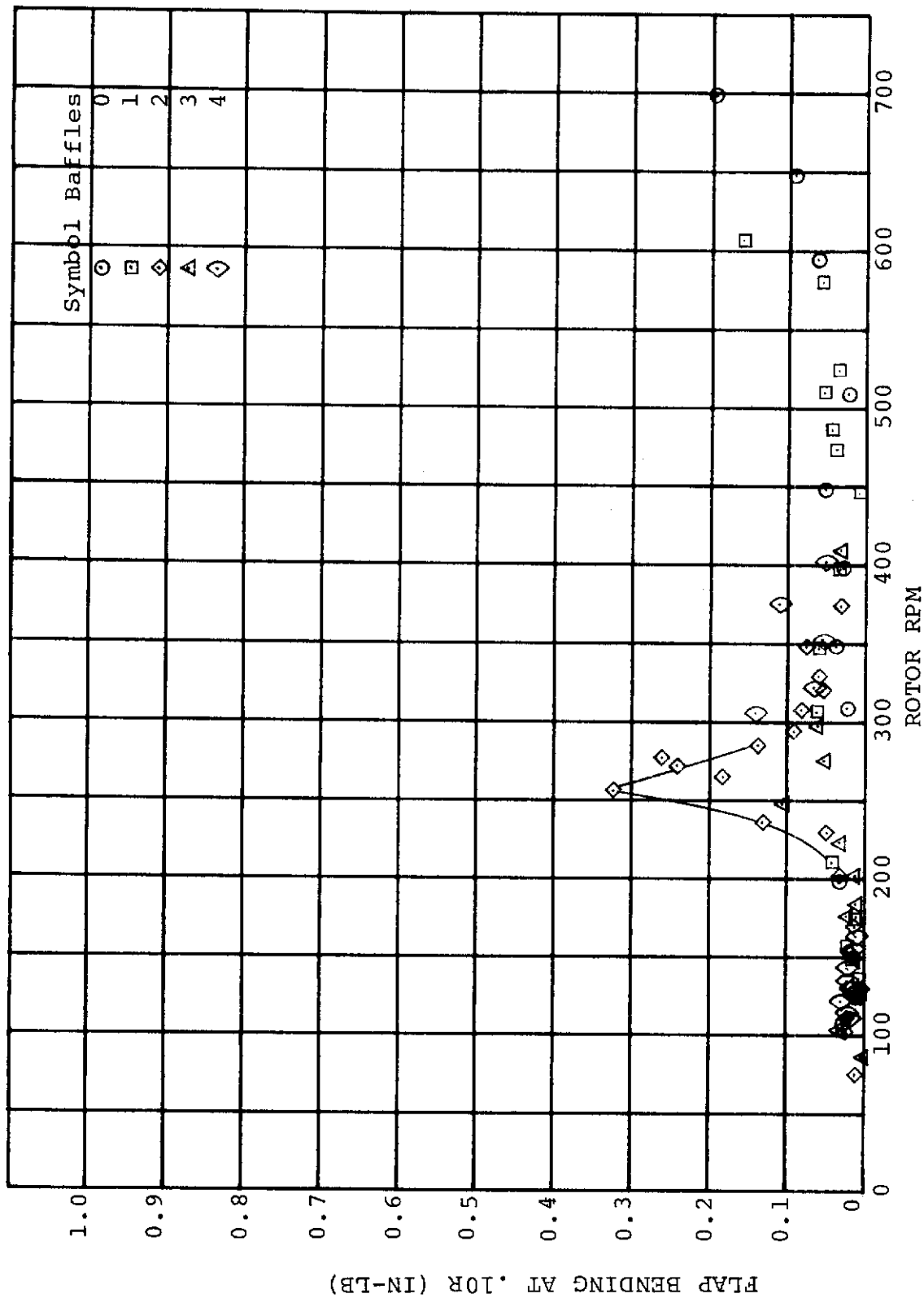


FIGURE 5-14. 5TH HARMONIC FLAP BENDING RESPONSE TO BAFFLES

6.0 BLADE LOADS

A major objective of the test program was to determine blade loads in hover, transition and cruise modes. Parameters varied were collective pitch, cyclic pitch, rotor speed, nacelle tilt, fuselage pitch and yaw, and dynamic pressure. Good results were obtained and the effects of each of the above parameters on blade alternating loads are presented herein.

Since the blade strain gages were bonded to the blade spar, all blade bending moments are with respect to the blade and not with respect to the disc plane. At collective angles ($\theta.75$) as low as 30° the measured root chordwise bending moment is primarily an out of plane deformation due to the high twist of rotor blade. This is discussed in Section 3.3 and illustrated in Figure 3-5.

During the initial portion of the test, one rotor was excessively unbalanced which resulted in higher blade loads and a restricted rotor speed range of operation. Corresponding results are discussed in Section 6.1.1. It was found that excessive unbalance increased not only the minimum values of loads, but also the variation of loads with cyclic. To achieve properly scaled rotor balance would require balancing the model to within 0.0001 in-lb which is not practicable. However, after the initial portion of the test a balance was achieved which gave low minimum loads and is considered to provide good loads data. Because residual unbalance was not zero, the loads data may be conservative.

The wind tunnel wall corrections are less than data scatter for all test conditions because the model operated at very low disc loading (Froude scaling), and the model to tunnel ratios are small. Recirculation is minimized by the slotted test section.

All data presented herein were obtained from the right rotor blade, SN-16 LB at 0.10R for flap and chord bending and 0.15R for torsion.

6.1 HOVER BLADE LOADS

Blade loads data were obtained in hover to show the effect of cyclic pitch, rotor-rotor interference, stall flutter, collective pitch, rotor spin-up and spin-down and low forward speed on blade loads.

Cyclic pitch test results showed that the slope of blade loads per degree of cyclic are not affected by ground effect but IGE

does increase the value of minimum blade loads at zero cyclic. Increased collective pitch increased blade loads sensitivity to cyclic pitch application.

At differential collective pitch values corresponding to that required for roll control power in hover, rotor-rotor interference had essentially no effect on blade alternating loads.

Low amplitude stall flutter inception occurred in hover at a collective pitch angle of approximately 11° ; however loads were low.

For a rotor precone of 5 degrees, the test data showed that the steady flap bending at the root is zero at approximately 10.5 degrees collective pitch at 705 RPM.

Rotor start-up and shut-down showed that maximum alternating chord bending lagged the one per rev chordwise frequency crossing by 50 RPM. The maximum chord bending loads during start-up were 1.3 times those during shut-down.

6.1.1 Effect of Cyclic Pitch

One of the primary objectives was to determine the effect of cyclic pitch on blade loads in hover. Additional considerations were the effect of collective pitch and ground interference on blade loads due to cyclic pitch. The results of cyclic pitch effects on blade loads are shown in Figures 6-1 through 6-11 and are discussed below. Samples of blade load wave forms are given in Figure 6-1 for a series of cyclic values. The primary one per rev loads vary with cyclic, as would be expected, and there is also a small amplitude 3 per rev load in the flap bending direction.

Figures 6-2 and 6-3 show alternating chord and flap bending data as cyclic pitch is varied for hovering IGE at 4.7 degrees collective pitch and 825 RPM. These data show a near linear increase with cyclic from a minimum value. The alternating chord bending gradient is 3 inch pounds per degree cyclic and the flap bending gradient is 2 inch pounds per degree cyclic. Figures 6-4 and 6-5 show blade loads data that were recorded early in the test in hover OGE at 4 degrees collective pitch and 750 RPM. The data in these figures were taken when the rotor was out of balance and illustrate the increased sensitivity of cyclic pitch on blade loads with rotor unbalance combined with reduced rotor speed (750 RPM). The design hover speed for the model was 825 RPM but 750 RPM was the optimum rotor speed for minimum blade loads with the unbalanced rotor.

The gradient of these blade loads with cyclic are 8 in lb chord bending per degree cyclic or 2.5 times the gradient for chord bending shown in Figure 6-3. The gradient for flap bending is 1.1 times the gradient for flap bending shown in Figure 6-3. Data for correlation purposes must therefore be chosen to contain minimum rotor unbalance.

Figures 6-6 through 6-9 show the effect of model height on blade loads in hover with cyclic pitch at the design model hover rotor speed. These data show that ground interference does not affect the gradient of blade loads per degree cyclic pitch but does affect the level of blade loads at minimum cyclic. In Figure 6-6, the alternating chord bending at minimum cyclic hovering IGE is 2 times the chord bending hovering OGE in Figure 6-8. Comparing Figures 6-7 and 6-9, model height has no effect on alternating flap bending.

Figures 6-2, 6-3, 6-9 and 6-11 show the effect of collective pitch on blade loads in hover IGE with cyclic pitch. These data show that collective affects the gradient of blade loads per degree of cyclic pitch. In Figure 6-10 at 11 degrees collective the gradient of alternating chord bending per degree cyclic is 2.5 times the gradient of chord bending at 4.7 degrees collective in Figure 6-2. Comparing Figures 6-3 and 6-11, increasing collective from 4.7 to 11 degrees increases the gradient of flap bending loads per degree of cyclic by 25 percent.

6.1.2 Rotor-Rotor Interference

To determine the effect of downwash from one rotor on the blade loads of the other rotor the collective pitch on the left rotor was varied between 5.9° and 13.3° while the collective on the right rotor whose blade loads were being monitored was kept constant. All other parameters were held constant. The test results show that the range of differential collective (10.5 to 13 degrees) required for roll control power when hovering at 1g OGE has essentially no effect on alternating blade loads. The phasing of the harmonic content changes significantly as shown in Figure 6-12. No scales are shown because the phasing and harmonic content are of primary interest. Recirculation was not a factor in these tests because the rotor disc loading was very small and the slotted walls minimized direct recirculation in the test section.

6.1.3 Effect of Collective Pitch

Full scale design analyses show that under 1g conditions five degrees of rotor blade precone produce zero steady

flap bending moment at the blade root with $\theta_{.75} = 10^\circ$ at design hover RPM. This is confirmed by the test results in Figure 6-13 which shows the variation of steady flap bending moment at 0.10R with collective pitch. In this case ($\Omega = 750$ RPM) low collective produces the expected negative steady bending moment at 0.10R (due to centrifugal force acting on the pre-coned blade), and zero steady bending moment results with $\theta_{.75} = 10.3^\circ$.

6.1.4 Rotor Start-up and Shut-down

Figures 6-14, 6-15 and 6-16 show the effect of rotor start-up and shut-down through the one per rev frequency crossing on blade loads in hover. Figure 6-16 shows that the rate of change of RPM with time through the one per rev crossing were nearly the same. Maximum chord bending during start-up are 1.3 times chord bending during shut-down and are equivalent to the loads obtained by 3.5 degrees of hover cyclic at 825 RPM, as shown in Figure 6-2.

6.1.5 Low Forward Speed

Testing was done OGE at low forward speed to determine whether blade-tip vortex interactions were present and, if so, how the blade loads were affected. Cyclic was varied at a tunnel q corresponding to a full-scale aircraft speed of 23 fps. The results in Figures 6-17 and 6-18 show a large decrease in blade loads as cyclic pitch is increased positively. The sensitivity of these loads to cyclic is in the same order of that in hover and the cyclic pitch value at which minimum load would occur (not reached in this run) had a notable shift to positive as expected.

6.1.6 Stall Flutter

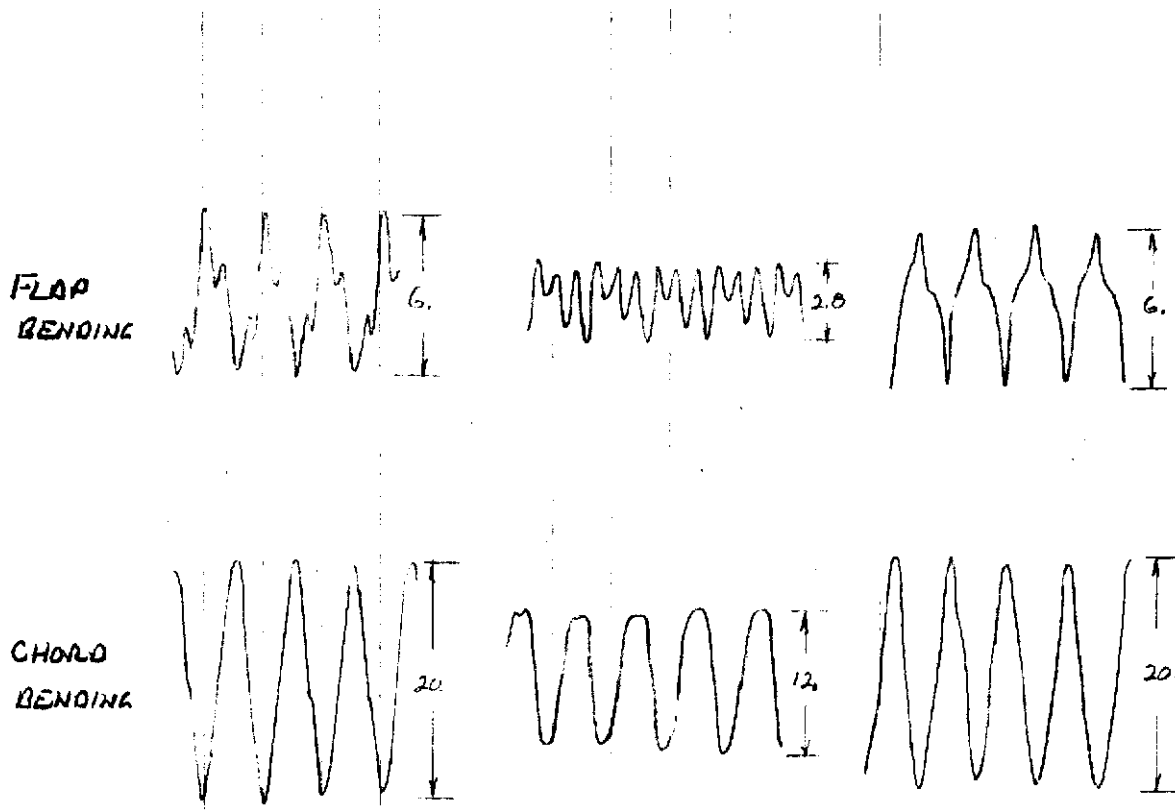
Stall flutter inception is considered to occur at the break in the blade torsion amplitude versus collective pitch. Figure 6-19 shows the alternating torques which resulted from two rotor speeds. Although the load amplitudes are very low, inception is considered to have occurred at $\theta_{.75} = 12^\circ$ for $\Omega = 750$ and $\theta_{.75} = 11^\circ$ for $\Omega = 830$. Blade torsion wave traces are presented in Figure 6-20 for the $\Omega = 850$ RPM case. The peak to peak amplitudes correspond to the circular data points on Figure 6-19.

Contrails

It is noteworthy that even at the highest collective pitch setting tested (14.2°), the absolute value of alternating torsion moment is very low - about ± 1.1 lb in.

A measurement of rotor thrust in hover was obtained from the steady wing flap bending moment. The maximum thrust values (shown in Figure 6-21) produce a thrust coefficient (C_T -- helicopter notation) of 0.01, and a corresponding value of $C_T/\sigma = 0.118$.

Contrails



CEC DATA POINT 7
 $\theta_2 = -1.5^\circ$

10
 -0.75°

15
 $+1.5^\circ$

- NOTES:
- PEAK-TO-PEAK BENDING MOMENT LOADS ARE INDICATED
 - VERTICAL LINES ARE 1/REV MARKER AT $\psi = 90^\circ$

FIGURE 6-1. WAVE-FORM OF ALTERNATING BLADE LOADS
 FOR A SERIES OF CYCLIC PITCH ANGLES
 - RIGHT BLADE .10R RUN 31
 $\theta_{1F} = 9.0^\circ$ HOVER
 $\Omega = 750 \text{ RPM}$

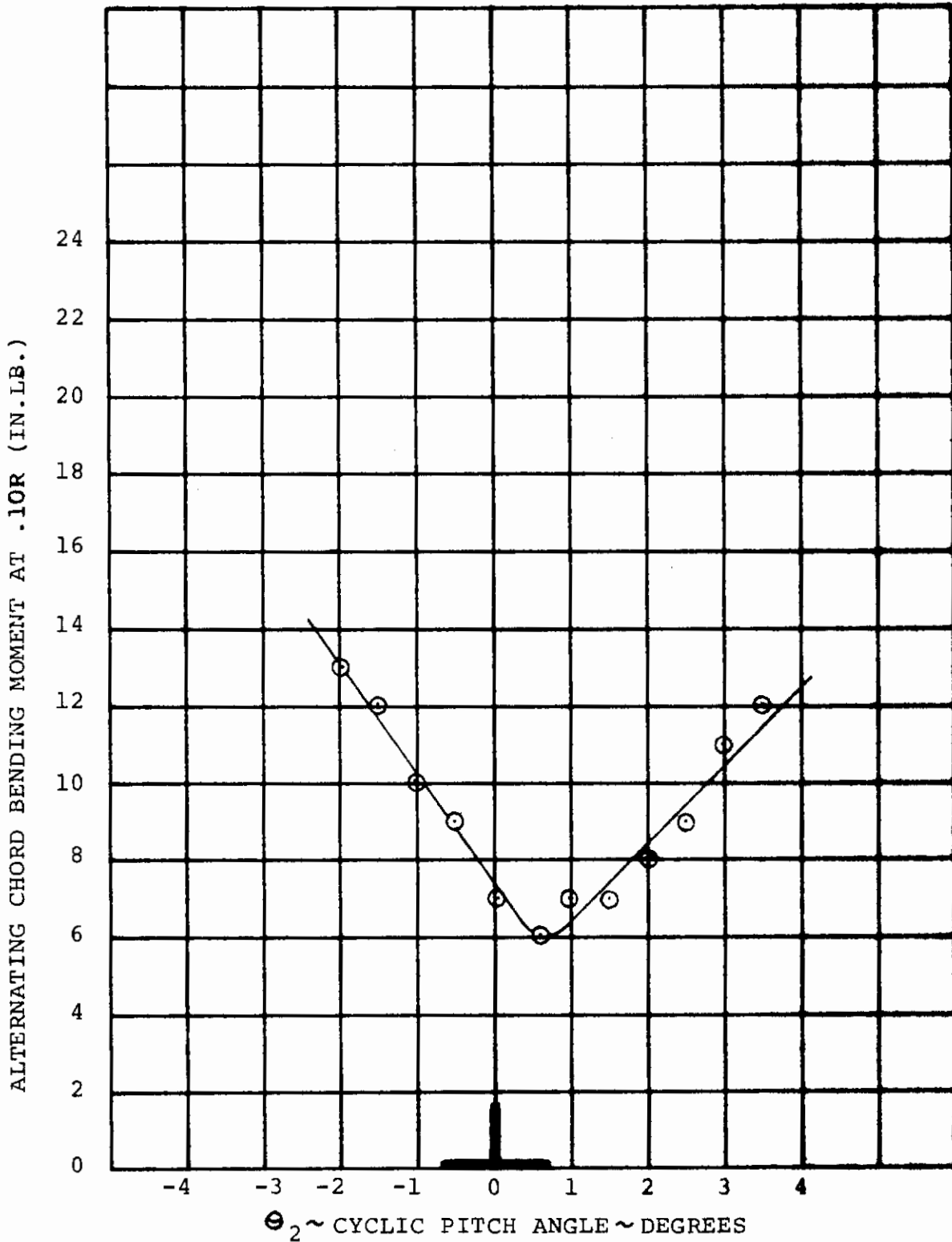
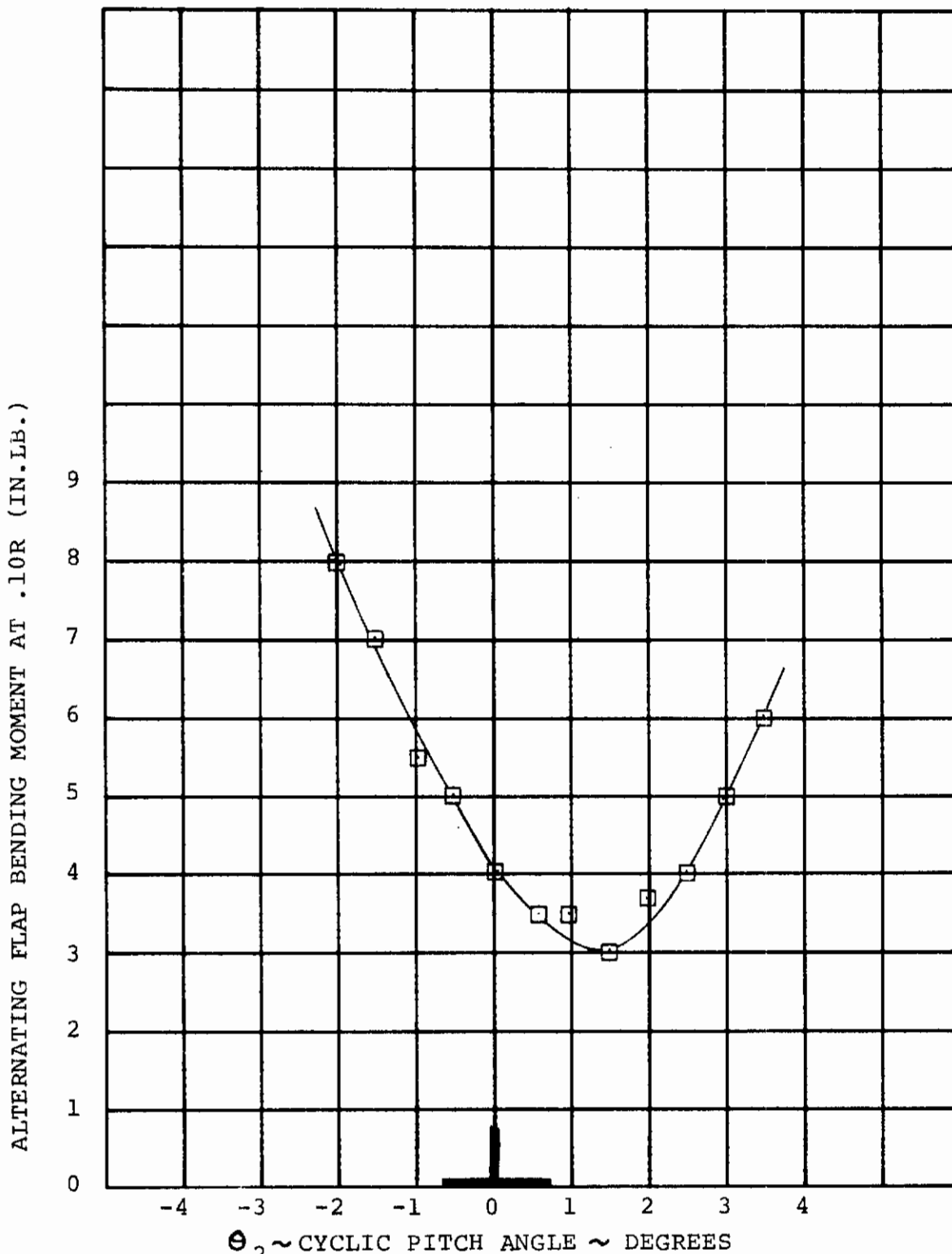
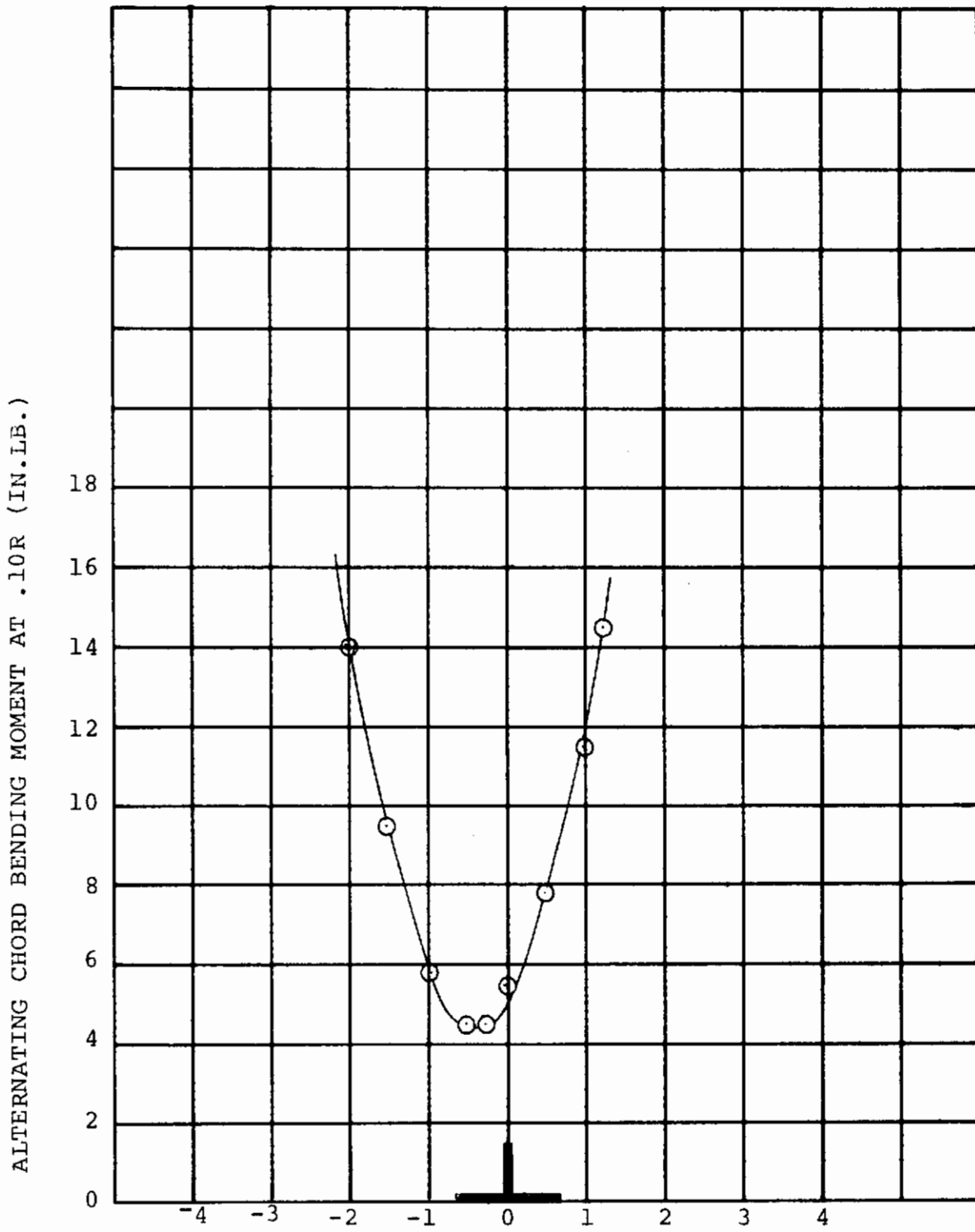


FIGURE 6-2. EFFECT OF CYCLIC PITCH ON RIGHT ROTOR ALTERNATING CHORD BENDING MOMENT IN HOVER IGE FOR $i_N = 90$ DEG., $\Theta_{.75} = 4.7$ DEG., AND 825 RPM RUN 61(16)

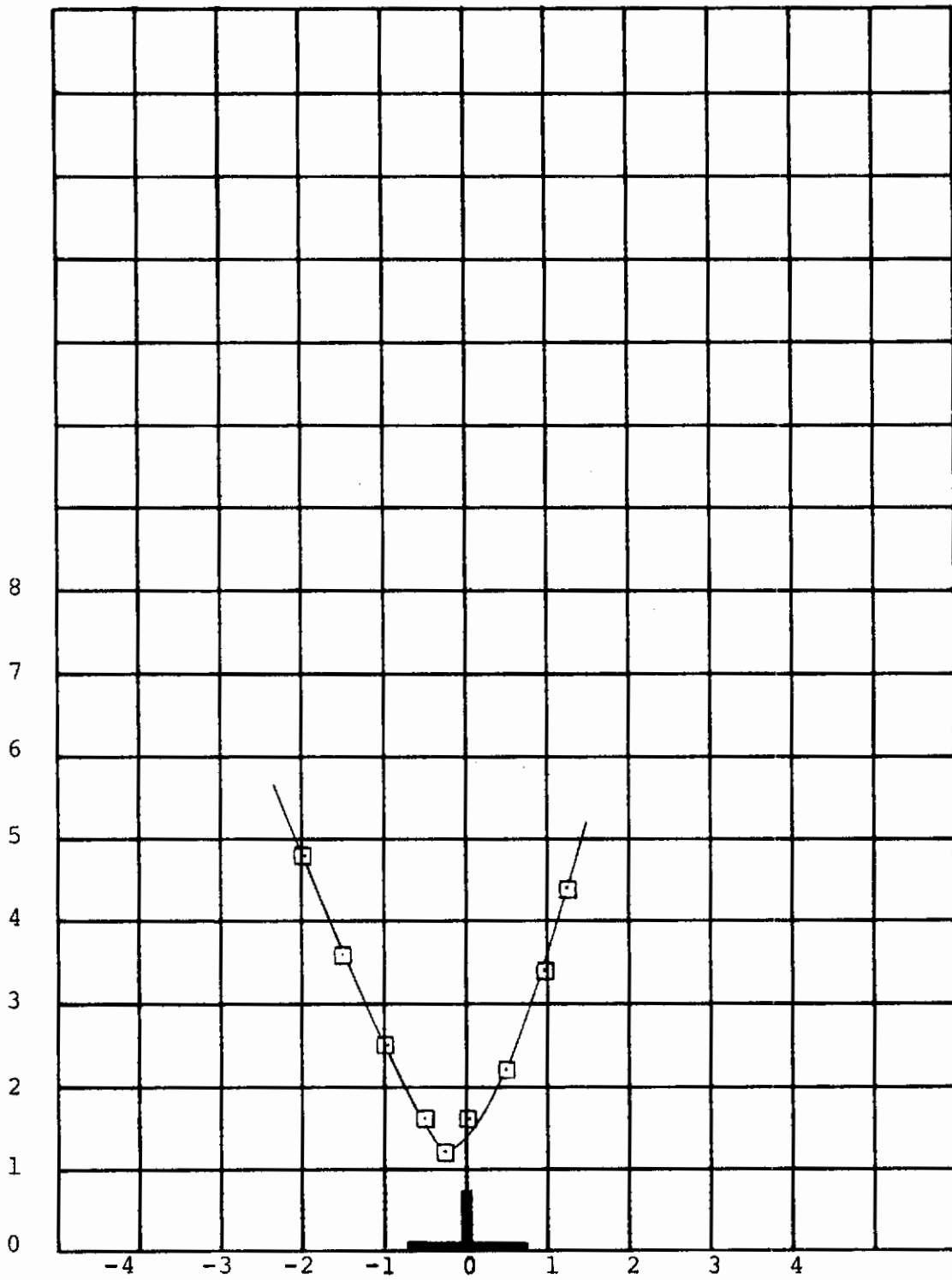


$\Theta_2 \sim$ CYCLIC PITCH ANGLE \sim DEGREES
 FIGURE 6-3. - EFFECT OF CYCLIC PITCH ON RIGHT ROTOR
 ALTERNATING FLAP BENDING MOMENT IN HOVER IGE FOR $i_N =$
 90 DEG., $\Theta_{.75} = 4.7$ DEG., AND 825 RPM.
 RUN 61(16)



$\Theta_2 \sim$ CYCLIC PITCH ANGLE ~ DEGREES
 FIGURE 6-4. - EFFECT OF CYCLIC PITCH ON RIGHT ROTOR
 ALTERNATING CHORD BENDING MOMENT IN HOVER OGE FOR $i_N =$
 90 DEG., $\Theta_{.75} = 4$ DEG, AND 750 RPM
 RUN 23(7) - UNBALANCED ROTOR

ALTERNATING FLAP BENDING MOMENT AT .10R (IN.LB.)



$\Theta_2 \sim$ CYCLIC PITCH ANGLE \sim DEGREES

FIGURE 6-5. - EFFECT OF CYCLIC PITCH ON RIGHT ROTOR ALTERNATING FLAP BENDING MOMENT IN HOVER OGE FOR $i_N = 90$ DEG., $\Theta_{.75} = 4$ DEG., AND 750 RPM.
 RUN 23(7) UNBALANCED ROTOR

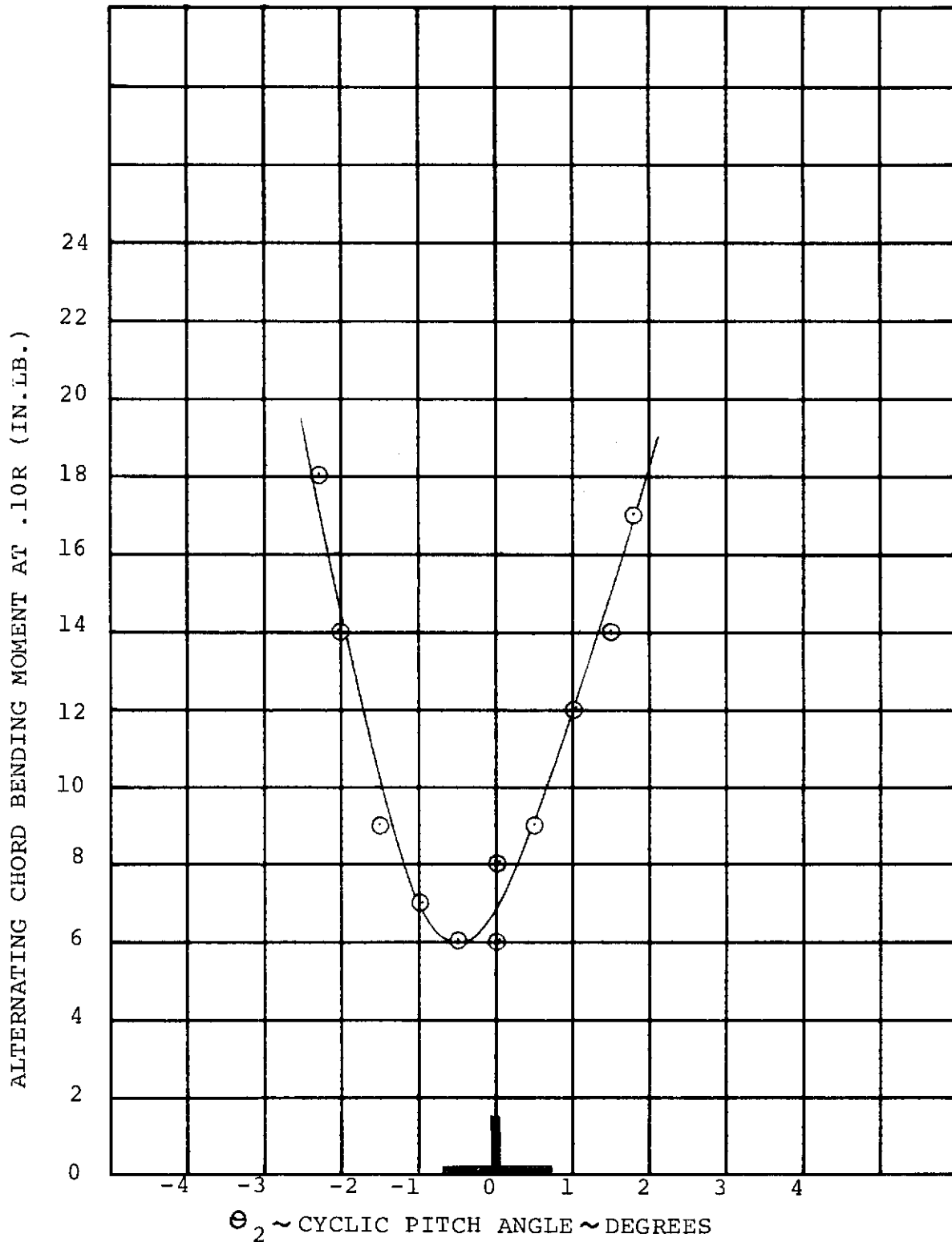


FIGURE 6-6. - EFFECT OF CYCLIC PITCH ON RIGHT ROTOR ALTERNATING CHORD BENDING MOMENT IN HOVER IGE FOR $i_N = 90$ DEG., $\theta_{.75} = 10.6$ DEG., AND 825 RPM.
RUN 61(3)

ALTERNATING FLAP BENDING MOMENT AT .10R (IN.LB.)

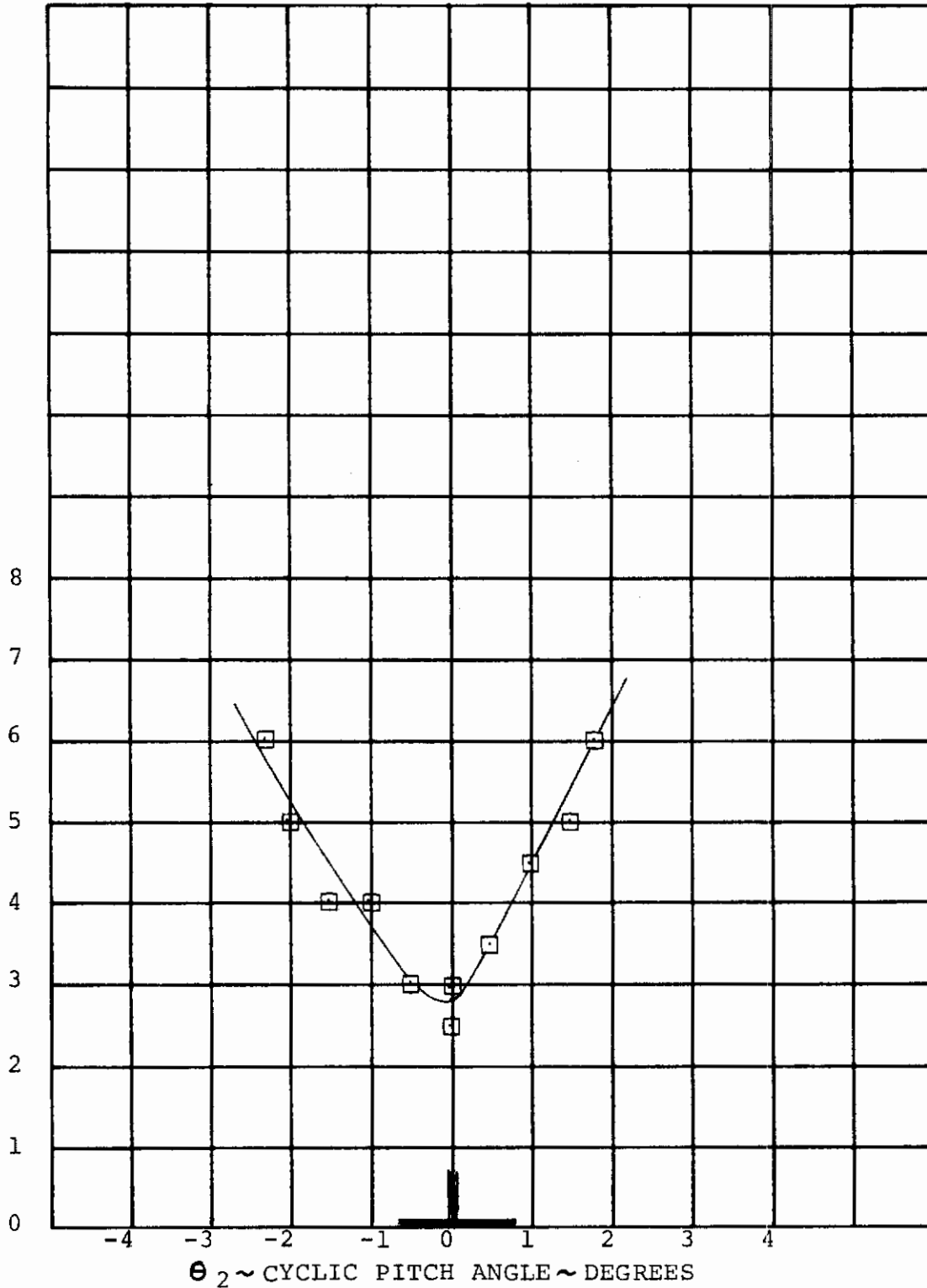


FIGURE 6-7. - EFFECT OF CYCLIC PITCH ON RIGHT ROTOR ALTERNATING FLAP BENDING MOMENT IN HOVER IGE FOR $i_N = 90$ DEG., $\Theta_{.75} = 10.6$ DEG., AND 825 RPM.
RUN 61(3)

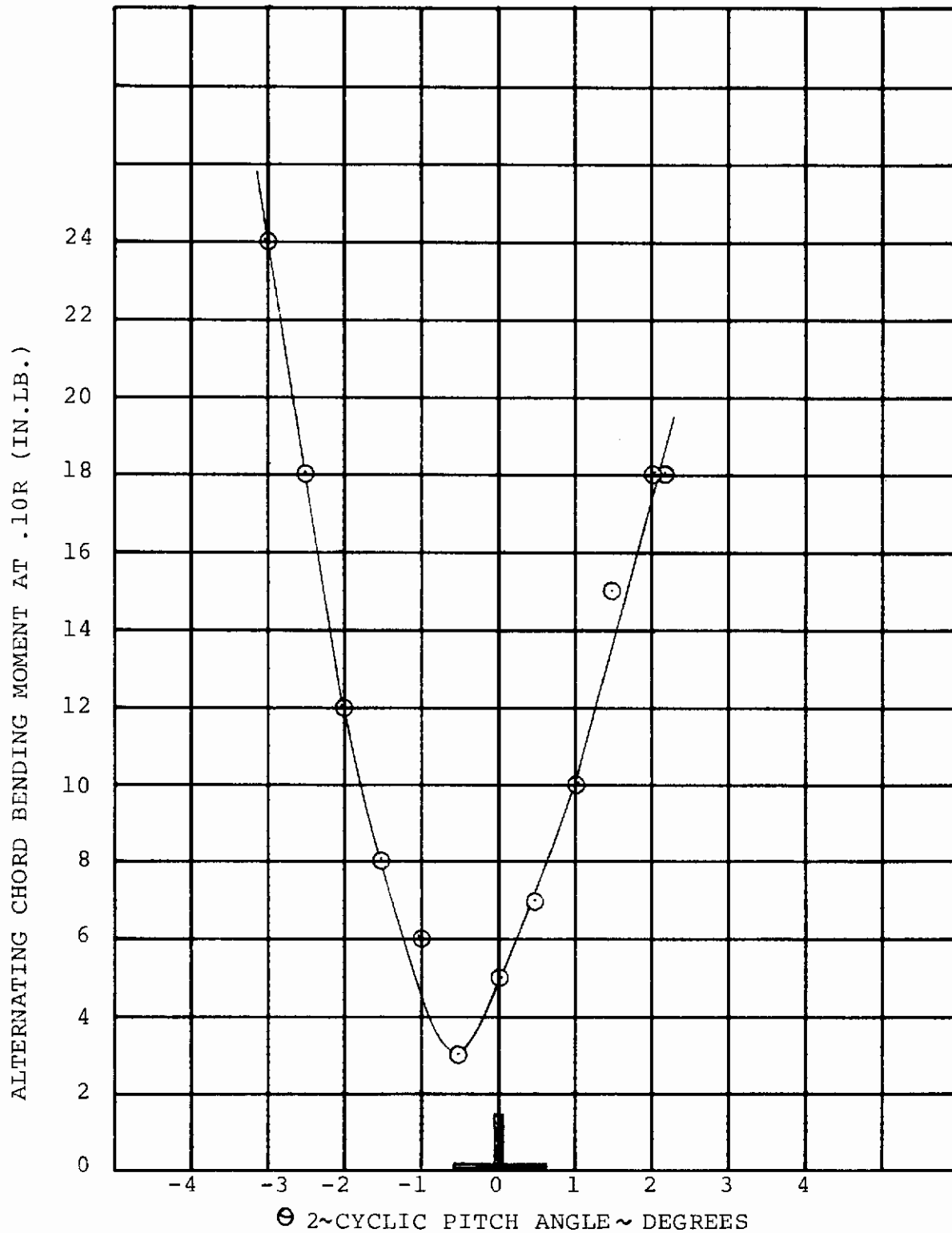


FIGURE 6-8. EFFECT OF CYCLIC PITCH ON RIGHT ROTOR ALTERNATING CHORD BENDING MOMENT IN HOVER OGE FOR $i_N=90$ DEG., $\Theta_{.75}=10.1$ DEG. AND 825 RPM.
RUN 65(12)

ALTERNATING FLAP BENDING MOMENT AT .10R (IN.LB.)

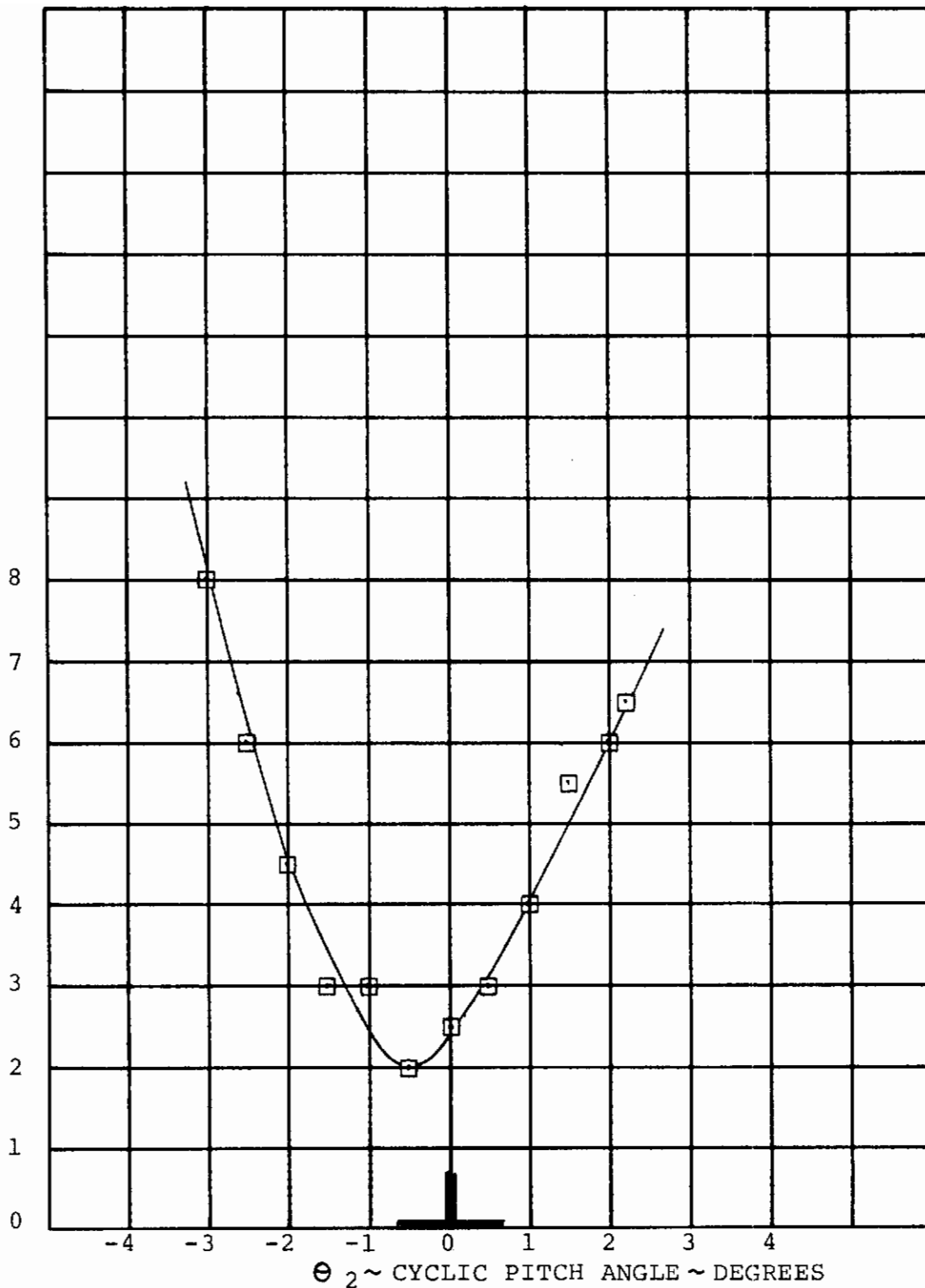


FIGURE 6-9. - EFFECT OF CYCLIC PITCH ON RIGHT ROTOR ALTERNATING FLAP BENDING MOMENT IN HOVER OGE FOR $i_N = 90$ DEG., $\Theta_{.75} = 10.1$ DEG., AND 825 RPM. RUN 65(12)

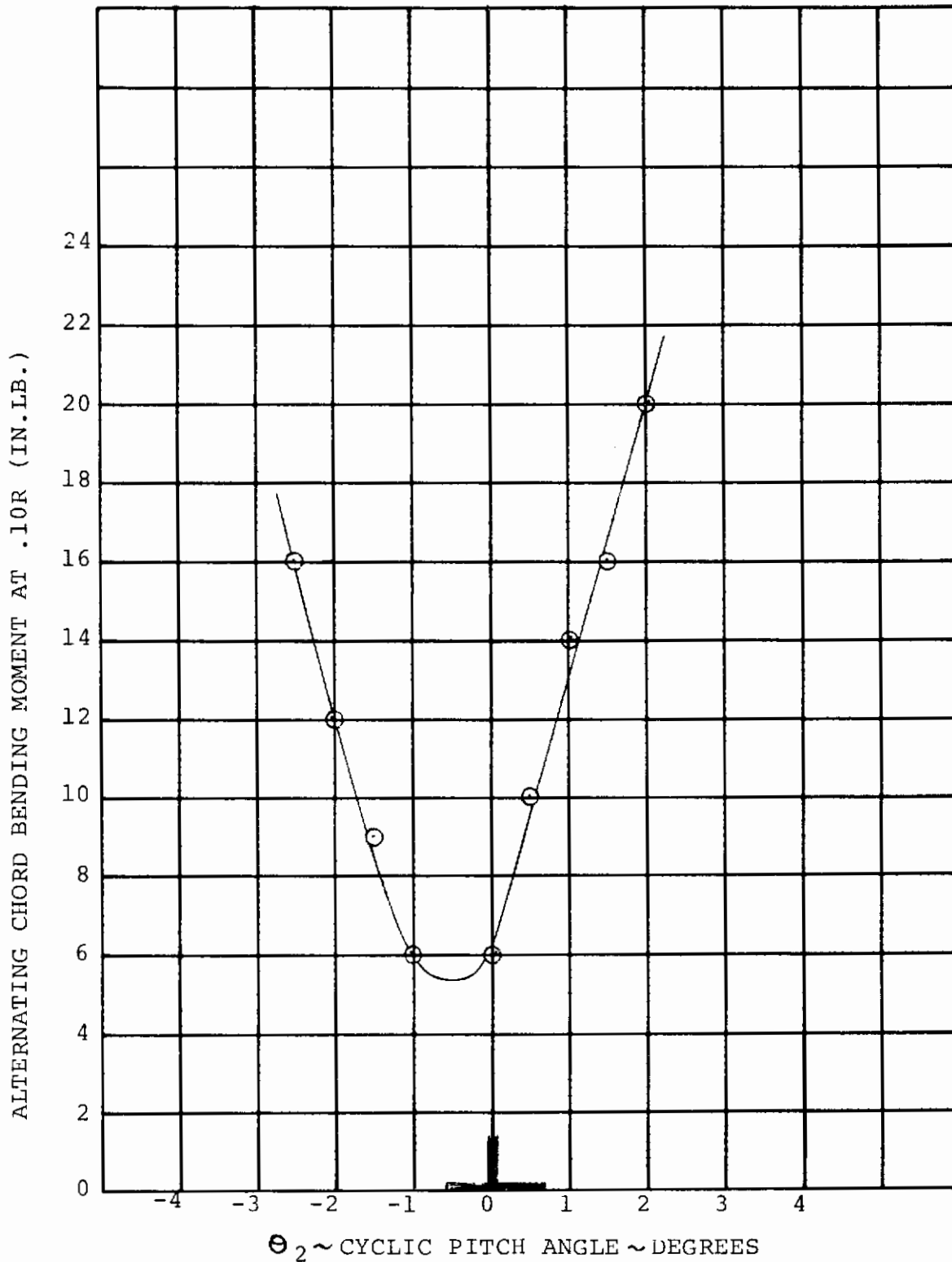


FIGURE 6-10. EFFECT OF CYCLIC PITCH ON RIGHT ROTOR ALTERNATING CHORD BENDING MOMENT IN HOVER IGE FOR $i_N = 90$ DEG., $\Theta_{.75} = 11$ DEG., AND 825 RPM.

RUN 62(17)

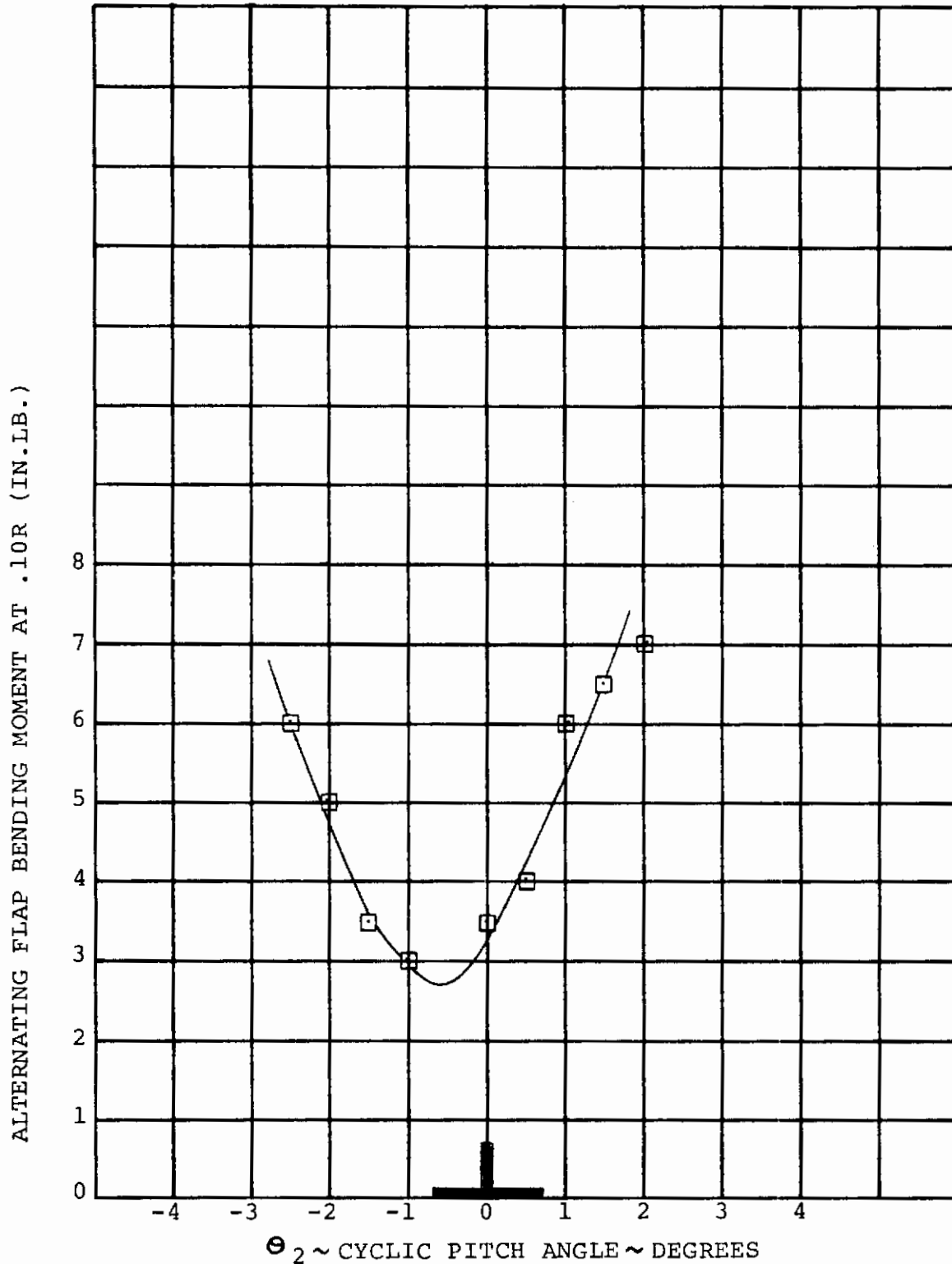


FIGURE 6-11. EFFECT OF CYCLIC PITCH ON RIGHT ROTOR ALTERNATING FLAP BENDING MOMENT IN HOVER IGE FOR $i_N = 90$ DEG., $\Theta_{.75} = 11$ DEG., AND 825 RPM. RUN 62(17)

Contrails

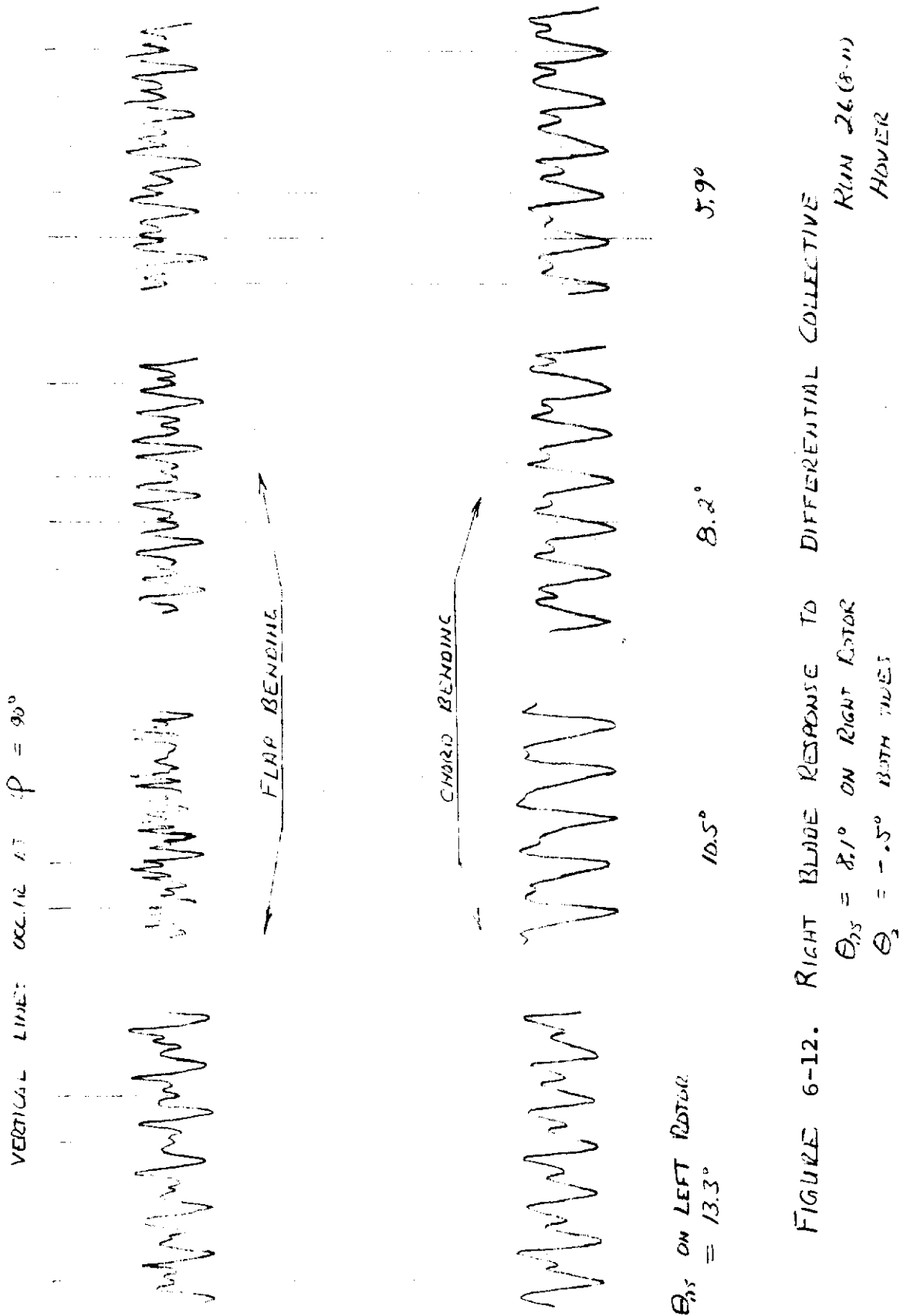


FIGURE 6-12. RIGHT BLADE RESPONSE TO DIFFERENTIAL COLLECTIVE

$\theta_{15} = 8.1^\circ$ ON RIGHT ROTOR

$\theta_2 = -0.5^\circ$ BOTH SIDES

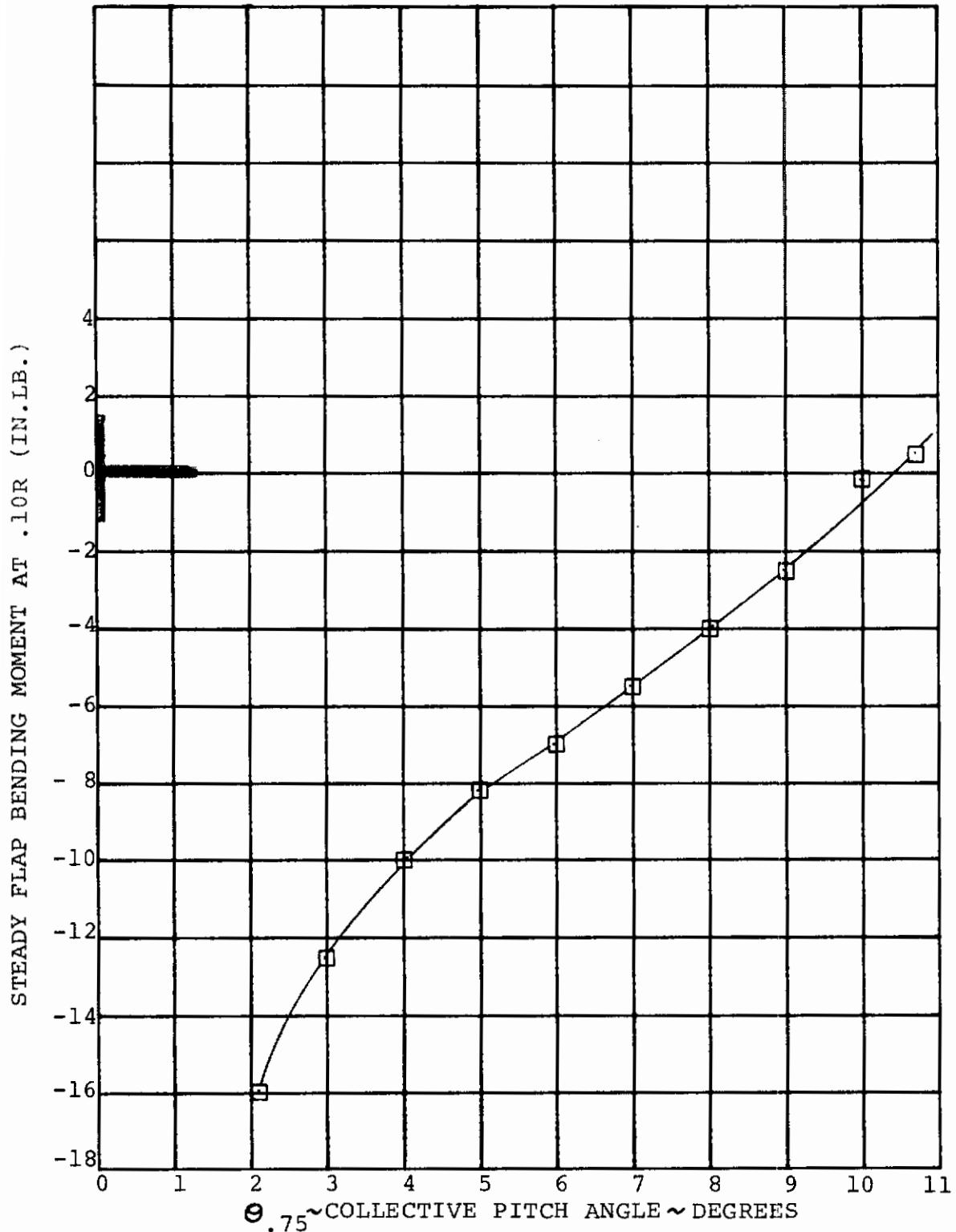


FIGURE 6-13. EFFECT OF COLLECTIVE PITCH ON RIGHT ROTOR STEADY FLAP BENDING MOMENT IN HOVER OGE FOR 90 DEG., $\theta_2 = -.75$ DEG., AND 750 RPM.
RUN 32(4)

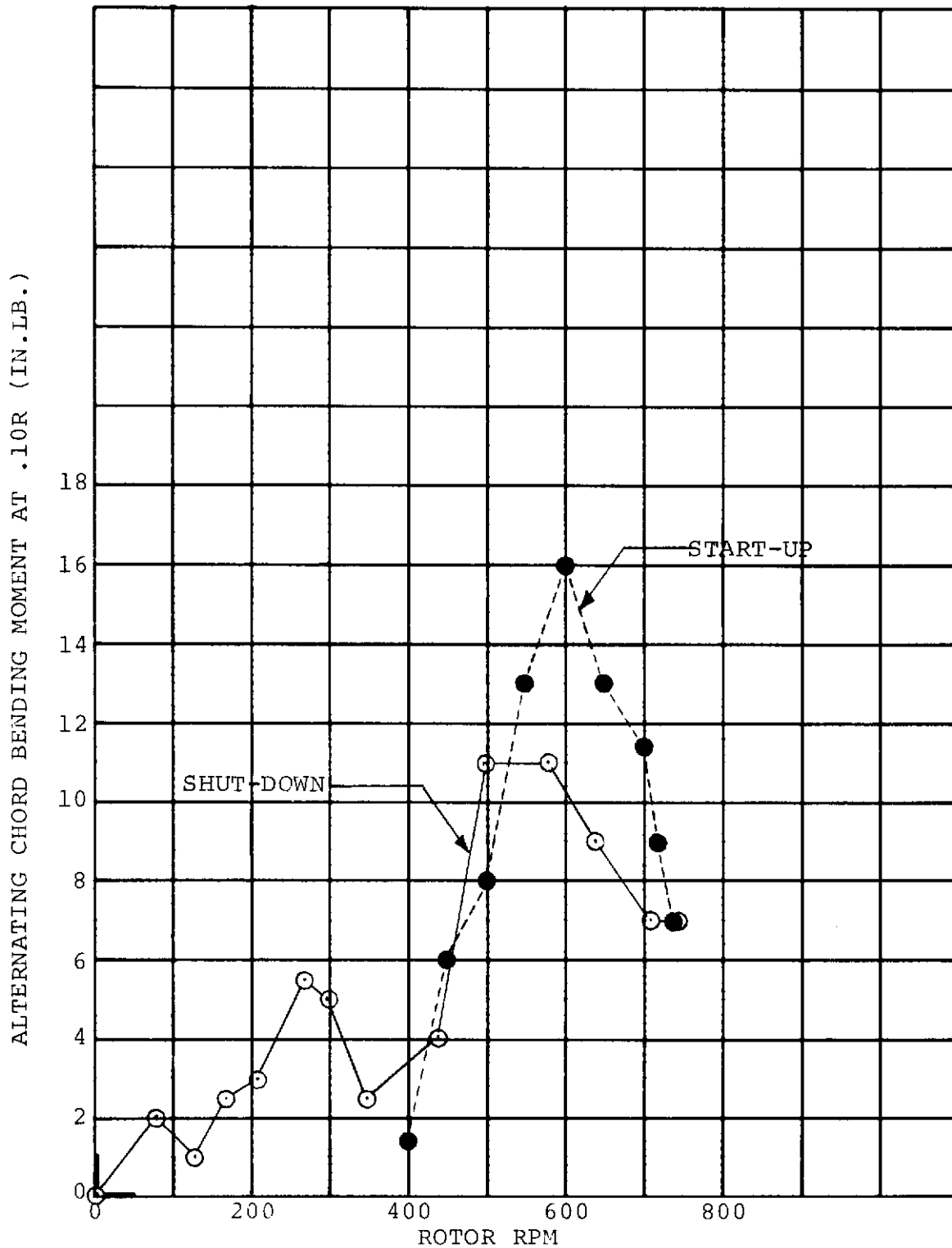


FIGURE 6-14. - EFFECT OF ROTOR START-UP AND SHUT-DOWN ON RIGHT HAND ALTERNATING CHORD BENDING MOMENT IN HOVER OGE FOR $i_N = 90$ DEG., $\theta_{.75} = 3.2$ DEG., AND $\theta_2 = 0$ DEG. RUN 24

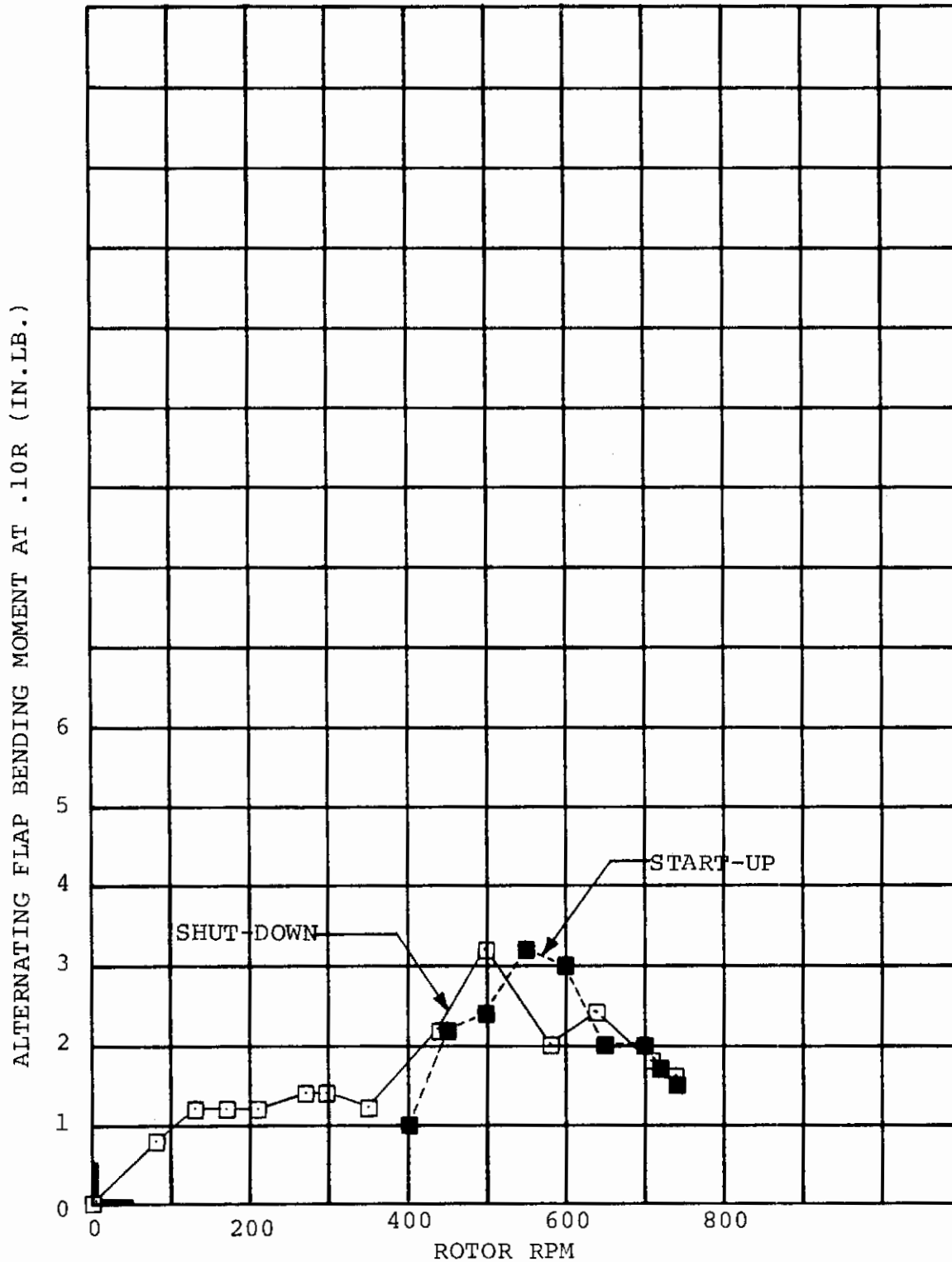


FIGURE 6-15. - EFFECT OF ROTOR START-UP AND SHUT-DOWN ON RIGHT HAND ALTERNATING FLAP BENDING MOMENT IN HOVER OGE FOR $i_N = 90$ DEG., $\theta_{.75} = 3.2$ DEG., AND $\theta_2 = 0$ DEG. RUN 24

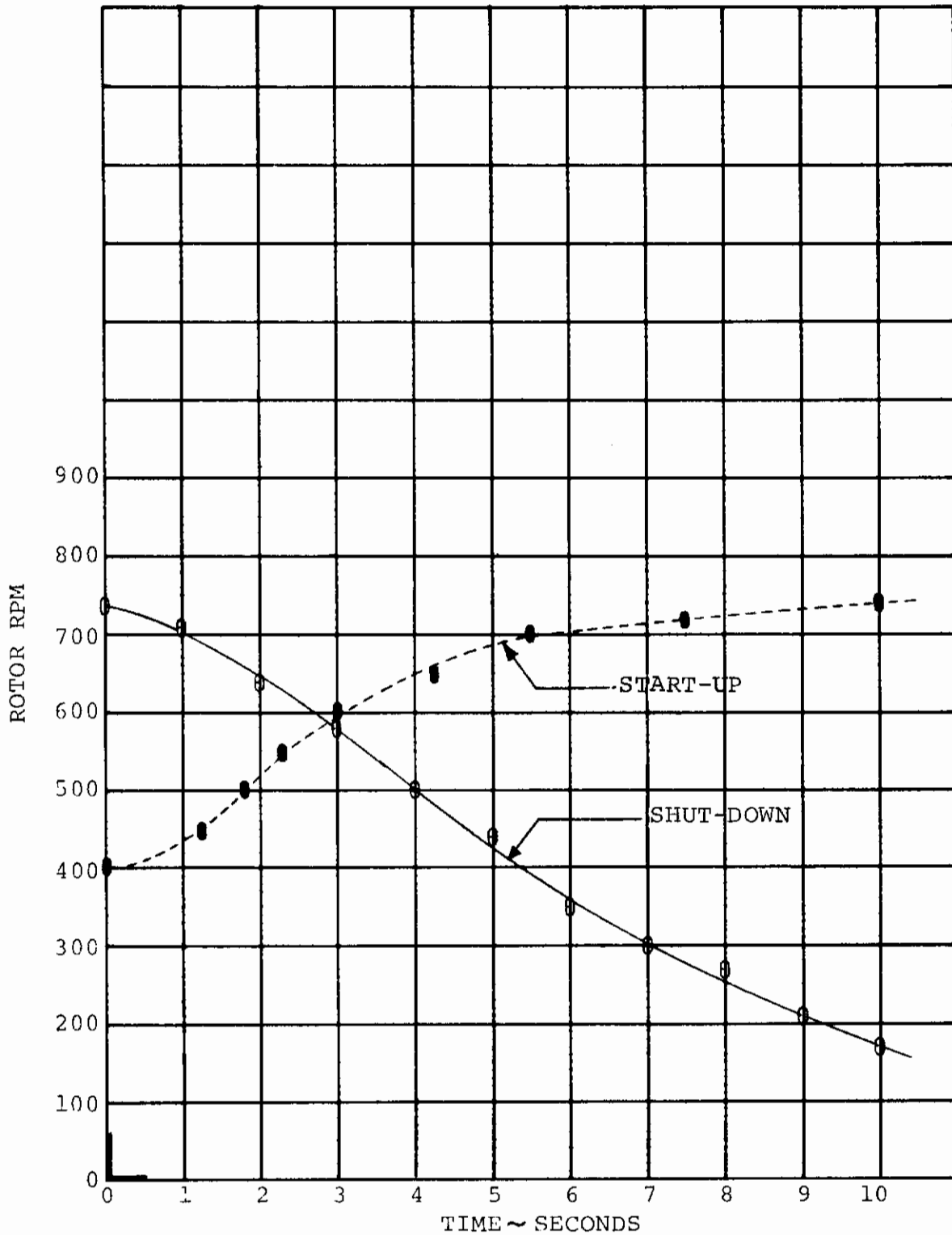


FIGURE 6-16.- ROTOR SPLED DURING START-UP AND SHUT-DOWN
IN HOVER OGE FOR $i_N = 90$ DEG., $\theta_{.75} = 3.2$ DEG., AND
 $\theta_2 = 0$ DEG. RUN 24

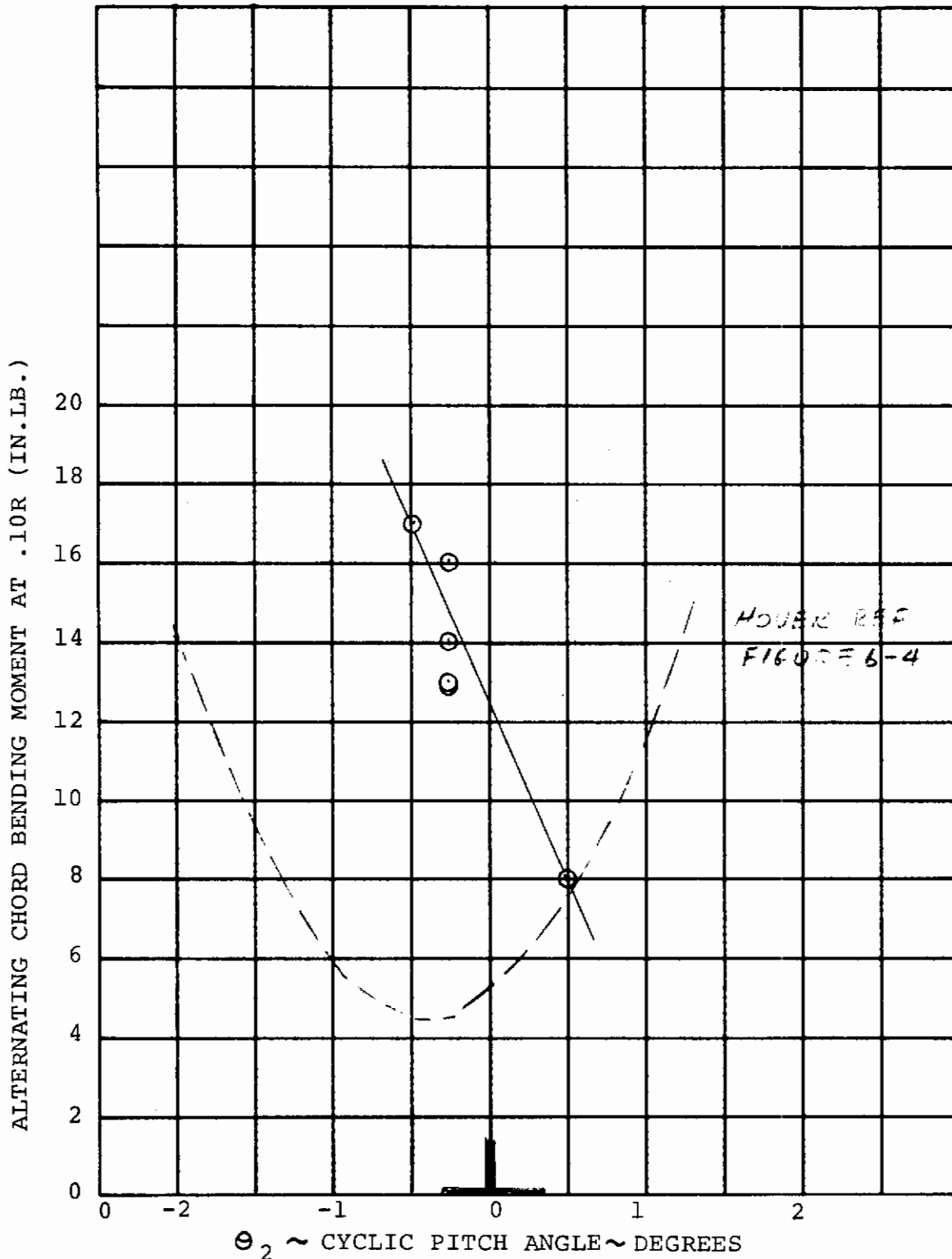


FIGURE 6-17. - EFFECT OF CYCLIC PITCH ON RIGHT ROTOR ALTERNATING CHORD BENDING MOMENT IN HOVER OGE FOR $i_N = 90$ DEG., $\theta_{.75} = 4$ DEG., 750 RPM, AND $q = 0.06$ PSF.
 RUN 33(2-6)

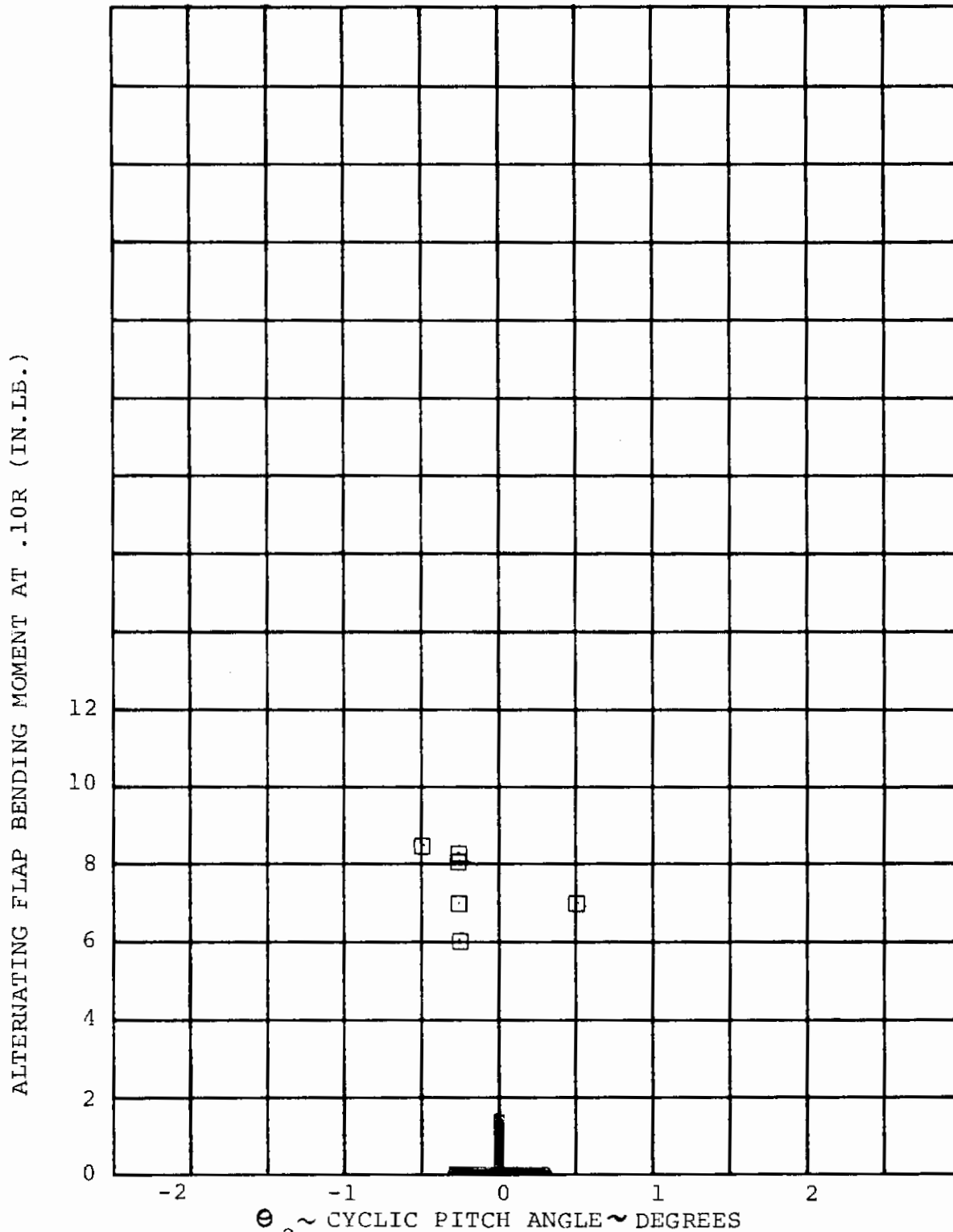


FIGURE 6-18. - EFFECT OF CYCLIC PITCH ON RIGHT ROTOR ALTERNATING FLAP BENDING MOMENT IN HOVER OGE FOR $i_N = 90$ DEG., $\theta_{.75} = 4$ DEG., 750 RPM, & $q = 0.06$ PSF.

RUN 33(2-6)

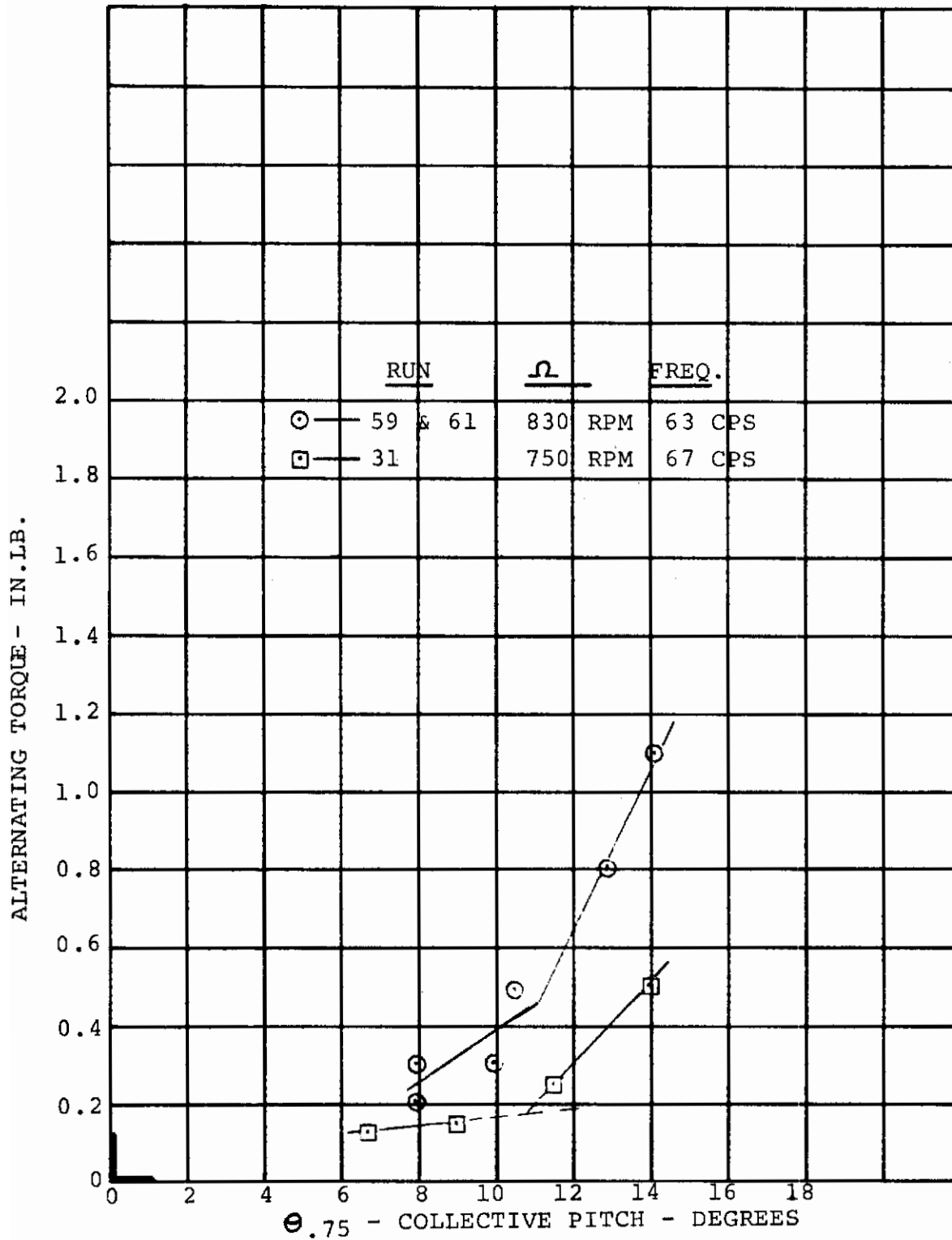


FIGURE 6-19.- EFFECT OF COLLECTIVE PITCH ON BLADE TORSION RESPONSE IN HOVER FOR $i_N = 90$ DEG., & $\theta_2 = 0$ DEG.

Contrails

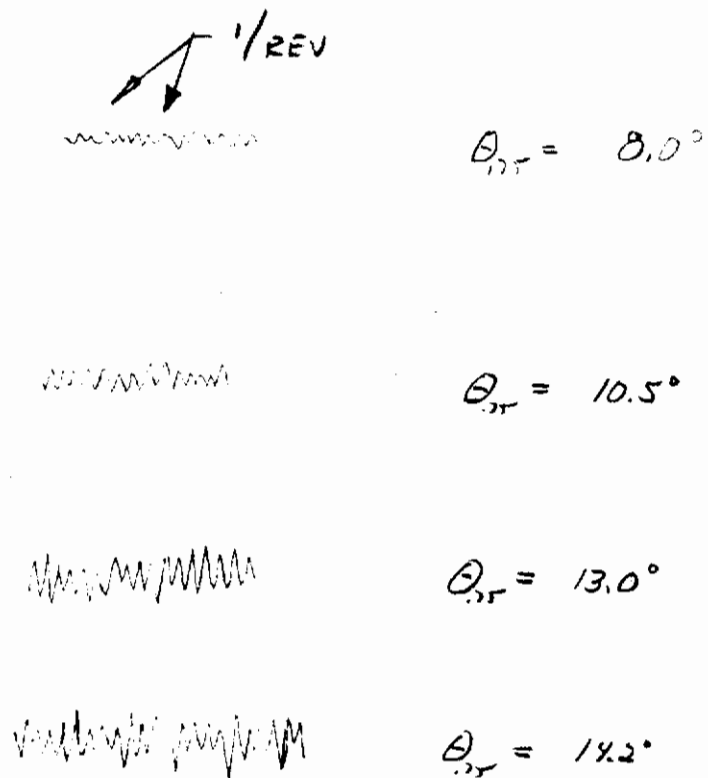


FIGURE 6-20. EFFECT OF COLLECTIVE PITCH ON
BLADE TORSION AMPLITUDE

-RIGHT BLADE .15R

$\Omega = 830$ RPM

RUN 6D-61

HOVER

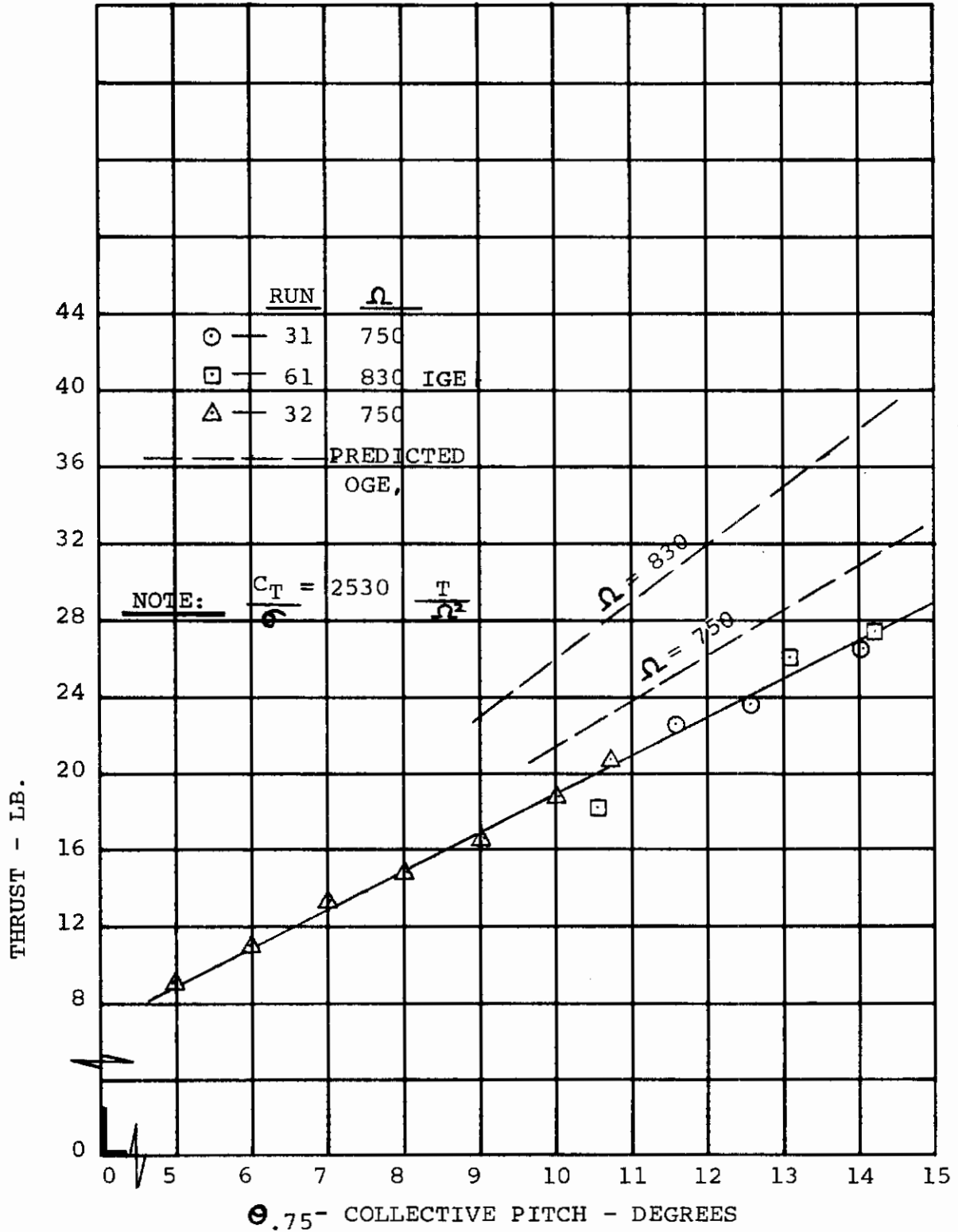


FIGURE 6-21. ROTOR THRUST — DETERMINED FROM WING STEADY FLAP BENDING MOMENT - RIGHT SIDE - HOVER

6.2 TRANSITION BLADE LOADS

Blade loads data were taken in transition at two nacelle tilt angles, 60 degrees and 40 degrees, to determine the effect of cyclic pitch, dynamic pressure, collective pitch and model pitch and yaw. Test results show that for each nacelle tilt, collective pitch and dynamic pressure, there is a value of positive cyclic pitch at which alternating chord bending loads are minimized. Decreasing the cyclic pitch angle increases the flap bending moments. For a constant nacelle tilt and collective pitch, increased dynamic pressure increased the minimum value of alternating chord bending. Increased collective pitch decreased the minimum value of chord bending. Model pitch and model yaw caused large changes in alternating chord bending with little effect on alternating flap bending.

6.2.1 Effect of Cyclic Pitch

The blade alternating flap and chord bending load data for nacelle tilt angles of 60° and 40° are presented in Figures 6-22 through 6-31 for cyclic pitch variations. Alternating torsion loads remained small throughout this series of tests. The effect of increasing dynamic pressure is shown in Figures 6-22, 6-24 and 6-26 to increase the minimum alternating chord bending load (cyclic bucket) for $i_N = 60^\circ$. Note, however, that in Figure 6-22 for $\beta = 9.8^\circ$ (Run 39), higher alternating loads occurred at $q = 0.2$ psf than at other q values. The loads at the $.2q$ value are suspected to be caused by the recirculation of the tip vortices with the rotor blades. This has also been found in other tests on both tilt rotor and helicopter rotor models. At this point the blade alternating chord load was composed primarily of 1 per rev response whereas 2 per rev was prominent at other points for this run. Figure 6-22 also shows that with increasing dynamic pressure, the value of cyclic pitch at which the minimum blade chord bending loads occur increases. These trends are summarized in Figure 6-28 which also shows that increasing collective pitch decreases the minimum (bucket) value of chord bending load.

The flap bending load is shown in Figure 6-23 to increase with increasing dynamic pressure. An apparent "bucket" also exists for flap bending alternating loads, the trend of which is similar to that for chord bending but it occurs at a higher value of cyclic than that for chord bending and was obtained during the test for $q = 0$, and 0.5 psf only.

Contrails

Figures 6-29, 6-30 and 6-31 show the trend of blade alternating loads with cyclic for $i_N = 40^\circ$ which are similar to those for $i_N = 60^\circ$.

6.2.2 Effect of Model Yaw

Figures 6-32 through 6-37 show the effect of model yaw on blade loads for 60 and 40 degrees nacelle tilt. Chord bending loads increased as the model was yawed to the right from zero and decreased as the model was yawed to the left from zero. When the right rotor is yawed to the left, the angle of attack on the advancing side of the disc is decreased, thus decreasing flapping and the resulting blade loads. Flapwise loads showed the same result but the sensitivity of alternating flap bending to changes in model yaw is much less than chord bending sensitivity due to the large amount of flapwise aerodynamic damping.

6.2.3 Effect of Model Pitch

Figures 6-38 through 6-41 show the effect of model pitch on blade loads in transition at 60 and 40 degrees nacelle tilt. At both nacelle tilts, alternating chord bending decreased and flap bending increased as the model was pitched nose up. Increasing model pitch has the same effect as increasing the cyclic pitch angle on the advancing side of the disc and the results are the same as those shown in Section 6.2.1. If model pitch had been increased more, the chord bending loads would have reached a minimum and then increased as they did in Section 6.2.1 when cyclic was varied.

6.2.4 Stall Flutter - Transition

In the transition regime for $i_N = 60^\circ$, blade torsion wave traces showed that the amplitude at its torsional frequency increases with increasing dynamic pressure. This is shown in Figure 6-42. Effects of collective and cyclic pitch are involved, however, and are not isolated from these data. Blade torsion wave shapes for two dynamic pressure conditions in Figure 6-42 are shown in Figure 6-43. Note the input at $\psi = 90^\circ$ (advancing side) which induces the torsional frequency. The blade torsional frequency response was also sensitive to the combined influence of fuselage pitch and yaw displacements as shown in Figure 6-44 for $i_N = 40^\circ$.

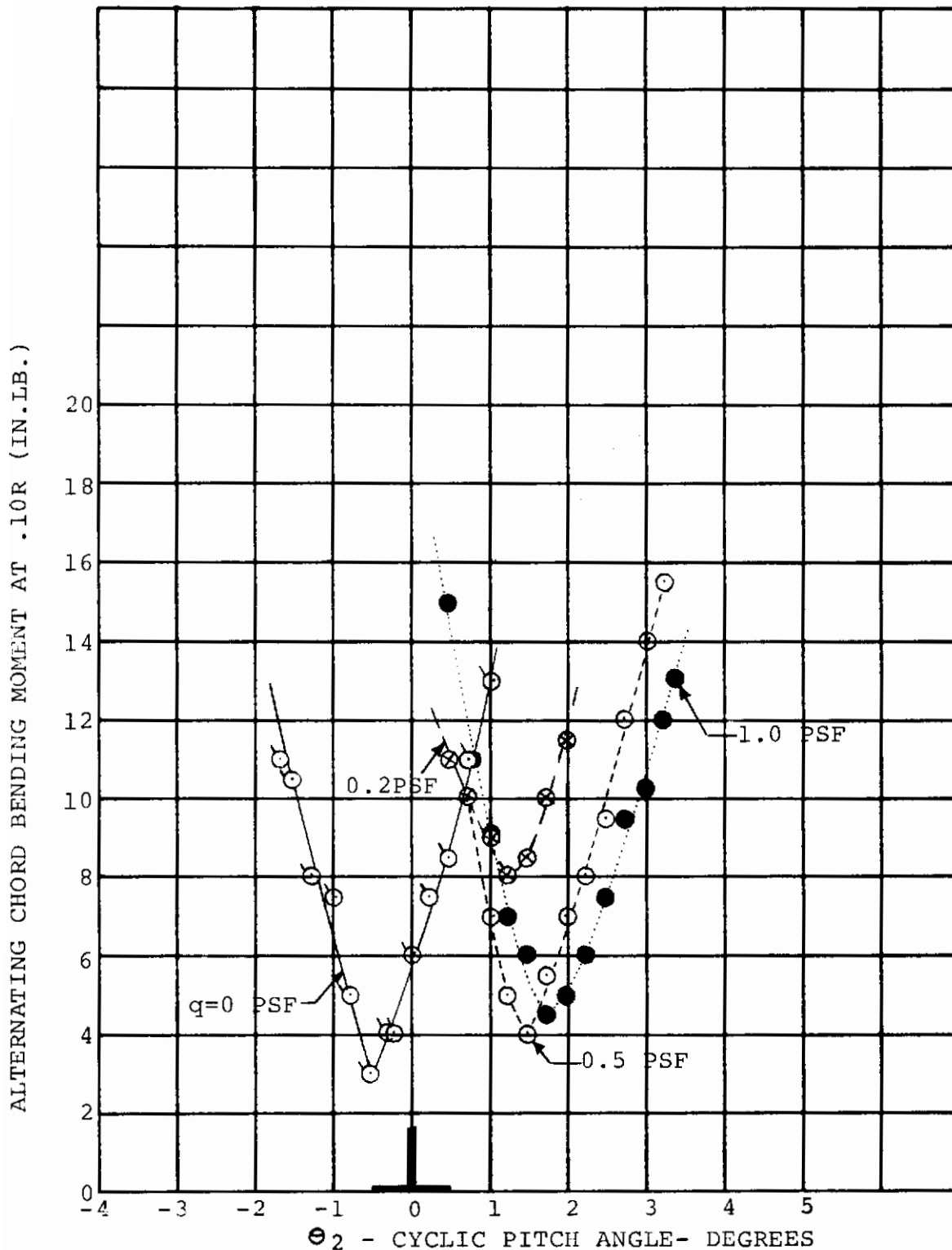


FIGURE 6-22 EFFECT OF DYNAMIC PRESSURE ON RIGHT ROTOR ALTERNATING CHORD BENDING MOMENT IN TRANSITION FOR $i_N = 60$ DEG., $\Theta_{.75} = 9.8$ DEG., AND 790 RPM. RUN 39 (6,8,9,12)

ALTERNATING FLAP BENDING MOMENT AT .10R (IN.LB.)

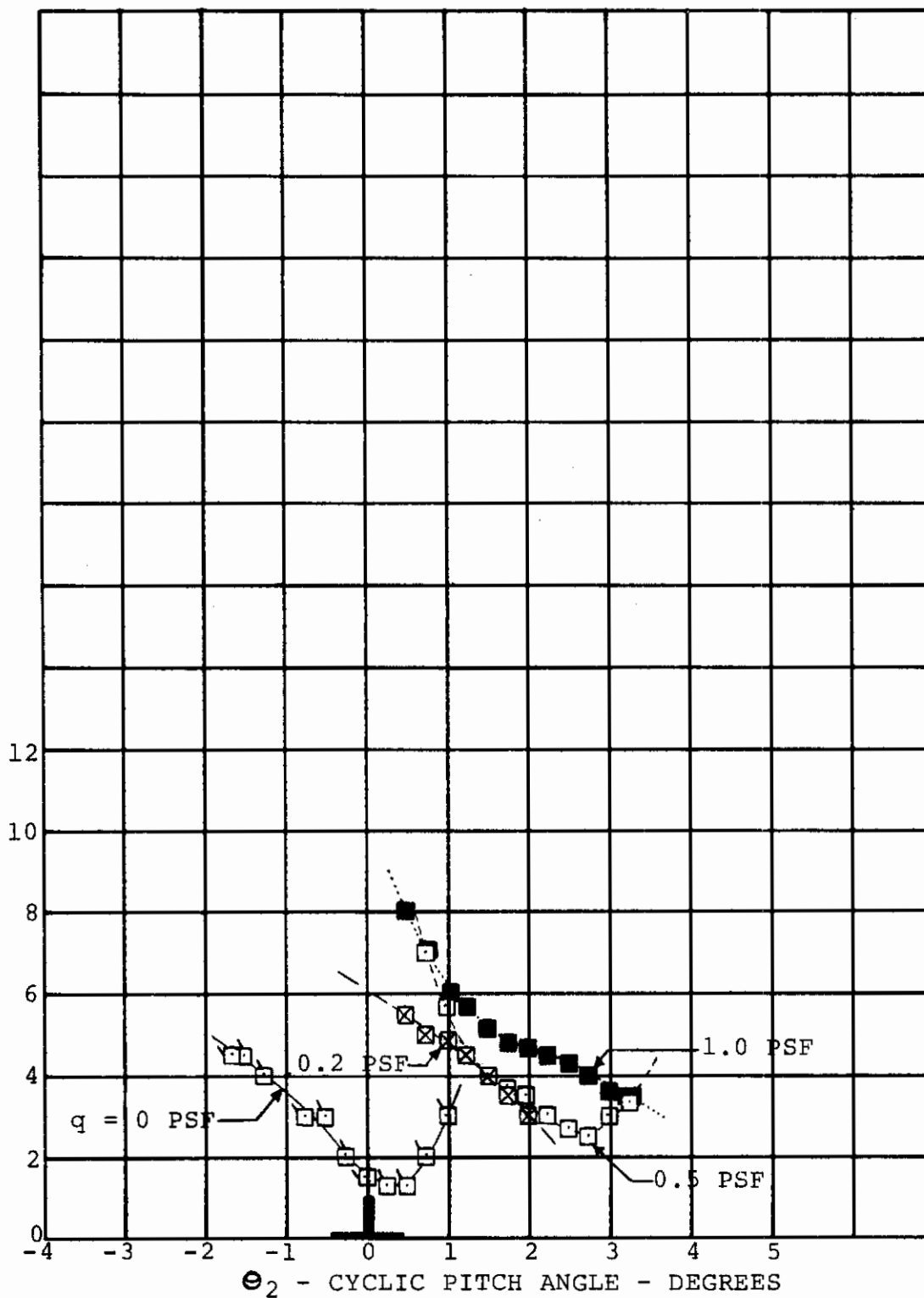


FIGURE 6-23 EFFECT OF DYNAMIC PRESSURE ON RIGHT ROTOR ALTERNATING FLAP BENDING MOMENT IN TRANSITION FOR $i_N = 60$ DEG., $\Theta_{.75} = 9.8$ DEG., AND 790 RPM. RUN 39 (6,8,9,12)

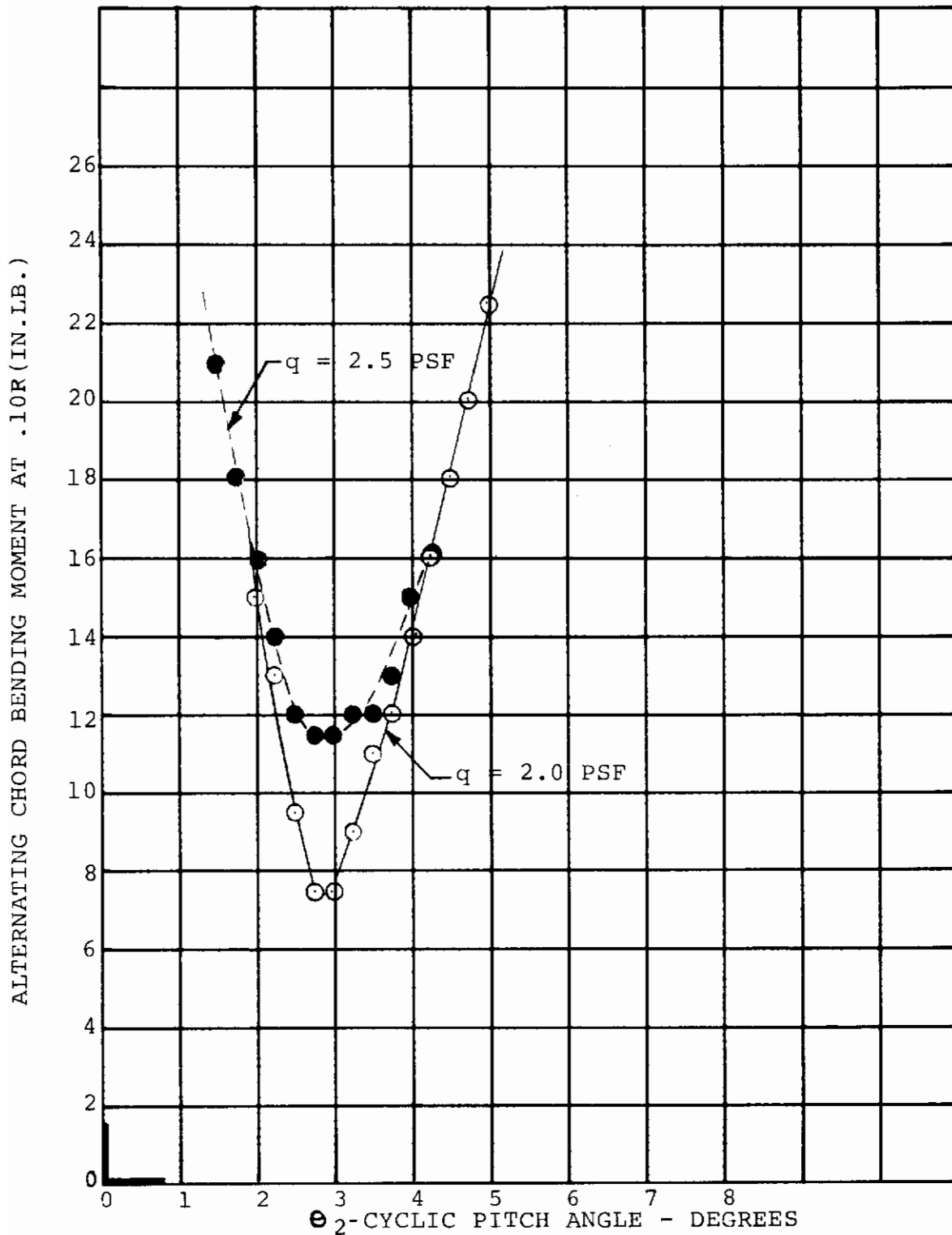


FIGURE 6-24. EFFECT OF DYNAMIC PRESSURE ON RIGHT ROTOR ALTERNATING CHORD BENDING MOMENT IN TRANSITION FOR $i_N = 60$ DEG., $\theta_{.75} = 14.2$ DEG., AND 790 RPM.
RUN 41(8,12)

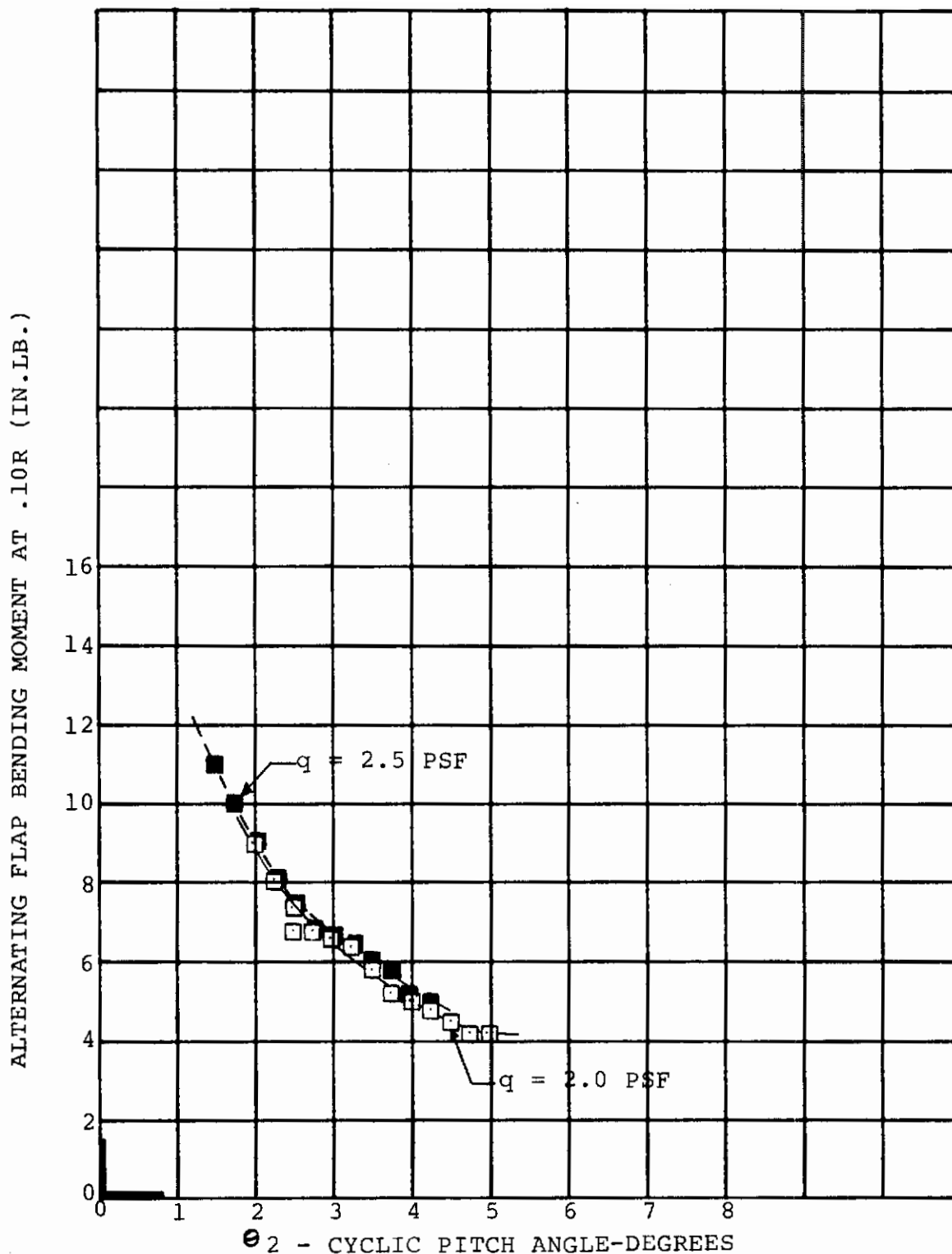


FIGURE 6-25. EFFECT OF DYNAMIC PRESSURE ON RIGHT ROTOR ALTERNATING FLAP BENDING MOMENT IN TRANSITION FOR $i_N = 60$ DEG., $\theta_{.75} = 14.2$ DEG., AND 790 RPM.
RUN 41(8,12)

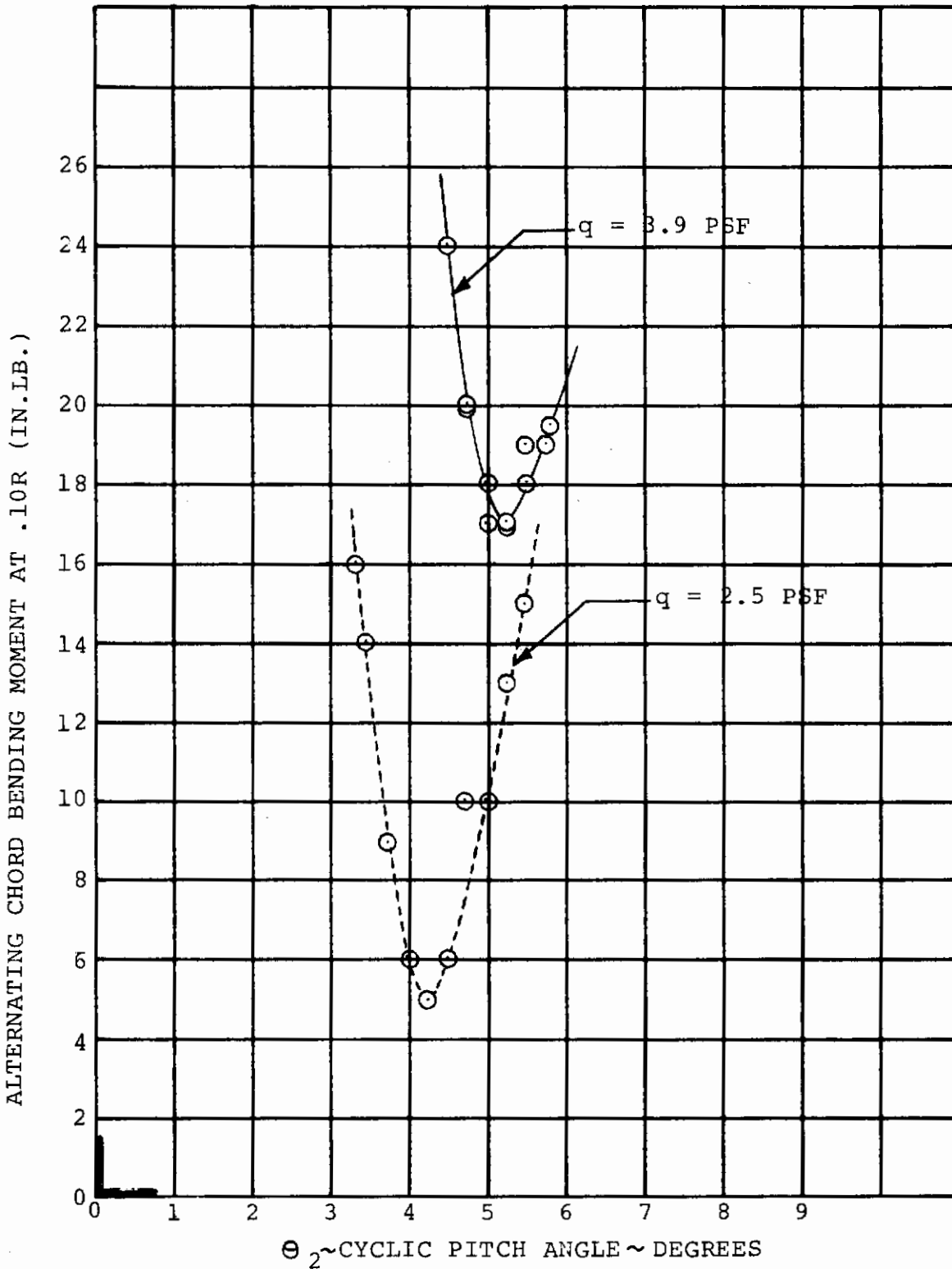


FIGURE 6-26. EFFECT OF DYNAMIC PRESSURE ON RIGHT ROTOR ALTERNATING CHORD BENDING MOMENT IN TRANSITION FOR $i_N = 60$ DEG., $\Theta_{.75} = 16$ DEG., AND 790 RPM. RUN 41(17,24)

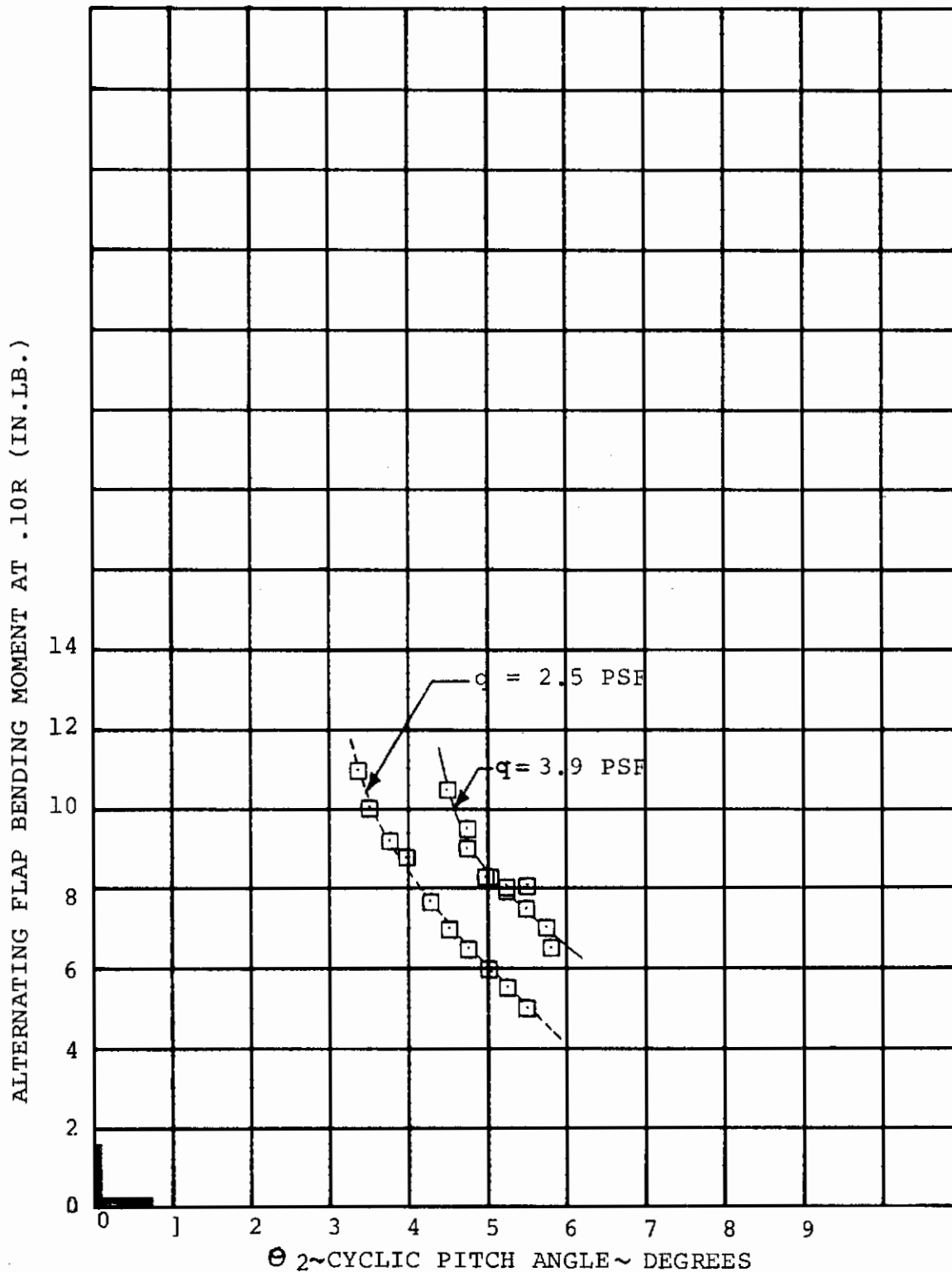


FIGURE 6-27. EFFECT OF DYNAMIC PRESSURE ON RIGHT ROTOR ALTERNATING FLAP BENDING MOMENT IN TRANSITION FOR $i_N = 60$ DEG., $\theta_{.75} = 16$ DEG., AND 790 RPM. RUN 41(17,24)

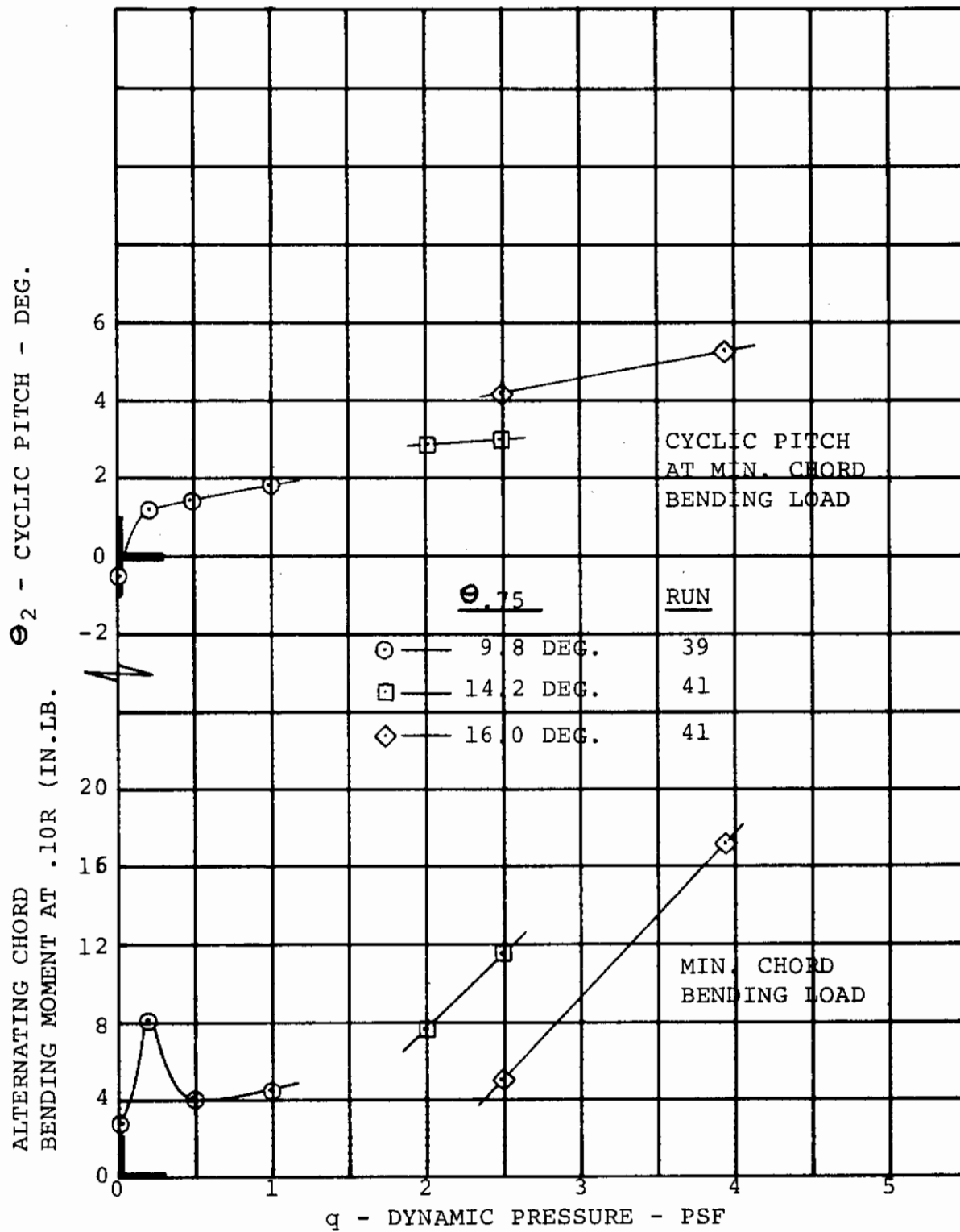


FIGURE 6-28. EFFECT OF DYNAMIC PRESSURE ON BLADE MINIMUM ALTERNATING CHORD BENDING LOAD IN TRANSITION FOR $i_N = 60$ DEG.

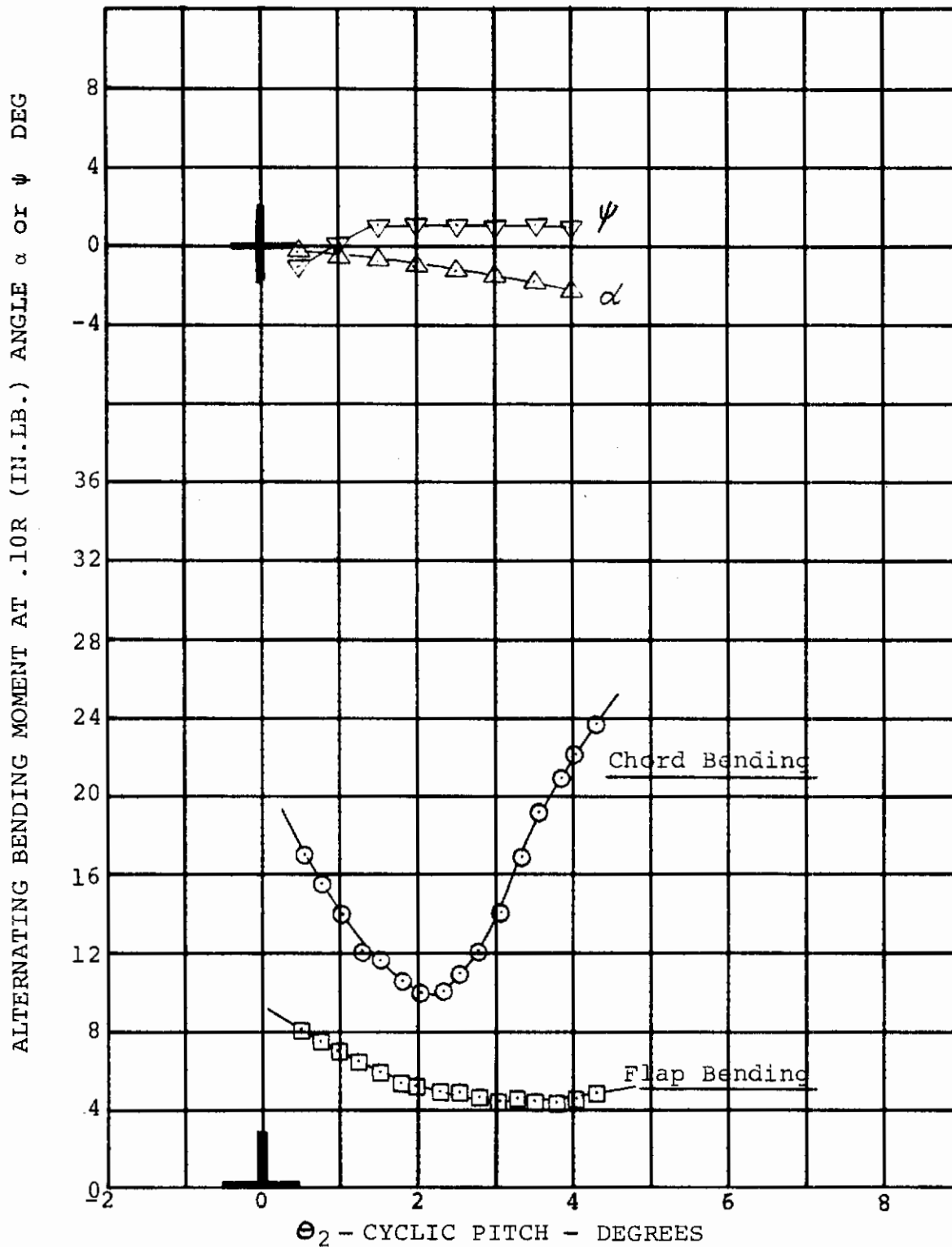


FIGURE 6-29. EFFECT OF CYCLIC PITCH ON RIGHT HAND BLADE ALTERNATING LOADS IN TRANSITION - $i_N = 40$ DEG., $\theta_{.75} = 16.2$ DEG., $q = 2.0$ PSF, AND $\Omega = 790$ RPM - RUN 43(3)

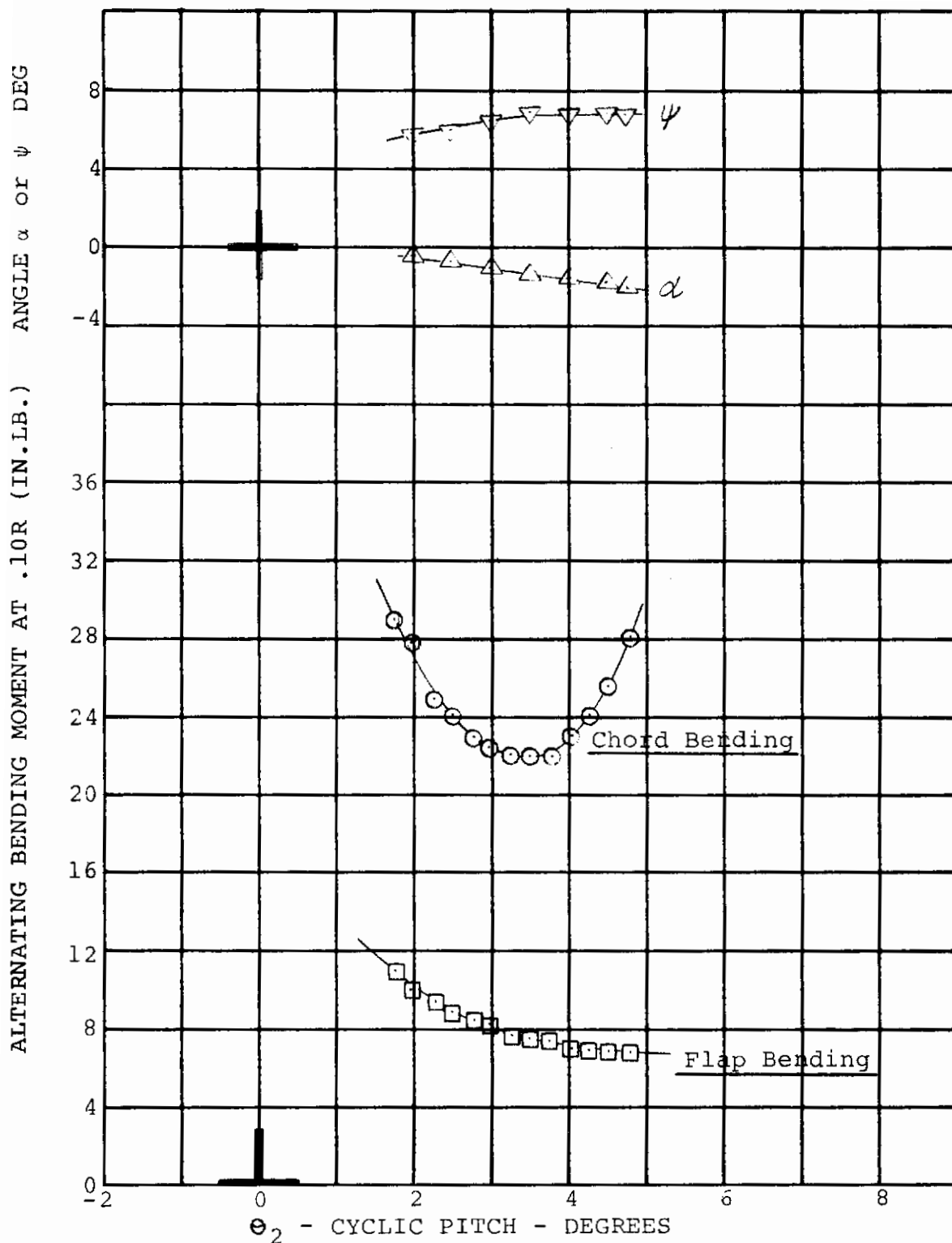


FIGURE 6-30. EFFECT OF CYCLIC PITCH ON RIGHT HAND BLADE ALTERNATING LOADS IN TRANSITION - $i_N = 40$ DEG., $\theta_{75} = 20.0$ DEG., $q = 4.0$ PSF, AND $\Omega = 790$ RPM - RUN 43(8)

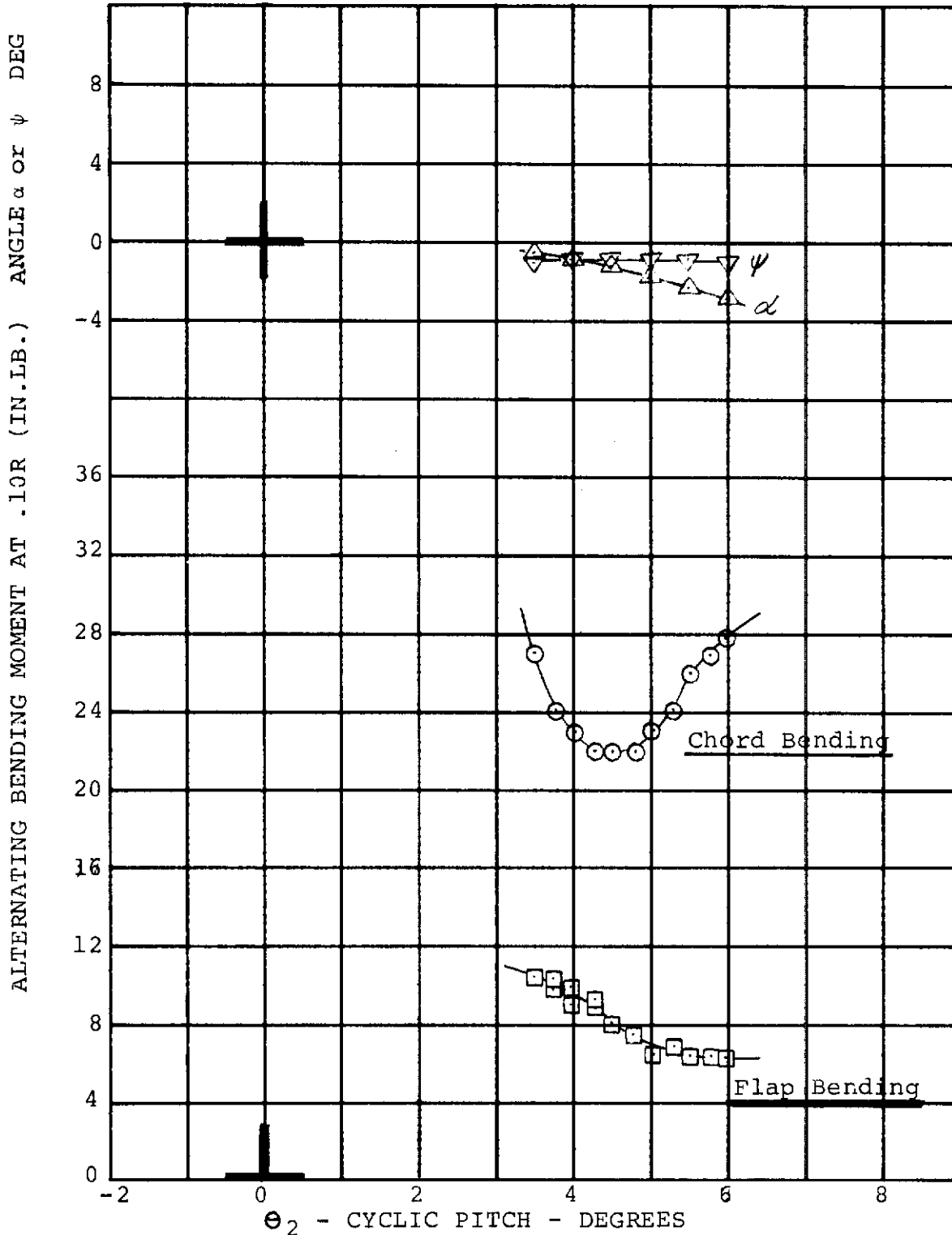


FIGURE 6-31. EFFECT OF CYCLIC PITCH ON RIGHT HAND BLADE ALTERNATING LOADS IN TRANSITION $-i_N = 40$ DEG., $\Theta_{.75} = 23$ DEG., $q = 5.25$ PSF, AND $\Omega = 790$ RPM - RUN 43 (14)

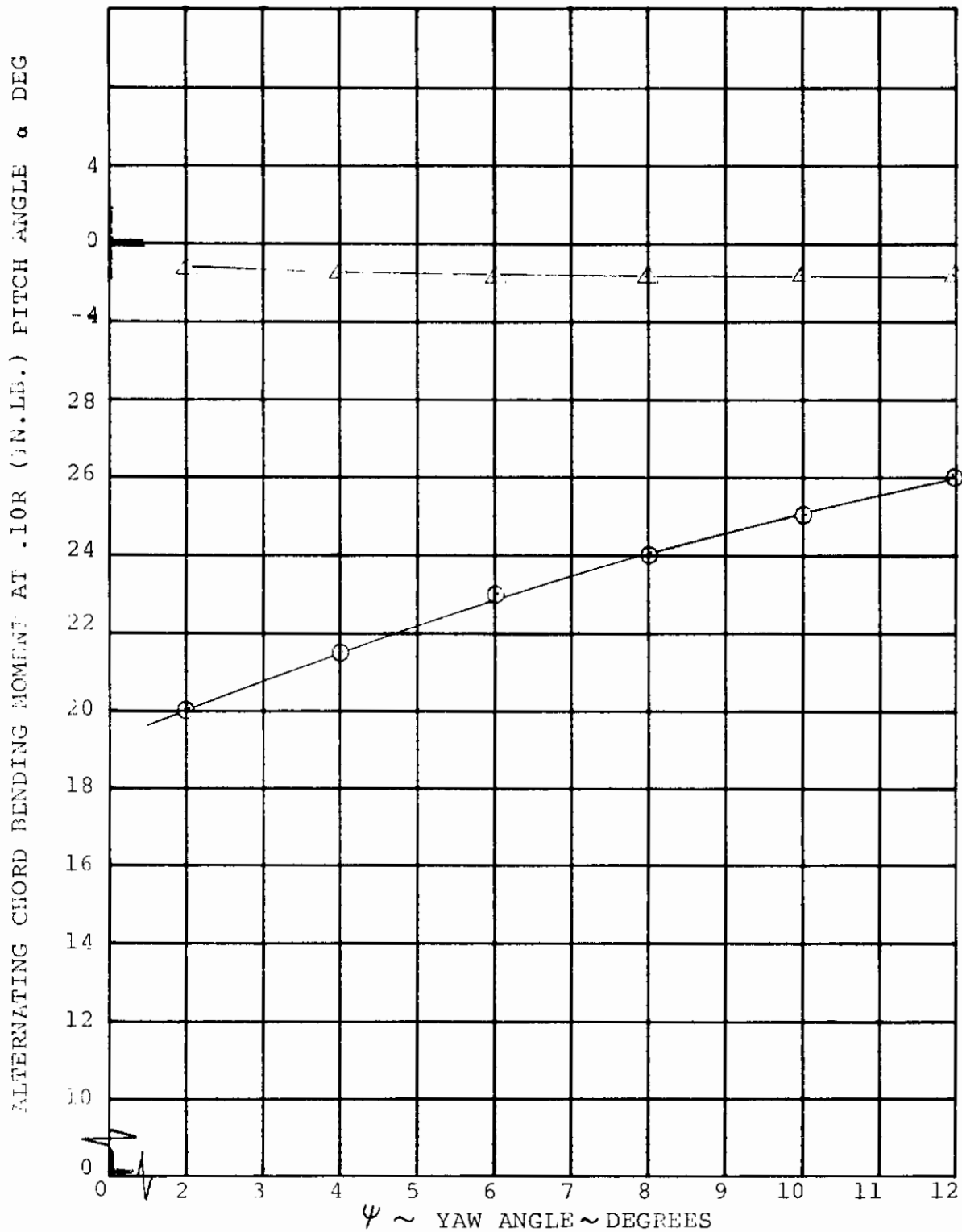


FIGURE 6-32. EFFECT OF MODEL YAW ANGLE ON RIGHT ROTOR ALTERNATING CHORD BENDING MOMENT IN TRANSITION FOR $i_N=60$ DEG., $\theta_{.75}=16$ DEG., $q=4.1$ PSF, $\theta_2=5.8$ DEG., AND 790 RPM.

RUN 41(27)

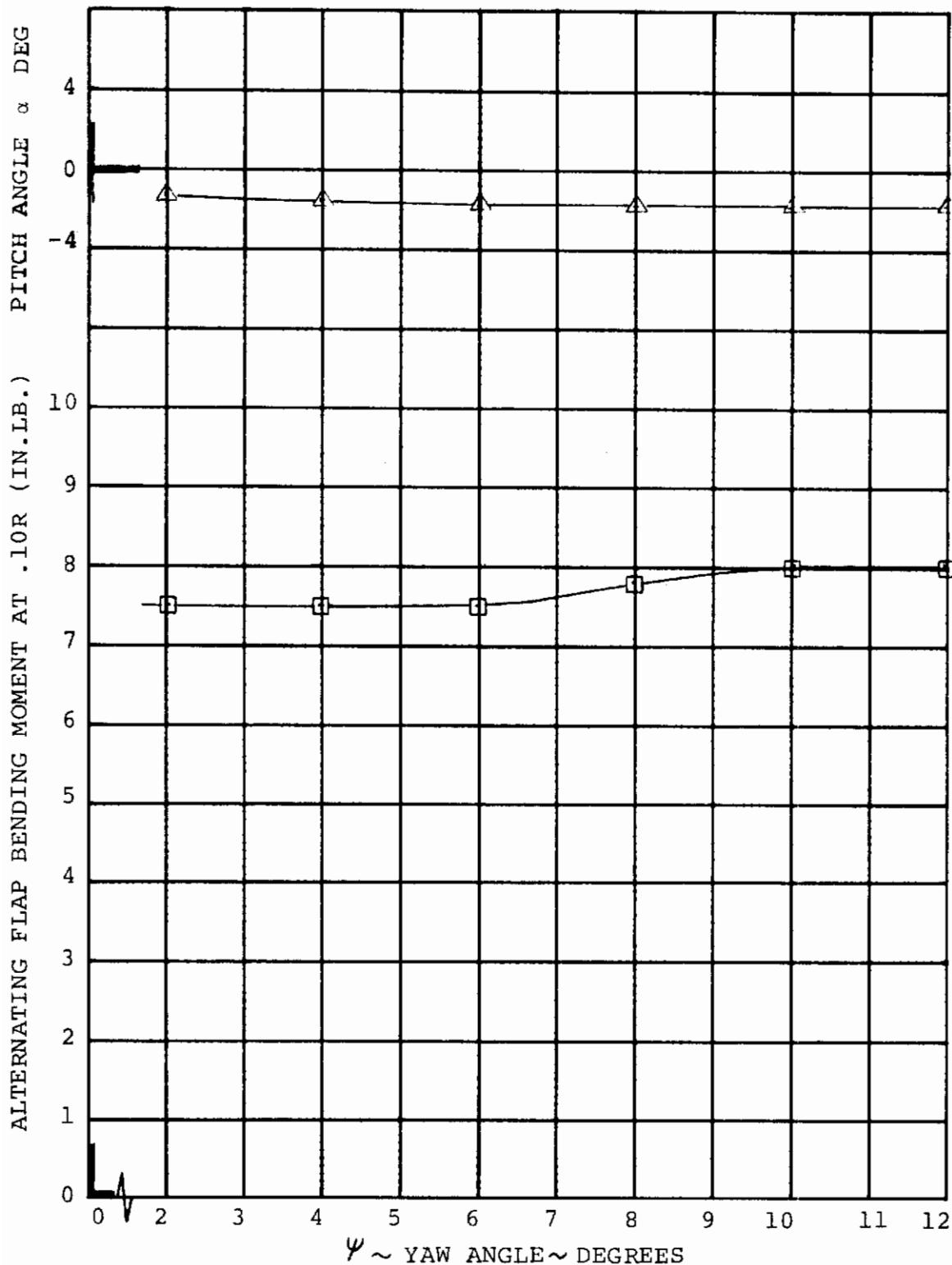


FIGURE 6-33. EFFECT OF MODEL YAW ANGLE ON RIGHT ROTOR ALTERNATING FLAP BENDING MOMENT IN TRANSITION FOR $i_N = 60$ DEG., $\theta_{.75} = 16$ DEG., $q = 4.1$ PSF, $\theta_2 = 5.8$ DEG., AND 790 RPM.

RUN 41(27)

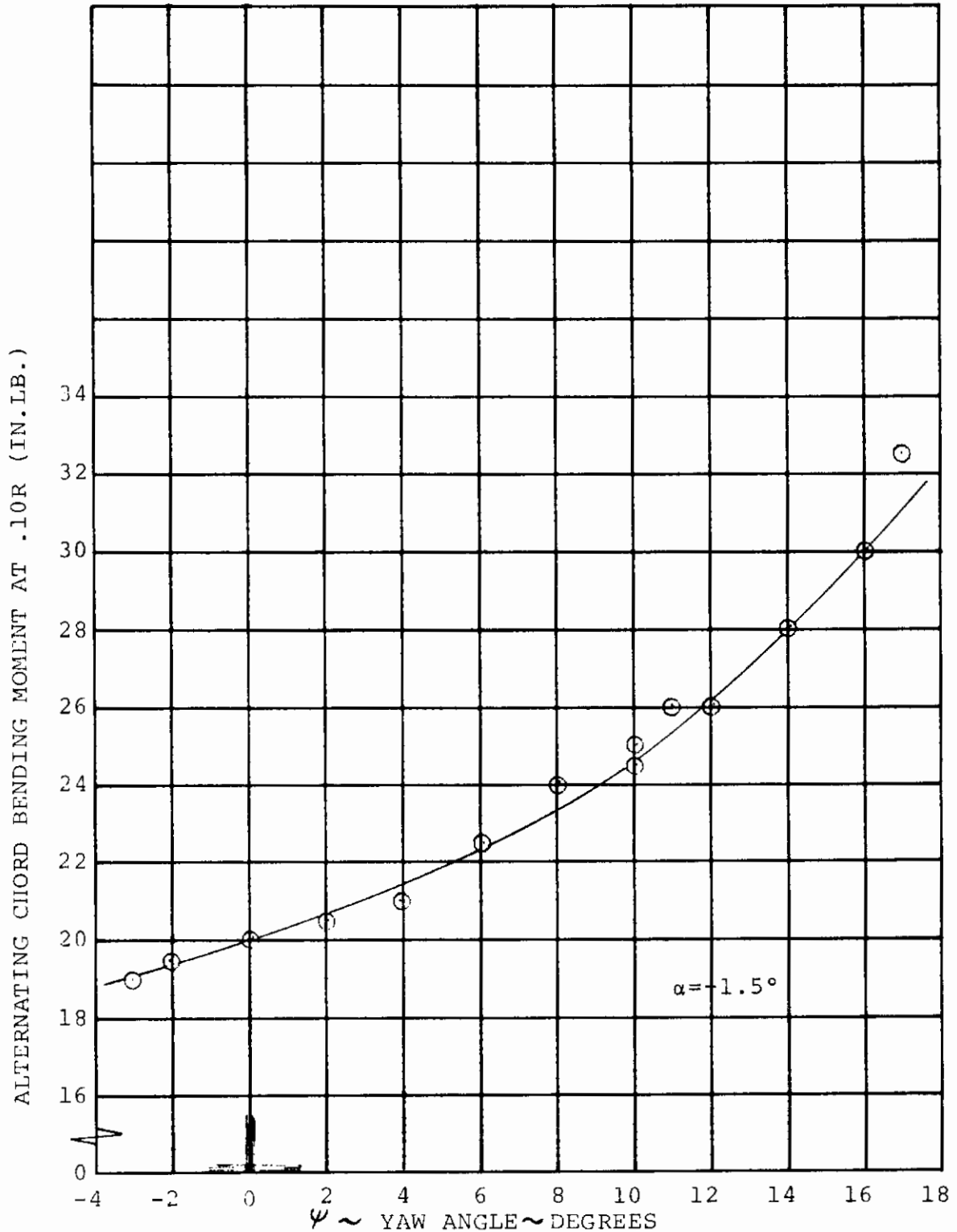


FIGURE 6-34. EFFECT OF MODEL YAW ANGLE ON RIGHT ROTOR ALTERNATING CHORD BENDING MOMENT IN TRANSITION FOR $i_N = 40$ DEG., $\theta_1 = 20$ DEG., $q = 4$ PSF, $\theta_2 = 3.8$ DEG., AND 790 RPM.

RUN 43 (10)

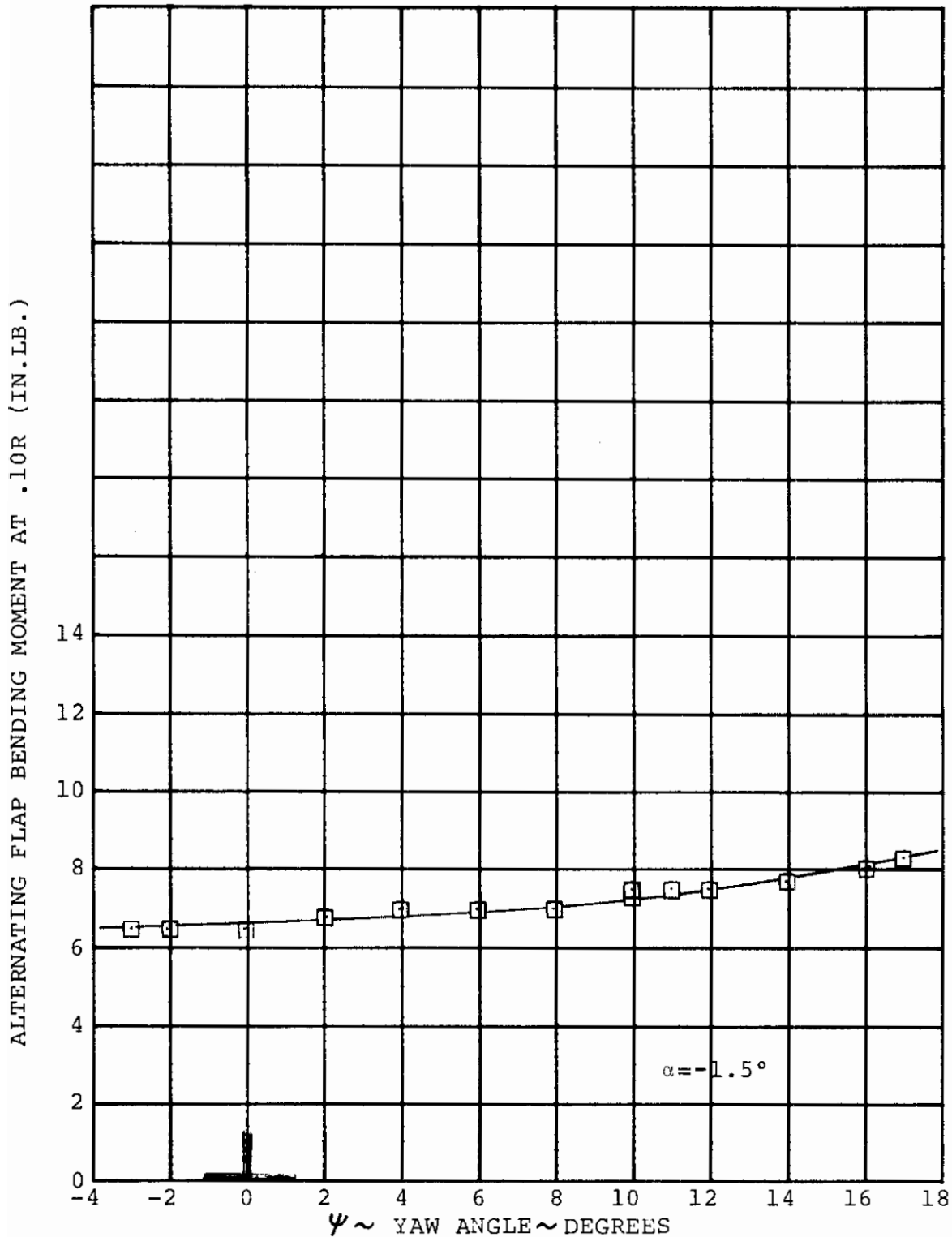


FIGURE 6-35 EFFECT OF MODEL YAW ANGLE ON RIGHT ROTOR ALTERNATING FLAP BENDING MOMENT IN TRANSITION FOR $i_N = 40$ DEG., $\theta_{.75} = 20$ DEG., $q = 4$ PSF, $\theta_2 = 3.8$ DEG., AND 790 RPM.
 RUN 43(10)

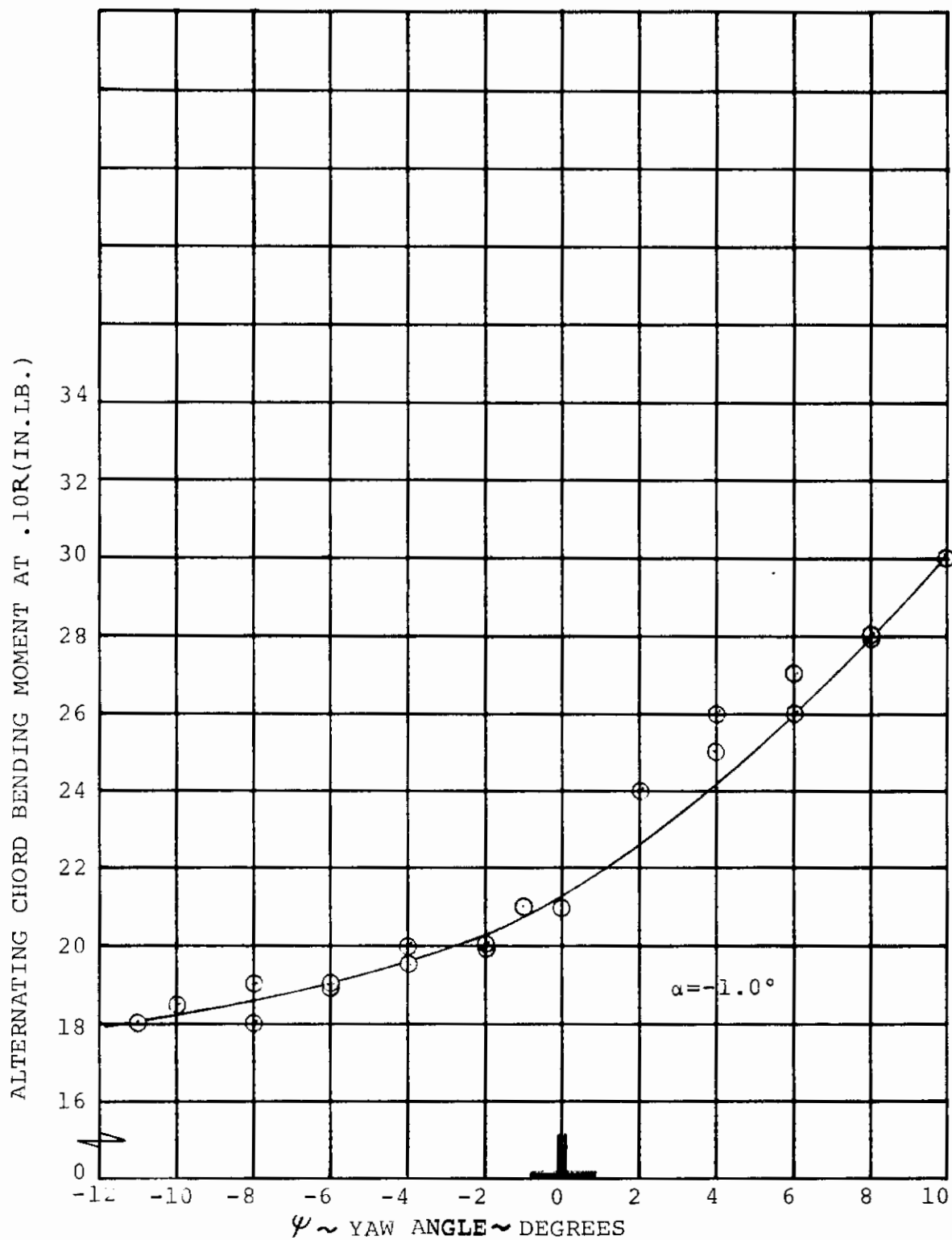


FIGURE 6-36. EFFECT OF MODEL YAW ANGLE ON RIGHT ROTOR ALTERNATING CHORD BENDING MOMENT IN TRANSITION FOR $i_N = 40$ DEG., $\theta_{.75} = 23$ DEG., $q = 5.25$ PSF, $\theta_2 = 4.3$ DEG., AND 790 RPM.

RUN 43 (16)

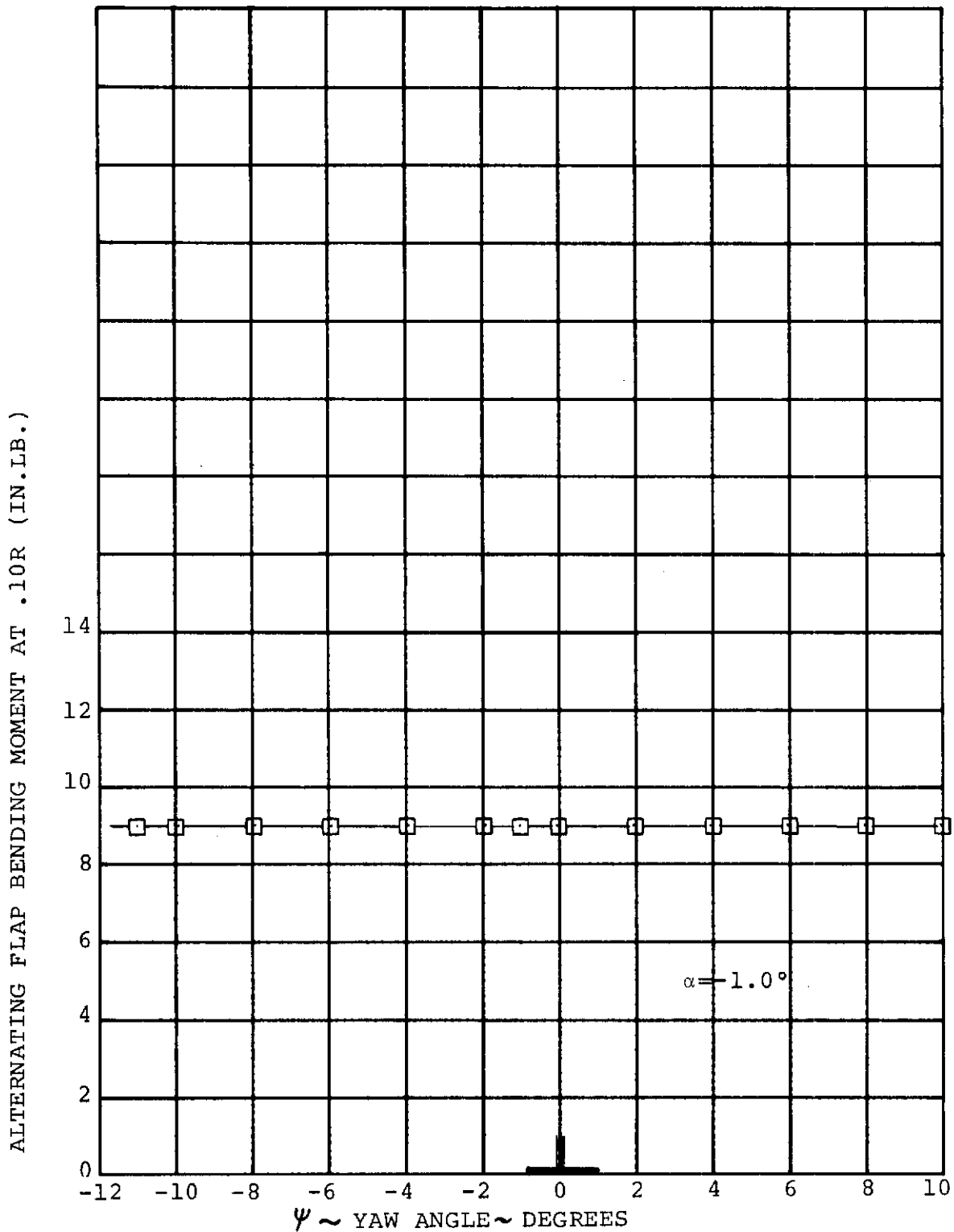


FIGURE 6-37. EFFECT OF MODEL YAW ANGLE ON RIGHT ROTOR ALTERNATING FLAP BENDING MOMENT IN TRANSITION FOR $i_N=40$ DEG., $\theta_{.75}=23$ DEG., $q=5.25$ PSF, $\theta_2=4.3$ DEG., AND 790 RPM.

RUN 43(16)

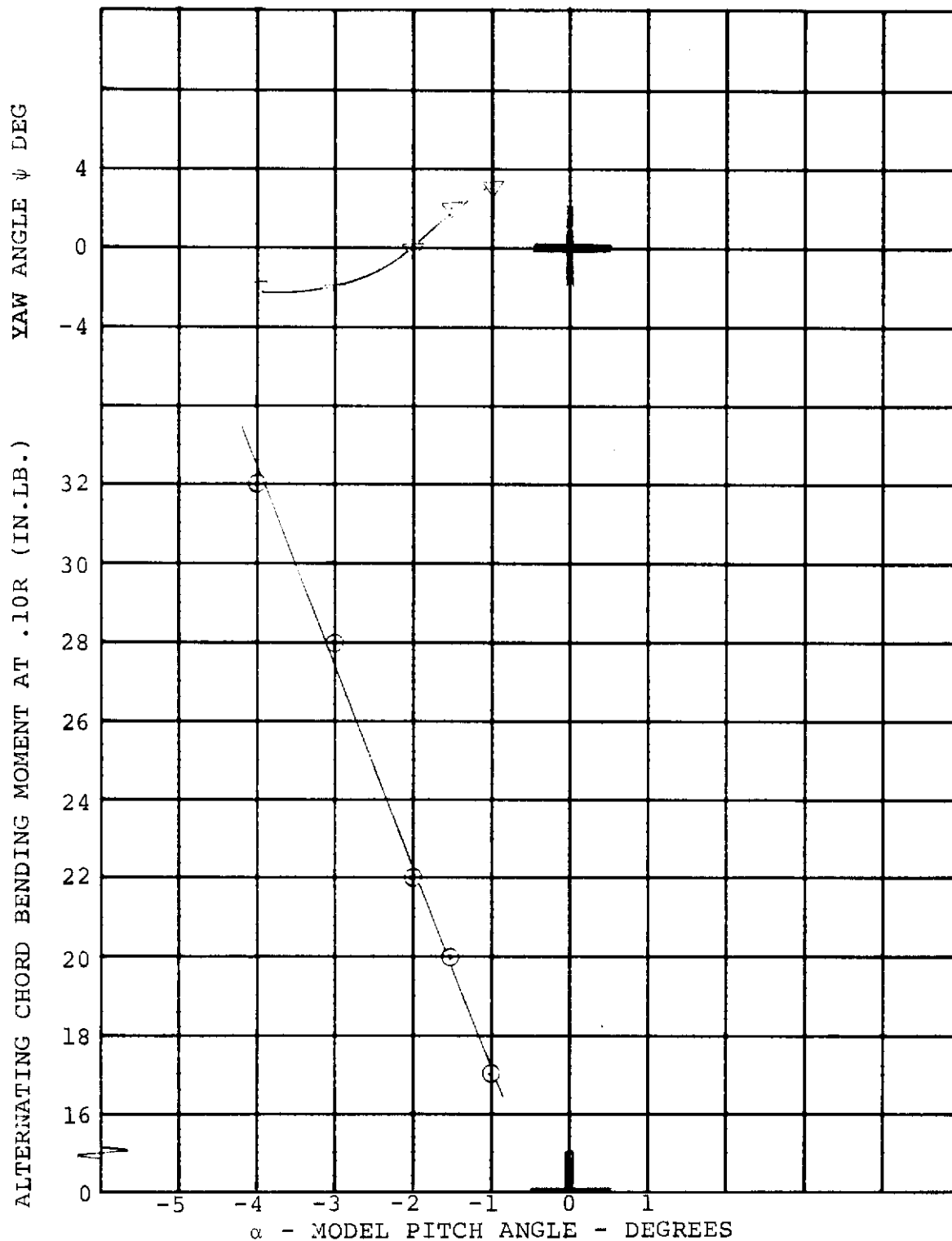


FIGURE 6-38 EFFECT OF MODEL PITCH ANGLE ON RIGHT ROTOR ALTERNATING CHORD BENDING MOMENT IN TRANSITION FOR $i_N=60$ DEG., $\theta_2=16$ DEG., $q=4.1$ PSF, $\theta_2=5.8$ DEG., AND 790 RPM

RUN 41(26)

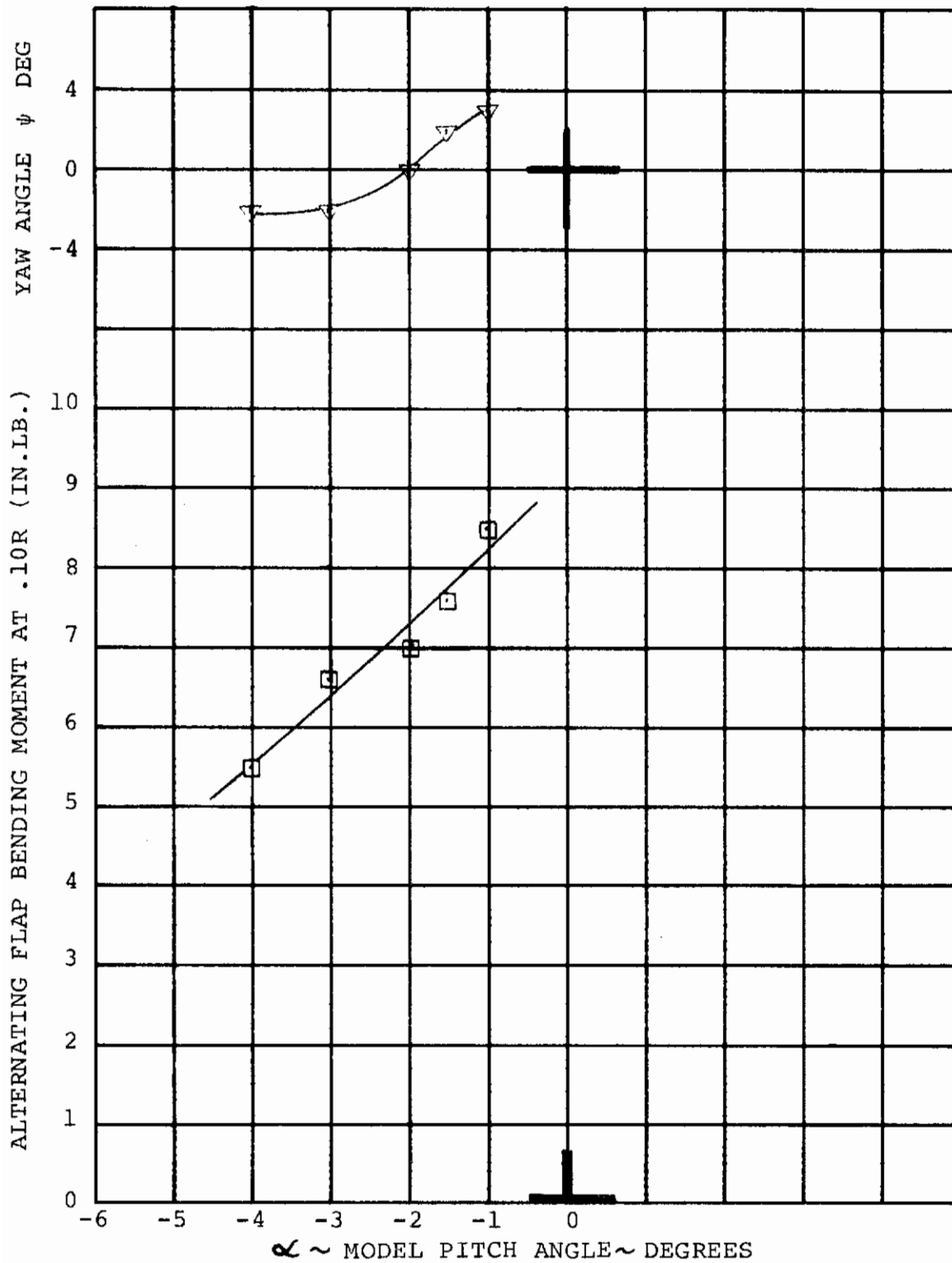


FIGURE 6-39. EFFECT OF MODEL PITCH ANGLE ON RIGHT ROTOR ALTERNATING FLAP BENDING MOMENT IN TRANSITION FOR $i_N=60$ DEG., $\theta_{.75}=16$ DEG., $q=4.1$ PSF, $\theta_2=5.8$ DEG., AND 790 RPM.

RUN 41(26)

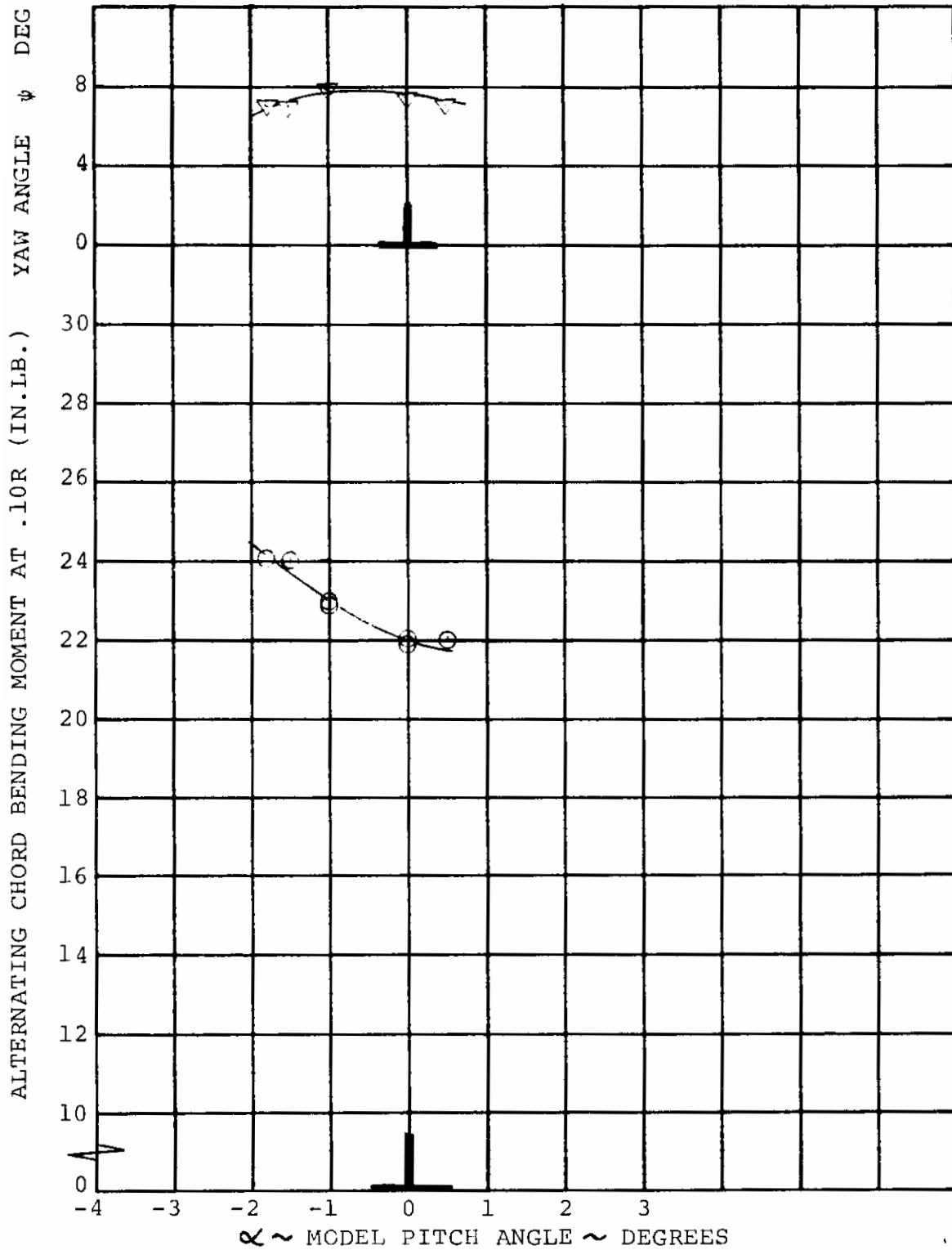


FIGURE 6-40. EFFECT OF MODEL PITCH ANGLE ON RIGHT ROTOR ALTERNATING CHORD BENDING MOMENT IN TRANSITION FOR $i_N=40$ DEG., $\theta_{.75}=20$ DEG., $q=4$ PSF, $\theta_2=3.8$ DEG., AND 790 RPM.
RUN 43(9)

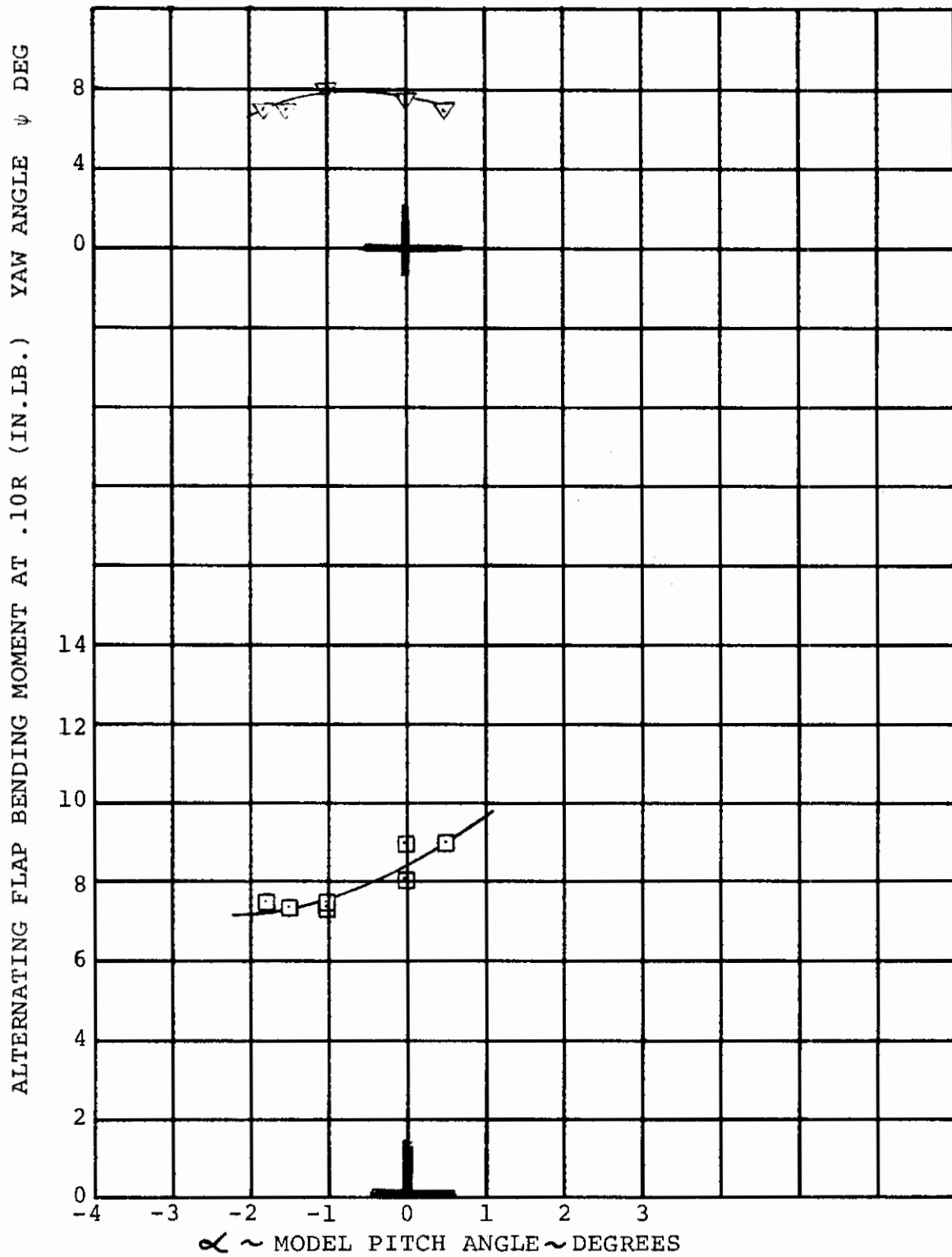
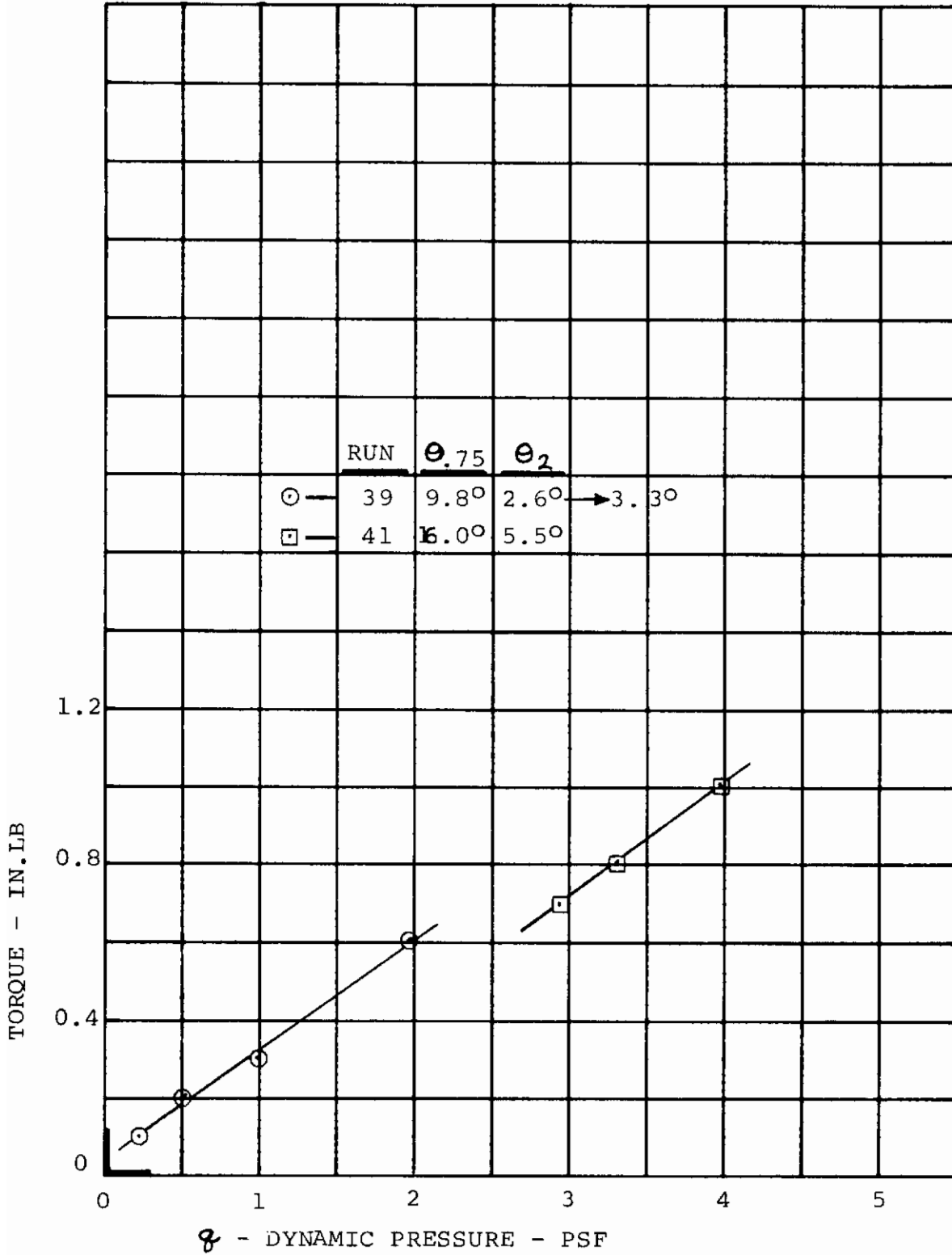


FIGURE 6-41. EFFECT OF MODEL PITCH ANGLE ON RIGHT ROTOR ALTERNATING FLAP BENDING MOMENT IN TRANSITION FOR $i_N = 40$ DEG., $\theta_{.75} = 20$ DEG., $q = 4$ PSF, $\theta_2 = 3.8$ DEG., AND 790 RPM.
 RUN 43 (9)



8 - DYNAMIC PRESSURE - PSF
 TORQUE - IN. LB

FIGURE 6-42. BLADE RESPONSE AT TORSIONAL FREQUENCY
 FOR $i_N = 60$ DEG., $f = 65$ CPS

Contrails

VERTICAL LINE: AT $\psi = 90^\circ$

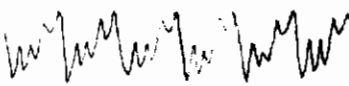

	Run	q	θ_{15}	θ_2	Ω
		PSF	DEG	DEG	RPM
	39	1.9	9.8°	3.3°	780
	41	3.9	16.0°	5.5°	780

FIGURE 6-43 BLADE TORSION RESPONSE IN TRANSITION
 - RIGHT BLADE -.15R $i_w = 60^\circ$

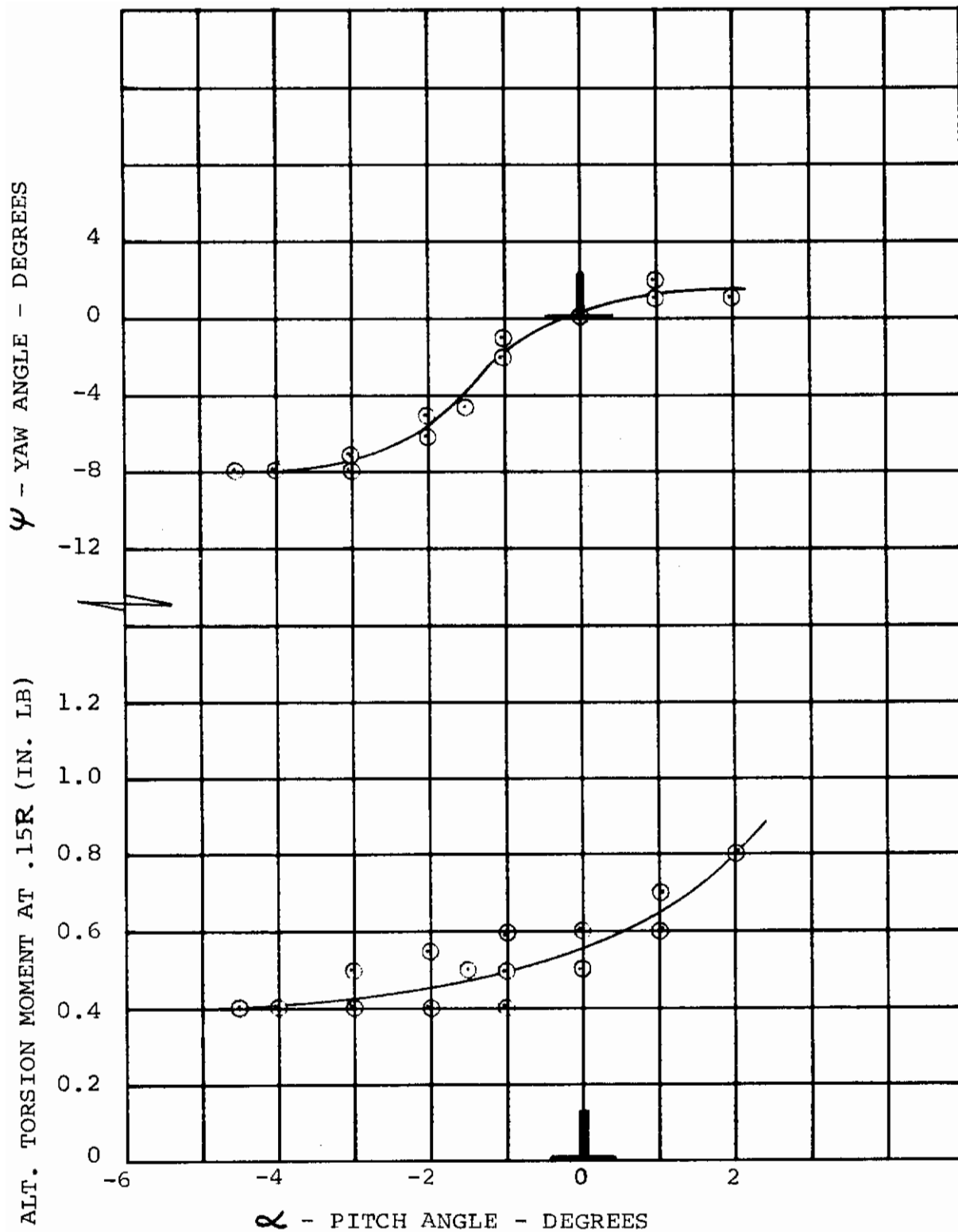


FIGURE 6-44 EFFECT OF FUSELAGE DISPLACEMENT ON RIGHT HAND BLADE ALTERNATING TORSION RESPONSE AT ITS TORSION NATURAL FREQUENCY FOR $i_N = 40$ DEG., $\theta_{.75} = 23$ DEG., $\theta_2 = 4.3$ DEG., $q_0 = 5.25$ PSF, AND 790 RPM-RUN 43 (15)

6.3 CRUISE CONFIGURATION BLADE LOADS

Blade loads data were taken in the cruise configuration to show the effect of cyclic pitch, model pitch, and model yaw, collective, and dynamic pressure.

At a tunnel dynamic pressure ($q = 4.9$ psf) corresponding to a full-scale speed of 120 knots, alternating chord bending sensitivity to cyclic pitch was twice that due to cyclic in hover - OGE. Cyclic pitch was shown to have little effect on alternating flap bending.

At a dynamic pressure ($q = 6.65$ psf) corresponding to a full-scale speed of 140 knots, 5 degrees of model yaw produced alternating chord bending equivalent to that due to .85 degrees of hover cyclic. Alternating flap bending was insensitive to model yaw.

The isolated effect of model pitch on blade loads could not be determined since the model tended to yaw as the model was pitched. The uncertainty of the physical position of the model in the tunnel after attitude changes through the snubber cables caused the coupling between model pitch and yaw. The yaw was not caused by any aerodynamic or gyroscopic effects.

6.3.1 Effect of Cyclic Pitch

Blade loads data taken in cruise at $q = 5$ to show the effect of cyclic pitch are shown in Figures 6-45 and 6-46. These data show the alternating flap bending moment to be insensitive to cyclic pitch while alternating chord bending moments increase at the rate of 12 in. lb. per degree of cyclic pitch. Referring to Figure 6-11 the sensitivity of chord bending to cyclic in hover was 6 in. lb. per degree cyclic.

6.3.2 Effect of Model Yaw

Figures 6-47 through 6-50 show the effect of model yaw on blade loads at $q = 6$ and $q = 7$ PSF. These data showed alternating chord bending to be sensitive to model yaw whereas alternating flap bending showed little increase with yaw. At a q of 6, 5 degrees of yaw produce alternating chord bending equivalent to .3 degree cyclic in hover. At a q of 7 PSF, 5 degrees of yaw produce alternating chord bending equivalent to .85 degree of hover cyclic.

6.3.3 Effect of Model Pitch

Figures 6-51 through 6-56 show the effect of model pitch on blade loads at $q = 6$ and $q = 7$ PSF. These data are inconclusive in determining the isolated effect of model pitch since the model yawed as the model pitch was increased. This was caused by soft model mount and the inability to keep model yaw constant with the snubber cables. However, the blade loads data show the same trend as when the model was yawed. Alternating chord bending is sensitive to changes in pitch whereas there is little change in alternating flap bending.

6.3.4 Effect of Collective Pitch

The effect of collective pitch on steady flap bending in cruise is shown in Figure 6-57. Steady flap bending increased sharply with increased collective and the gradient of steady flap bending with collective increased as dynamic pressure increased. In Figure 6-13 the variation of steady flap bending with collective in hover was 0.7 in. lb per degree collective. As shown in Figure 6-57, at $q = 6$, the gradient of steady flap bending with collective in cruise is 8 in. lb per degree or 10 times as sensitive as in hover. This is a direct result of the typically increased sensitivity of rotor thrust with collective as advance ratio is increased in cruise, as shown in Figure 6-58.

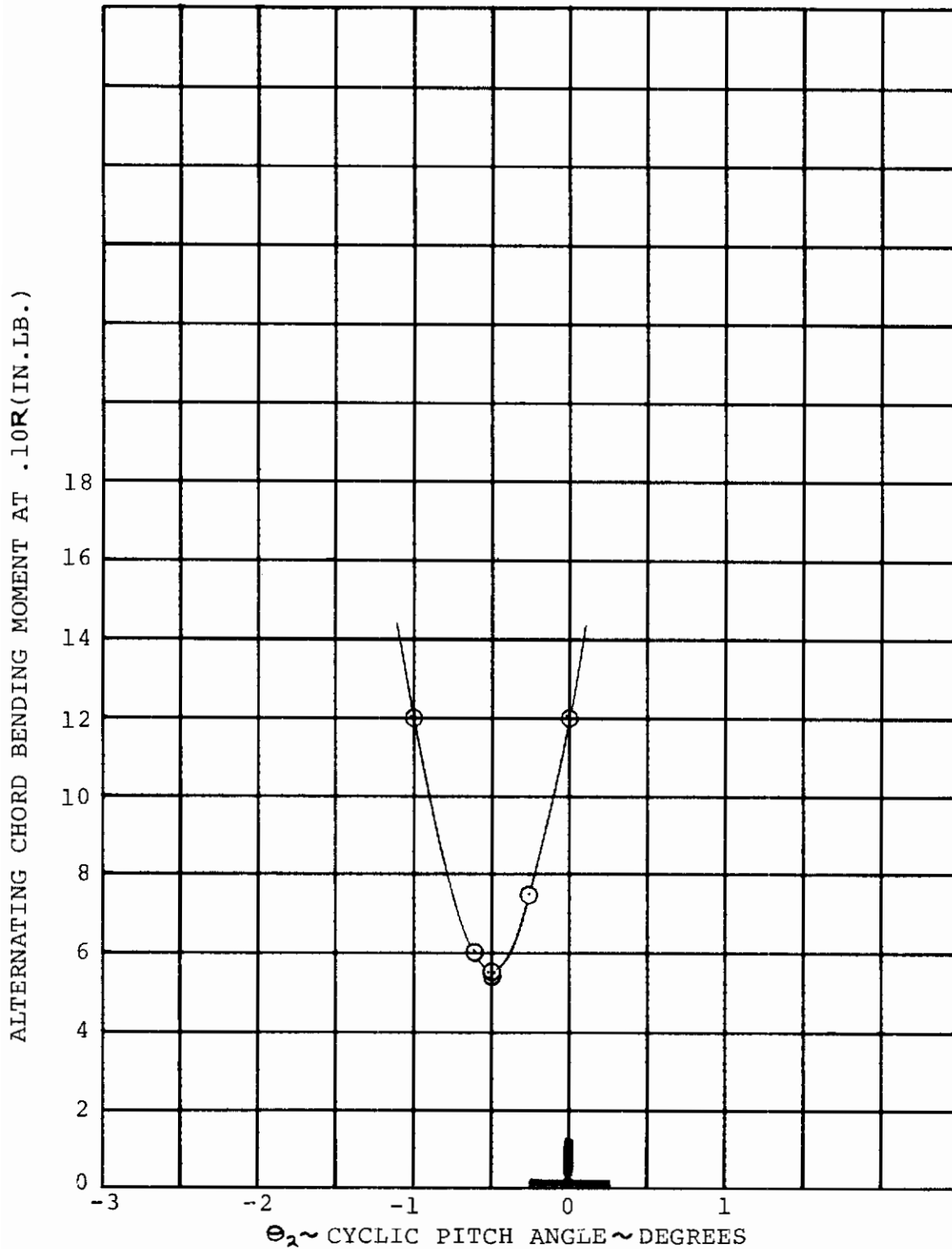


FIGURE 6-45 EFFECT OF CYCLIC PITCH ON RIGHT ROTOR ALTERNATING CHORD BENDING MOMENT IN CRUISE FOR $i_N = 0$ DEG., $\Theta_{.75} = 24.5$ DEG., $q = 5$ PSF, AND 790 RPM. RUN 37 (33-37)

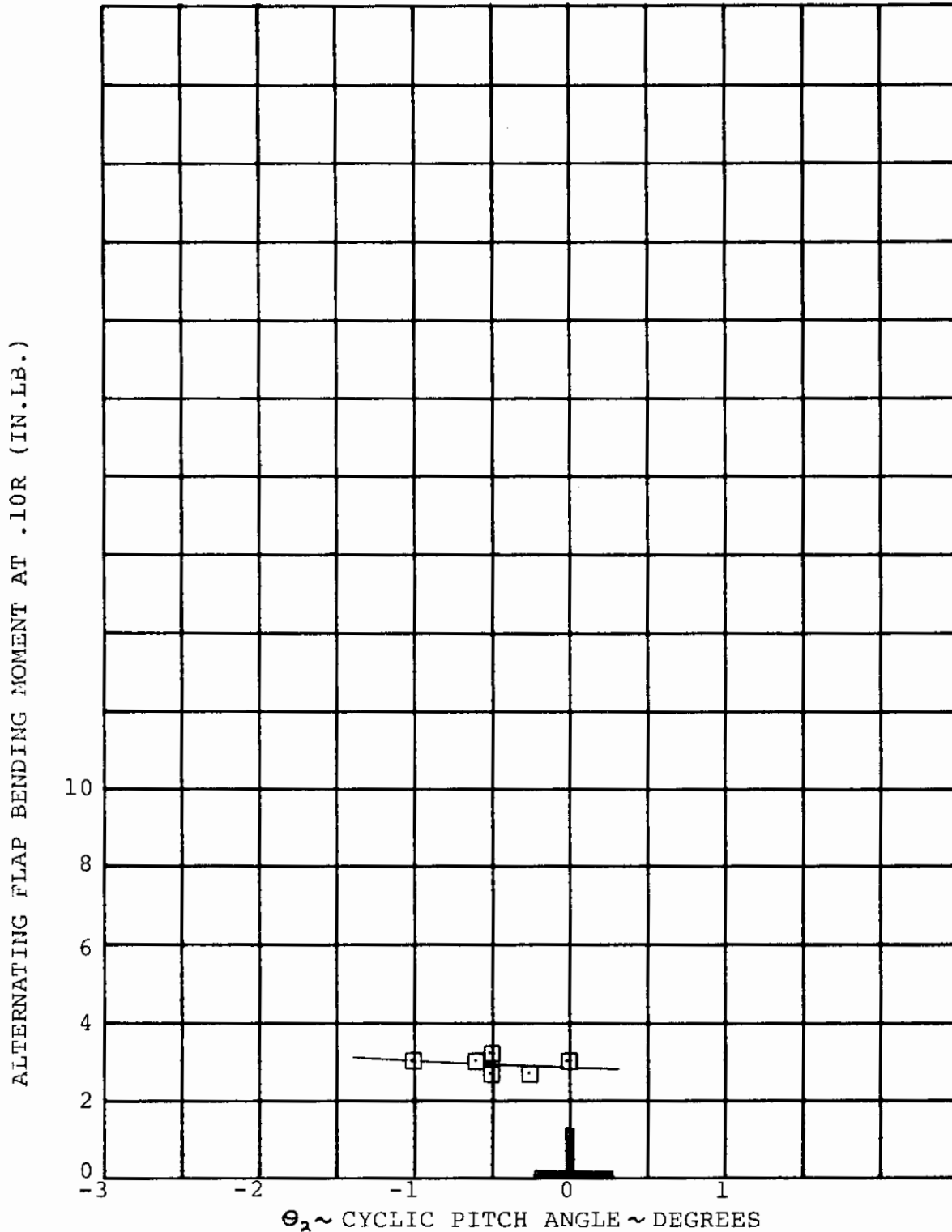


FIGURE 6-46 EFFECT OF CYCLIC PITCH ON RIGHT ROTOR
 ALTERNATING FLAP BENDING MOMENT IN CRUISE FOR $i_N = 0$.DEG.
 $e_{.75} = 24.5$ DEG., $q = 5$ PSF, AND 790 RPM.
 RUN 37(33-37)

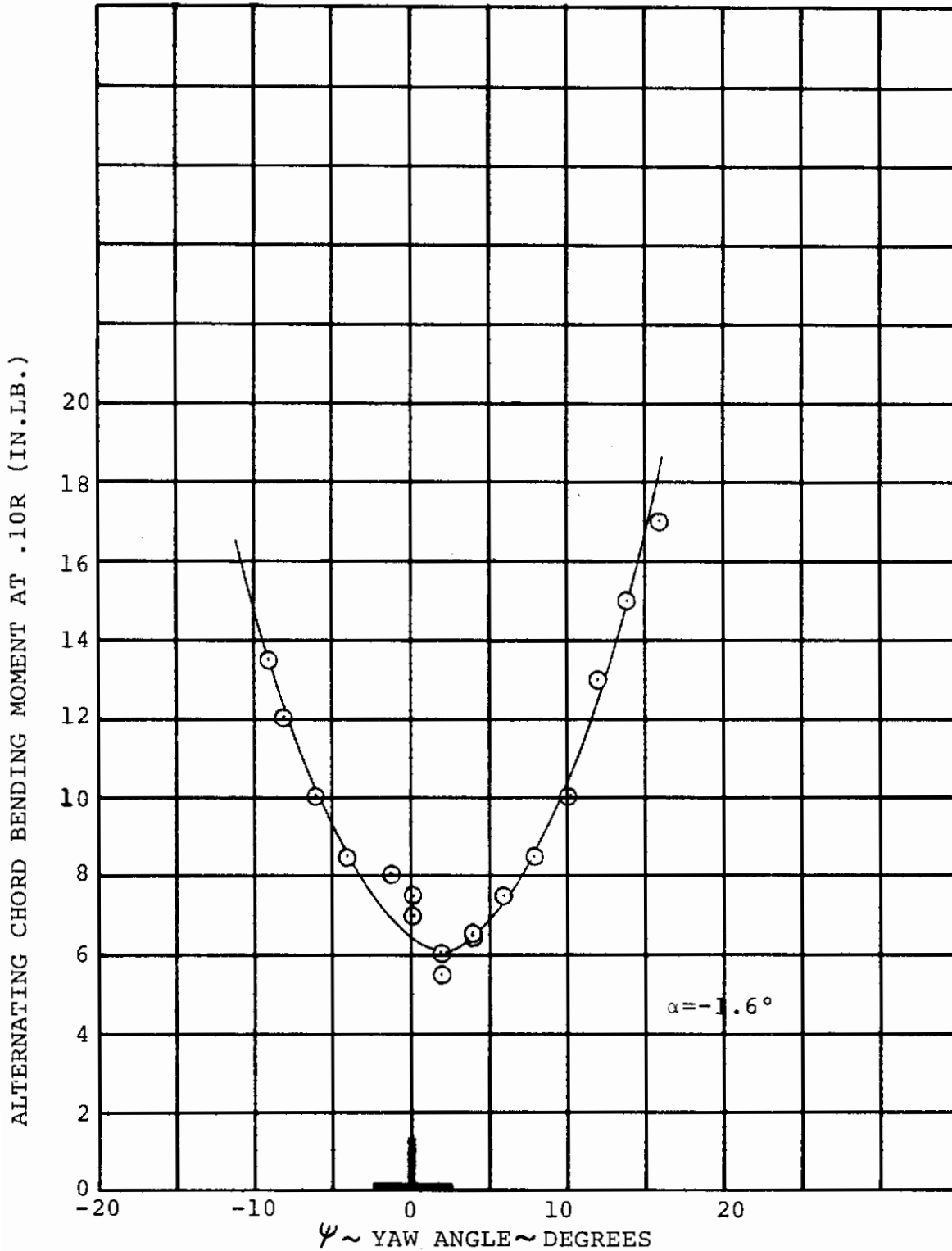


FIGURE 6-47. EFFECT OF MODEL YAW ANGLE ON RIGHT ROTOR ALTERNATING CHORD BENDING MOMENT IN CRUISE FOR $i_N = 0$ DEG. $\Theta_{.75} = 26.7$ DEG., $q = 6$ PSF, $\Theta_2 = -0.7$ DEG., AND 790 RPM. RUN 38 (4)

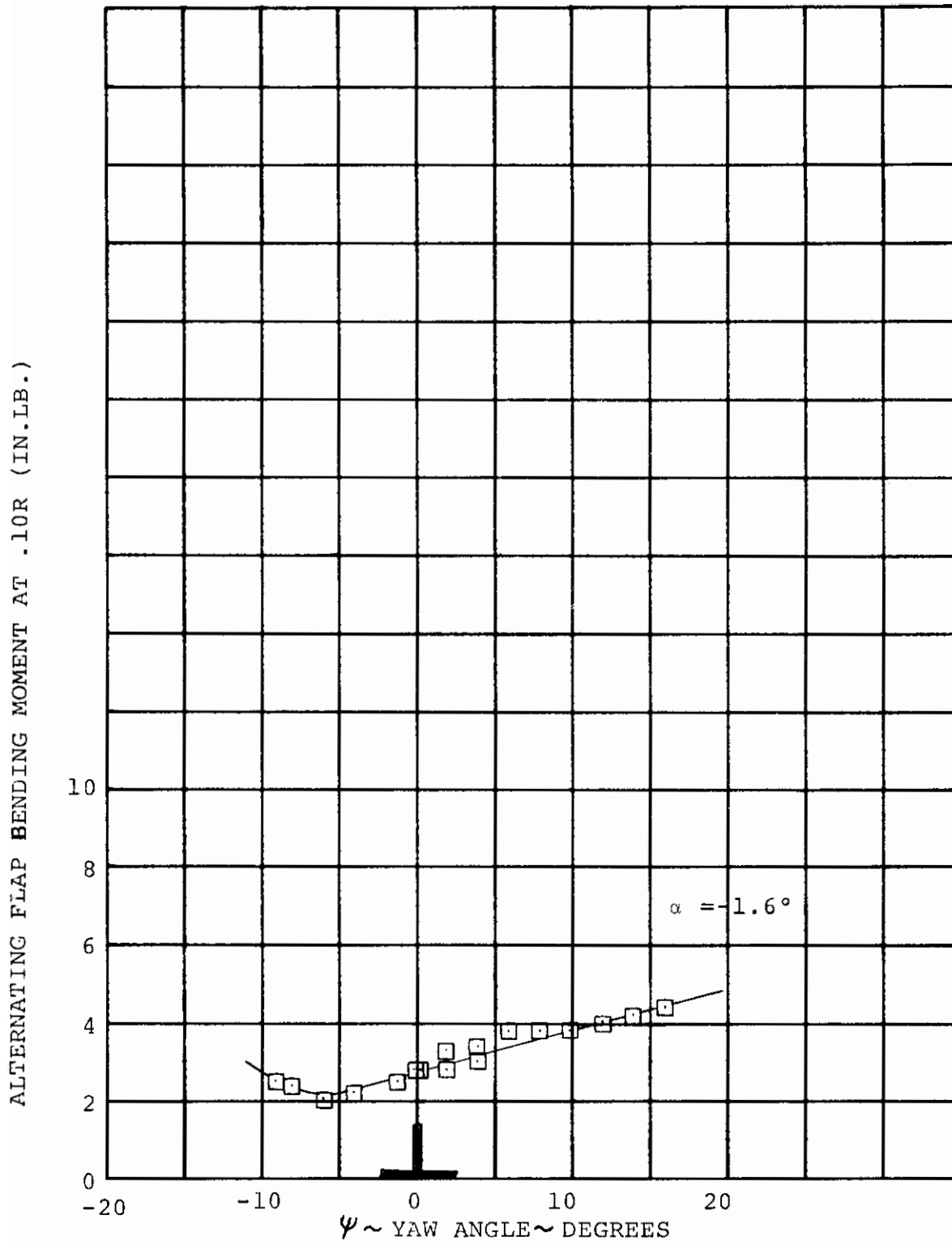


FIGURE 6-48. EFFECT OF MODEL YAW ANGLE ON RIGHT ROTOR ALTERNATING FLAP BENDING MOMENT IN CRUISE FOR $i_N = 0$ DEG. $\Theta_{.75} = 26.7$ DEG., $q = 6$ PSF, $\Theta_2 = -0.7$ DEG., AND 790 RPM. RUN 38(4)

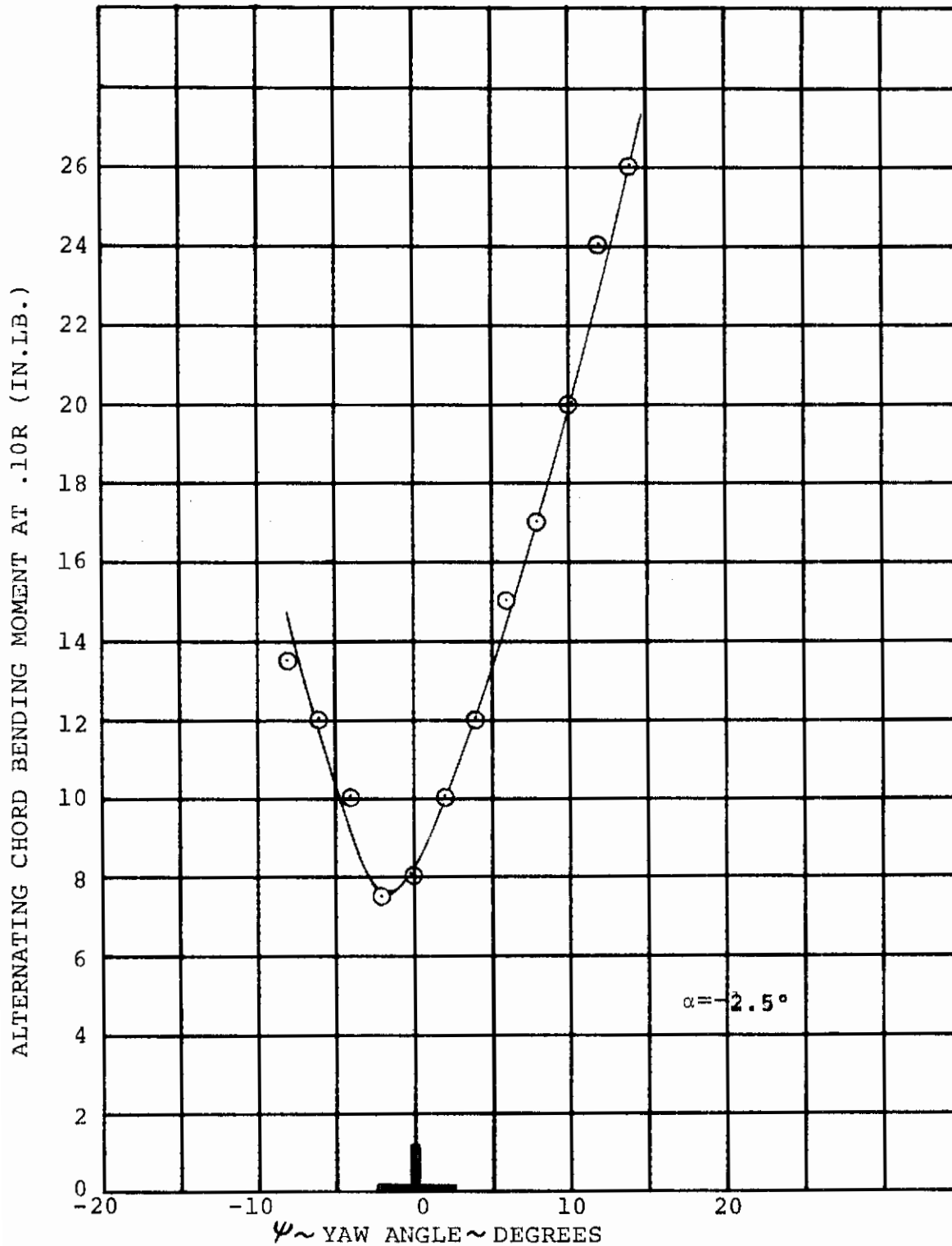


FIGURE 6-49. EFFECT OF MODEL YAW ANGLE ON RIGHT ROTOR ALTERNATING CHORD BENDING MOMENT IN CRUISE FOR $i_N = 0$ DEG. $\theta_1 = 30.7$ DEG., $q = 7$ PSF, $\theta_2 = -0.7$ DEG., AND 790 RPM. RUN 38(10)

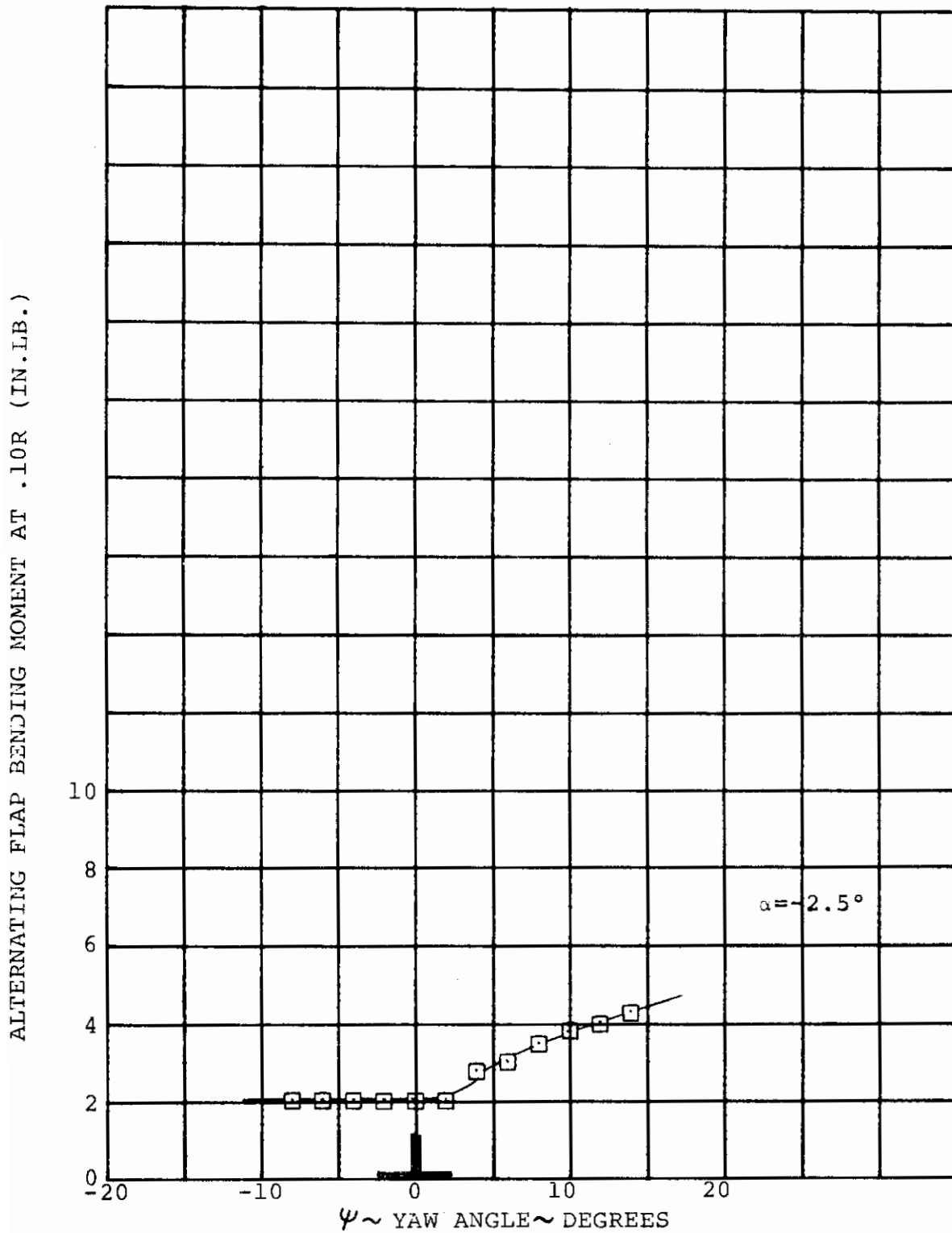


FIGURE 6-50. EFFECT OF MODEL YAW ANGLE ON RIGHT ROTOR ALTERNATING FLAP BENDING MOMENT IN CRUISE FOR $i_N = 0$ DEG. $\Theta_{.75} = 30.7$ DEG., $q = 7$ PSF, $\Theta_2 = -0.7$ DEG., AND 790 RPM. RUN 38(10)

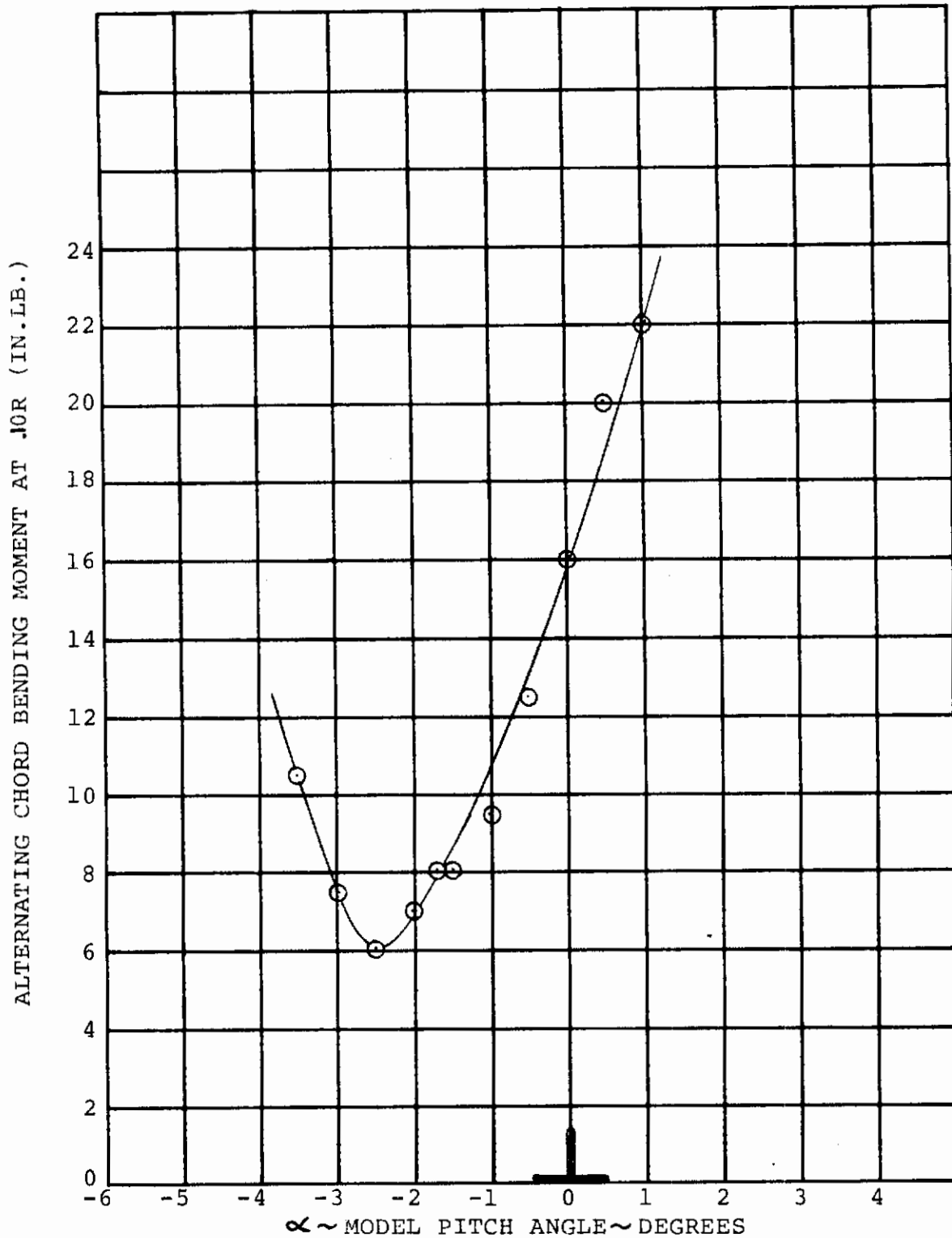


FIGURE 6-51. EFFECT OF MODEL PITCH ANGLE ON RIGHT ROTOR ALTERNATING CHORD BENDING MOMENT IN CRUISE FOR $i_N=0$ DEG. $\theta_{.75}=26.7$ DEG., $q=6$ PSF, $\theta_2=-0.7$ DEG., AND 790 RPM. RUN 38(3)

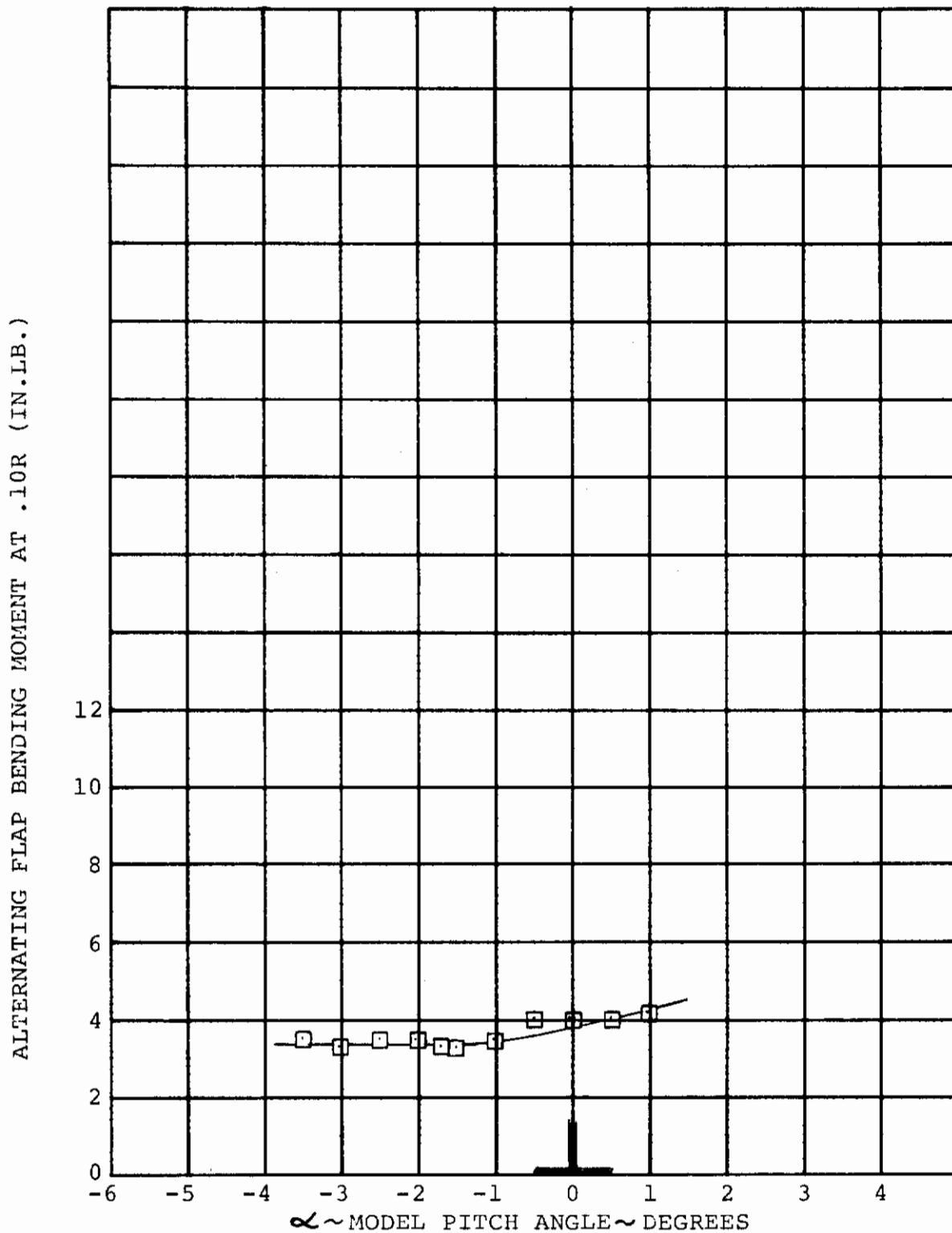


FIGURE 6-52. EFFECT OF MODEL PITCH ANGLE ON RIGHT ROTOR ALTERNATING FLAP BENDING MOMENT IN CRUISE FOR $i_n = 0$ DEG.
 $\Theta_{.75} = 26.7$ DEG., $q = 6$ PSF, $\Theta_2 = -0.7$ DEG., AND 790 RPM.
 RUN 38(3)

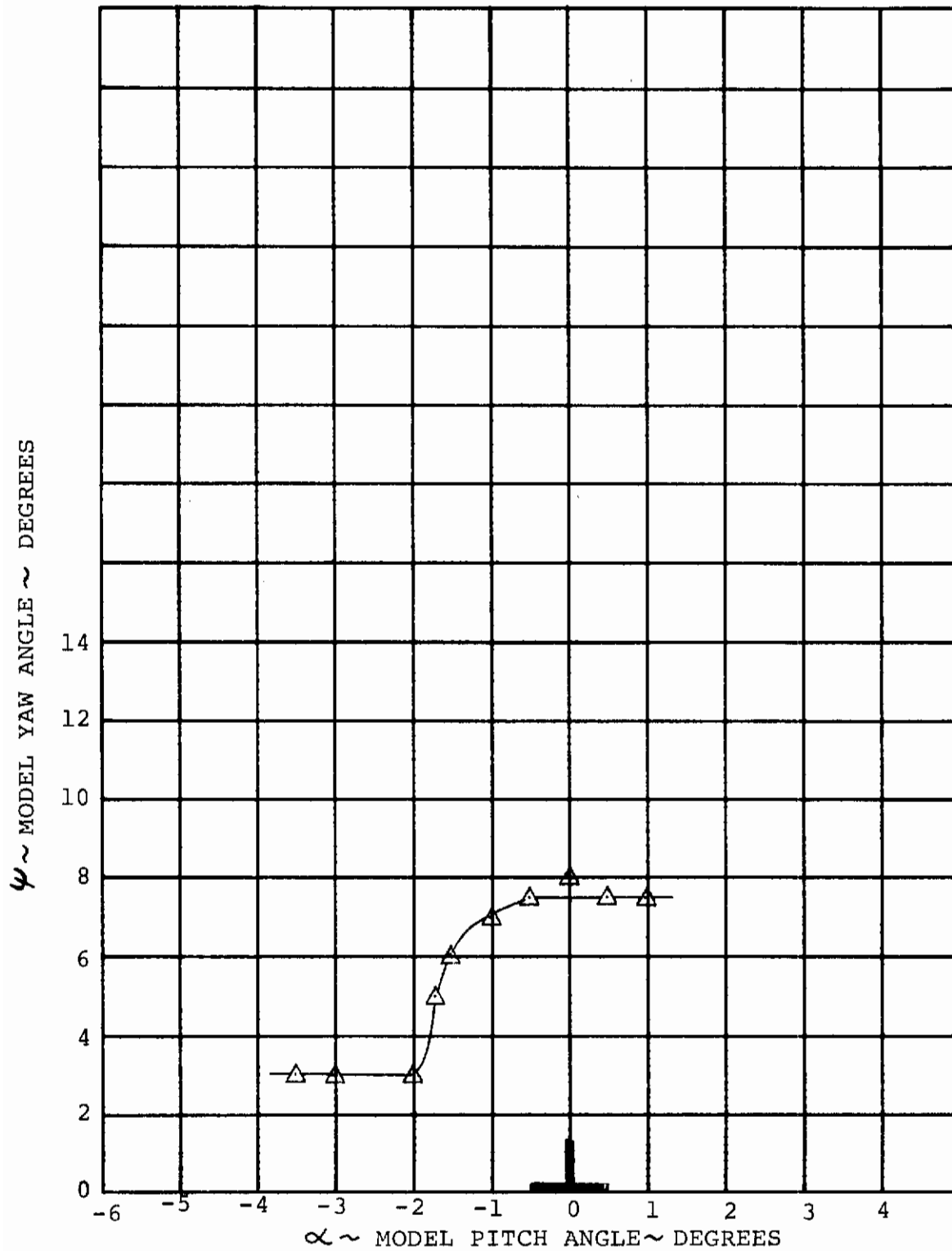


FIGURE 6-53. VARIATION OF MODEL YAW WITH MODEL PITCH ANGLE IN CRUISE FOR $i_N = 0$ DEG., $\Theta_{.75} = 26.7$ DEG., $q = 6$ PSF, $\Theta_2 = -0.7$ DEG., AND 790 RPM. RUN 38(3)

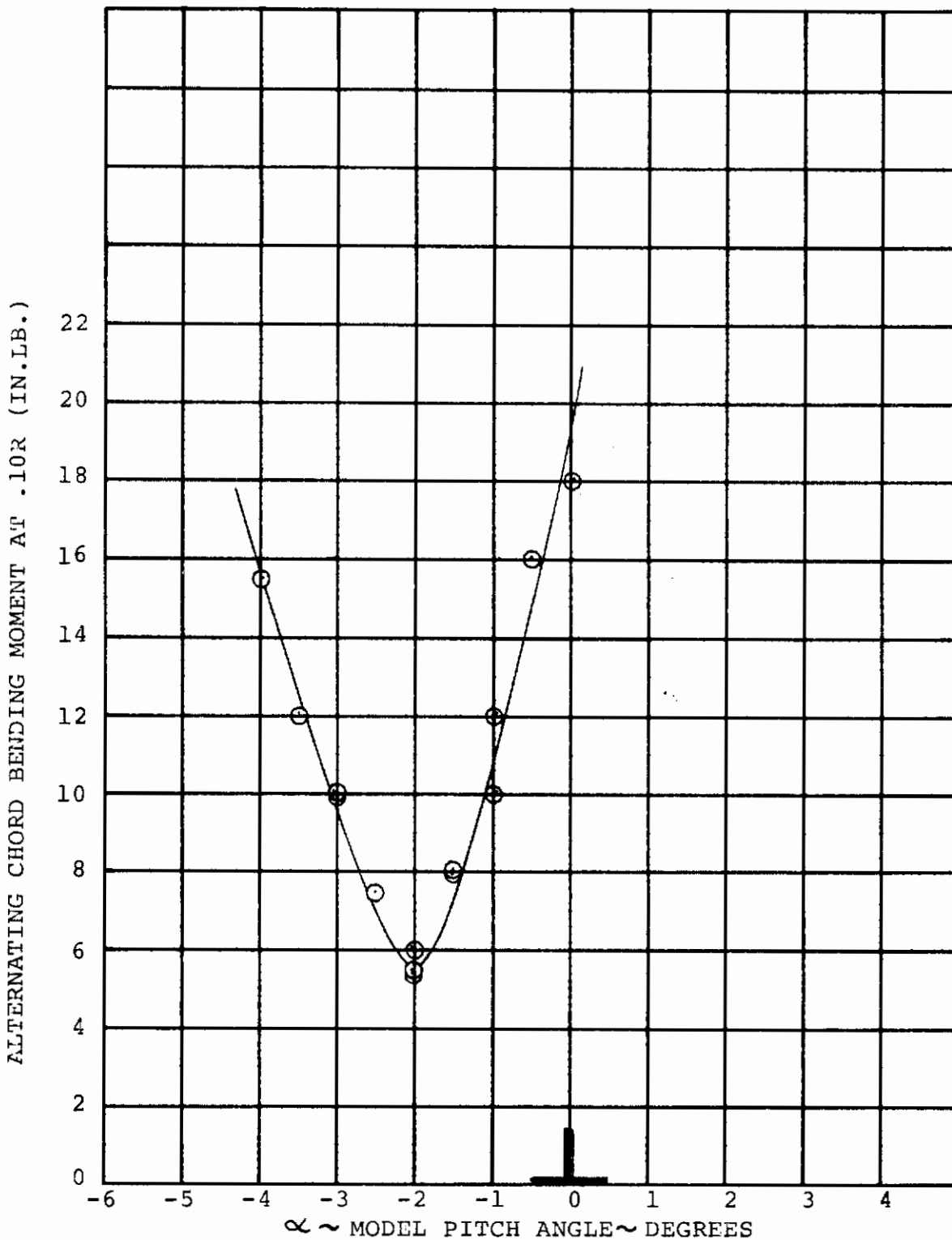


FIGURE 6-54. EFFECT OF MODEL PITCH ANGLE ON RIGHT ROTOR ALTERNATING CHORD BENDING MOMENT IN CRUISE FOR $i_N = 0$ DEG.
 $\Theta_{.75} = 30.7$ DEG., $q = 7$ PSF, $\Theta_2 = -0.7$ DEG., AND 790 RPM.
RUN 38(9)

ALTERNATING FLAP BENDING MOMENT AT .10R (IN.LB.)

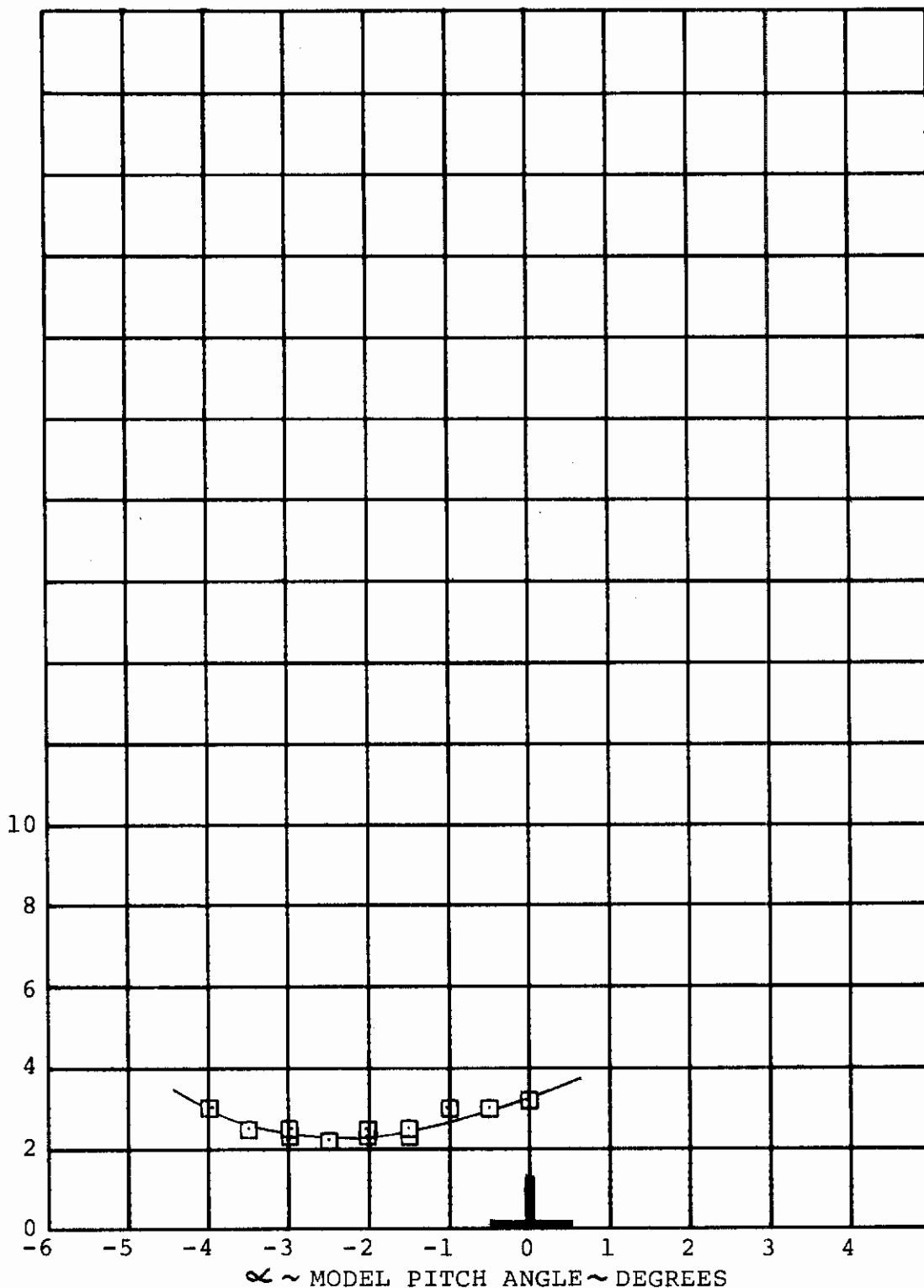


FIGURE 6-55. EFFECT OF MODEL PITCH ANGLE ON RIGHT ROTOR ALTERNATING FLAP BENDING MOMENT IN CRUISE FOR $i_N = 0$ DEG. $\Theta_{.75} = 30.7$ DEG., $q = 7$ PSF, $\Theta_2 = -0.7$ DEG., AND 790 RPM. RUN 38(9)

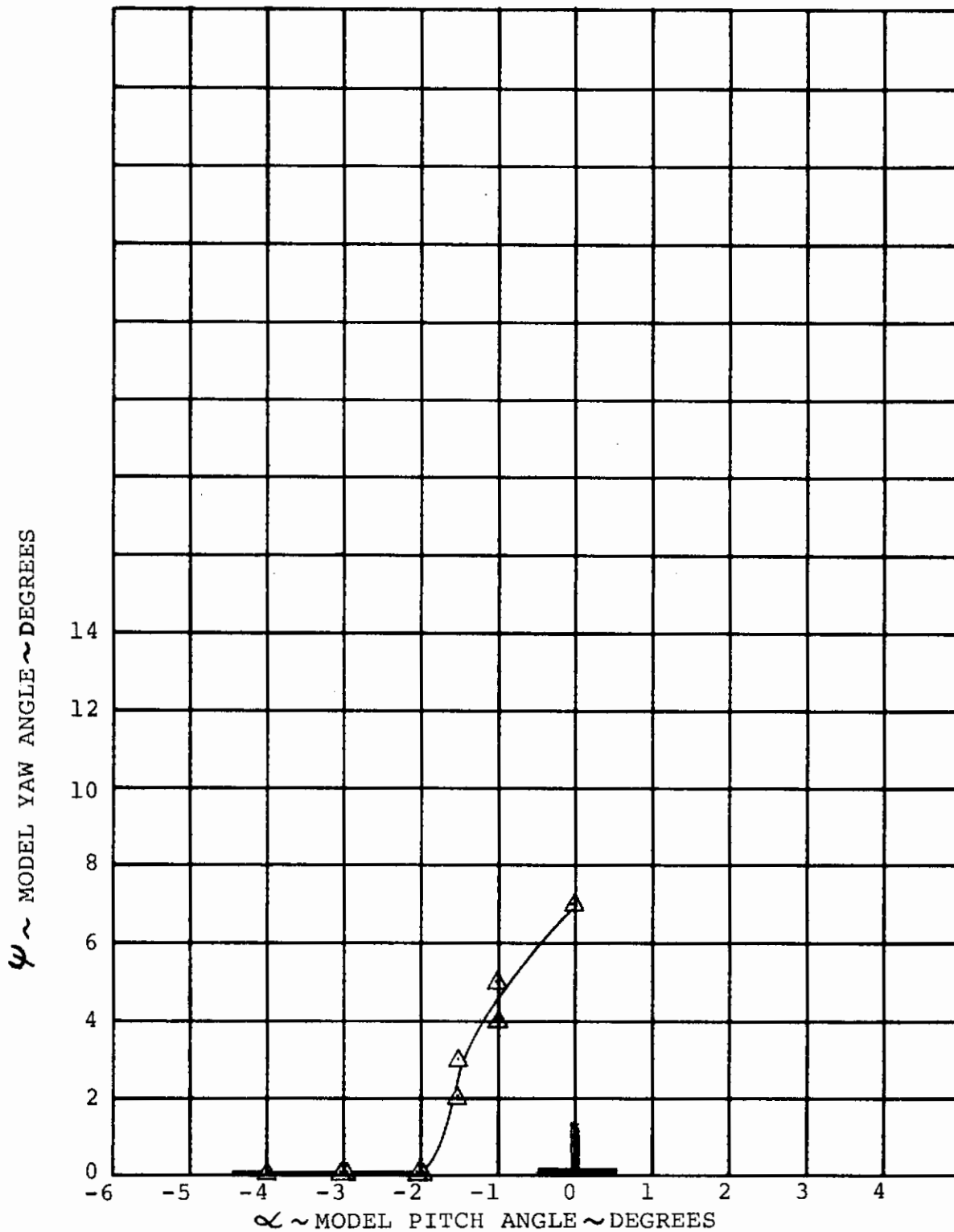


FIGURE 6-56. VARIATION OF MODEL YAW WITH MODEL PITCH ANGLE IN CRUISE FOR $i_N = 0$ DEG., $\theta_{75} = 30.7$ DEG., $q = 7$ PSF, $\theta_2 = -0.7$ DEG., AND 790 RPM.

RUN 38(9)

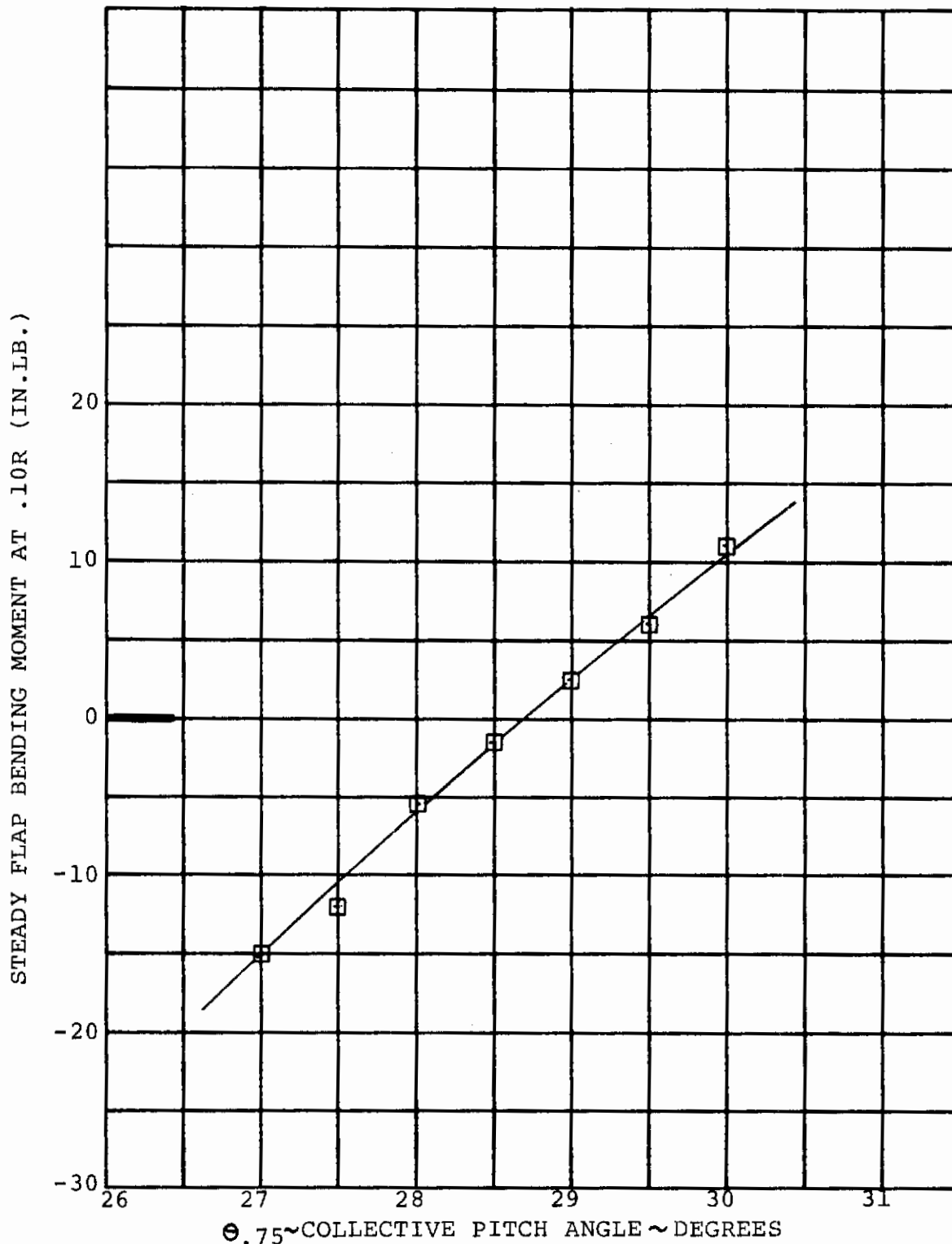
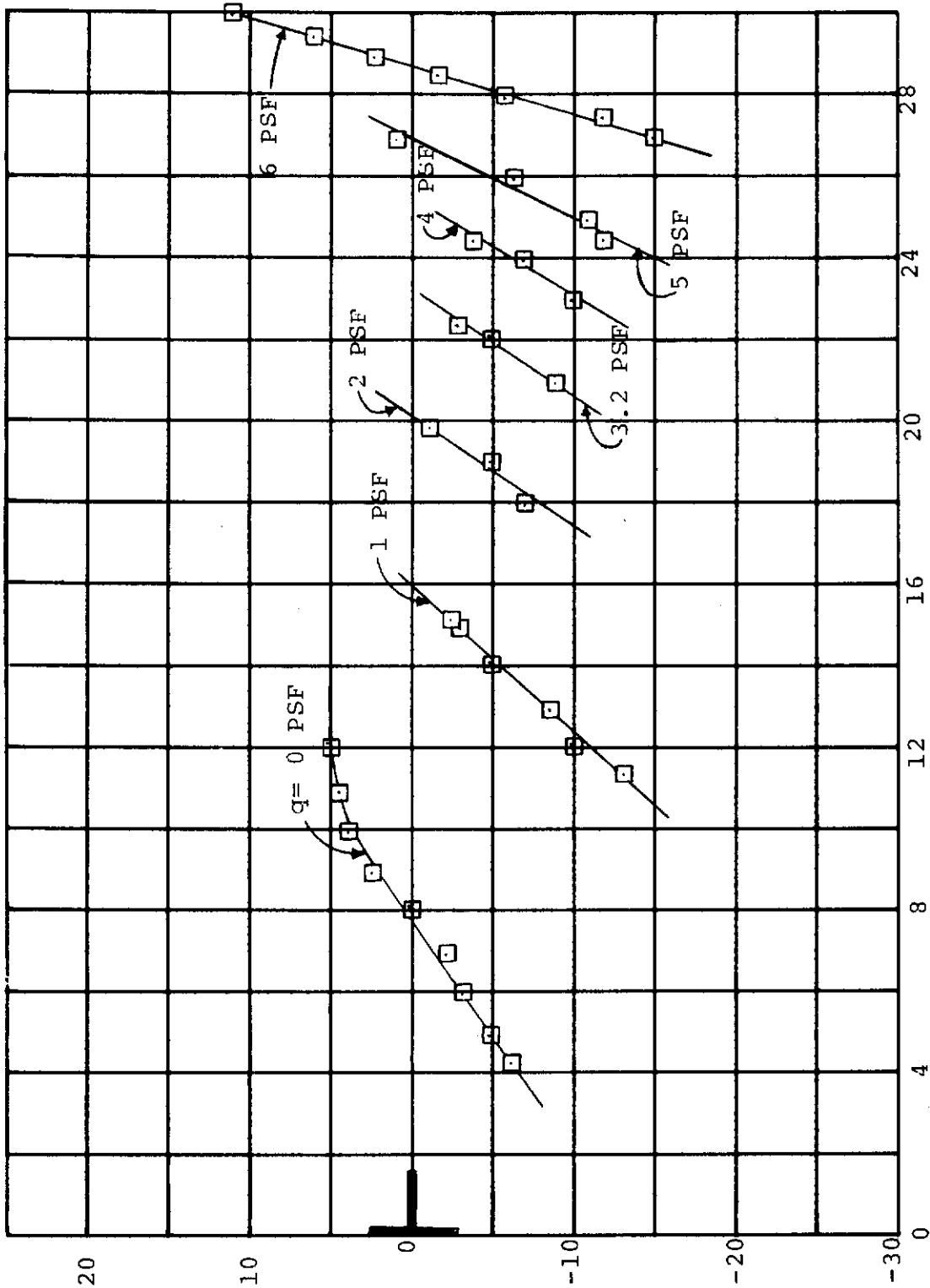


FIGURE 6-57. EFFECT OF COLLECTIVE PITCH ANGLE ON RIGHT ROTOR STEADY FLAP BENDING MOMENT IN CRUISE FOR $i_N=0$ DEG., $q = 6$ PSF, $\theta_2 = -0.5$ DEG., AND 790 RPM.

RUN 39(41)



STEADY FLAP BENDING MOMENT AT .10R (IN.LB.)

FIGURE 6-58. EFFECT OF COLLECTIVE PITCH ANGLE ON RIGHT ROTOR STEADY FLAP BENDING MOMENT IN CRUISE FOR $i_n = 0$ DEG., $\Theta_2 = -0.4$ DEG., AND 790 RPM.

6.4 BLADE RESPONSE TO MODEL DISTURBANCE

Pitch disturbances were manually induced to the model under various conditions during the test. Resulting blade load responses are presented in Figure 6-59 and 6-60 for some typical cases representing hover and cruise conditions respectively. In the hover case (Figure 6-59) the disturbance caused the alternating load to momentarily increase with the peak load occurring at the time when the pitching motion was at its maximum rate, approximately $60^\circ/\text{sec}$.

The blade loads which resulted from a pitch disturbance in the cruise condition (Figure 6-60) were primarily due to angle of attack change and contained essentially no dynamic amplification. The model modes, both rigid body and blade, were heavily damped.

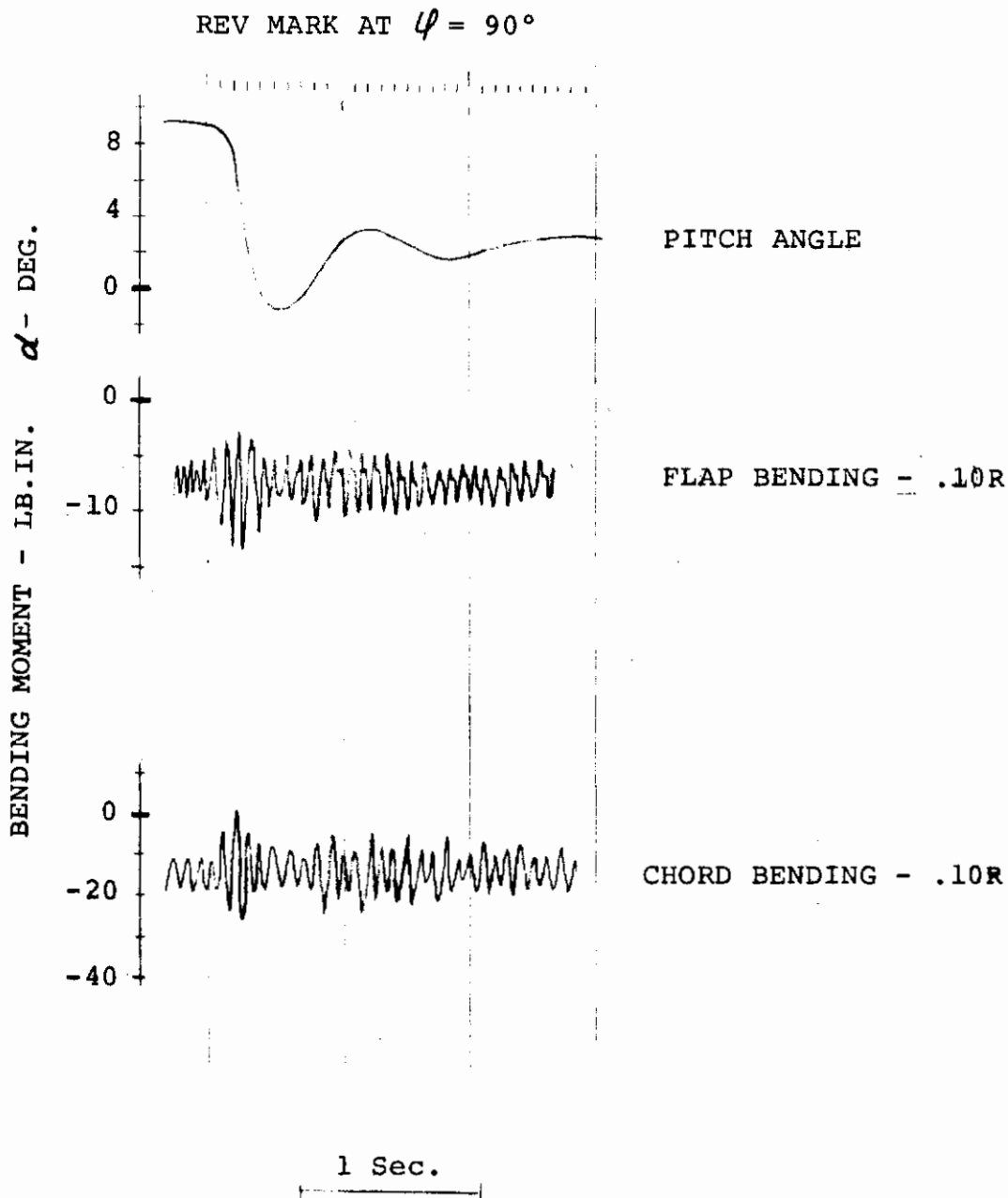


FIGURE 6-59. BLADE RESPONSE TO PITCH DISTURBANCE
IN HOVER, $\theta_{.75} = 6.0 \text{ DEG.}$, $\theta_2 = -0.5 \text{ DEG.}$,
 $\Omega = 830 \text{ RPM}$, RUN 65

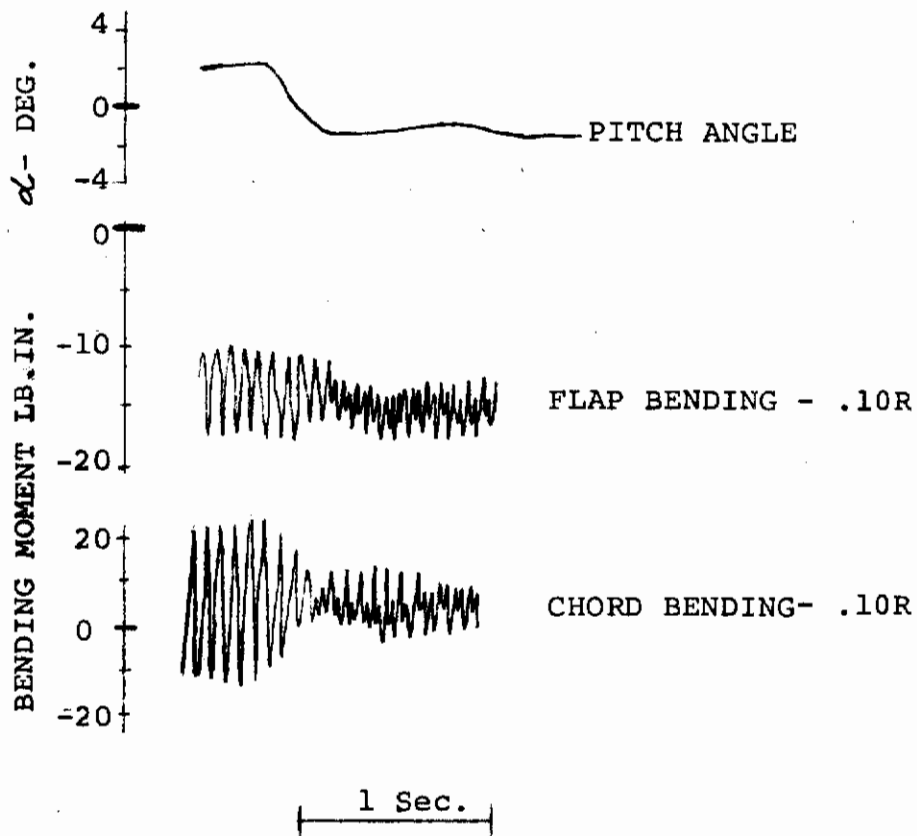


FIGURE 6-60 BLADE RESPONSE TO PITCH DISTURBANCE
IN CRUISE ATTITUDE: $\theta_{.75} = 28$ DEG.,
 $\Omega = 790$ RPM, $q = 7.0$ PSF, $\alpha_w = 0$ DEG.,
RUN 50

7.0 VEHICLE DYNAMICS

7.1 PREDICTED FREQUENCY AND DAMPING SPECTRUM

Figures 7-1 through 7-5 present the predicted modal frequencies (f vs Ω) and damping (% critical vs Ω) curves. The circled numbers in the figures serve only to identify the frequency roots without specific order. As noted, the modal characteristics of a given frequency root can change considerably with rotor speed. It can be seen in Figure 7-1 that the root "one" response is predominantly wing torsion at low rotor speeds and changes to predominantly blade response above 600 rpm (damping spectrum plots are associated to the frequency plots by root number). Representative tweak and shake test frequency results are shown at zero rpm on Figures 7-1 and 7-3. Correlation of the observed test frequencies with predictions, in general is good. Comparison of Figures 7-2 and 7-3 shows that the predicted damping values have significant dependence upon collective for this model.

7.2 VEHICLE FREQUENCIES

7.2.1 Rotors Non-Rotating

Modal frequencies and damping for the non-rotating system were obtained from tweak (initial displacement) and shake tests. Test results of the tweak test for the symmetric condition only at various nacelle tilt angles, encompassing cruise through hover, are shown in Table 7-1.

TABLE 7-1

WING FREQUENCIES AND DAMPINGS FROM TWEAK TEST

NACELLE INCIDENCE	SYM.WING FLAP		SYM.WING CHORD		SYM.WING TORSION	
	FREQ. (CPS)	DAMPING %	FREQ. (CPS)	DAMPING %	FREQ. (CPS)	DAMPING %
0° (Cruise)	5.2	.022	10.5	.012	16.8	.010
40°	5.1	.041	10.5	.015	17.0	X
60°	5.1	.032	10.3	.017	X	X
90° (Hover)	5.1	.033	10.5	.017	17.5	.012

Contrails

The effect of tilt angle on frequency was found to be negligible; however, wing flap modal damping varied to some extent.

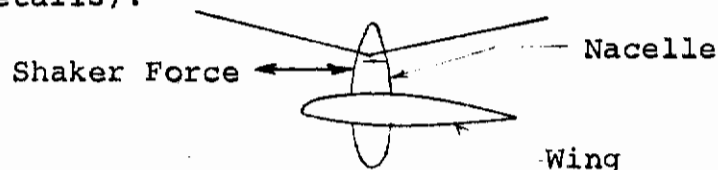
The symmetric and antisymmetric root bending moment frequency response curves from the hover configuration shake tests are shown by Figures 7-6 through 7-11. An index of the data is shown in Table 7-2. A response peak which is predominantly wing flap bending, occurs at a shaker frequency of 6 cps. The response at 9.3 cps is predominantly wing symmetric chord bending with considerable coupling with wing symmetric torsion. The blade chordwise bending frequency at $\Omega=0$ is also in this vicinity. The response near 17.5 cps is wing torsion. No test data is available between shaker frequencies of 10.5 cps and 14 cps for symmetric excitation. Data from tests conducted in this range was incorrect due to a malfunction in the computer analysis system and the test response data was irretrievable.

TABLE 7-2

SHAKE TEST INDEX - ROTORS NON-ROTATING

FIGURE	TYPE OF EXCITATION	FREQUENCY RESPONSE CURVE
7-6	Symmetric	Wing Flap Bending
7-7	Symmetric	Wing Chord Bending
7-8	Symmetric	Wing Torsion
7-9	Antisymmetric	Wing Flap Bending
7-10	Antisymmetric	Wing Chord Bending
7-11	Antisymmetric	Wing Torsion

The shake test was performed employing two air jet shakers, one mounted on each nacelle. These shakers were mounted approximately 4 inches ahead of the wing elastic axis and provided excitation normal to the nacelle as shown below (see Figure 3-6 for details).



The phase between the left and right shakers was adjusted to provide both symmetric and antisymmetric excitation to the wings, with the frequency of excitation varying from zero to 20 cps.

7.2.2 Rotating Rotors

Figures 7-12 through 7-17 show the wing symmetric root bending moment frequency response curves from the cruise and hover configuration shake tests; and an index of the data is shown in Table 7-3. The rotor speed for these shake tests was 790 RPM and 825 RPM respectively.

TABLE 7-3

SHAKE TEST INDEX -- ROTATING ROTORS

FIGURE	NACELLE POSITION	FREQUENCY RESPONSE CURVE
7-12	Cruise	Wing Flap Bending
7-13	Cruise	Wing Chord Bending
7-14	Cruise	Wing Torsion
7-15	Hover	Wing Flap Bending
7-16	Hover	Wing Chord Bending
7-17	Hover	Wing Torsion

An examination of the rotating data indicates that the wing bending frequencies are not significantly changed from the non-rotating ones. The large peak around 13.5 cps is predominantly the 1st harmonic of the rotor excitation caused by an unbalance in the rotor system. A summary of the wing natural frequencies determined from tweak test, shake test and analysis is shown in Table 7-4.

TABLE 7-4
WING FREQUENCY SUMMARY

TWEAK TEST (SYM)	SHAKE TEST				NON-ROTATING CALCULATED		MODE
	SYM.		ANTI-SYM.		SYM	ANTI-SYM	
	ROTAT.	NON ROTAT.	ROTAT.	NON ROTAT.			
5.1CPS	6.9	6.0	*	*	4.6	> 20	Flap Bending
10.5	10.0	9.0	*	*	9.1	> 20	Chord Bending
17.5	17.2	17.5	-	17.5	18.0	15.4	Torsion

*Not observed during the shake test and predicted to be above the maximum shaker frequency.

7.3 ELASTIC MODE STABILITY

The model was run through an equivalent full scale nacelle tilt/airspeed envelope as shown in Figure 3-8 to check for whirl flutter, divergence, classical flutter or air resonance. There was no evidence of any of these phenomena throughout the test range. The presence of substantial 1/rev loads due to model unbalance and the limited force available from the shaker made it impossible to obtain good quantitative modal damping data, but there was clearly no tendency for any of these modes to be self excited or to persist if excited by abrupt airplane motions or by the shaker unit in the natural frequency tests described in Section 7-1. A model response occurred associated primarily with blade chord bending under conditons near zero thrust in hover and at low velocities in transition. In some cases a limit cycle oscillation developed. This response did not occur at the higher tunnel speeds tested in the cruise mode.

The mode was always sufficiently stable that a substantial volume of test data could be taken at the conditions where it was encountered. These data are presented and the phenomenon is discussed in more detail under Item 7.3.2.

7.3.1 Input Disturbances

The model was disturbed with the snubber cables from its trim position at various conditions throughout the test to determine its rigid body and elastic modal response. The rigid body data were obtained by gradually displacing the model from trim and then releasing the cables quickly. In all cases throughout the test the rigid body modes were very stable. Results are discussed in Section 8.0. Typical pitch and roll responses are shown in Figure 8-1.

7.3.2 Blade Chord Bending Mode Oscillations

As mentioned under 7.3 there were some conditions where a mode, associated primarily with blade chord bending, was lightly damped or developed a limit cycle oscillation. As can be seen from Figure 7-18 the conditions at which the oscillation occurred followed closely the conditions for zero thrust. The data points shown by circles (indicating zero thrust conditions) were obtained from Figure 6-59. A typical oscillograph tape showing the nature of the mode as a **limit cycle oscillation** is given in Figure 7-19.

The primary characteristic is the blade chord bending trace, which shows a substantial .72 per rev (blade chord bending natural frequency) superimposed on the normal one per rev. This shows up as the .28 per rev beat visible in the trace. The blade flap bending and torsion show the same frequencies though with less amplitude, while wing torsion (fixed system) shows a corresponding $1-.72=.28$ per rev superimposed on the one per rev. Aircraft pitching motion also shows a small response at the same .28 per rev frequency. There is very little response at this frequency in wing chord bending or wing torsion.

Correlation of the predicted $\Omega - \omega_1$ mode damping with some limited test data is presented in Figure 7-20. The same type of low frequency beat response was observed over a range of conditions during transition and cruise testing. Boundaries for occurrence of the oscillations are given in Figures 7-21 and 7-22 by showing the regions of non-occurrence, in low damping and limit cycle. Additional data are desirable to define these boundaries more fully.

The beat oscillation could also be found during a rapid shutdown, and the beat frequency used as an additional check on rotating blade chordwise frequencies.

Contrails

During the shutdown period of Run 40, the rotor was windmilling and beat frequencies occurred which changed with rotor speed (controlled by q). These beat frequencies are shown in the lower portion of Figure 7-29 and when added to the rotor speed ($\Omega + \omega$ beat) below the resonant crossover and subtracted from the rotor speed ($\Omega - \omega$ beat) above the crossover they appear as shown in the frequency spectrum in the upper part of Figure 7-29. Note the correlation with the baffle test and predicted frequencies. Note also that the crossover decreased from the 550 rpm baffle test to 510 rpm. This corresponds almost exactly with the decrease in chord bending tweak frequency which occurred from the start of testing to Run 40 as noted in Figure 4-1 due apparently to monocoat deterioration.

This type of oscillation has been found also on some helicopter models and on one other tilt rotor model (a stiff model with in-plane and out-of-plane frequencies of about 2.2Ω and 1.5Ω respectively). Theory indicates that it is generally associated with large initial out-of-plane deflections of the blade, especially in the negative thrust direction. This is confirmed by the fact that this model, which had 5° precone experienced the instability only near zero thrust, where the blades are bent back from their 5° precone position by centrifugal force. On a full scale aircraft it will be necessary to give careful consideration to this type of instability in selecting the precone angle.

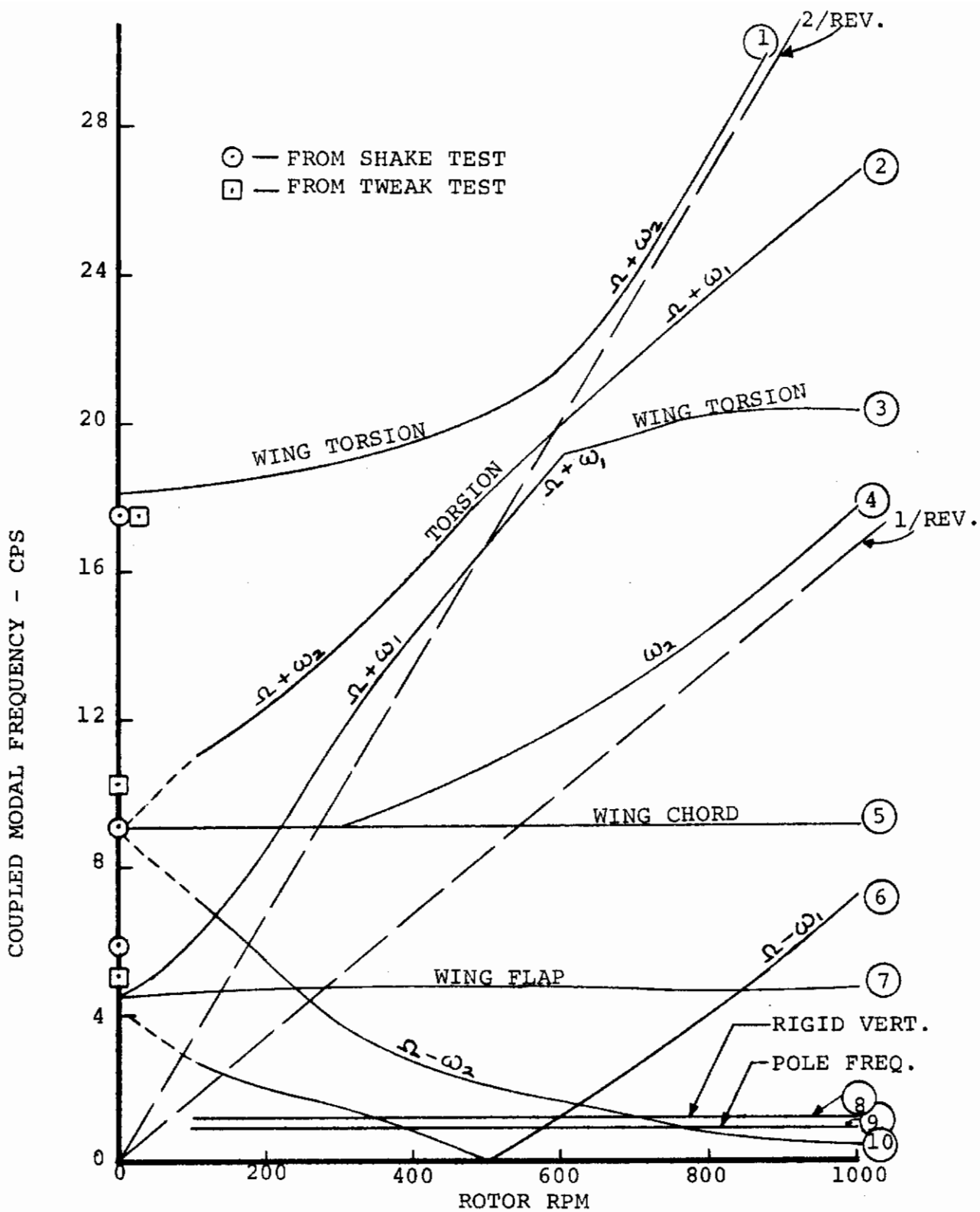


FIGURE 7-1. FREQUENCY SPECTRUM FOR SYMMETRICAL HOVER MODES

Contrails

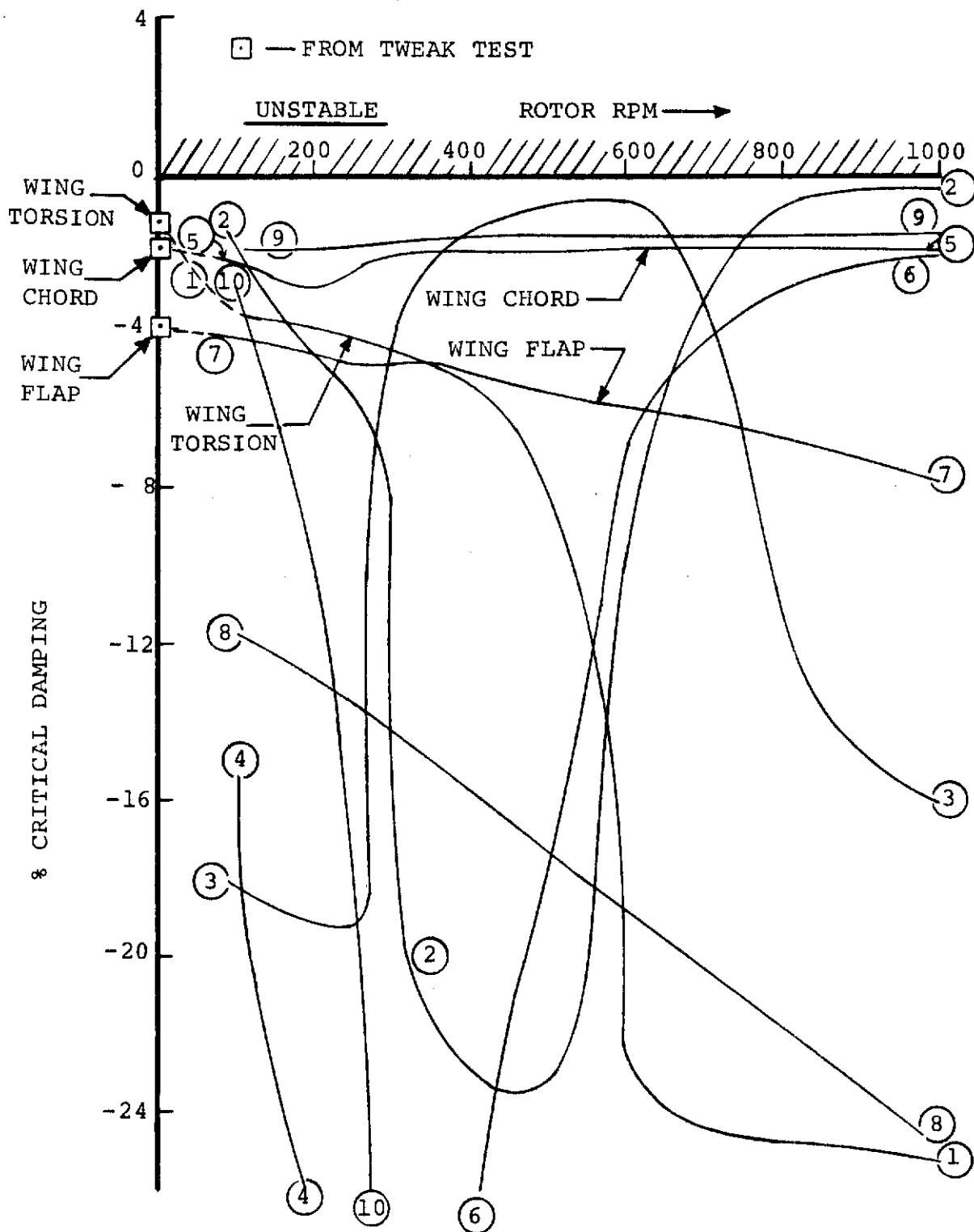


FIGURE 7-2. DAMPING SPECTRUM FOR SYMMETRICAL HOVER MODES, $\theta_{.75} = 11$ DEG.

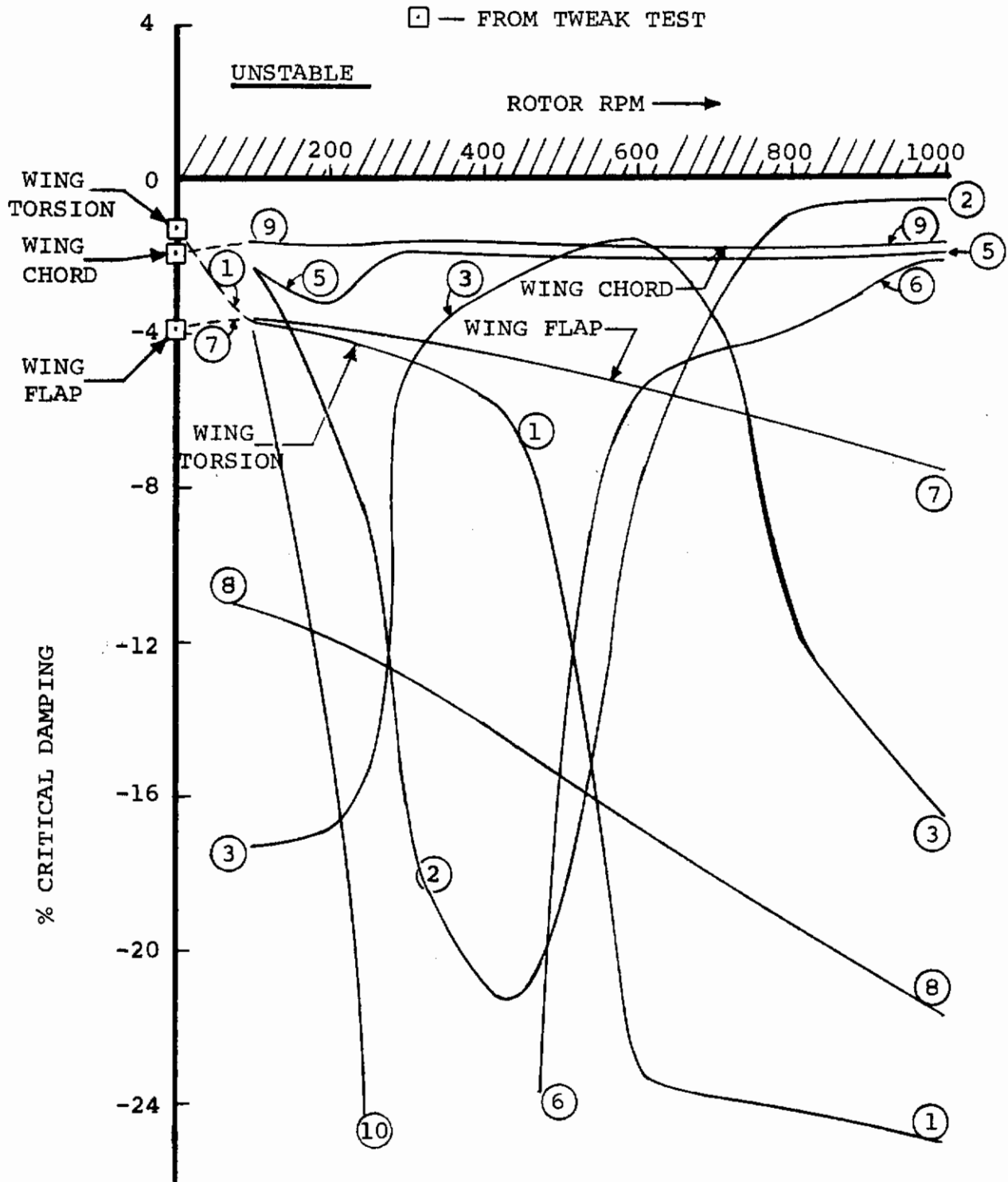


FIGURE 7-3. DAMPING SPECTRUM FOR SYMMETRICAL HOVER MODES ($\theta_{.75} = 0$)

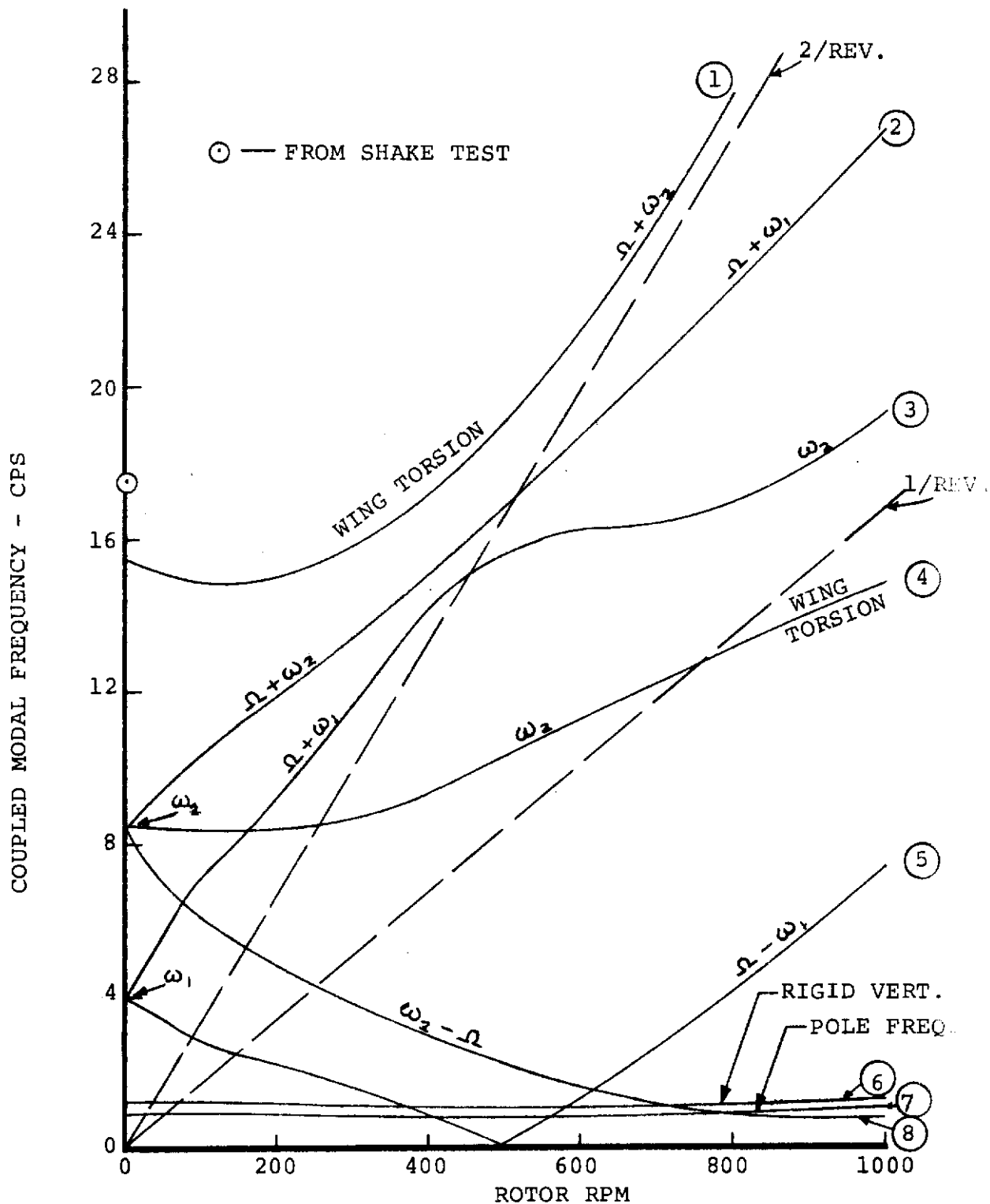


FIGURE 7-4. FREQUENCY SPECTRUM FOR ANTI-SYMMETRICAL HOVER MODES ($\sigma_{.75} = 0$)

Contrails

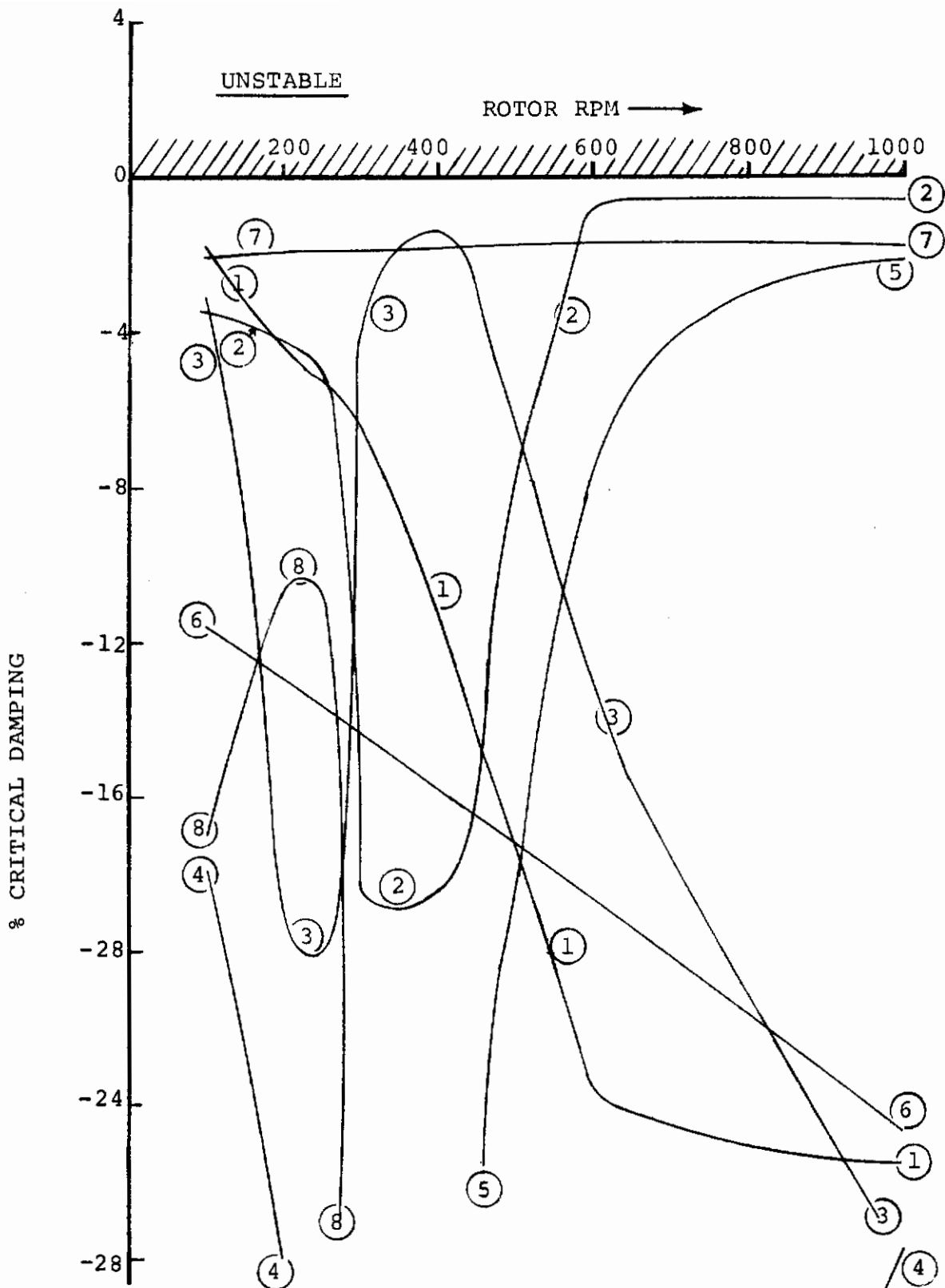


FIGURE 7-5. DAMPING SPECTRUM FOR ANTI-SYMMETRICAL HOVER MODES ($\sigma_{.75} = 0$)

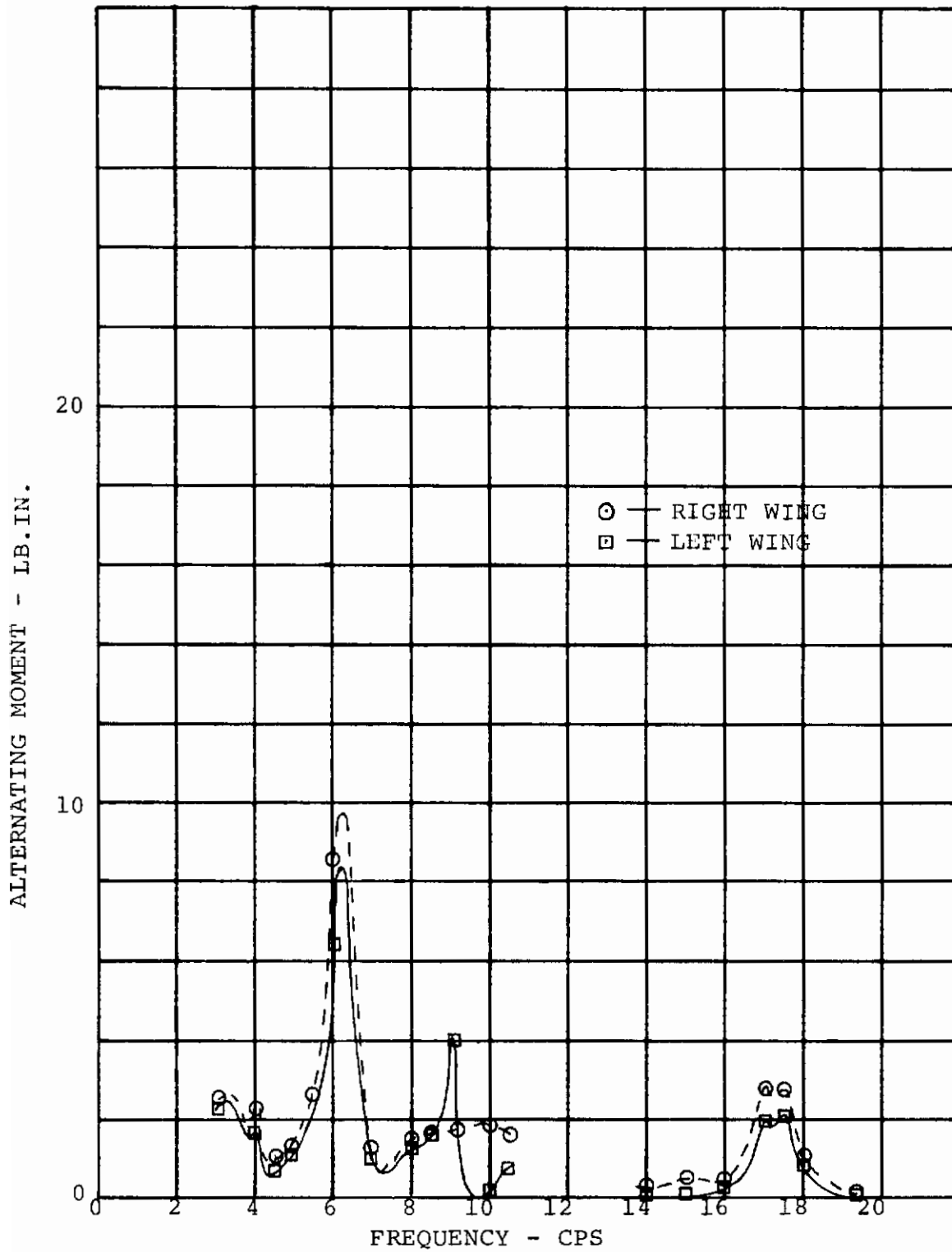


FIGURE 7-6: WING FLAP BENDING RESPONSE TO SYMMETRICAL EXCITATION-NON-ROTATING BLADES, $i_N = 90\text{DEG}$.

Contrails

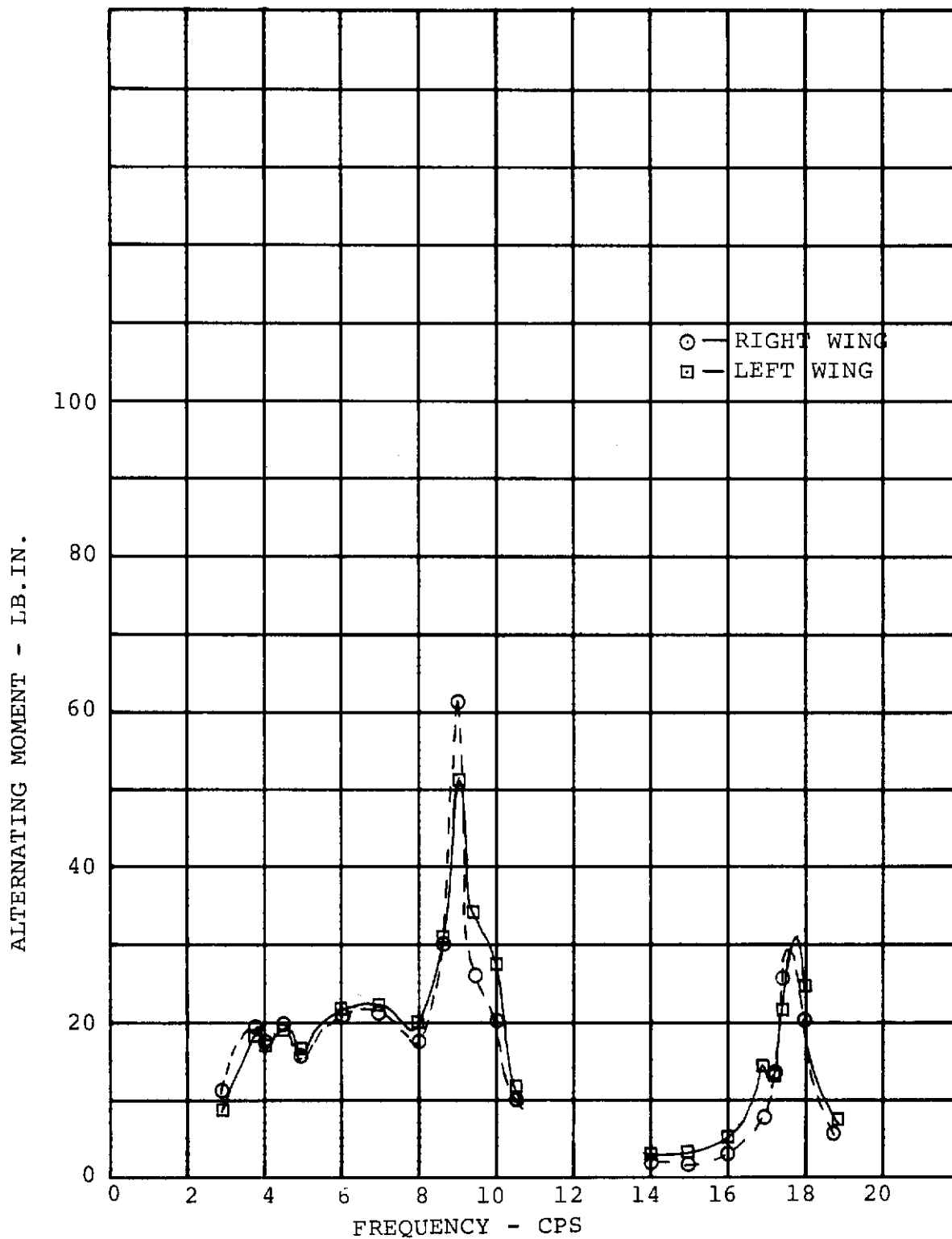


FIGURE 7-7: WING CHORD BENDING RESPONSE TO SYMMETRICAL EXCITATION-NON-ROTATING BLADES, $i_N = 90$ DEG.

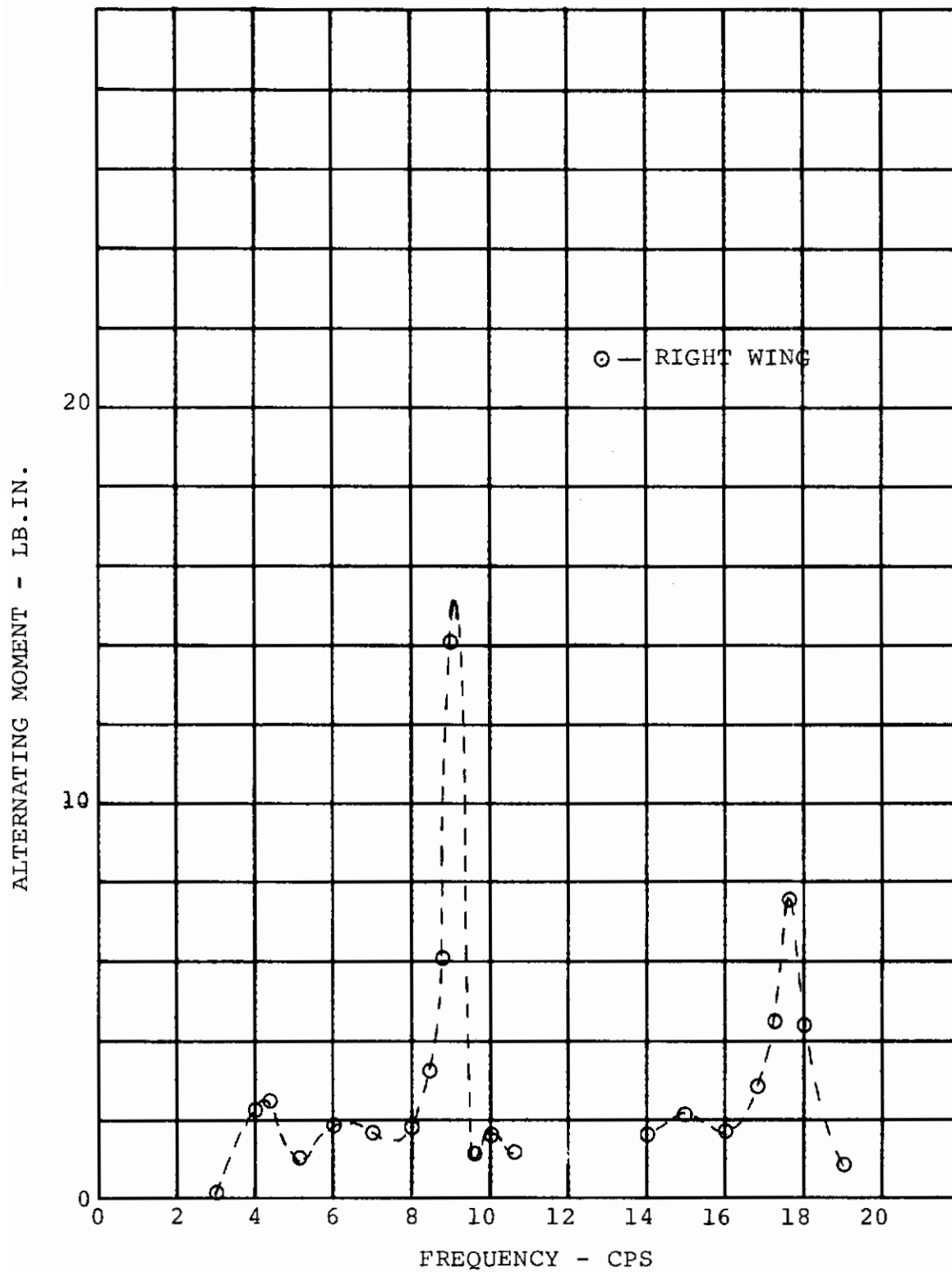


FIGURE 7-8: WING TORSION RESPONSE TO SYMMETRIC EXCITATION
NON-ROTATING BLADES, $i_N = 90$ DEG.

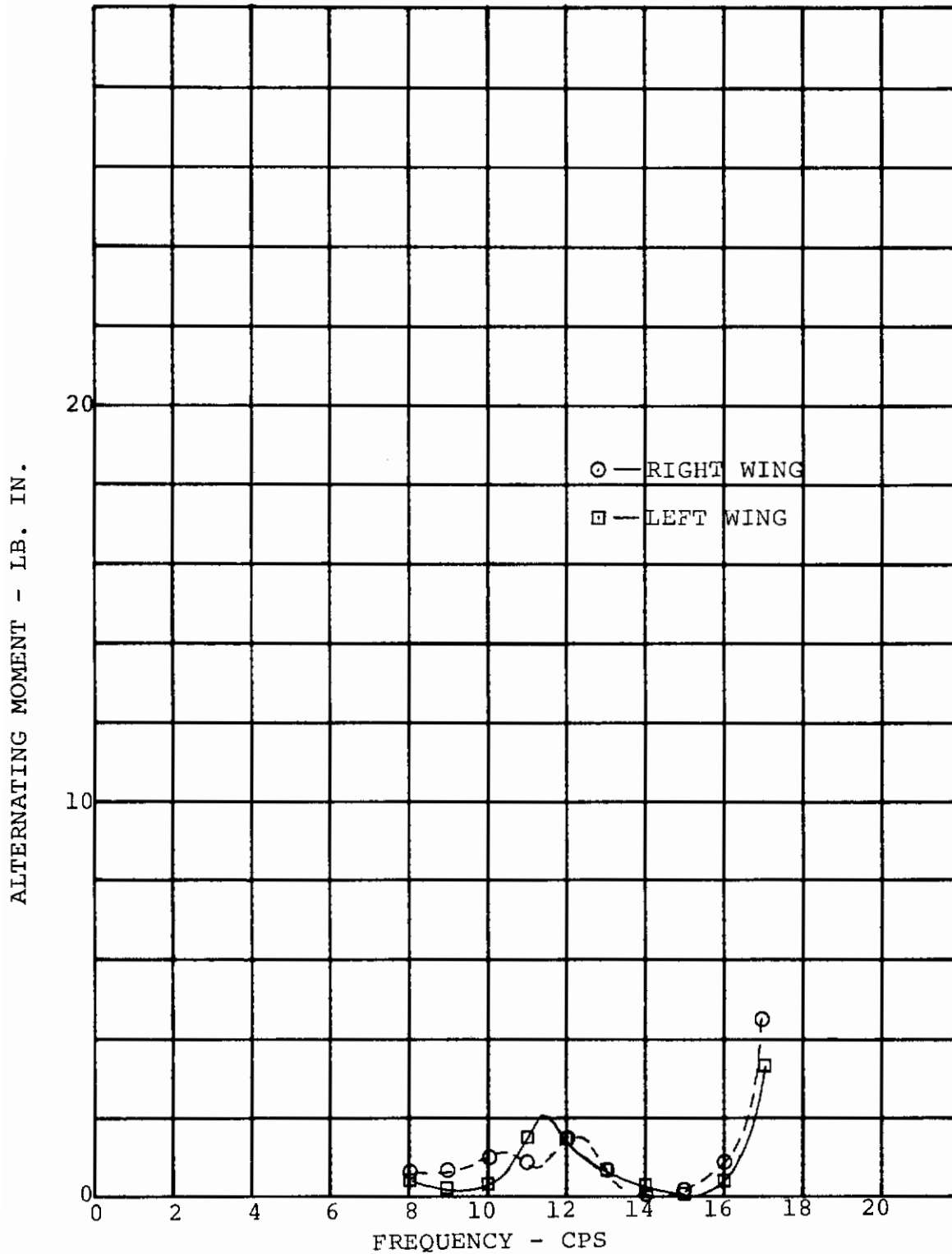


FIGURE 7-9: WING FLAP BENDING RESPONSE TO ANTI-SYMMETRIC EXCITATION-NON-ROTATING BLADES, $i_N = 90$ DEG.

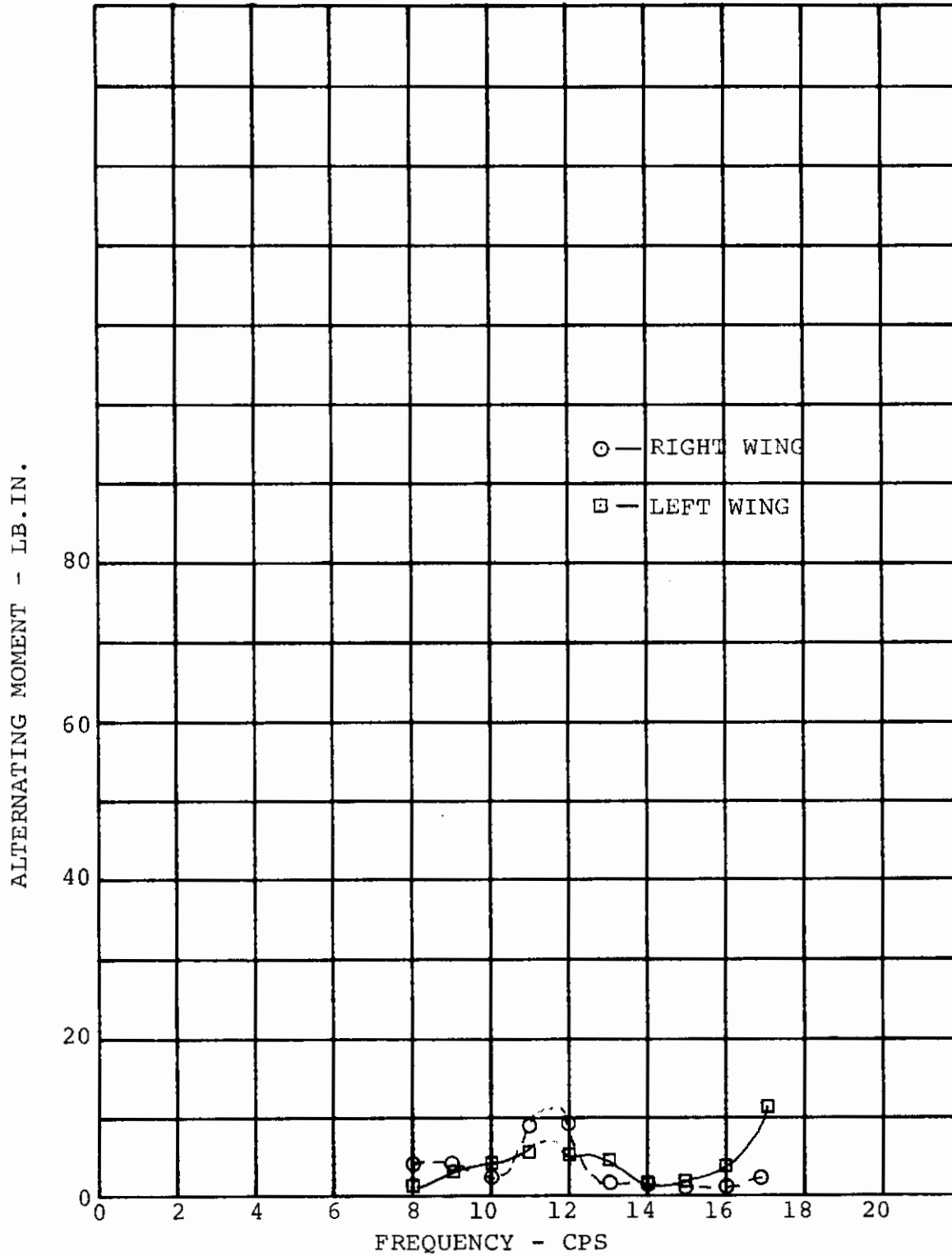


FIGURE 7-10: WING CHORD BENDING RESPONSE TO ANTI-SYMMETRIC EXCITATION-NON-ROTATING BLADES, $i_N = 90$ DEG.

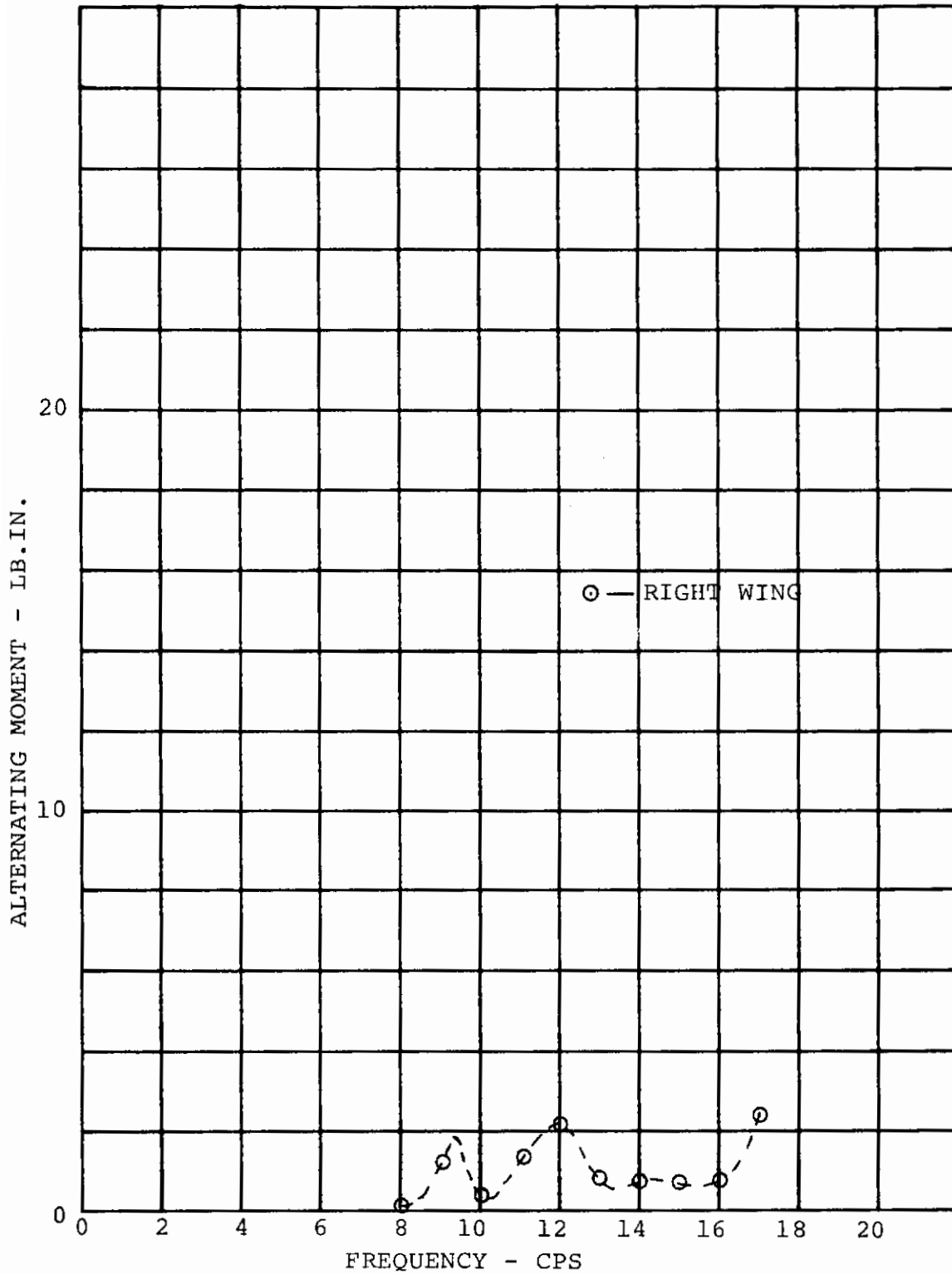


FIGURE 7-11: WING TORSION RESPONSE TO ANTI-SYMMETRIC EXCITATION, NON-ROTATING BLADES, $i_N=90$ DEG.

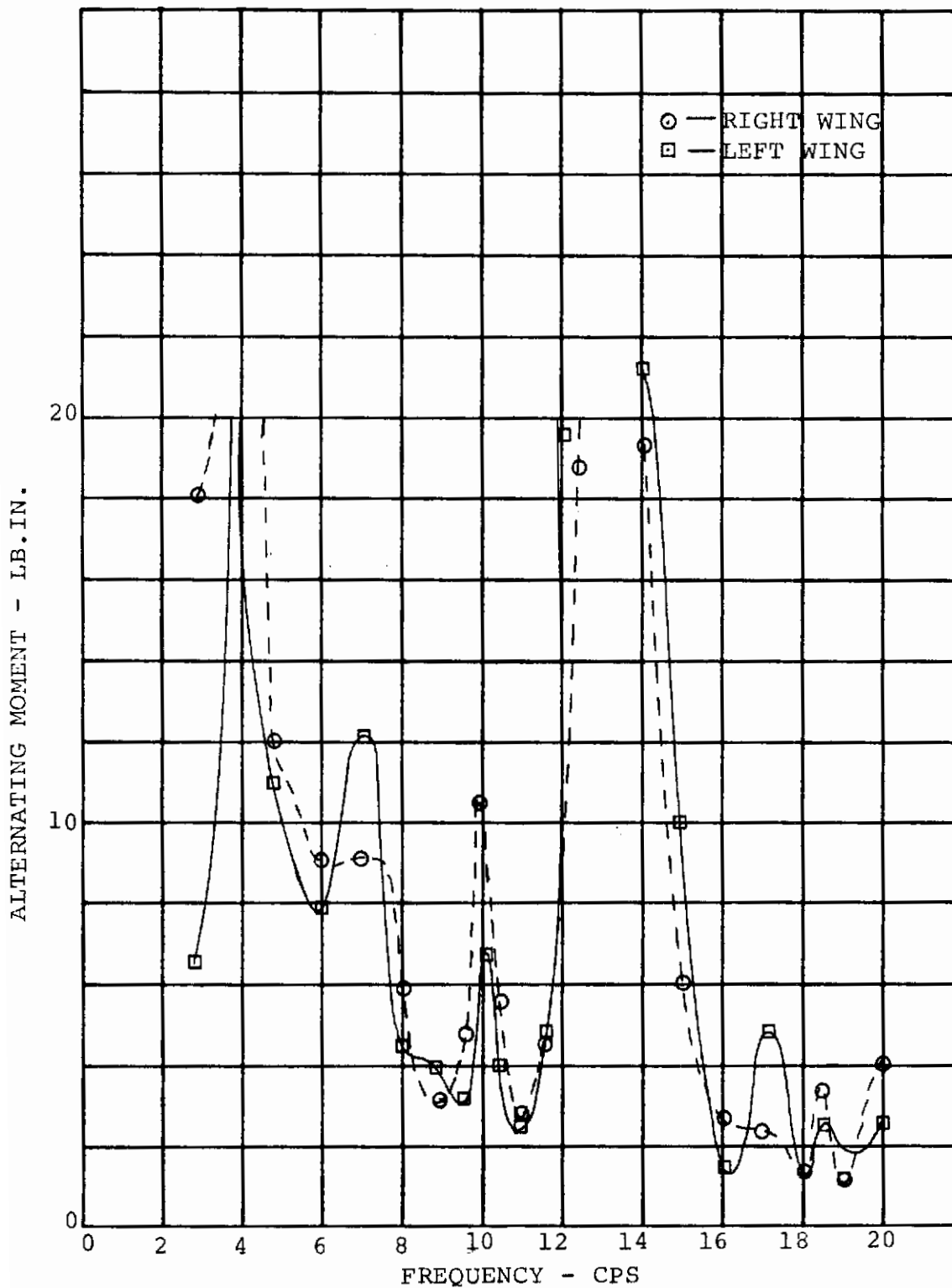


FIGURE 7-12: WING FLAP BENDING RESPONSE TO SYMMETRIC EXCITATION, $\Omega = 790$ RPM, $q = 0$ PSF., $\Theta_{.75} = 6$ DEG., $i_N = 0$ DEG., RUN 45

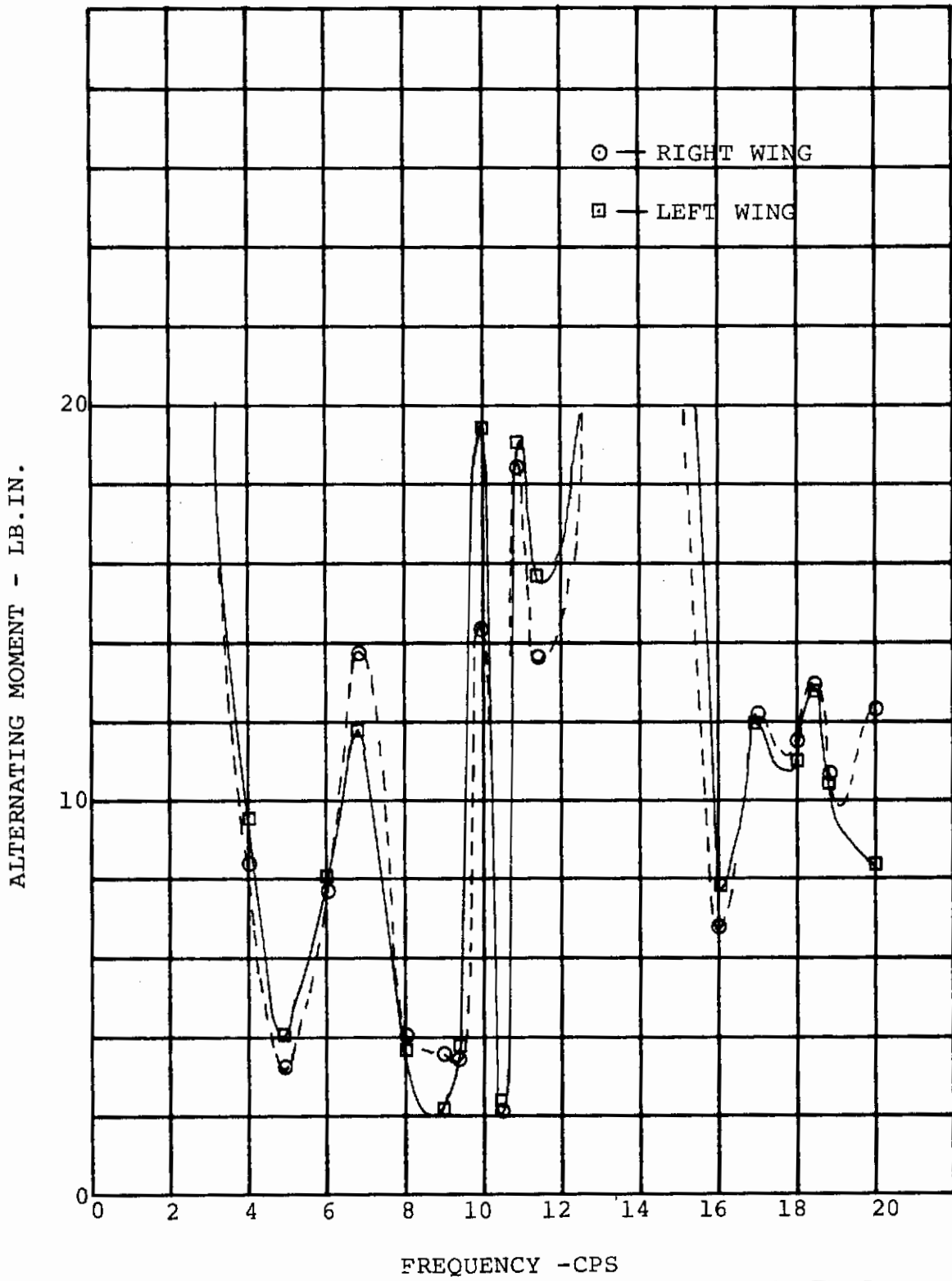


FIGURE 7-13: WING CHORD BENDING RESPONSE TO SYMMETRIC EXCITATION, $\Omega = 790$ RPM, $q = 0$ PSF., $\theta_{.75} = 6$ DEG., $i_N = 0$ DEG., RUN 45

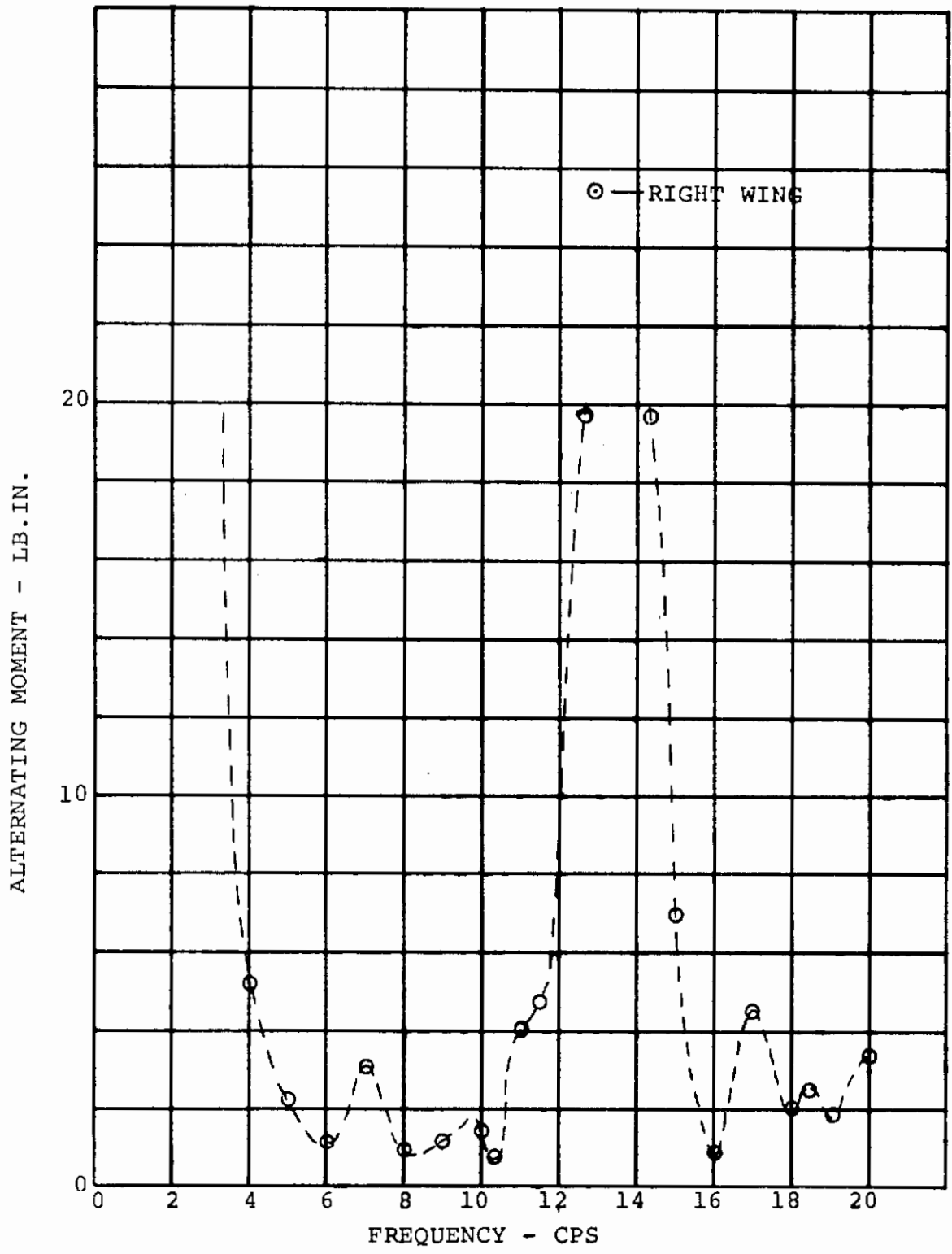


FIGURE 7-14: WING TORSION RESPONSE TO SYMMETRIC EXCITATION - $\Omega = 790$ RPM, $q = 0$ PSF, $\Theta_{.75} = 6$ DEG. $i_N = 0$ DEG., RUN 45

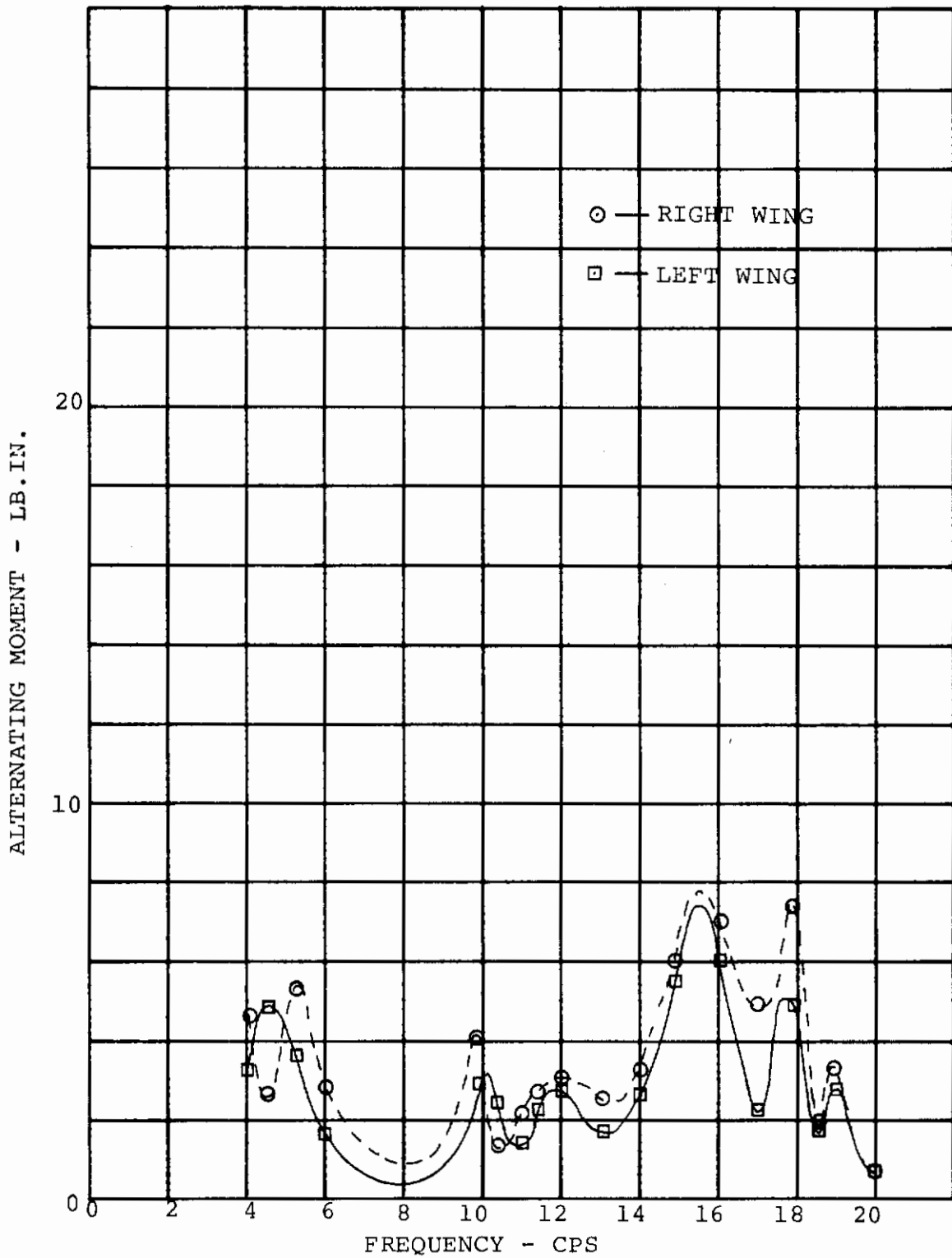


FIGURE 7-15: WING FLAP BENDING RESPONSE TO SYMMETRIC EXCITATION - $\Omega = 825$ RPM, $q = 0$ PSF., $\theta_{.75} = 10$ DEG., $i_N = 90$ DEG., RUN 52

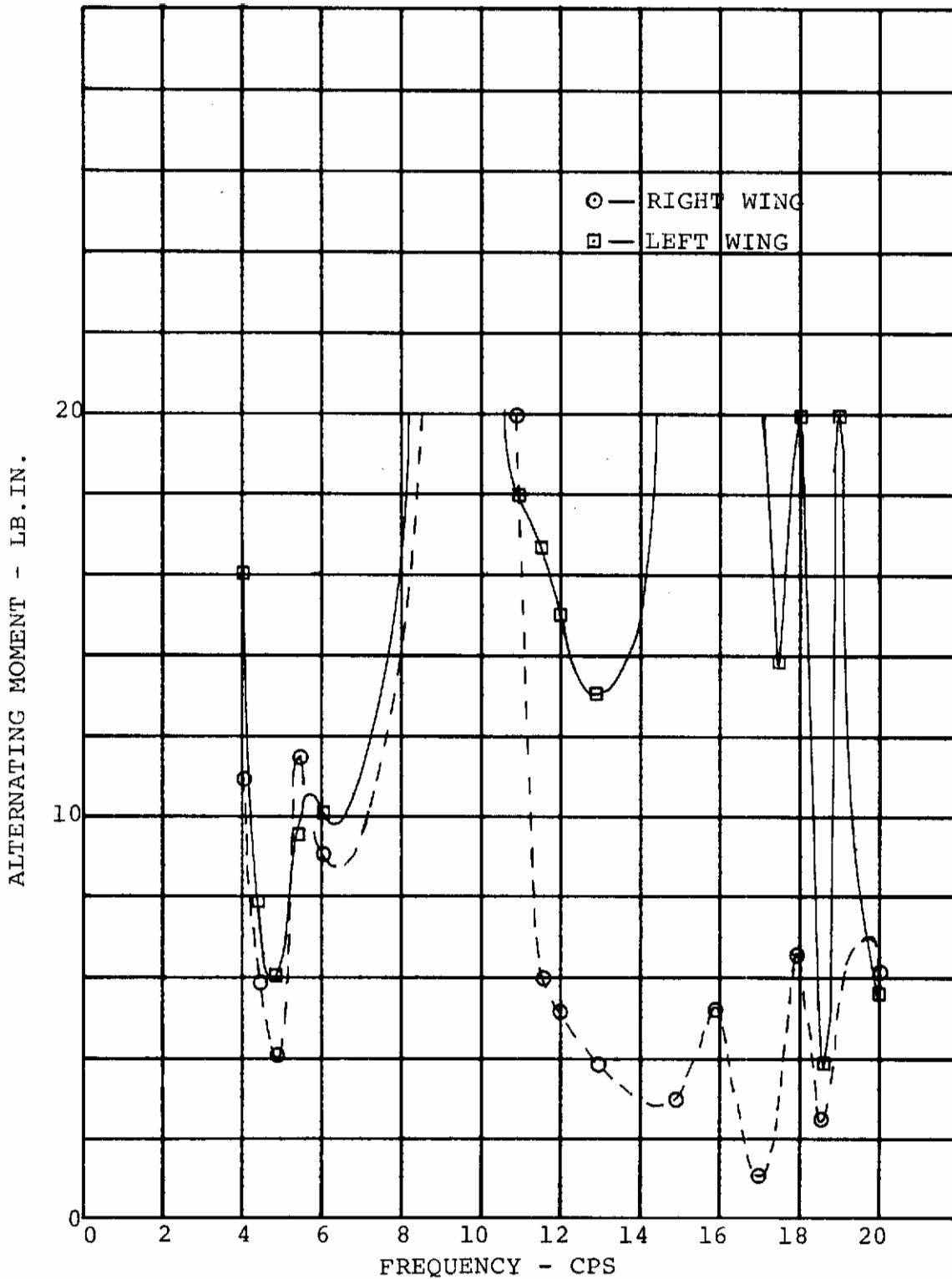


FIGURE 7-16: WING CHORD BENDING RESPONSE TO SYMMETRIC EXCITATION, $\Omega = 825$ RPM, $q = 0$, $\theta_{.75} = 10$ DEG. $i_N = 90$ DEG., RUN 52

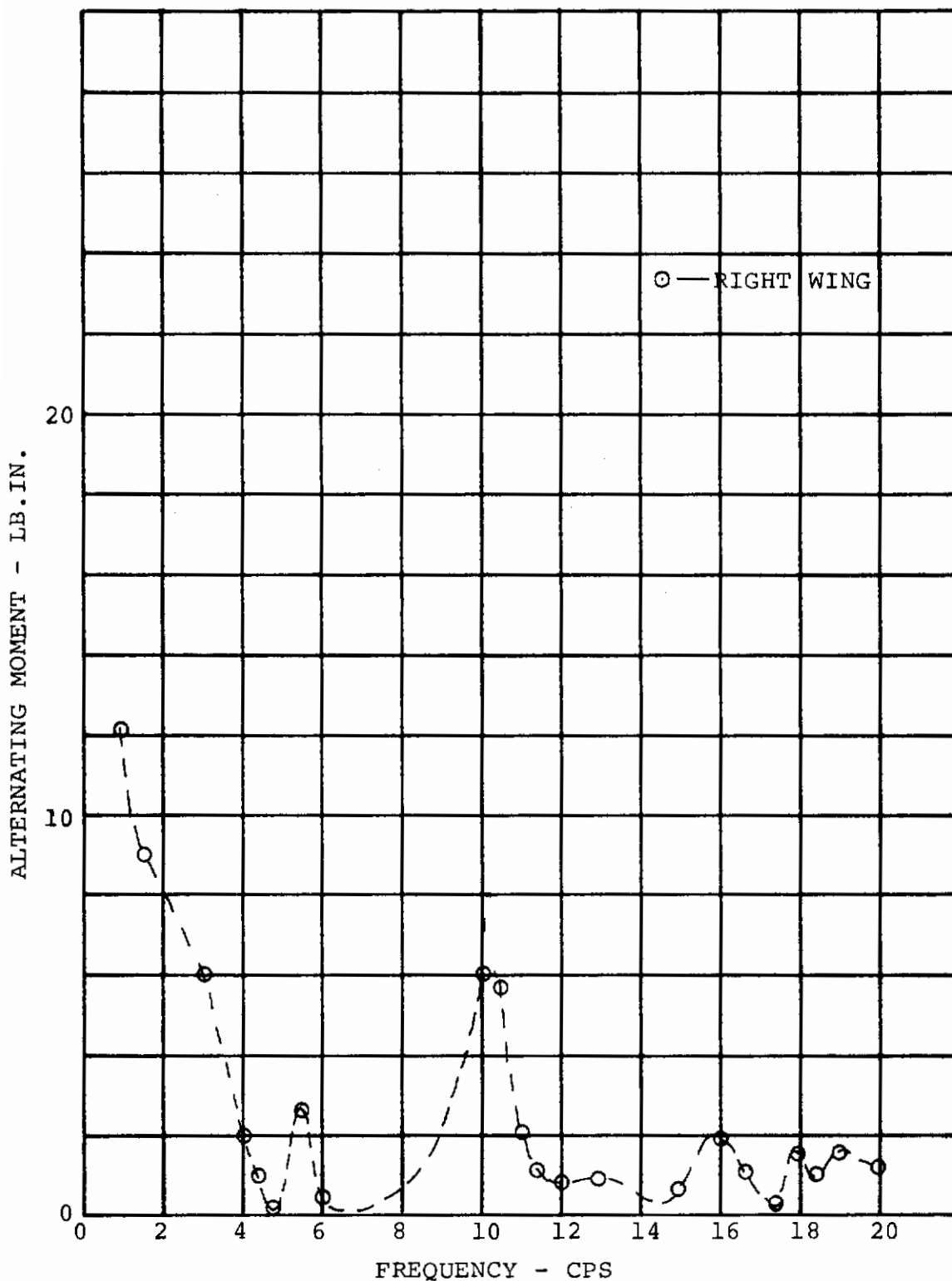


FIGURE 7-17: WING TORSION BENDING RESPONSE TO SYMMETRIC EXCITATION $-\Omega = 825$ RPM, $q = 0$, $\theta_{.75} = 10$ DEG. $i_N = 90$ DEG., RUN 52

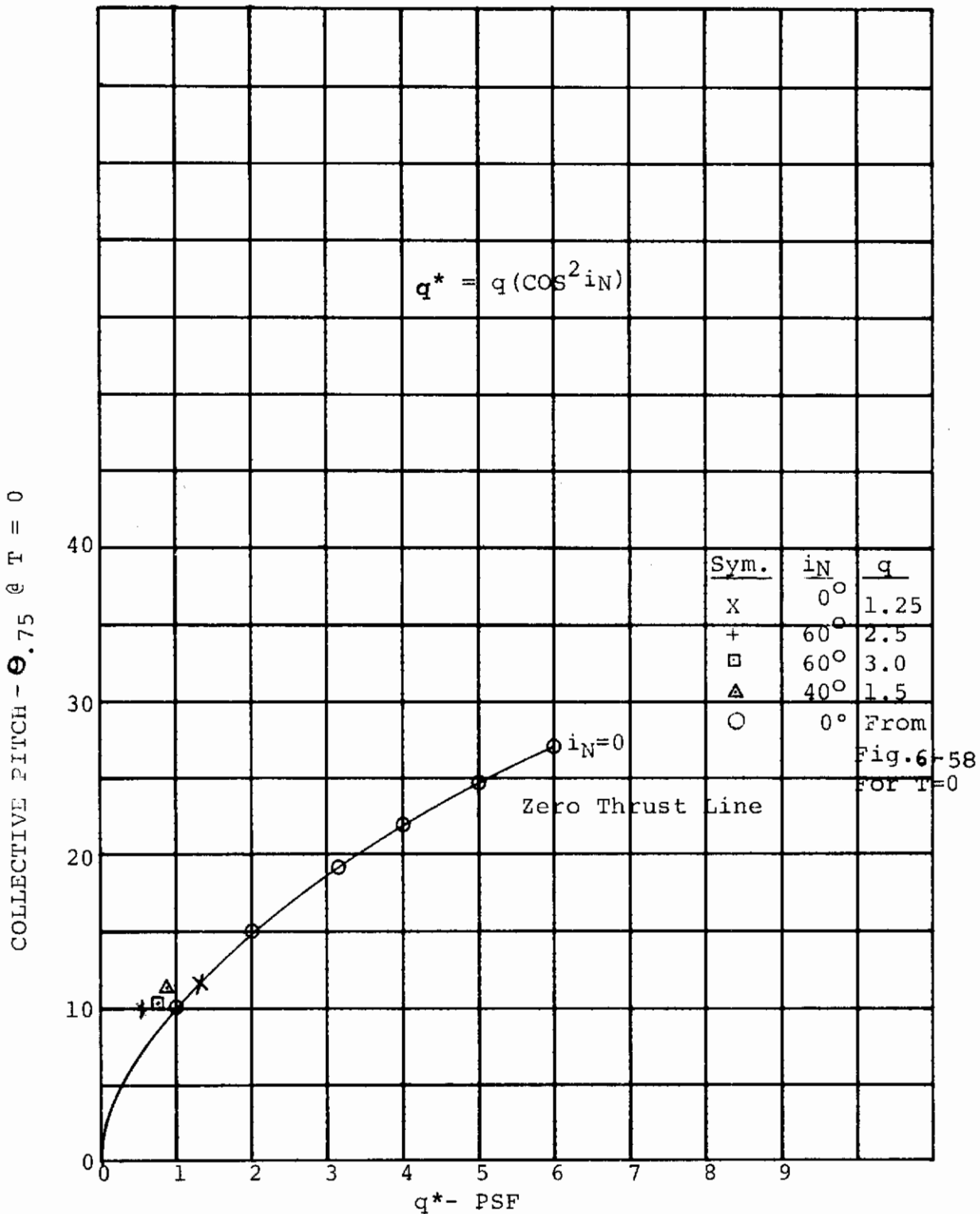
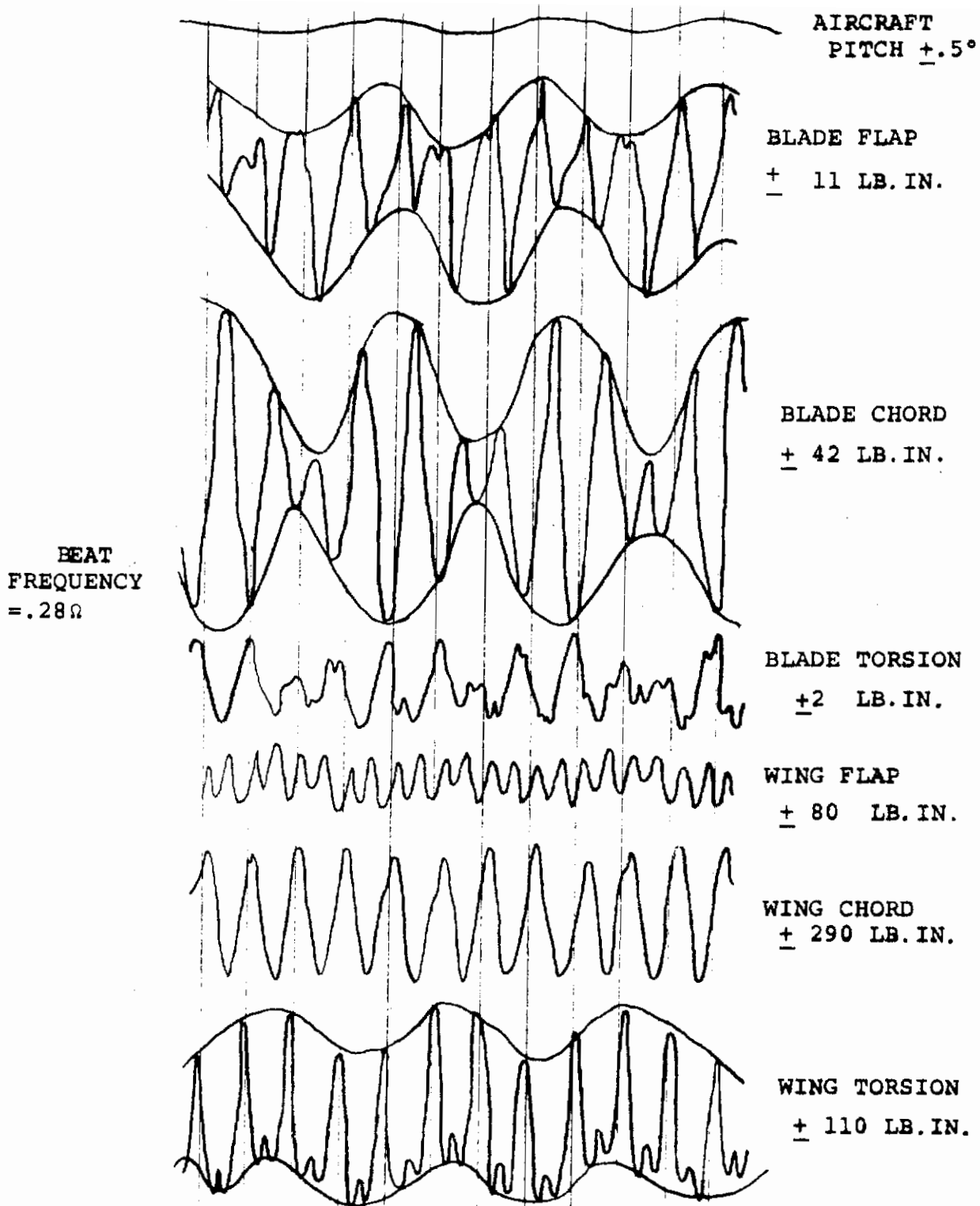


FIGURE 7-18 - LOW FREQUENCY OSCILLATION OCCURRENCES RELATIONSHIP TO ZERO THRUST

Contrails



NOTE: Oscillation started at $q = 2.5$ psf

FIGURE 7-19 BEAT FREQUENCY RESPONSE OSCILLOGRAM
RIGHT BLADE AND WING, $\Omega = 790$ RPM, $\theta_{75} = 10.2$ DEG.,
 $\theta_2 = 3.5$ DEG. $q = 2.75$ PSF, $i_N = 60$ DEG., RUN 40(12).

Contrails

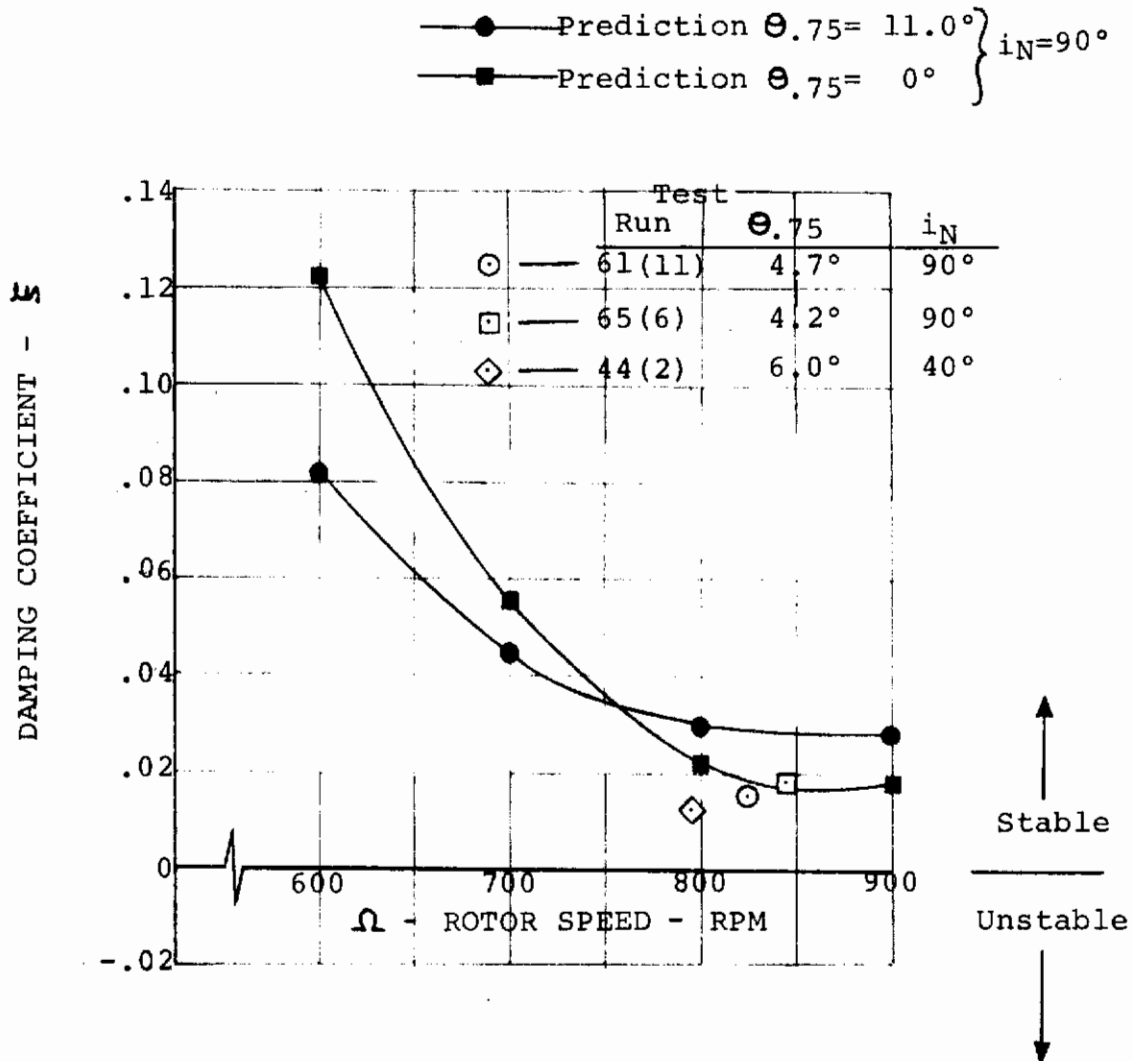


FIGURE 7-20. - CORRELATION OF OBSERVED LOW FREQUENCY MODE DAMPING WITH PREDICTION. $q = 0$

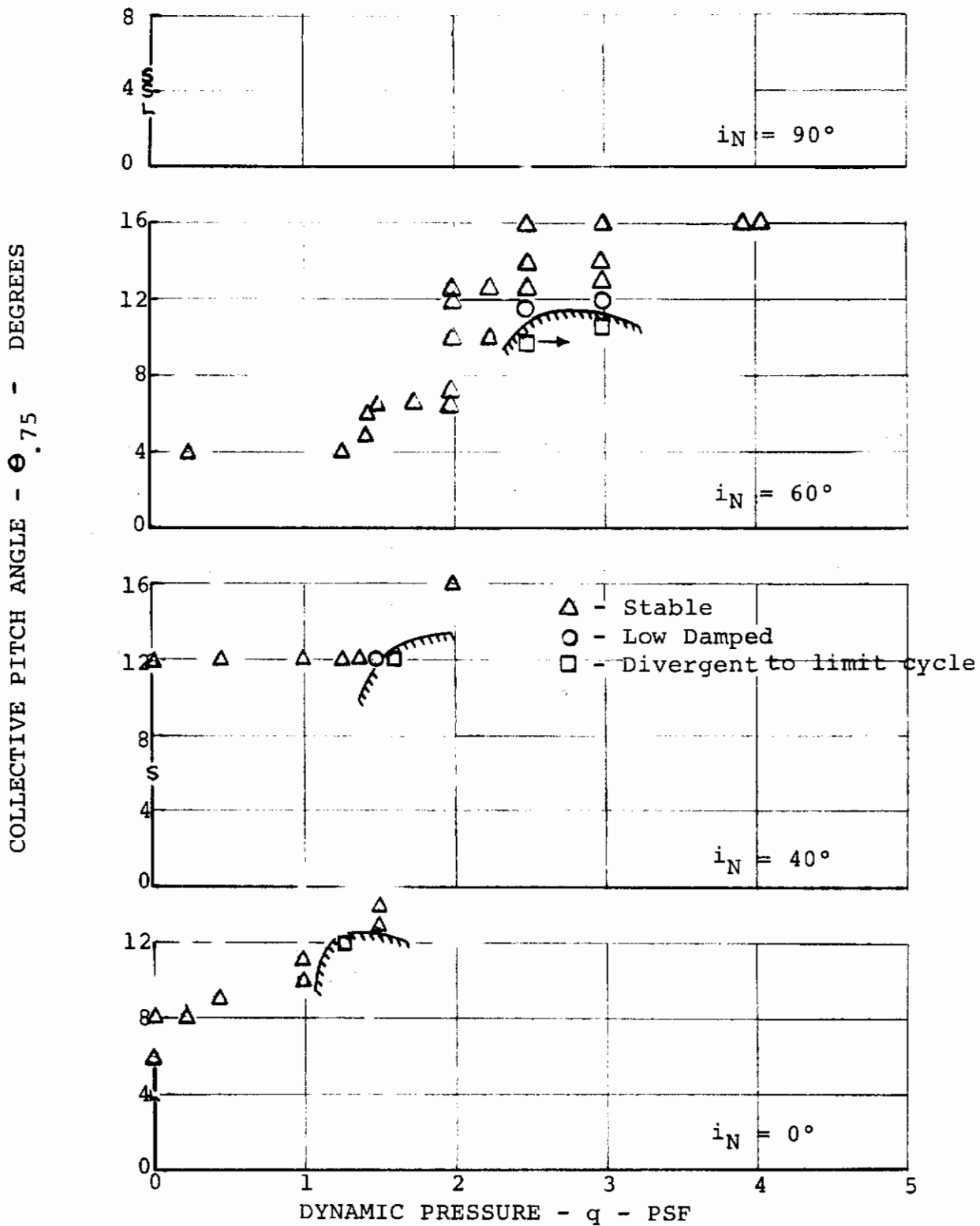


FIGURE 7-21. REGIONS OF LOW FREQUENCY OSCILLATION OCCURRENCES

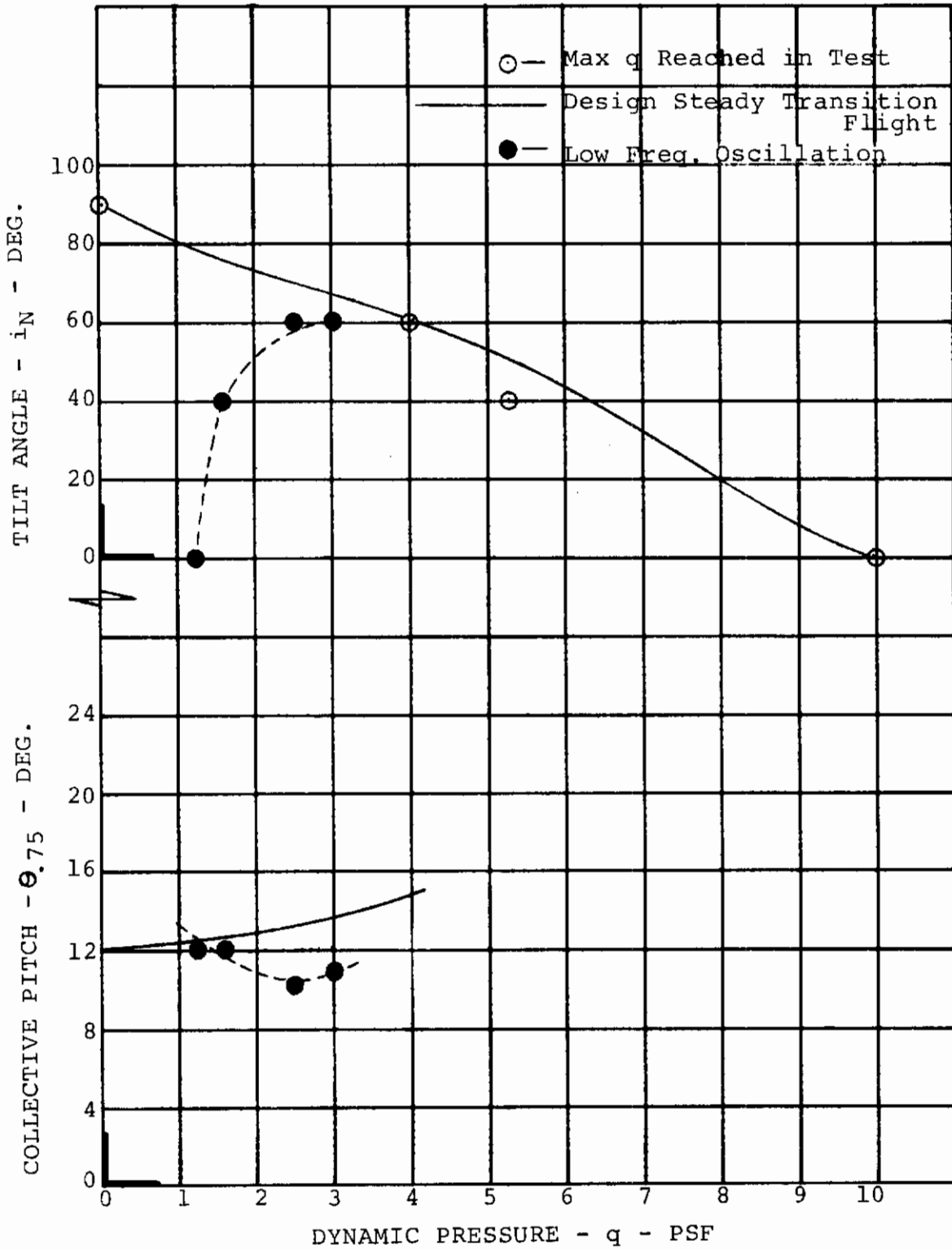


FIGURE 7-22. SUMMARY OF CONDITIONS AT WHICH LOW FREQUENCY OSCILLATION OCCURRED.

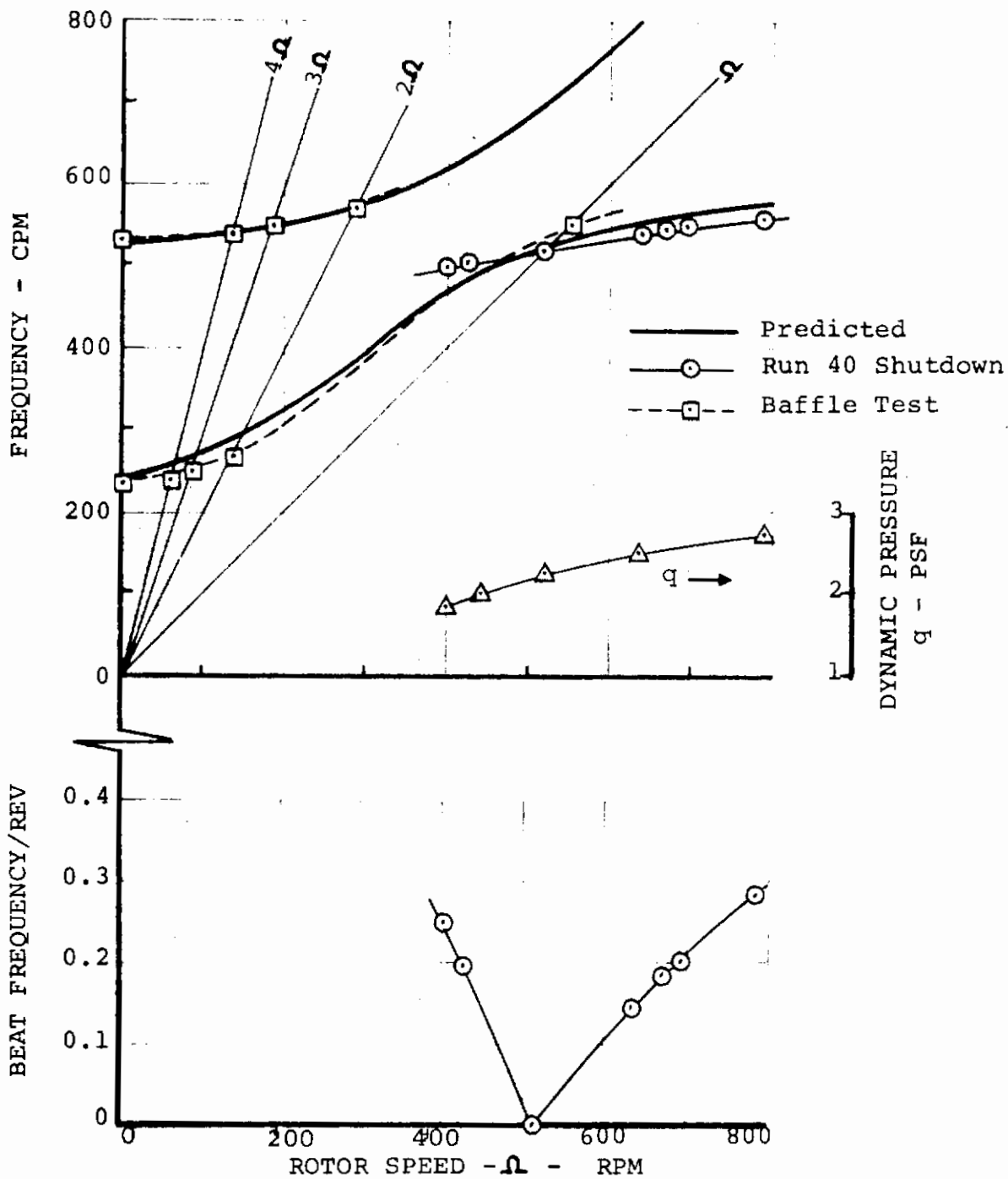


FIGURE 7-23. CORRELATION OF BLADE FREQUENCY OBTAINED FROM BEAT OSCILLATION DURING EMERGENCY SHUTDOWN, $\theta_{.75} = 10.2$ DEG., $i_N = 60$ DEG. RUN 40 (12)

8.0 FLYING QUALITIES

8.1 INSTALLED RIGID BODY DYNAMICS

For pure free flight simulation a model must be mounted such that all six rigid body degrees of freedom are unrestrained. Realistic mounting arrangements, however, can only approach this ideal condition with the result that finite built in stiffness and damping exist.

"Tweak" tests were performed prior to the power-on tests specifically to determine the rigid body dynamic properties (frequency and damping). The effects of the umbilical and snubber cables were determined. Prior to the wind tunnel installation an assessment of the umbilical effect was made by conducting simple tests to determine the optimum umbilical arrangement, the results of which showed that the installation used in this test (Figure 3-1) does not change the stiffness and inertia of the rigid body modes. This was confirmed by the data shown in Table 4-2. The model was "tweak" tested periodically throughout the program and the corresponding results are listed in Table 4-1. All damping data were reduced from the motion decrements recorded on the oscillograph in terms of viscous damping coefficients.

8.2 PITCH AND ROLL SPRINGS

The capability of evaluating the effect of a simple attitude feedback control system was provided by installing springs in the pitch and roll axes. These springs added a stiffness of 15.0 in.lb/deg in pitch and 5.0 in.lb/deg in roll, or in terms of control sensitivity in the hover mode, 1.01 rad/sec² and 0.061 rad/sec², respectively, per degree of fuselage attitude. The power-off, rigid body dynamic effect of the springs is shown by the data in the following table for the hover configuration.

AXIS	SPRINGS REMOVED-RUN 62		SPRINGS ON - RUN 28	
	f	ξ	f	ξ
Pitch	.87	.14	1.5	.027
Roll	.31	.10	.54	.028

8.3 HOVER CHARACTERISTICS

8.3.1 Rigid Body Damping

Rigid body damping data were obtained by gradually displacing the model from the neutral trimmed position with the snubber cables and then releasing the cables quickly. In all cases throughout the test the rigid body modes were very stable. A summary of all data relating to rigid body stability is contained in Table 8-1.

An example of increased stability provided by the rotor in hover is shown by the damping decrements in Figure 8-1 which illustrate a more rapid decay with power on. This is the case for both pitch and roll. Collective has an apparent stabilizing effect in itself as illustrated in the bar chart of Figure 8-2. Here it is shown that the rotors turning with no induced flow ($\theta_{.75} = 0^\circ$) provides no added stability in pitch whereas the high collective substantially increases the damping. Data were not obtained for roll motion at low collective and no ordinate values are given since frequency and damping are of primary interest.

8.3.2 Collective Pitch Effectiveness - Roll Controllability

Differential collective pitch effectiveness for roll control was determined from the wing root flap bending moment data of Figure 8-3. The data reflects the hovering configuration bending moments measured at butt line 6.62 as collective pitch of the prop/rotor is varied. The thrustline is located at butt line 40.68. Except for the non-linearity at the 2.0 degree collective setting, the moment response is essentially linear to 9.0 degrees collective with some increased effectiveness noted between 9.0 and 10.7 degrees.

At the maximum collective value ($\theta_{.75} = 10.7^\circ$) shown in Figure 8-3 the rotor has developed 20.6 lb. of thrust which represents 2/3 of the thrust required to balance the model total weight (61 lb.). Extrapolation of the data indicates that approximately 12° of collective would be required to lift 50 lb. (the equivalent full scale aircraft gross weight).

8.3.3 Cyclic Pitch Effectiveness - Pitch Controllability

Wing root torque arising from the application of longitudinal cyclic pitch on one prop/rotor is shown in Figure 8-4. In the hover configuration ($i_N = 90^\circ$), control effectiveness is

essentially linear. Comparative data are also presented for the cruise configuration ($i_N = 0^\circ$) at a dynamic pressure (q) of 0.2 PSF. The steady torque measured at zero cyclic is attributed to a residual control input of approximately -1.0 degree cyclic and possibly a distorted wing torsion wave form due to rotor unbalance.

The average torque or pitching moment data per degree of cyclic pitch were measured about zero cyclic and converted to non-dimensional coefficient form. The resulting coefficients are plotted in Figure 8-5 and are compared with predicted levels for the cruise configuration.

8.4 TRANSITION AND CRUISE CHARACTERISTICS

The limited amount of data which were obtained in transition indicates that the pitch stability increases slightly over that in hover. The effect of dynamic pressure on the rigid body pitch frequency and damping is illustrated in Figure 8-6 which shows a general increase in damping with increased dynamic pressure. These data are composed of $i_N = 40^\circ$, 60° , and 90° tilt angles. Additional data are required for each tilt angle to completely define the damping trend.

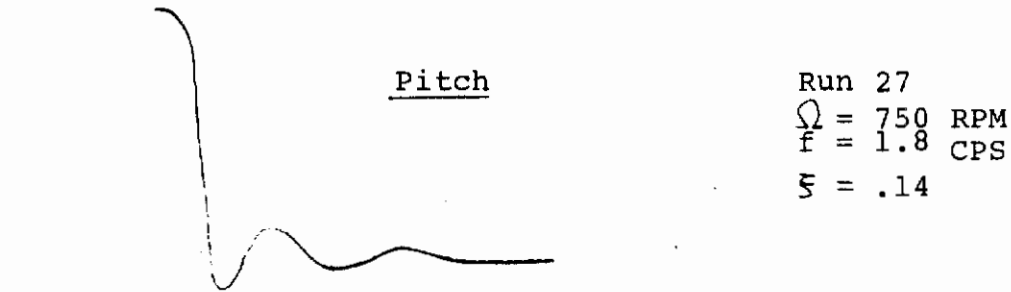
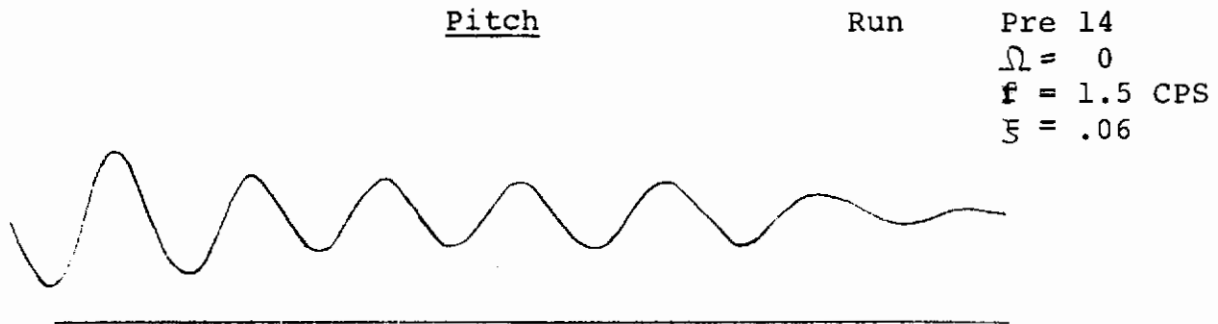
Data obtained with the rotors off (Run 57) are presented in Figure 8-7 and show that although the damping with wind-on is greater than that with wind-off, a decreasing trend exists with increasing dynamic pressure. Insufficient data exist to establish positive conclusions, but correlations with the data of Figure 8-7 and Run 50(5) in Table 8-1 suggests that the rotor provides added damping in the cruise attitude.

TABLE 8-1

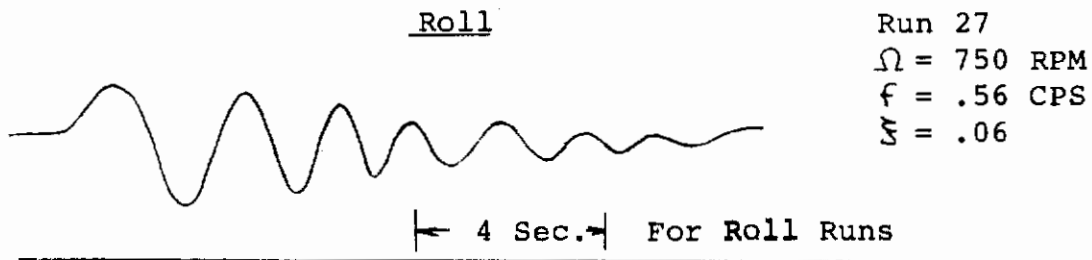
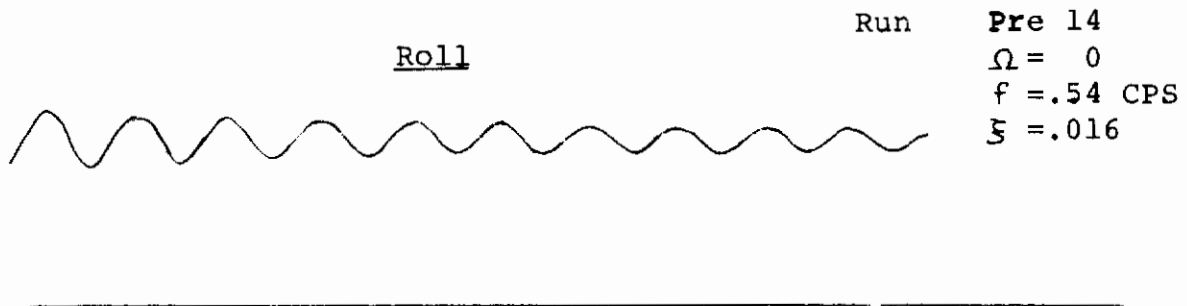
RIGID BODY DAMPING DATA SUMMARY

RUN	i_N	q	Ω	$\theta_{.75R}$	MODE	FREQ. CPS	DAMPING COEFF.
PRE 14	90	0	0	-	PITCH	1.5	.06
					ROLL	.54	.016
21	90	0	750	0	PITCH	1.65	.06
27	90	0	750	8.2	PITCH	1.8	.14
					ROLL	.56	.06
40 (9)	60	2.0	790	10.2	PITCH	1.7	.16
42 (5)	60	3.0	790	16.	PITCH	1.8	.18
43 (9)	40	4.0	790	20.	PITCH	1.7	.22
PRE 44	40	0	0	-	PITCH	1.5	.07
					ROLL	.55	.02
44 (4)	40	0	790	6.	PITCH	2.0	.11
50 (5)	0	10.0	790	32.	PITCH	1.7	VERY HIGH
					PITCH	1.5	.05
PRE 57	0	0	ROTORS OFF				
					ROLL	.60	.02
57	0	VARY	ROTORS OFF		PITCH	SEE FIG. 8-7	

Contrails



← 1 Sec. → For Pitch Runs



← 4 Sec. → For Roll Runs

Figure 8-1. Pitch and Roll Damping Decrements -
Hover Condition

$\theta_{.75} = 10.2^\circ\text{L}, 8.2^\circ\text{R}$ for Run 27

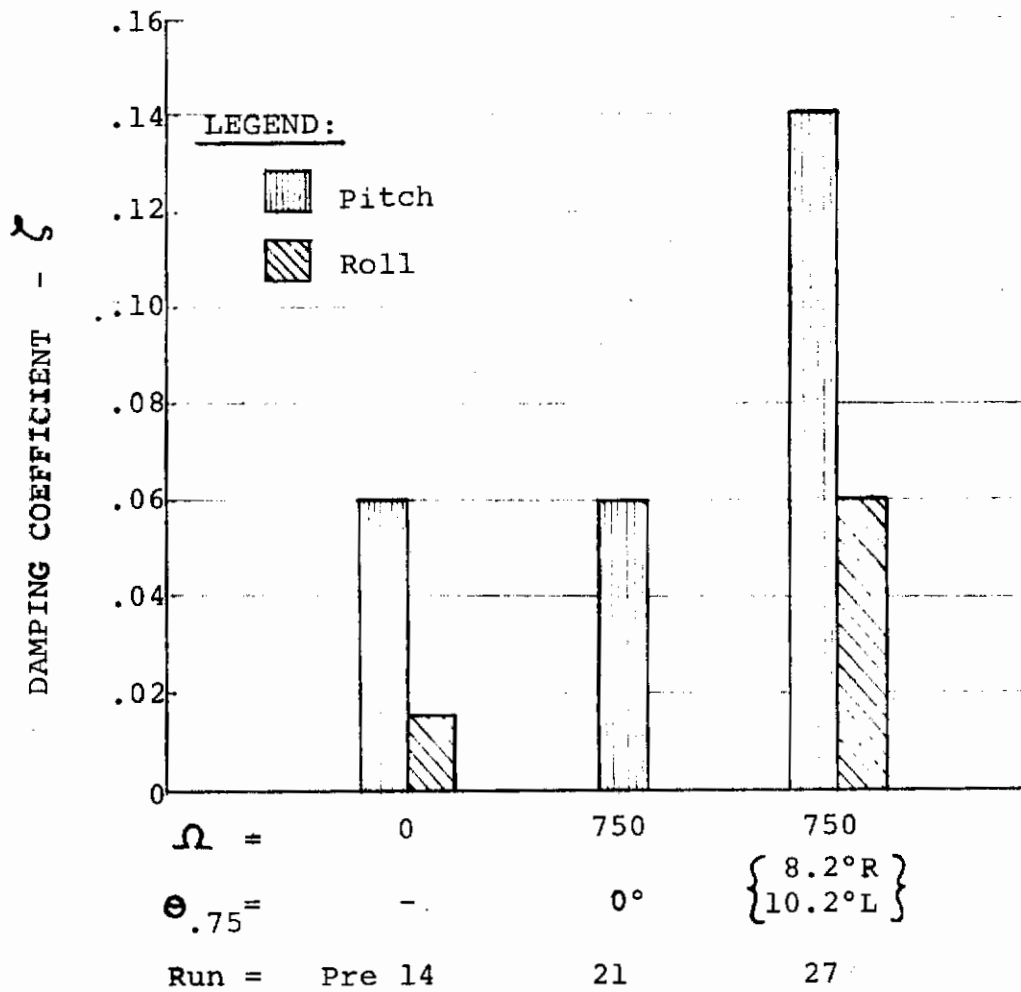


FIGURE 8-2. RIGID BODY DAMPING IN HOVER.

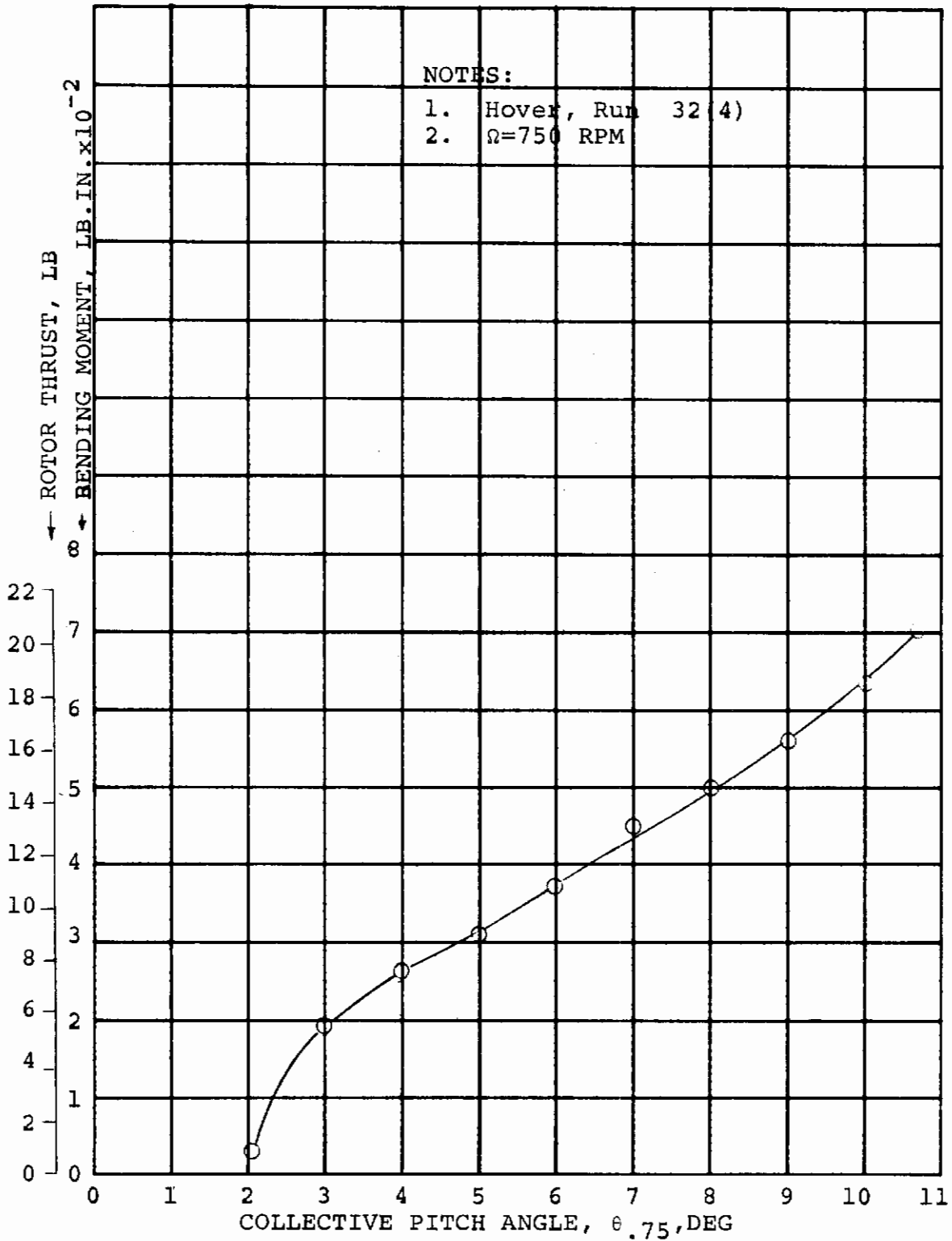


FIGURE 8-3 EFFECT OF COLLECTIVE PITCH ON WING STEADY FLAP BENDING MOMENT

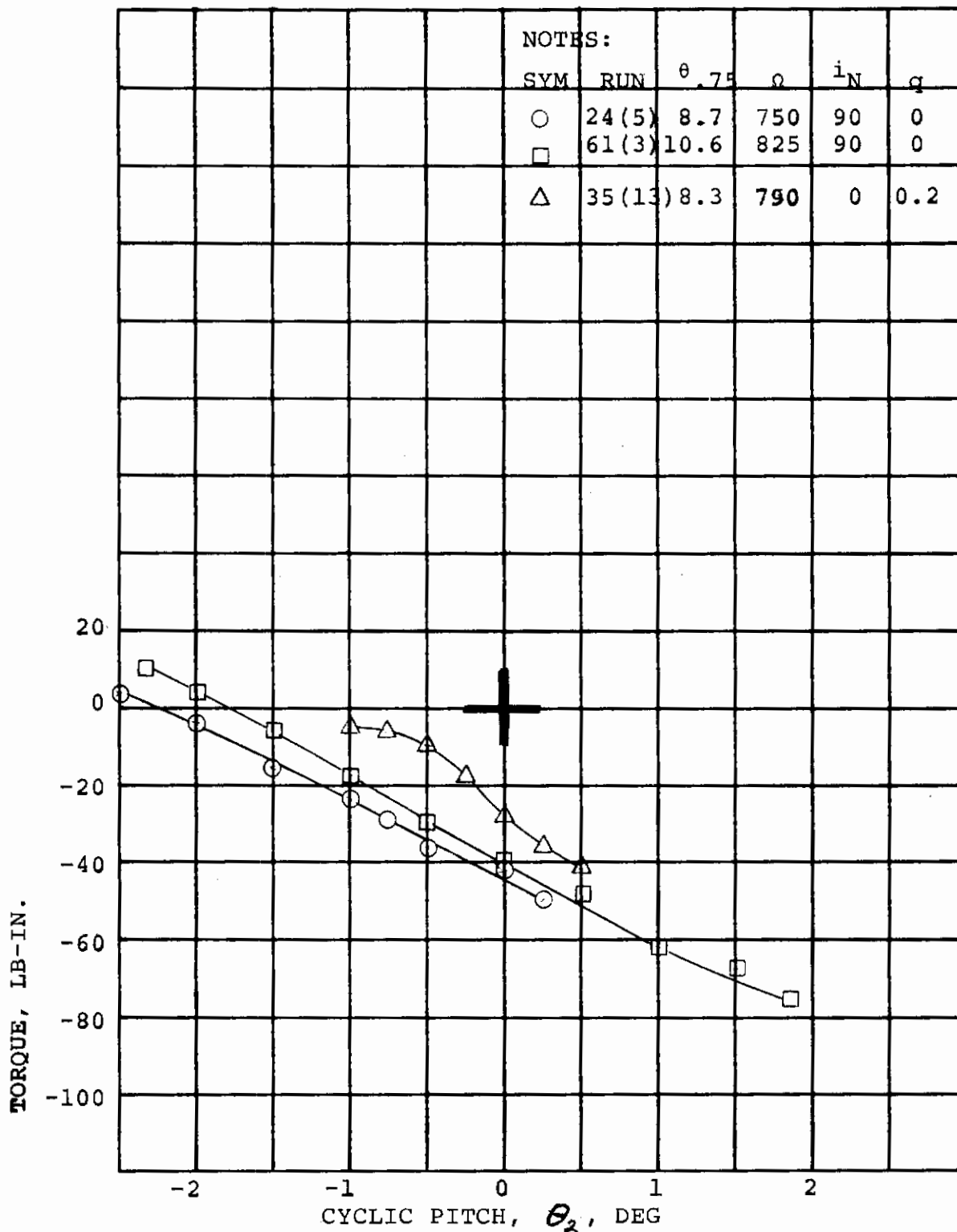


FIGURE 8-4 EFFECT OF CYCLIC PITCH ON WING STEADY TORQUE LOAD ILLUSTRATING CONTROL EFFECTIVENESS

Contrails

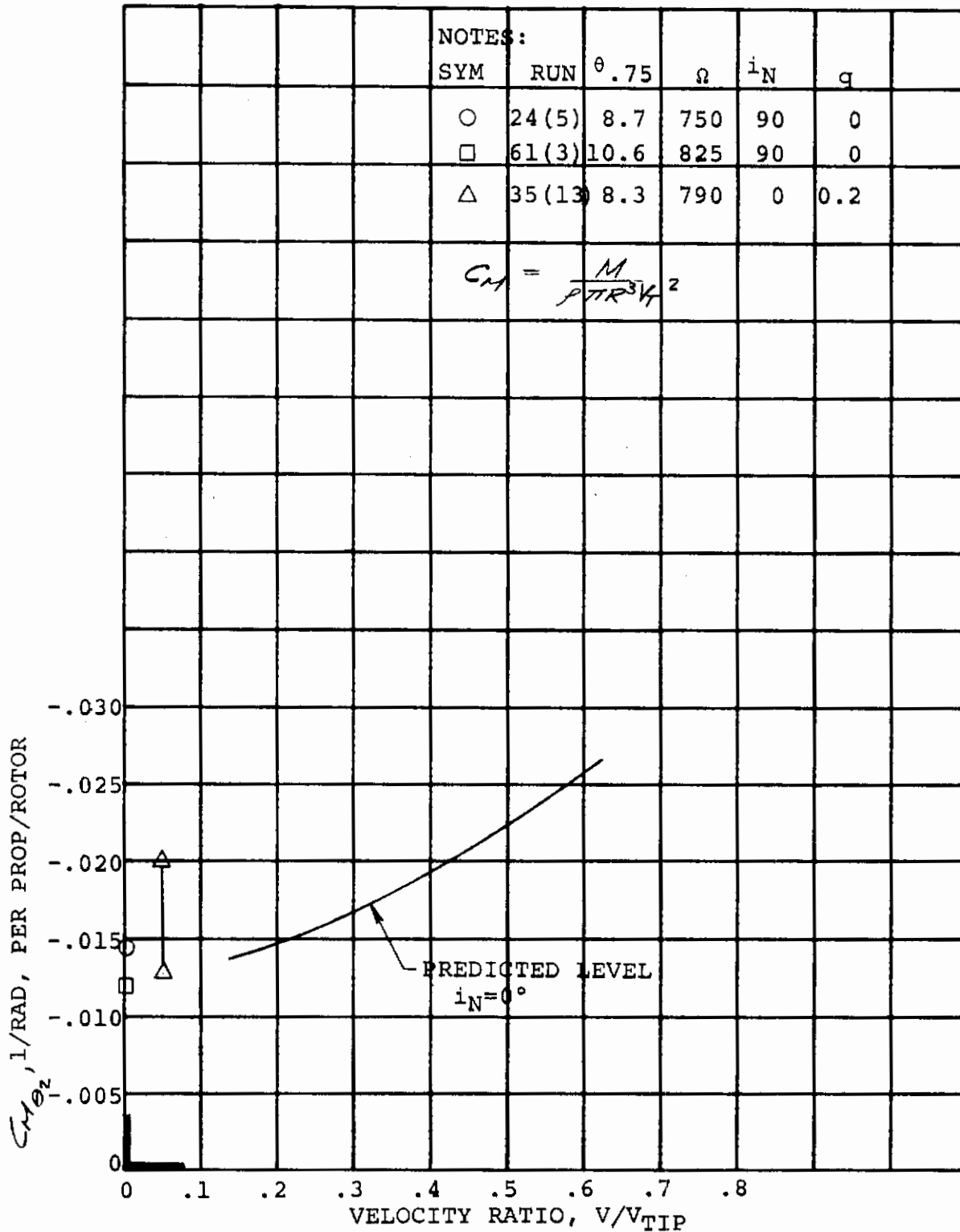


FIGURE 8-5 CYCLIC PITCH CONTROL POWER

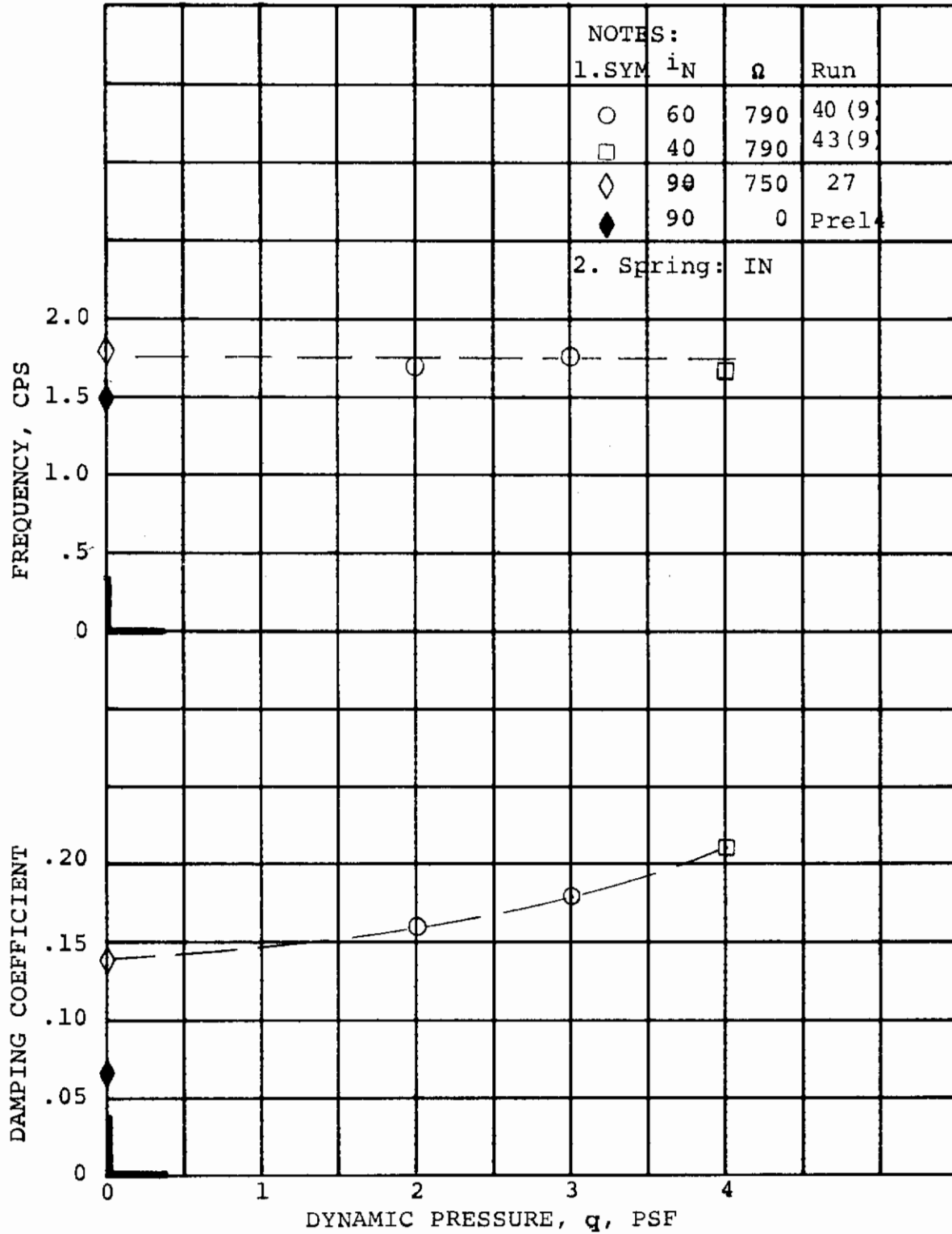


FIGURE 8-6 EFFECT OF DYNAMIC PRESSURE ON RIGID BODY PITCH FREQUENCY AND DAMPING

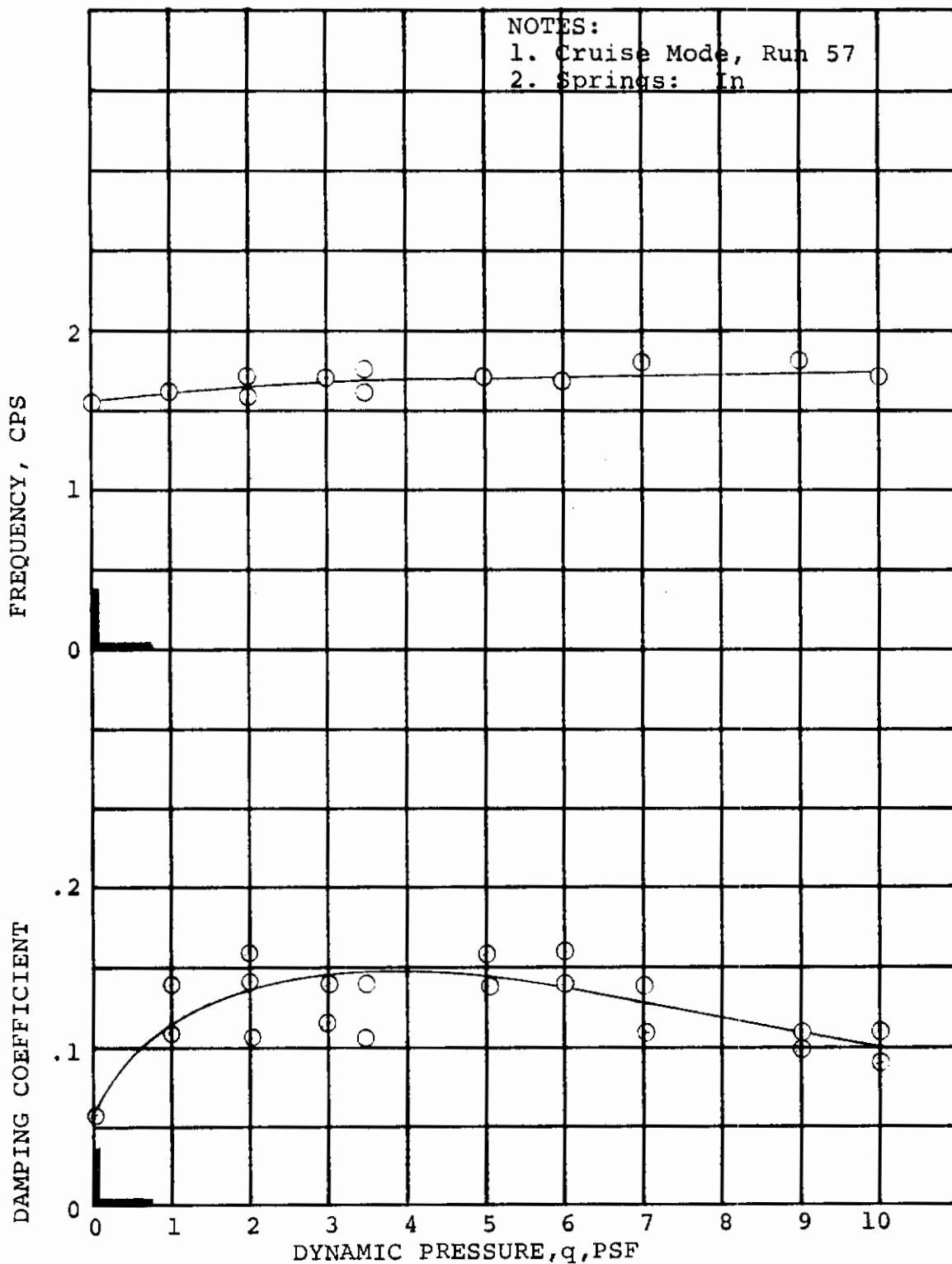


FIGURE 8-7 EFFECT OF DYNAMIC PRESSURE ON THE RIGID BODY PITCH FREQUENCY AND DAMPING WITH ROTORS OFF

9.0 SKITTISHNESS

It is believed that the "skittishness" demonstrated here is caused by unsteady flow around the wings and rotor system and is possibly triggered by flow asymmetries in the vicinity of the fuselage. The lateral oscillation is probably augmented by the lateral restraint of the pole mount. Without the mount, the motion would probably still be oscillatory but of longer period and accompanied by lateral translation of the airplane. Further description would require tests with tufts on the model or smoke for flow visualization to obtain insight as to the actual mechanics of the flow. The motions exhibited are typical of V/STOL aircraft operation in this flight regime and a SAS (Stability Augmentation System) will compensate for the disturbances, as discussed below.

9.1 GROUND EFFECT

In-ground-effect roll attitude motion of the unrestrained model in the hover configuration is shown in Figure 9-1, Run 64, in response to a manual induced disturbance to represent a gust input. The h/D ratio for this data was 0.41. The resulting roll motion is stable and the 0.33 cps oscillations are at least neutrally damped. Long-term self-induced motions which indicate the skittishness of the vehicle are shown in the lower time history as "undisturbed roll motion". The skittish motions are stable and are at least neutrally damped with an average frequency of 0.35 cps. Maximum unperturbed roll displacements are in the order of $\pm 2^\circ$.

An out-of-ground effect response is shown in Figure 9-2 along with the comparable in-ground-effect time history. The OGE response is highly damped and there is no tendency for the model to be excited by any other disturbance other than the initial, intentionally imposed upset.

9.2 EFFECT OF ADDED ROLL STIFFNESS

The neutrally damped oscillations observed in-ground-effect were easily controlled by adding a mounting spring in the roll axis. The mounting spring which provided the restraint characteristic discussed in Section 8-2 represented the attitude stiffness of a simple attitude feedback control system. Figure 9-1, Run 61, shows a damped 0.45 cps oscillation with a damping coefficient of 0.165. Since there is no tendency for the model to respond

Contrails

to any unintentional disturbances, it is possible to eliminate IGE skittishness by providing attitude stiffness. The equivalent full-scale frequencies based on these test results would be sufficiently low (<0.15 cps) so that pilot control would be sufficient. It should be remarked here that the model was restrained laterally by the cable mount. Roll motion in-ground-effect resulting from a completely free model although coupled with an unrestrained lateral mode are not expected to create problems for the full scale aircraft.

Contrails

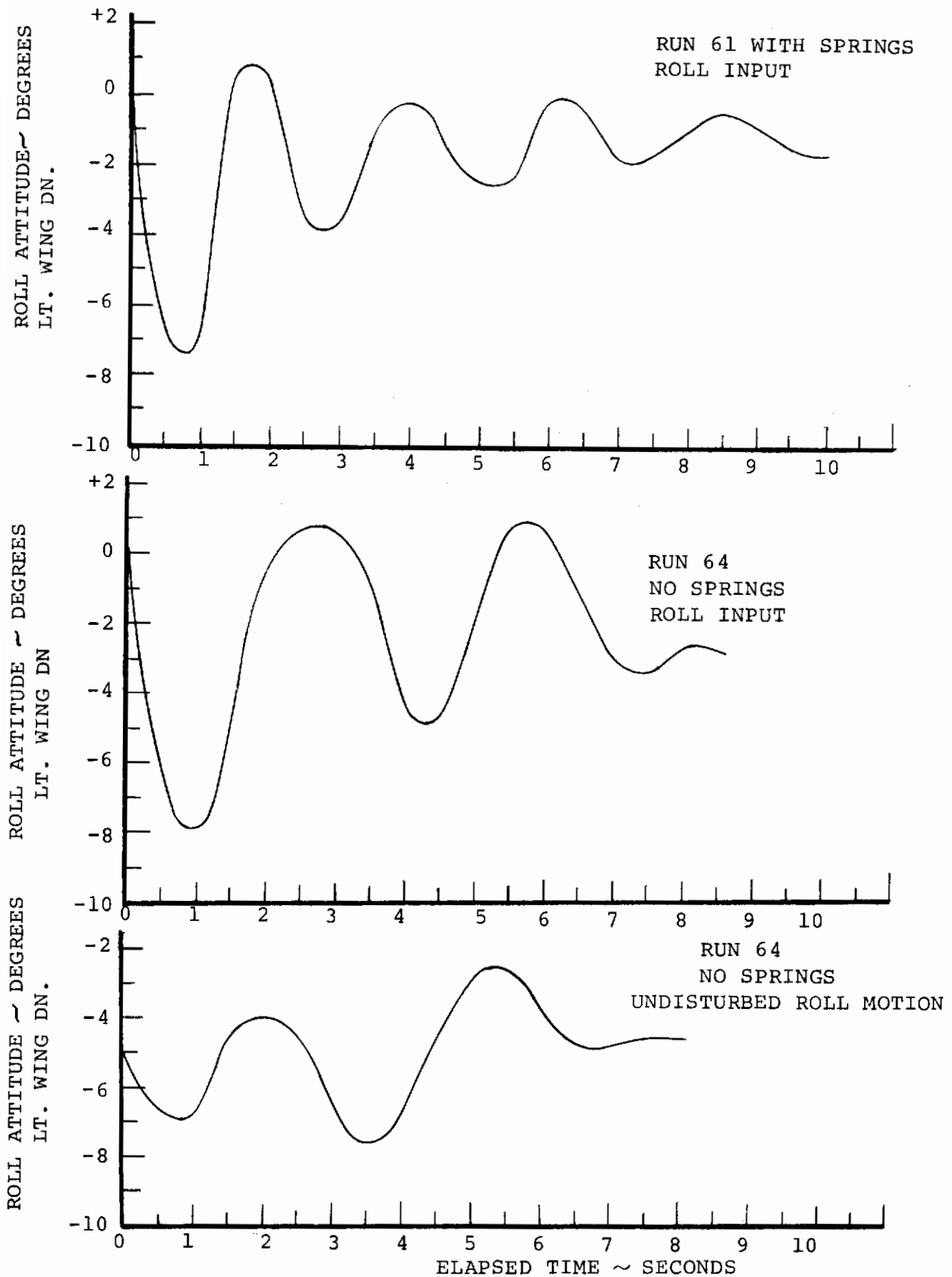


FIGURE 9.1: MODEL ROLL STABILITY IN GROUND EFFECT $h/D = .41$
HOVER, $i_N = 90^\circ$, $\Omega = 825$ RPM

ROLL INPUT

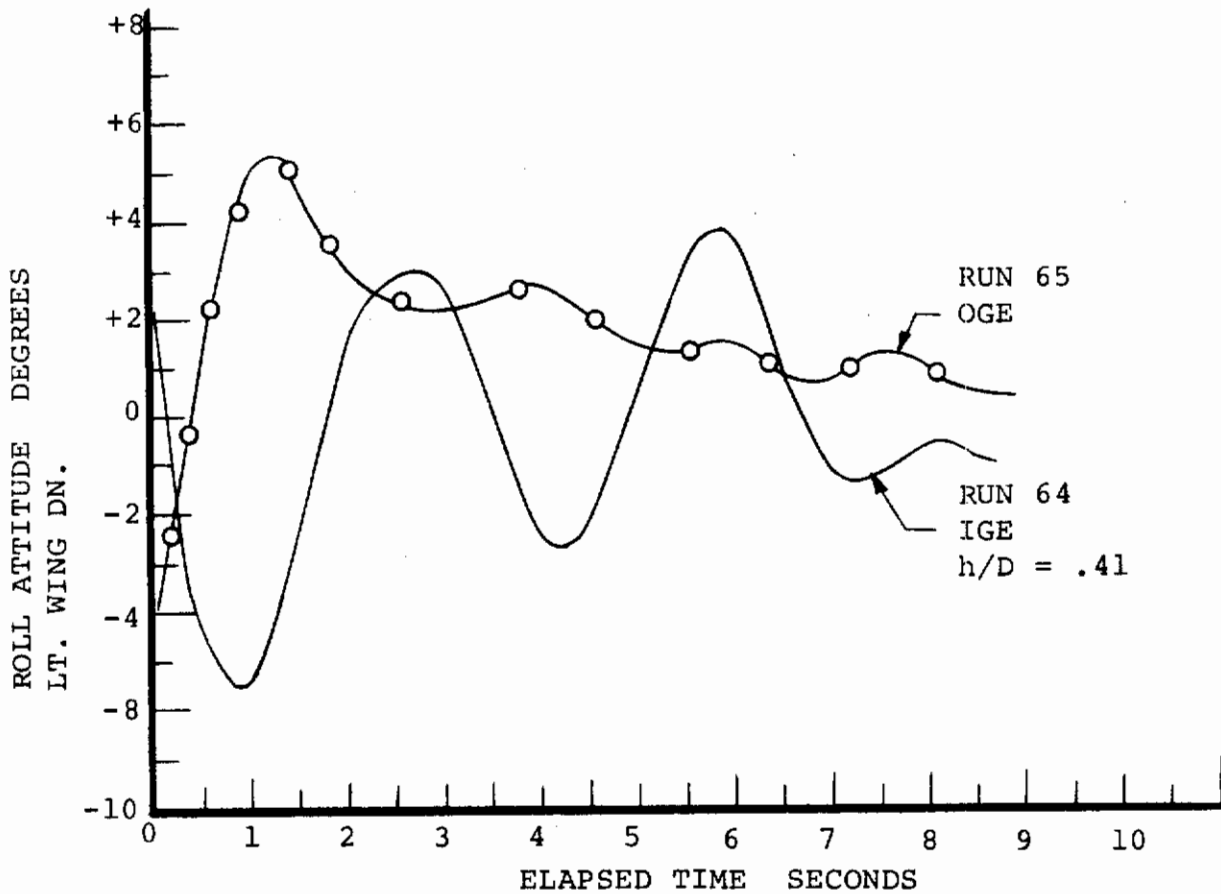


FIGURE 9.2. ROLL STABILITY IN AND OUT OF GROUND EFFECT WITHOUT SPRINGS HOVER, $i_N = 90^\circ$, $\Omega = 825$ RPM

10.0 CONCLUSIONS

10.1 BLADE LOADS

- 1) The rotating coupled bending frequencies are accurately predicted by the coupled flap-lag frequency analysis.
- 2) The sensitivity of blade loads to cyclic pitch in hover are increased by increased collective pitch and are not affected by ground interference.
- 3) In transition for a specific nacelle tilt and advance ratio, there is a value of cyclic pitch at which alternating chord bending is minimized. For minimum chord bending load the value of cyclic pitch increases positively with increasing dynamic pressure, and the value of the minimum blade load decreases with increasing collective.
- 4) In all flight modes, alternating chord bending was more sensitive than alternating flap bending to blade section angle changes caused by cyclic pitch, Aq conditions, or model attitude.

10.2 VEHICLE DYNAMICS

- 1) As predicted, the model did not encounter classical flutter, whirl flutter, air resonance or divergence instabilities in the range tested.
- 2) Good agreement between measured and predicted wing frequencies was obtained.
- 3) Wing bending frequencies were found to be independent of nacelle tilt angles.
- 4) A low frequency limit cycle oscillation consisting predominantly of blade chord bending was identified at conditions near zero thrust at low tunnel speeds.

10.3 STABILITY AND CONTROL

- 1) Rigid body motions with the prop/rotors removed are well damped over the range of q investigated.

- 2) Some increase in the damping of rigid body motions is evident with the prop/rotors installed.

10.4 SKITTISHNESS

- 1) Without artificial damping in-ground effect disturbances are controllable. Oscillations are at least neutrally damped with an average frequency of 0.35 cps (model scale) and maximum amplitude of $\pm 2.0^\circ$.
- 2) In-ground effect disturbances can be well damped with a simple roll attitude feedback system.

11.0 RECOMMENDATIONS

It is recommended that in the next test the cyclic input axis should be varied in transition tests to determine effect on blade loads and optimum control effectiveness.

12.0 REFERENCES

1. Test results of Ground/Air Mechanical Stability and Wind Tunnel Test of the Full-Span 1/10 Scale Powered Dynamic Model of the M-160 Tilt Rotor Aircraft.
N. Bean
Boeing-Vertol D160-10012-1, January 8, 1971.
2. Procurement Specification for a Powered 1/10 Scale, Flutter/Mechanical Stability Wind Tunnel Model.
R. E. Patterson
Boeing-Vertol D8-0976, November 1967.
3. Data Report
Boeing-Vertol Model 160
L. Wasserman
Dynamic Devices, Inc., February 1968.
4. Summary and Analysis of a 5.5 Foot Diameter Boeing-Vertol Model 160, Dynamic Rotor "AQ" Loads Wind Tunnel Test, With Wind Tunnel Data Report Included as Appendix.
R. Hartman
Boeing-Vertol D160-10001-1, August 1969.
5. Wind Tunnel Results for the Model 160 Dynamic Propeller Blade Loads Extended Test Program, November 1968.
J. Zola
Boeing-Vertol D8-2475-1, June 1969.

13.0 APPENDICES

APPENDIX A - MODEL MASS PROPERTIES

1. MODEL COMPONENT WEIGHTS

All items listed were weighed on balance-arm platform scales during model assembly at the Vertol Wind Tunnel. Weights are given in pounds. Component center of gravities (C.G.) were determined either by balancing on knife edge or by suspension. The longitudinal locations of C.G. are given in inches from model nose.

		<u>Weight (LB)</u>
a) <u>Assembled Model Total Weight</u>		61.0
b) <u>Major Components</u>		
(1) Nacelle and contents, including jet shaker, less rotor blades (C.G. on rotor ξ , 4.55" above drive shaft ξ) Inertia about pivot = 1.14 lb.in.sec ²		11.65
(3) Rotor blades		1.20
(1) Wing and contents		2.28
(1) Fuselage including empennage		30.74
c) <u>Sub-component</u>	<u>C.G.</u>	<u>Weight (LB)</u>
Air motor and gearbox	24.45	7.44
Fuselage keel	25.68	5.43
Wing support: horizontal web, fwd	23.90	0.36
horizontal web, aft	28.95	5.36
vertical web, L.H.	26.40	0.44
vertical web, R.H.	26.40	0.44
Fuselage balsa section, No.1	5.85	0.61
2 & 8	13.23	0.57
3 & 9	19.48	0.62
4 & 10	24.08	0.62
5 & 11	31.52	0.80
6 & 12	37.15	0.61
7 & 13	43.35	0.53
14	51.75	0.62

Contrails

	<u>C.G.</u>	<u>Weight (LB)</u>
Nose Landing Gear, less wheels	7.40	0.54
Axle + 2 tires	-	0.31
Main Landing Gear, less wheels	33.20	1.01
2 Axles + 4 tires	-	0.62
Landing gear damper bar		0.91
Misc. fuselage contents		0.65

d) External Umbilical Line

Air hose (each - 5/8" I.D.)	.13 lbs/ft	
Instrumentation wire bundle	0.327 lbs/ft	
Air hose fitting	1.18 lbs	
Effective umbilical weight (estimated)	.88 lbs	

2. MOMENTS OF INERTIA

Moments of inertia of a nacelle and the assembled model were determined by suspending the units on a two-string (bifilar) pendulum. The supports were equidistant from the center of gravity so the inertias given are about the C.G. The model was rotationally displaced and 20 free oscillations counted against a stopwatch to determine the period. The pendulum length and distance between the supports were measured.

	<u>LB-IN-SEC²</u>
a. Nacelle, complete less rotor blades including shaker Pitching about pivot	I = 1.14
b. Model, complete less rotor blades	
Yawing about C.G., $i_N=90^\circ$	I = 108.7
Rolling about C.G., $i_N=0^\circ$	I = 82.8
Pitching about C.G., $i_N=90^\circ$	I = 14.84
Pitching about C.G., $i_N=0^\circ$	I = 13.87

APPENDIX B - ROTOR BLADE AND WING PROPERTIES

Table B-1 and Figures B1 through B-3 define the properties of the rotor blade. Figures B-4, B-5, and B-6 define the wing stiffness of the model.

Contracts

TABLE B-1
BLADE PROPERTIES

STATION r/R	CHORD c/c .75	TWIST DEG.	MASS PROPERTIES		STIFFNESS PROPERTIES		
			WEIGHT LB./IN.	INERTIA LB.IN ² /IN	EI-FLAPE LB.IN ² X 10 ⁴	EI-CHORD LB.IN ² X 10 ⁴	GJ LB.IN ² X 10 ⁴
1.0					.0217	.2736	
.975	.815	-9.0	.0036	.0012			
.9375							.016
.9	.880	-5.6	.0056	.0014	.0234	.4770	
.85							.018
.8	.961	-1.9	.0075	.0022	.0279	.5364	
.75							.023
.7	1.036	1.5	.0093	.0034	.0358	.7128	
.65							.026
.6	1.114	4.9	.0112	.0050	.0378	.8946	
.55							.028
.5	1.196	8.3	.0130	.0071	.0392	1.0746	
.44							.030
.383					.0504	1.3140	
.38	1.291	12.5	.0150	.0089			
.315							.048
.267					.867	1.6704	
.25	1.394	18.0	.0208	.0110			
.21							.074
.17	1.458	23.6	.0241	.0125			
.15					.1330	2.520	.090
.13	1.480	27.0	.0248	.0076			
.1163							.100
.1025			.0253	.0060			
.096					.1196	1.8000	
.095							.106
.0875			.0200	.0043			
.08					.576	.1220	.132
.0725			.0071	.00007			
.0613							.132
.05			.0071	.00007			
.033					.576	.1220	.132
.033					.102	19.58	
.0175			.0071	.00007			
0					.102	19.58	

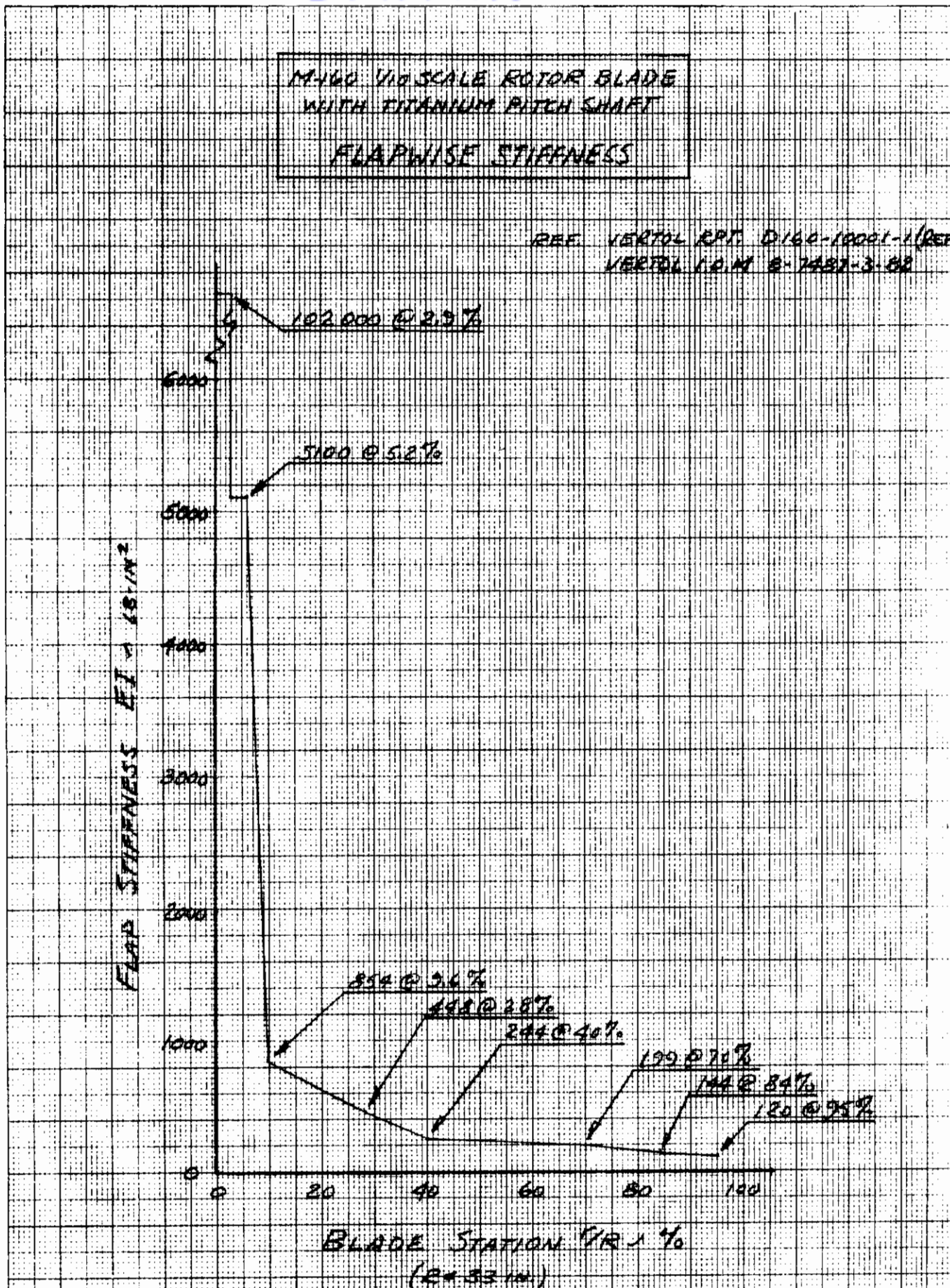


FIGURE B-1 1/10 SCALE M-160 ROTOR BLADE FLAPWISE STIFFNESS

Contrails

M-160 1/10 SCALE ROTOR BLADE
WITH TITANIUM PITCH SHAFT
CHORDWISE STIFFNESS

REF VERTOL RPT D160-10001-1 (REV 3)
VERTOL COM E-7407-3-1

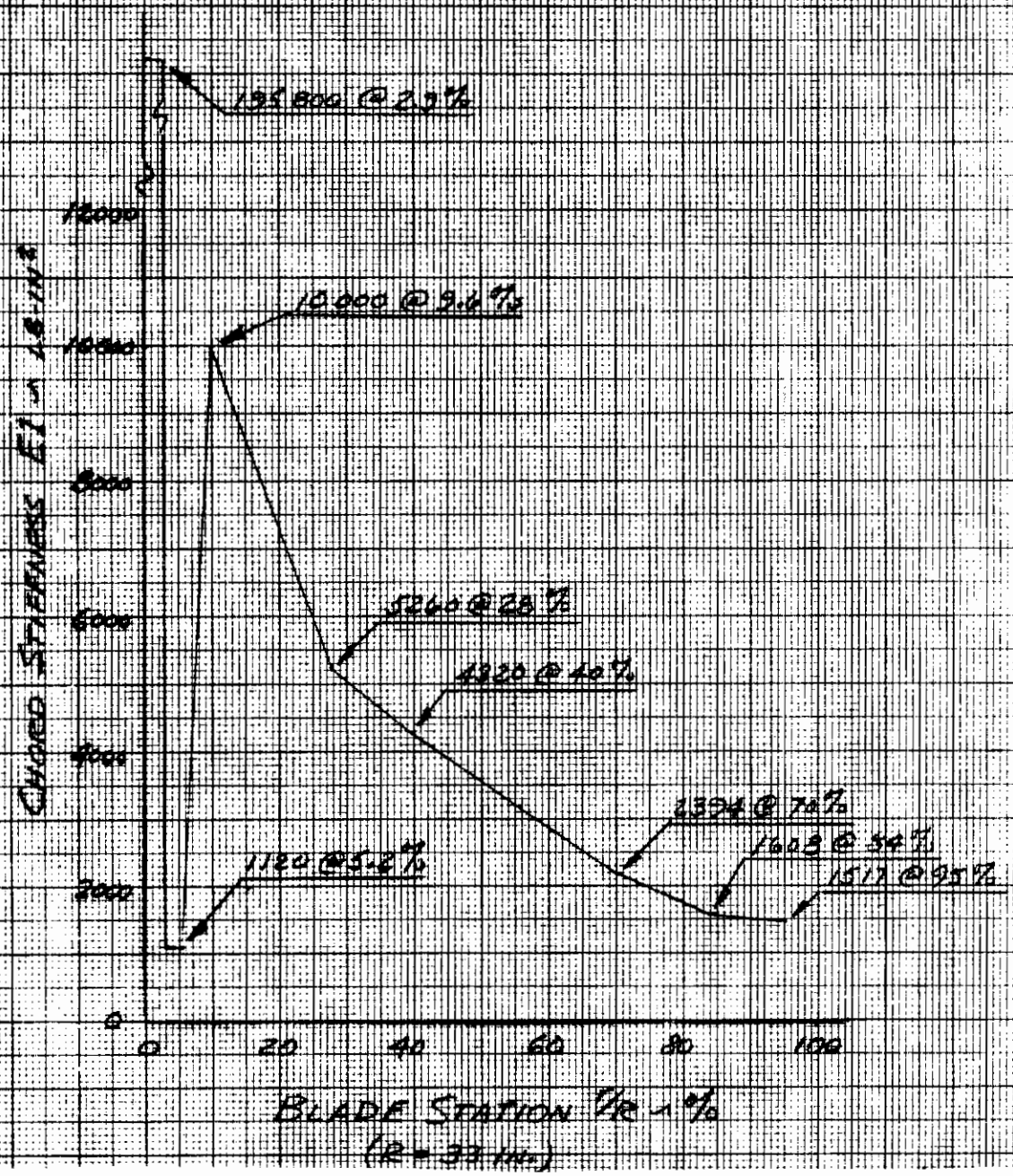


FIGURE B-2 1/10 SCALE M-160 ROTOR BLADE CHORDWISE STIFFNESS

Contrails

M-160 1/10 SCALE ROTOR BLADE
WITH TITANIUM PITCH SHAFT
TORSIONAL STIFFNESS

REF. VERTOL RPT. D160-10001-V(RR-3)

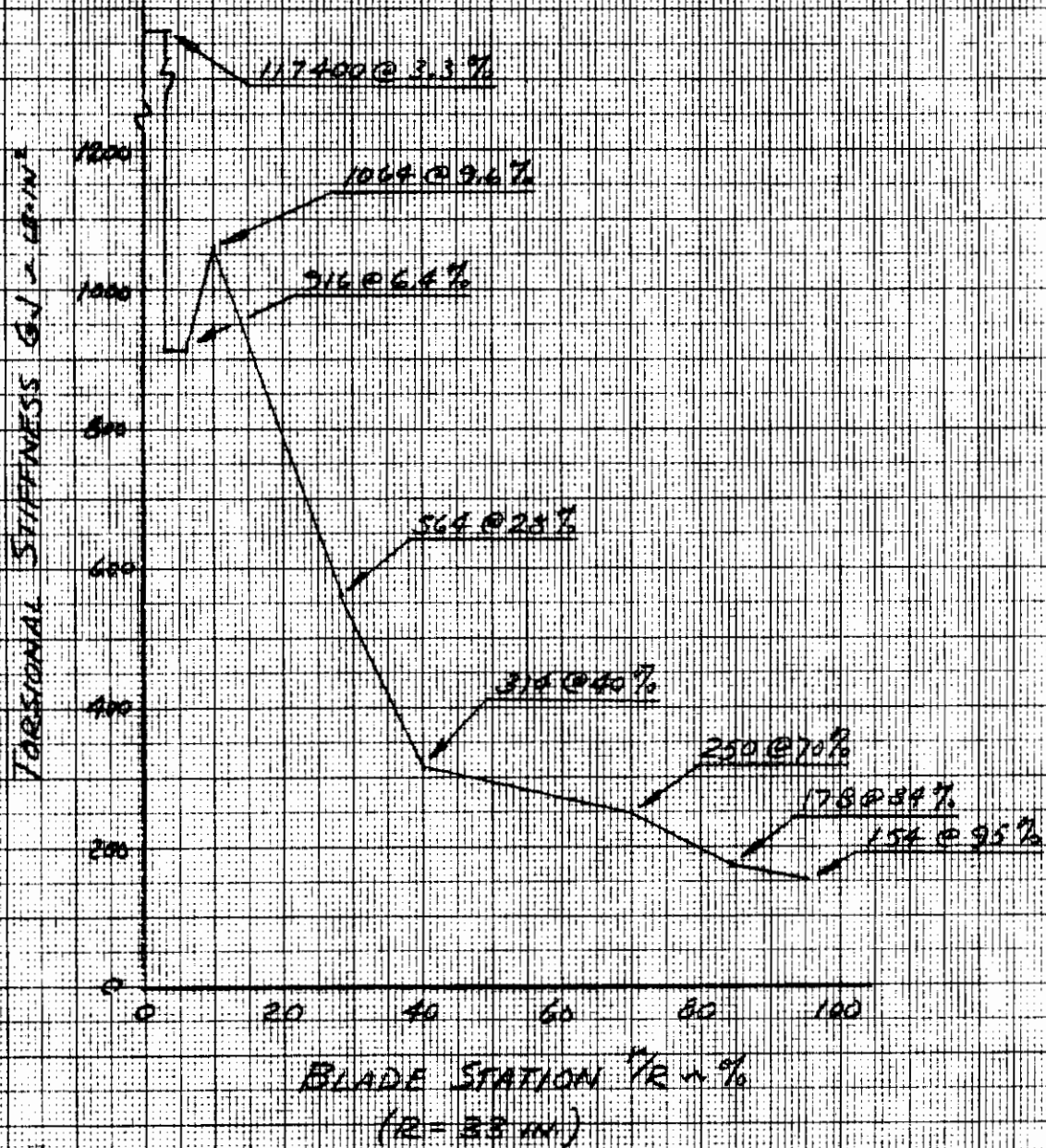


FIGURE B-3 1/10 SCALE M-160 ROTOR BLADE TORSIONAL STIFFNESS

M-160 1/10 SCALE MODEL WING
 100% SCALED STIFFNESS SPAR
 WING
 FLAPWISE STIFFNESS

NOTE:

STARBOARD WING CALIBRATED 10-4-69
 WING BOXES, DRIVE SHAFT & NACELLE REMOVED
 LOAD APPLIED ON SPARTUBE & @ STA. 37.5

- WING TIP DOWN
- △ WING TIP UP

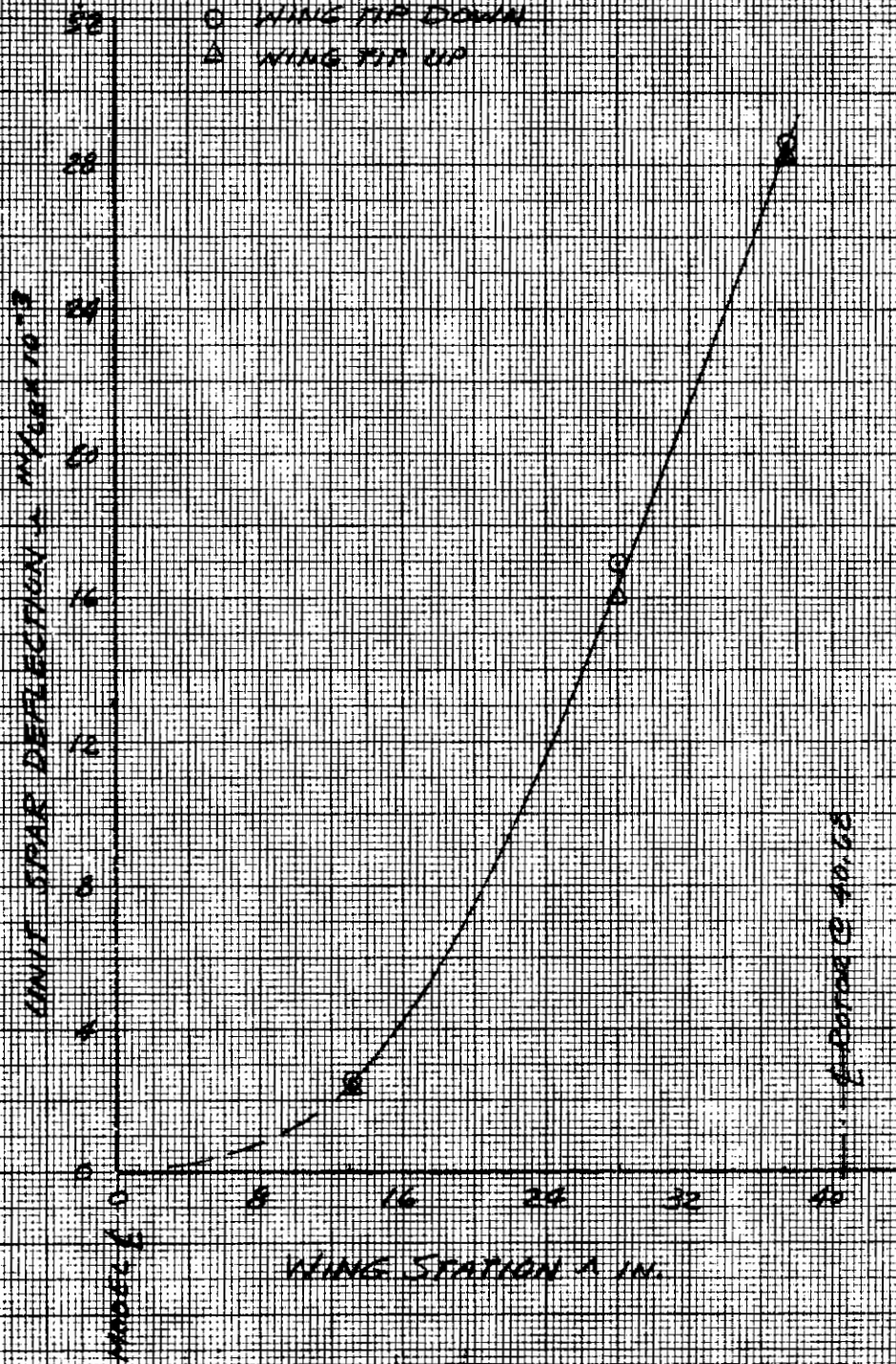


FIGURE B-4 1/10 SCALE M-160 WING FLAPWISE STIFFNESS

M-160 1/10 SCALE MODEL WING
 100% SCALED STIFFNESS SPAR
 WING
CHORDWISE STIFFNESS

NOTE:

STARBOARD WING CALIBRATED 10-4-68
 WING BONES, DRIVE SHAFT & NACELLE REMOVED
 LOAD APPLIED ON SPAR TUBE @ STA. 37.5

- WING TIP AFT
- △ WING TIP FWD

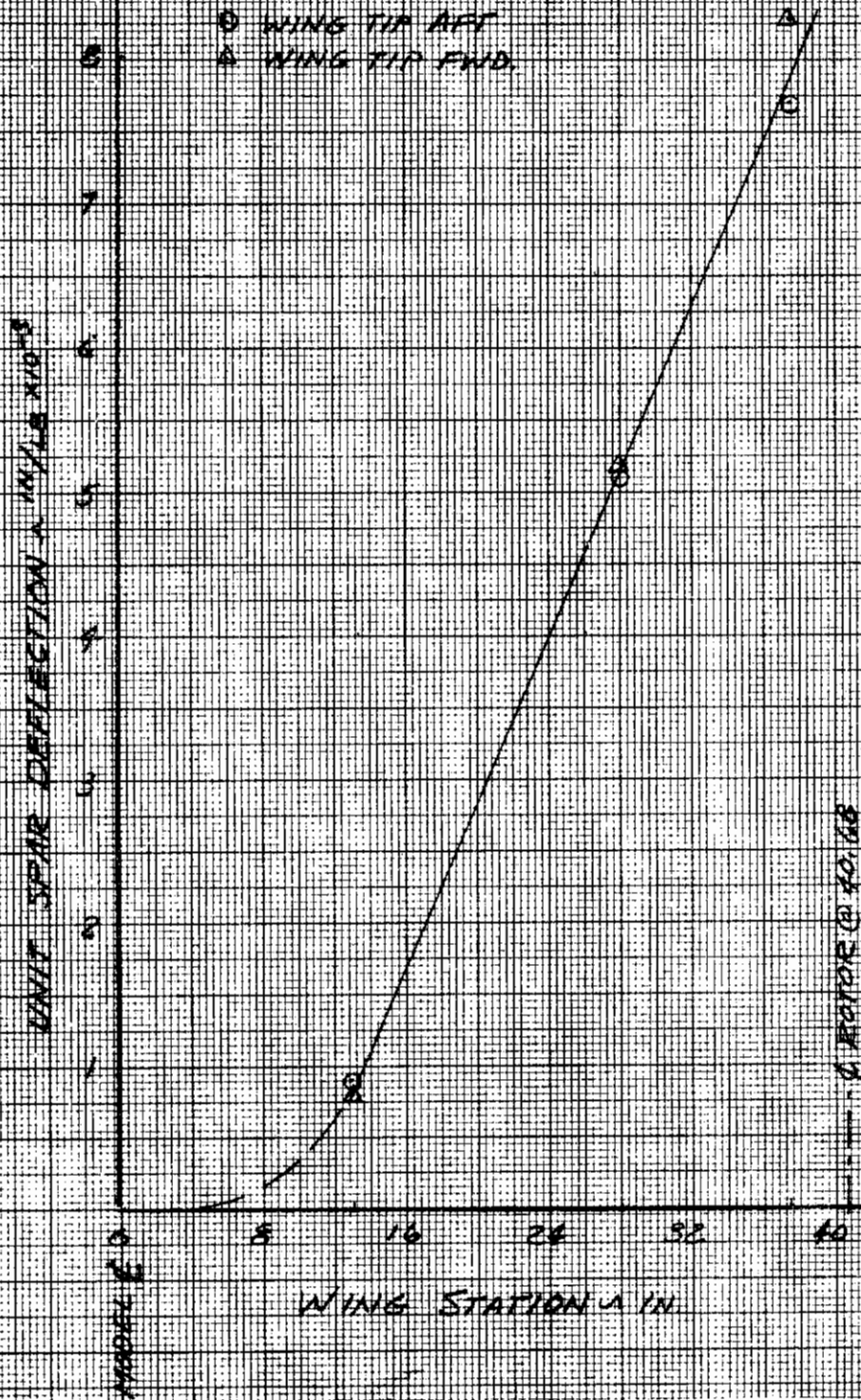


FIGURE B-5 1/10 SCALE M-160 WING CHORDWISE STIFFNESS

Contrails

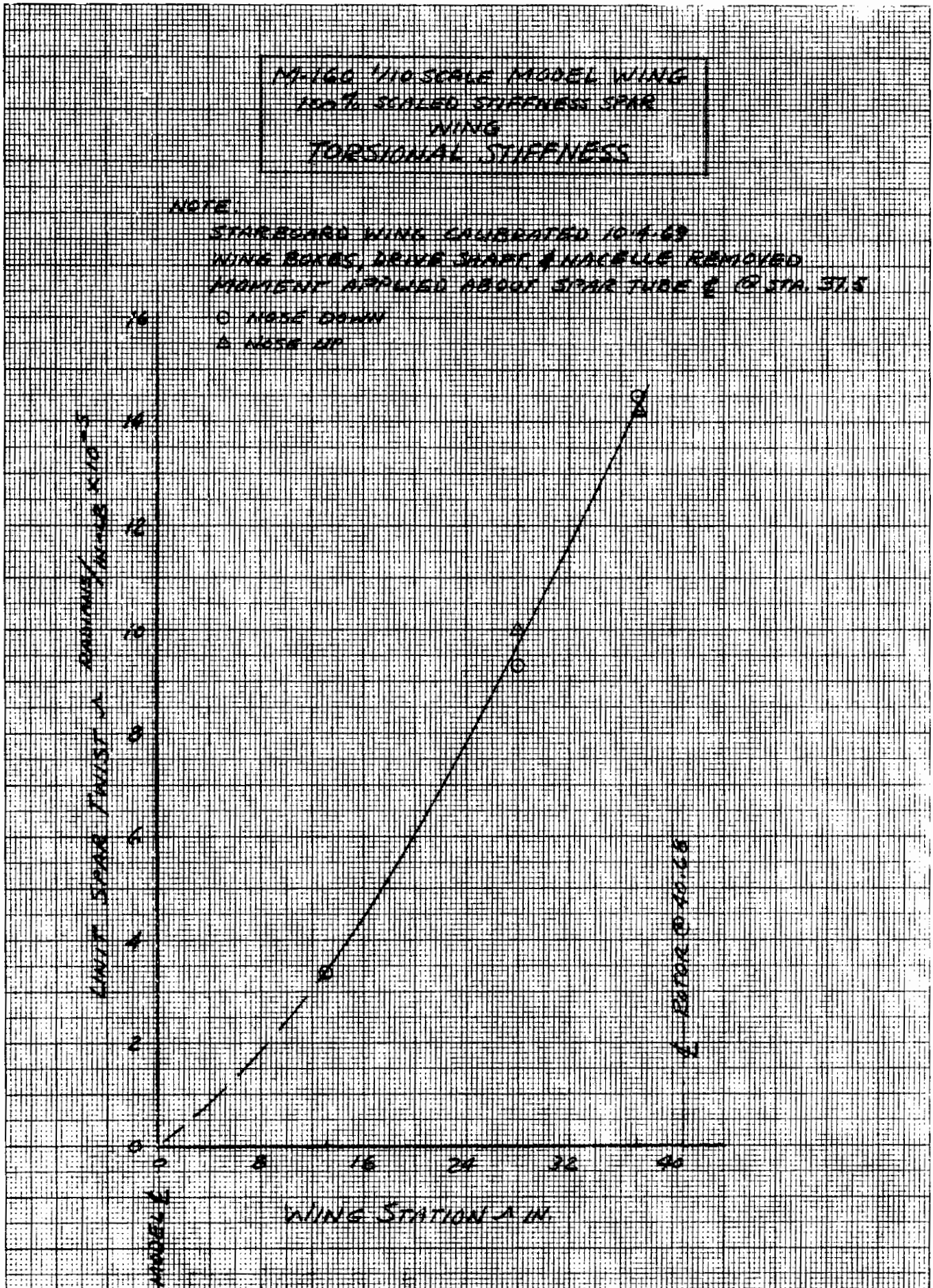


FIGURE B-6 1/10 SCALE M-160 WING TORSIONAL STIFFNESS

Approved for Public Release

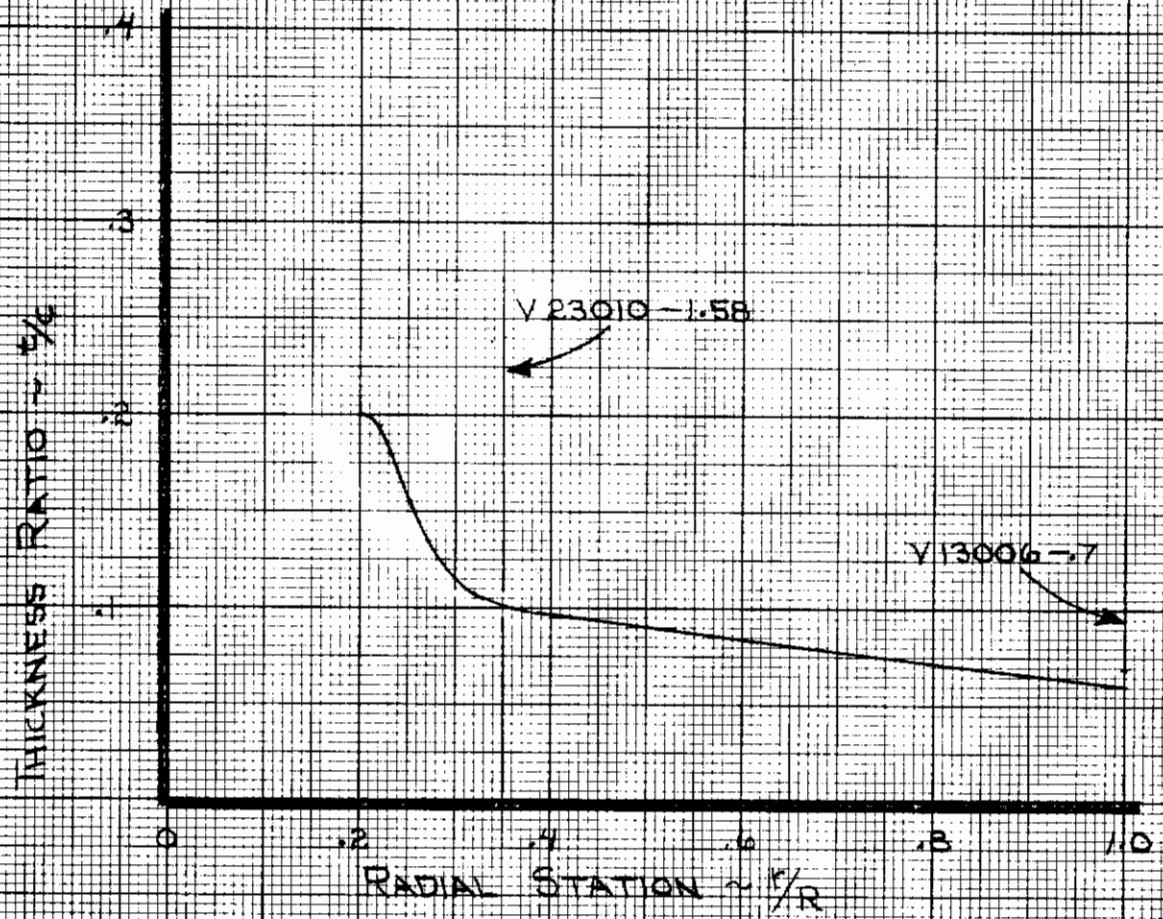


FIGURE B-7 ROTOR BLADE THICKNESS AND AIRFOIL DISTRIBUTION.

APPENDIX C - RUN LOG

A copy of the run log recorded during the test is enclosed in the following pages. This log lists the test conditions by run number and contains added descriptive notes.

PREP.	CHK.	APPR.	REVISD	DATE	DATE / TIME						
RUN NO.	CONFIGURATION	TYPE OF RUN	WT. TARE RUN	R.R. ϕ_{75} DEG	R.R. B_1 DEG	LR ϕ_{75} DEG	LR B_1 DEG	RPM	δ_3 DEG	α DEG	J
1	R.H.R.	BAFFLE TEST		3	0	OFF	OFF	VARY	0	90	0
2	R.H.R. WITH BAFFLE AT $\psi = 90^\circ$	✓		3	✓	✓	✓	✓	✓	✓	✓
3	R.H.R. WITH BAFFLES AT $\psi = 90, 270$	✓		3	✓	✓	✓	✓	✓	✓	✓
4	R.H.R. WITH BAFFLES AT $\psi = 90, 210, 330$	✓		3	✓	✓	✓	✓	✓	✓	✓
5	R.H.R. WITH BAFFLES AT $\psi = 90, 180, 270$	✓		3	✓	✓	✓	✓	✓	✓	✓
6	SEE NOTE BELOW.			-	-	-	-	-	-	90	-
7	SEE NOTE BELOW			-	-	-	-	-	-	0	-
8	SEE NOTE BELOW			-	-	-	-	-	-	0	-
9	SEE NOTE BELOW			-	-	-	-	-	-	0	-
10	SEE NOTE BELOW			-	-	-	-	-	-	0	-

1. MODEL LOCATED IN ASSEMBLY AREA FOR BAFFLE TEST
NO BAFFLE-ROTOR & 5.5 FT ABOVE FLOOR
2. V-CAL & BLADE BANG TEST ON CEC, RHR BLADE ONLY
3. BLADE BANG TEST ON CEC. RHB ONLY. BAFFLES AT $\psi = 90$ & 270°
4. BAFFLES AT $\psi = 90, 210$ & 330°
5. BAFFLES AT $\psi = 90, 180, 270$ & 0°
6. MODEL ON MONKEY WITHOUT UNBILICAL AND SNUBBERS. RIGID BODY FREQUENCY AND DAMPING CHARACTERISTICS WERE OBTAINED.
7. SAME AS 6 EXCEPT $\alpha = 0^\circ$
8. MODEL ON MONKEY WITH UNBILICAL ATTACHED. AIR HOSES TO MOTOR AND SHAKERS PRESSURISED. EFFECTS OF UNBILICAL AND PRESSURE ON RIGID BODY FREQUENCY AND DAMPING CHARACTERISTICS WERE OBTAINED. SNUBBERS OFF.
9. SAME AS 8 EXCEPT SNUBBERS ARE ON AND LOOSE
10. SAME AS 9 EXCEPT MODEL IS SNUBBED

1/10 SCALE 160 MODEL
VRO54D

BYWT
070

Contrails

PREP.	CHK.	APPR.	RUN NO.	CONFIGURATION	TYPE OF RUN	WT. TARE RUN	R.R. B, Deg.	L.R. B, Deg.	R.R. B, Deg.	L.R. B, Deg.	RPM	ds	W	f	J	DATE TIME
			11	SEE NOTE BELOW			-	-	-	-	-	-	90	-	-	1-27-71; 22:50
			12	SEE NOTE BELOW			-	-	-	-	-	-	90	-	-	1-28-71; 18:00
			13	SEE NOTE BELOW			-	-	-	-	-	-	90	-	-	19:00
			14	SEE NOTE BELOW			-	-	-	-	-	-	90	-	-	19:25
			15	HOVER	TRAP BAL.		4	4	0	0	830	0	90	0	0	23:30
			16		✓		0	0	0	0	830	0	90	0	0	1-29-71 16:30
			17		✓		4	4	-	-	830	0	90	0	0	
			18		✓		2.5	4.6	-	-	830	0	90	0	0	
			19		✓		2.5	-	-	-	830	0	90	0	0	
			20		✓		2.5	-	-	-	758	OFF	90	0	0	19:15

11. MODEL ON MONKEY WITH UNBICIAL ON AND SNUBBERS OFF. AIR HOSE TO SHAKERS ARE PRESSURISED. AIR HOSES ^{TO MOTOR} NOT PRESSURISED. MODEL IS IN HOVER CONFIGURATION. SHAKER FREQUENCY FROM 0 TO 22 CPS WITH PRESSURES OF 20 AND 40 CPS. SYMMETRICAL AND ANTI-SYMMETRICAL SHAKE.
12. SAME AS 11 EXCEPT DATA NOW BEING RECORDED ON COMPUTER. SYMMETRICAL SHAKE ONLY AND 40 PSI SHAKER PRESSURE.
13. SAME AS 12 EXCEPT ANTI-SYMMETRICAL SHAKE.
14. SAME AS 12. BLADE BANG TEST PRIOR TO THIS RUN TRACK AND BALANCE RUN.
15. TRACK, BALANCE AND HORIZONTAL TAIL VIBRATION TEST VERTICAL ^{AND HORIZONTAL} TAIL REINFORCED
16. VERTICAL TAIL AND HORIZONTAL TAILS REINFORCED ADDITIONAL REINFORCEMENT ON HORIZONTAL TAIL AND BALANCE WTS ON L.H. ROTOR
17. BALANCE WTS. OFF- TRACK CHECK.
18. ADDITIONAL STIFFNESS REMOVED FROM HORIZONTAL TAIL- TRACK ADJUSTMENT TO L.H. ROTOR PRIOR TO THIS RUN. HORIZONTAL TAIL REMOVED.

1/10 SCALE 160 MODEL
VRO54D

BY WT
070

PREP.	CHK.	APPR.	DATE	REMARKS	TYPE OF RUN	WT. TARE RUN	R.R. Θ_{75} DEG	R.R. B_1 DEG	L.R. Θ_{75} DEG	L.R. B_1 DEG	RPM	δS DEG	i_N DEG	Ψ	J	DATE TIME
					HOVER		0	0	0	0	VARY	OFF	90	0	0	1-29-71; 19:40
					✓		VARY	0	VARY	0	750	OFF	90	0	0	21:40
					✓		3.2	VARY	4.0	VARY	750	OFF	90	0	0	21:53
					✓		VARY	VARY	VARY	VARY	750	OFF	90	0	0	23:31
					✓		3.2	VARY	4.3	VARY	750	OFF	90	0	0	23:38
					✓		8.1	-1.0	VARY	-1.0	750	OFF	90	0	0	
					✓		8.1	-1.0	10.2	-1.0	750	OFF	90	0	0	23:60
					✓		3.2	-0.5	4.0	-1.0	750	OFF	90	0	0	END 24:45
					✓		-	3.5	-	-1.0	✓	0	90	✓	✓	FEB 1, 11:00 16:30

21. HORIZONTAL TAIL OFF FOR ALL HOVER RUNS. AFTER RUN FOUND CUFF ON RB6 RUBBING AGAINST THE SPINNER. ALSO NOTICED HIGH BLADE TORSION LOADS FOR THIS BLADE DURING RUN.

23. B_1 FROM -4 TO 2 DEG.

24. Θ_{75} R.R. Θ_{75} LB. B,R,R B,L,R.

5.8°/0.4° 4.5/8.7 -1.6°/0° -1.5°/0° RANGE

26. COULD NOT DECREASE L.R. Θ_{75} AFTER THIS RUN DOWN FOR REPAIR

26. DIFFERENTIAL COLLECTIVE

27. RIGID BODY FREQUENCIES

28. 1/REV IN COMPUTER REPLACED WITH OSCILATOR-FREQUENCY VARIED.

BLADE FREQ. BANG TEST AFTER THIS RUN.

29. VARIOUS RUN-UPS TO INVESTIGATE HORIZONTAL TAIL VIBRATION

ADDED 4.5 BK. POINT MASS TO TIP (ONE EACH SIDE) OF HORIZONTAL TAIL.

1/10 SCALE 160 MODEL
VRO54D

BVWT
070

PREP.	CHK.	APPR.	REVISED	DATE	RUN NO.	CONFIGURATION	TYPE OF RUN	WT. TARE RUN	R.R. θ_{15} Deg	L.R. θ_{15} Deg	L.R. θ_{15} Deg	RPM	δ_s Deg	δ_w Deg	δ' Psf	J	DATE	TIME	
					30	HOVER			VARY	VARY	VARY	750	0	90	0	0		2-1-71	19:30
					31	HOVER			VARY	VARY	VARY	750	0	90	0	0			20:15
					32	TRANS			1.5	1.5	-1.5	750	0	90	-0.6				21:47
					33	TRANS			4.0	4.7	VARY	750	0	90	0.06				22:51
					34	CRUISE			VARY	-0.5	VARY	790	0	0	0	0			23:01
					35	CRUISE			4.24	4.25	-0.6	790	0	0	0	0			00:52
					36	CRUISE			4.8	-0.6	4.8	VARY	-6.5	0	0	0			01:13
					37	CRUISE			4.8	-0.6	4.8	VARY	-6.5	0	0	0			2-2-71
					38	CRUISE			4.8	-0.6	4.8	VARY	-6.5	0	0	0			19:18
									27	32	-1.5	790	-6.5	0	0	0			22:55

- 30. ELECTRICAL POWER TO AIR OIL MIST LOST DURING RUN. MODEL WITHOUT AIR-OIL MIST FOR 17 MIN. ALSO A MECHANICAL PROBLEM WITH L.H. B1 CHANGING WHILE RUNNING. DOWN TO REPAIR B1 PROBLEM.
- 32. HIGH BLADE LOADS (100%)
- 33. PITCHED FUSELAGE TO -10° BLADE LOADS STILL HIGH. 150%
- 34. (RPM = 790) COULD NOT RUN AT 750 DUE TO WING SYMMETRICAL BENDING AND HIGH C.B. LOADS ON L.H. BLADE.
- 35. YAW SNUBBERS ADDED
- 37. LOST AIR PRESSURE TO MODEL. ACTIVATED EMERGENCY TUNNEL SHUT DOWN. ALL LOADS LOW DURING SHUT DOWN - LOOKS LIKE A GOOD WAY TO SHUT DOWN FROM HIGH δ CONDITIONS. [LEFT HAND CYCLIC PITCH READOUT IS IN OPERATIVE]
- 38. PROBLEM WITH DRIVE SYSTEM AT $\theta_{15} = 32^\circ$ AND $\delta = 7^\circ$ AFTER RUN FOUND TRANSMISSION SHEAR PIN SHEARED.

1/10 SCALE 160 MODEL
YR054D

BVWT
070

PREP.	CHK.	APPR.	RUN NO.	CONFIGURATION	WT. TARE RUN	R.R. θ_{75} Deg	L.R. θ_{75} Deg	L.R. RPM	δ_3 Deg	γ Deg	γ PSF	I	DATE TIME
			39	TRANSITION		VARY	VARY	790	0	70	0/2		2-3-71 17:20
			40	TRANSITION		10	9.75	790	0	70	0/2.8		18:30
			41	TRANSITION		VARY	VARY	790	-10	70	0/4		19:30
			42	TRANSITION		VARY	VARY	790	-10	70	0/3		21:51
			43	TRANSITION		VARY	VARY	790	-3.8	40	0/5.2		23:25
			44	SEE NOTE BELOW		5.9	5.4	790	-4.2	40	0		00:38
			45	SHAKE TEST CRUISE MODE		6.0	5.6	790	-4.2	0	0		2-4-71 14:37
			46	SHAKE TEST CRUISE MODE									15:47
			47	CRUISE		10/28	10/51	900	-8.2	0	0/20		18:58
			48	CRUISE		28.2	0	790	-4	0	0/40		21:51

40 YAW AND PITCH SWEEPS AT $\gamma = 2$ PSF.
 41 YAW AND PITCH SWEEPS
 42 DECREASED THE TENSION ON VERTICAL SUPPORT CABLE
 43 YAW AND PITCH SWEEPS AT $\gamma = 4$ AND 5.25 PSF
 44 YAW, PITCH AND ROLL DISPLACEMENTS TO OBTAIN RIGID BODY STABILITY
 ALSO SHAKE FREQUENCY SWEEP FROM 4 TO 18 CPS. SYMMETRIC
 SHAKE AT 40 PSF

47 DURING AN ATTEMPT TO WINDMILL UP TO 790 RPM - TWO BLADES ON
 THE R.H.S (LB 14 & LB 22) CONTACTED THE WING L.E. AND BROKE OFF
 THE BLADE TIPS - SLIGHT OVERSPEED DUE TO R.H. ROTOR COLLECTIVE
 PITCH MOTOR SHORTING OUT. PRIOR TO RUN 45 THE RIGHT HAND ROTOR
 WAS STATICALLY BALANCED BY ADDING 32 GRMS TO BLADES LB 14
 + LB 22. PRIOR TO RUN 47 ALL LISTED B, FOR R.H. ROTOR ARE IN ERROR
 BY A FACTOR OF 2.0
 SYMMETRICAL SHAKE AT $\gamma = 7.0$

* ALL IN LISTED AS 70" SHOULD BE 60"

1/10 SCALE 160 MODEL
VR054D

48
BVWT
070

PREP.	CHK.	APPR	RUN NO.	CONFIGURATION	TYPE OF RUN	WT. TARE RUN	R.R. θ_{15} Deg	R.R. β Deg	L.R. θ_{15} Deg	L.R. β Deg	RPM	δ_s Deg	α_N Deg	β Deg	J	DATE TIME
			49	CRUISE			28.2	0	29.3	0	790	-4	0	7		2-4-71 22:30
			50	CRUISE			32.9	0	33.6	0	790	-4	0	10		✓ 23:00
			51	HOVER			4.15	VARY	4.15	VARY	900	0	90	0		✓ 00:25
			52	HOVER			10.0	-35	10.0	1.0	825	0	90	0		2-5 13:43
			53	HOVER			11.8	-35	10.0	1.0	825	0	90	0		✓ 15:10
			54	HOVER			4	-35	4	-35	-	0	90	0		18:45
			55	AUTOROTATION			VARY	0	VARY	0	-	0	105	1		25:27
			56	HOVER			VARY	0	VARY	0	825	0	90	0		2-8 15:00
			57	CRUISE-ROTORS OFF			-	-	-	-	-	VARY	0	0/10		✓ 23:09
			58	HOVER - IN GROUND EFFECT			4.0	0	4.0	0	825	0	90	0		2-7 00:30

49. ANTISYMMETRICAL SHAKE AT $\beta = 7$

50. RIGID BODY PITCH ~~NET~~ DISPLACEMENT

51. RIGID BODY PITCH DISPLACEMENT

52. RIGID BODY PITCH DISPLACEMENT AT VARIOUS θ_{15} & RPM.

53. SYMMETRICAL SHAKE. STATICALLY BALANCED L.H. ROTOR (23.9 gm ON RBI 4.20 ON RB5)

54. ANTI SYMMETRICAL SHAKE - TRANSMISSION SHEAR PIN SHERRED ON THIS RUN. THE SHEAR PIN WAS NOT SHERRED IN RUN 53 - THIS WAS A TRANSMISSION PROBLEM. SPROCKET HAD SLIPPED OFF SHAFT.

55. MOTOR & TRANSMISSION HAVE BOTH BEEN REMOVED FROM THE MODEL ATTEMPTED TO AUTOROTATE HOWEVER WAS UNSUCCESSFUL IN GETTING THE ROTORS UP TO SPEED.

56. DURING HOVER RUN-UP DIFFERENTIAL COLLECTIVE PITCH WAS INADVERTENTLY APPLIED CAUSING THE ROLL SNUDDER TO BREAK RESULTING IN LOSS OF THE L.H. ROTOR AND THE CROSS SHAFT TO BREAK.

57. RIGID BODY STABILITY ROTORS OFF.

58. TRACK RUN.

1/10 SCALE 160 MODEL
VROS4D

BYWT	070
------	-----

PREP.	CHK.	APPR.	RUN NO.	CONFIGURATION	TYPE OF RUN	WT. TARE RUN	R.R. θ_{15} Deg.	R.R. θ_{15} Deg.	L.R. θ_{15} Deg.	L.R. θ_{15} Deg.	RPM	ϕ_5 Deg.	ψ Deg.	δ Deg.	J	DATE TIME
			59	HOVER - IN GROUND EFFECT			8.8	0	4.4	0	825	0	90	-	-	2-10-71/0935
			60	" "			8.8	0	4.5	0	825	0	90	-	-	10:23
			61	" "			8.8	VARY	8.12	VARY	825	0	90	-	-	11:22
			62	" "			8.8	VARY	4.96	-0.7	825	0	90	-	-	13:40
			63	" "			11.3	-0.65	9.6	-0.7	825	0	90	-	-	14:33
			64	" "			VARY	VARY	VARY	-0.7	825	0	90	-	-	15:14
			65	HOVER			VARY	VARY	VARY	-0.7	825	0	90	-	-	17:51
			66	HOVER TRANSITION			11.9	VARY	9.7	VARY	825	18	60	0/3	-	19:01
			67	TRANSITION			11.9	VARY	9.2	VARY	825	18	40	0/2	-	

1/10 SCALE 160 MODEL VRO54D

60 RIGID BODY STABILITY DATA IN ROLL AND PITCH WITH & WITHOUT TENSION IN YAW SNUBBERS.

61 RIGID BODY STABILITY DATA IN ROLL AND PITCH WITH & WITHOUT TENSION IN YAW SNUBBERS.

62 REMOVED PITCH AND ROLL SPRINGS RIGID BODY PITCH AND ROLL STABILITY DATA.

63 REPEAT OF RUN 62 - NO DATA BECAUSE LEFT WING WAS AGAINST ROLL STOPS.

64 REPEAT OF RUN 62

65 RIGID BODY PITCH AND ROLL STABILITY.

66 YAW DISPLACEMENTS

67 RIGID BODY PITCH OSCILLATION NEAR 1.7 g RESULTING IN HIGH BLADE LOADS. VISUALLY IT SEEMS TO BE A LIMIT OSCILLATION AT ABOUT 1 CPS WITH THE MODEL SNUBBED.

Contrails

UNCLASSIFIED

Security Classification

DOCUMENT CONTROL DATA - R&D

(Security classification of title, body of abstract and indexing annotation must be entered when the overall report is classified)

1. ORIGINATING ACTIVITY (Corporate author) The Boeing Company, Vertol Division Boeing Center, P.O. Box 16858 Philadelphia, Pa. 19142		2a. REPORT SECURITY CLASSIFICATION Unclassified	
		2b. GROUP	
3. REPORT TITLE VOLUME VI. WIND TUNNEL TEST OF A POWERED TILT-ROTOR DYNAMIC MODEL ON A SIMULATED FREE FLIGHT SUSPENSION SYSTEM			
4. DESCRIPTIVE NOTES (Type of report and inclusive dates) Final Report, January to July 1971			
5. AUTHOR(S) (Last name, first name, initial) John E. Tomassoni Leon N. Delarm Robert B. Taylor Edward B. Schagrin			
6. REPORT DATE October 1971		7a. TOTAL NO. OF PAGES 195	7b. NO. OF REFS 5
8a. CONTRACT OR GRANT NO. F33615-69-C-1577		9a. ORIGINATOR'S REPORT NUMBER(S) D213-10000-6	
b. PROJECT NO.		9b. OTHER REPORT NO(S) (Any other numbers that may be assigned this report) AFFDL-TR-71-62, Volume VI	
c.			
d.			
10. AVAILABILITY/LIMITATION NOTICES Approved for Public Release - Distribution Unlimited			
11. SUPPLEMENTARY NOTES		12. SPONSORING MILITARY ACTIVITY Air Force Flight Dynamics Laboratory Air Force Systems Command Wright-Patterson Air Force Base, Ohio	
13. ABSTRACT This report presents the results of a wind tunnel test on a powered dynamic model of the Boeing M-160 tilt rotor aircraft with 5.5 foot diameter rotors. The model was tested in the Boeing V/STOL 20 x 20 foot wind tunnel during January-February 1971 and was supported to simulate free flight conditions with mount frequencies much lower than the dynamic aircraft frequencies. Blade loads, wing loads, flying qualities and skittishness in ground effect data were obtained.			

14. KEY WORDS	LINK A		LINK B		LINK C	
	ROLE	WT	ROLE	WT	ROLE	WT
Stowed Rotor Hover Cruise Blade Frequency Stall Flutter Tilt Rotor Transition Rotor Loads Skittishness Flying qualities						

INSTRUCTIONS

1. **ORIGINATING ACTIVITY:** Enter the name and address of the contractor, subcontractor, grantee, Department of Defense activity or other organization (*corporate author*) issuing the report.

2a. **REPORT SECURITY CLASSIFICATION:** Enter the overall security classification of the report. Indicate whether "Restricted Data" is included. Marking is to be in accordance with appropriate security regulations.

2b. **GROUP:** Automatic downgrading is specified in DoD Directive 5200.10 and Armed Forces Industrial Manual. Enter the group number. Also, when applicable, show that optional markings have been used for Group 3 and Group 4 as authorized.

3. **REPORT TITLE:** Enter the complete report title in all capital letters. Titles in all cases should be unclassified. If a meaningful title cannot be selected without classification, show title classification in all capitals in parenthesis immediately following the title.

4. **DESCRIPTIVE NOTES:** If appropriate, enter the type of report, e.g., interim, progress, summary, annual, or final. Give the inclusive dates when a specific reporting period is covered.

5. **AUTHOR(S):** Enter the name(s) of author(s) as shown on or in the report. Enter last name, first name, middle initial. If military, show rank and branch of service. The name of the principal author is an absolute minimum requirement.

6. **REPORT DATE:** Enter the date of the report as day, month, year, or month, year. If more than one date appears on the report, use date of publication.

7a. **TOTAL NUMBER OF PAGES:** The total page count should follow normal pagination procedures, i.e., enter the number of pages containing information.

7b. **NUMBER OF REFERENCES:** Enter the total number of references cited in the report.

8a. **CONTRACT OR GRANT NUMBER:** If appropriate, enter the applicable number of the contract or grant under which the report was written.

8b, 8c, & 8d. **PROJECT NUMBER:** Enter the appropriate military department identification, such as project number, subproject number, system numbers, task number, etc.

9a. **ORIGINATOR'S REPORT NUMBER(S):** Enter the official report number by which the document will be identified and controlled by the originating activity. This number must be unique to this report.

9b. **OTHER REPORT NUMBER(S):** If the report has been assigned any other report numbers (*either by the originator or by the sponsor*), also enter this number(s).

10. **AVAILABILITY/LIMITATION NOTICES:** Enter any limitations on further dissemination of the report, other than those

imposed by security classification, using standard statements such as:

- (1) "Qualified requesters may obtain copies of this report from DDC."
- (2) "Foreign announcement and dissemination of this report by DDC is not authorized."
- (3) "U. S. Government agencies may obtain copies of this report directly from DDC. Other qualified DDC users shall request through _____."
- (4) "U. S. military agencies may obtain copies of this report directly from DDC. Other qualified users shall request through _____."
- (5) "All distribution of this report is controlled. Qualified DDC users shall request through _____."

If the report has been furnished to the Office of Technical Services, Department of Commerce, for sale to the public, indicate this fact and enter the price, if known.

11. **SUPPLEMENTARY NOTES:** Use for additional explanatory notes.

12. **SPONSORING MILITARY ACTIVITY:** Enter the name of the departmental project office or laboratory sponsoring (*paying for*) the research and development. Include address.

13. **ABSTRACT:** Enter an abstract giving a brief and factual summary of the document indicative of the report, even though it may also appear elsewhere in the body of the technical report. If additional space is required, a continuation sheet shall be attached.

It is highly desirable that the abstract of classified reports be unclassified. Each paragraph of the abstract shall end with an indication of the military security classification of the information in the paragraph, represented as (TS), (S), (C), or (U).

There is no limitation on the length of the abstract. However, the suggested length is from 150 to 225 words.

14. **KEY WORDS:** Key words are technically meaningful terms or short phrases that characterize a report and may be used as index entries for cataloging the report. Key words must be selected so that no security classification is required. Identifiers, such as equipment model designation, trade name, military project code name, geographic location, may be used as key words but will be followed by an indication of technical context. The assignment of links, rules, and weights is optional.